Chair of Mining Engineering and Mineral Economics

Doctoral Thesis

Development of a quantitative risk assessment method to address the rock mechanics issues of applying TBMs in deep mines

Roohollah Narimani Dehnavi

November 2023

MONTANUNIVERSITÄT LEOBEN
www.unileoben.ac.at

AFFIDAVIT

I declare on oath that I wrote this thesis independently, did not use other than the specified sources and aids, and did not otherwise use any unauthorized aids.

I declare that I have read, understood, and complied with the guidelines of the senate of the Montanuniversität Leoben for "Good Scientific Practice".

Furthermore, I declare that the electronic and printed version of the submitted thesis are identical, both, formally and with regard to content.

Date 24.11.2023

Signature Author
Roohollah Narimani Dehnavi

Acknowledgements

I extend my gratitude to Prof. Nikolaus August Sifferlinger for his support during the completion of this thesis. Additionally, I am sincerely appreciative of the insightful feedback provided by Prof. Jamal Rostami. His mentorship has been instrumental in shaping my journey throughout this thesis.

I express deep gratitude to my beloved family, particularly my dear parents. Their enduring support and constant encouragement has propelled me towards my goals and ambitions.

I am also grateful to those wonderful colleagues and friends I had the privilege of meeting in the enchanting city of Leoben.

Abstract

For fast roadway development in deep underground mining, Tunnel Boring Machines are sometimes brought into operation. However, such machines might get entrapped if squeezing behavior develops and the machine advance rate is not high enough because of breakdowns. This research investigates the suitability of different types of Tunnel Boring Machines for development of infrastructure in deep mines and tunneling projects, with an emphasis on geological risks including squeezing and rockburst. The main consequences linked to these hazards are identified as worker injuries and support system and equipment damage in regions susceptible to rockbursts, and occurrences of shield jamming, support system damage, and challenges related to gripper bracing in squeezing grounds. In pursuit of the primary objective of this research, a probabilistic approach is used to quantitatively assess these consequences, leading to the development of an index called the TBM Risk Index, which assesses the cumulative effect of geological risks and mitigating measures.

To conduct an initial evaluation of shield jamming, as the most critical consequence in squeezing scenarios, a combination of parametric studies based on preconducted 3D numerical models and an approach derived from convergence confinement (CC) concept were used. The adapted convergence confinement method was also employed to assess the risk of support system damage. As for the rockburst consequences, the procedure highly relies on factors such as rockburst intensity and location, which are notably challenging to anticipate. To analyze these risks, preliminary rockburst prediction tools together with a probabilistic approach based on data from a relevant project were applied.

The methodologies introduced in this research were implemented in two primary

case studies, each focusing on a specific category of geological risks, leading to the following key findings: The case study with only squeezing consequences highlighted the effectiveness of a single-shielded TBM with shield lubrication in mitigating the risk. On the contrary, the case study with rockburst hazards demonstrated the higher risks associated with shorter shields in rockburst-prone areas.

Recognizing the uniqueness of each individual project, the research considered multiple hypothetical scenarios with varying proportions of squeezing grounds, areas susceptible to rockbursts, and regions characterized as normal grounds. Using the introduced TBM risk index, insights were gained for an optimum decision to be made between different available machines and mitigating measures. In scenarios with both squeezing and rockburst risks of roughly the same percentage, a single-shielded TBM with lubrication and a gripper TBM with associated mitigating measures were shown to have the lowest extent of rock mechanics issues. When rockburst risk is predominant, shielded TBMs are the preferred option, reducing exposure to seismic events. In scenarios with predominant squeezing grounds, gripper TBMs had the lowest TBM risk index. However, it is noteworthy that in severely squeezing grounds with prevalent squeezing proportion, the application of TBMs are generally questionable and conventional tunneling must be considered instead.

Zusammenfassung

Für die rasche Auffahrung von Zugangsstrecken im Untertagebau werden manchmal Vollschnittmaschinen zum Einsatz gebracht. Allerdings können diese Maschinen bei starker Setzung des Gebirges während Betriebsstörungen eingeklemmt werden. Diese Forschungsarbeit untersucht die Eignung von unterschiedlichen Typen von Tunnelbohrmaschinen zur Auffahrung der Strecken in tiefen Bergbauen und Tunnelbauprojekten. Ein Schwerpunkt liegt dabei auf den geologischen Risken einschließlich Einklemmen und Gebirgsschlag. Als wesentliche Konsequenzen dieser Gefahren wurden Verletzungen von Personen und Schäden an der Maschine in Bereichen mit Gebirgsschlägen sowie Einklemmen des Schildes, Schäden am Sicherungssystem und Probleme am Grippersystem in Bereichen starker Gebirgssetzung identifiziert. In Verfolgung des primären Zieles dieser Forschungsarbeit, wurde ein probabilistischer Ansatz verwendet um die Konsequenzen quantitativ zu bewerten. Dies führte zur Entwicklung des TBM Risk Index (TBM_{RI}), der den kumulativen Effekt der geologischen Risken und mildernden Maßnahmen berücksichtigt.

Zur Durchführung einer ersten Beurteilung des Blockieren des Schildes, als kritische Konsequenz durch Einklemmszenarios durch das Gebirge, wurde eine Kombination von parametrischen Studien basierend vorherigen 3D numerischen Modellen und ein Ansatz, abgeleitet vom "Convergence Confinement (CC) Concept", verwendet. Um die Risiken einer Beschädigung des Sicherungssystems zu beurteilen, wurde dieselbe CC Methode angewendet. Für Gebirgsschlagauswirkungen hängt die angenommene Vorgangsweise stark von Faktoren wie der Gebirgsschlags-Intensität und der Örtlichkeit, welche sehr schwer vorherzusagen sind, ab. Um diese Risiken zu analysieren wurden vorläufige Gebirgsschlags-Vorhersagemethoden gemeinsam

mit einem probabilistischen Ansatz, basierend auf Daten eines relevanten Projektes, verwendet.

Die in dieser Forschungsarbeit eingeführten Methoden wurden in zwei primären Fallstudien implementiert. Jede fokussierte sich auf eine spezielle Kategorie von geologischen Risiken, was zu folgenden Kernerkenntnissen führte: Die Fallstudie nur mit Einklemm-Konsequenzen zeigte die Effektivität einer TBM mit Einzelschild und Schildschmierung zur Verringerung der Risiken. Im Gegensatz dazu zeigte die Fallstudie mit Gebirgsschlag-Gefahren die höheren Risiken welche mit kürzeren Schilden in Gebieten mit größerer Gebirgsschlag-Wahrscheinlichkeit verbunden sind.

In Anerkennung der Einzigartigkeit jedes individuellen Projekts hat die Forschungsarbeit mehrere hypothetische Szenarien mit variierenden Anteilen von drückendem Boden, Bereiche mit Gebirgsschlags-Gefahr und Regionen die als störungsfrei charakterisiert werden, in Betracht gezogen. In Szenarien, in denen sowohl das Risiko von Einklemm- als auch von Gebirgsschlags-Gefahr etwa gleich hoch ist, hat sich gezeigt, dass eine Einzelschild-TBM mit Schmierung und eine Gripper-TBM mit damit verbundenen mildernden Maßnahmen den geringsten Umfang an Gebirgsmechanikproblemen aufweisen. Wenn das Gebirgsschlags-Risiko prädominant ist, sind Schild-TBMs die bevorzugte Option, um die Gefährdung bei seismischen Ereignissen zu reduzieren. In Szenarios mit Regionen mit prädominanter Einklemmgefahr wiesen Gripper-TBMs den niedrigsten TBM-Risikoindex auf. Es bleibt festzuhalten, dass in Regionen mit großer Quetschungsgefahr der Einsatz von Vollschnitt-TBMs fraglich bleibt, und es vorzuziehen ist, andere Tunnelbaumethoden zu verwenden.

Contents

Chapter 1

Introduction

Due to the rising demand for minerals, underground mining has been increasingly growing. However, with many upper orebodies already depleted, mines are going deeper, leading to higher in-situ stresses that pose stability risks for excavations. To mitigate these risks, proper excavation methods must be chosen and considered for designing the mine's development, and extraction operations.

Mechanized excavation has demonstrated advantages, including faster progress rates in sound rock masses, less damage to the development profile, lower ventilation requirements, and safer excavation and working conditions. Consequently, there is a rising interest in their application within the mining industry as a viable substitute for conventional drilling and blasting methods. Full-face cutting machines, such as TBMs, are gaining attention for their ability to cut hard rock at high production and advance rates. However, there are limited experiences with TBMs in underground mining. Their utilization in hard rock mines did not achieve comparable levels of success as that of partial-face cutting machines such as Roadhdeaders in soft rock (coal, salt, potash, etc.) mines, mostly because of their susceptibility to difficult ground conditions [1]. In underground metal mining, ideal operating circumstances like homogenous rock conditions and shallow to intermediate depths are relatively rare. Furthermore, the setup and logistics of operating these machines are highly challenging because of the lack of adaptability to mining infrastructures, low mobility, and unique requirements for TBM construction. Another impediment is the

lengthy manufacturing and launch process as well as the capital expenses [2]. Moreover, compared to civil engineering projects, mining is very site and case-specific, meaning that any mine has its own geological, geometrical, and environmental conditions. This results in the implementation of various mining methods. Therefore, it is logical to evaluate the challenges of applying full-face cutting machines (mostly TBMs) in different categories of mining methods. Three of the most common shapes of deposits namely, flat tabular deposits, massive steeply dipping deposits, and non-tabular deposits with irregular shapes are discussed further to better clarify the differences:

1. Flat tabular deposits

   In the category of flat tabular deposits such as coal mines, one can see many potentials for the application of TBMs. Indeed, the geometry of the deposit is not varying significantly and TBMs can be planned and organized more easily to develop roadways. Besides, statistics show that the geological complications and subsequent difficult ground conditions in coal mining formations have been less compared to metallic ores. China is planning to develop very deep roadways in coal mining in the coming years. Explorations indicate that 53 percent of coal resources in China are buried deeper than 1000 m [3]. Thus, faster and safer excavation of roadways using TBMs is gaining popularity.

2. Massive steeply dipping deposits

   Excavation of developments for accessing rather massive steep mineral deposits can also be planned easier. An illustrated example of using two TBMs to develop beyond 2 km depth is shown in Figure 1.1.

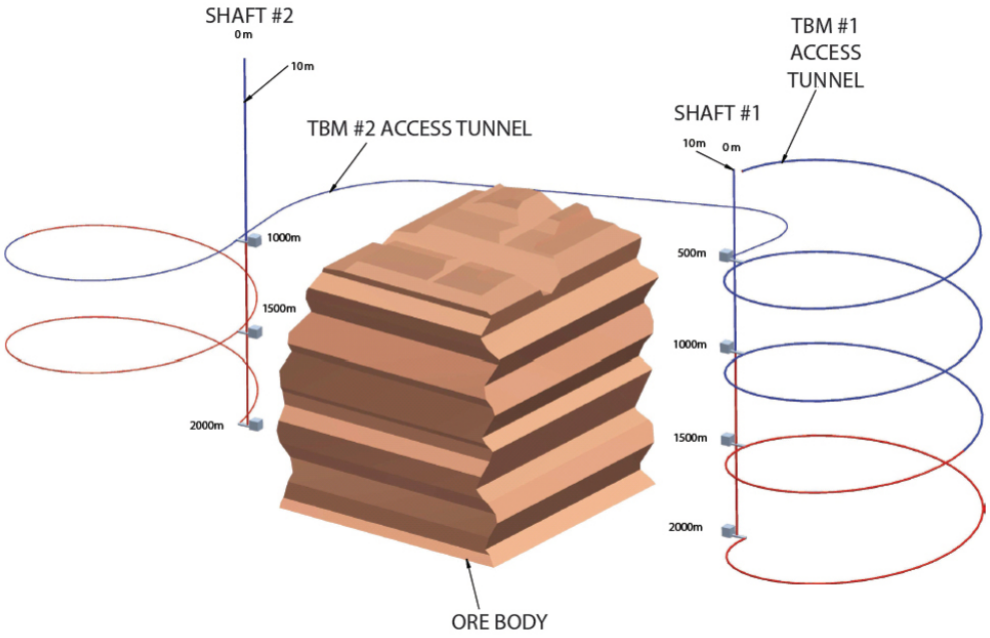

Figure 1.1: An illustration of a plan for accessing and transporting ore from a deep ore body through main access and haulage developments [4]

One of the mining methods for the extraction of massive mineral deposits is block caving (Figure 1.2). By knowing the depth of the undercutting and production level, the access decline shafts can be designed for TBM application. In Magma Copper mine, TBMs with a rather low turning radius were applied to also excavate the undercutting and production levels. Fully mechanized excavations using such approaches can significantly reduce the time required to construct infrastructures for a block-caving mine.

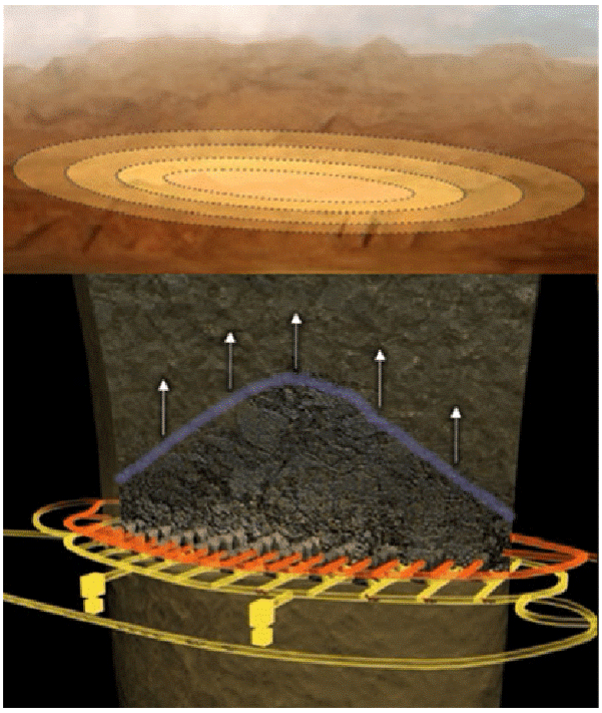

Figure 1.2: Production and undercutting level developments in a block caving mine [5]

3. Non-tabular deposits in vain mining

   An important factor in terms of non-tabular deposits is the uncertainty in their extent. The exploration of these mines is an ongoing procedure. In such mines, developing the whole infrastructure to the deepest areas is dependent on exploration operations. Since the current technology of TBMs does not provide enough flexibility in turning radius, the tunneling routes cannot be easily adapted and optimized. Figure 1.3 shows an example of the geometry of a non-tabular deposit in an underground mine.

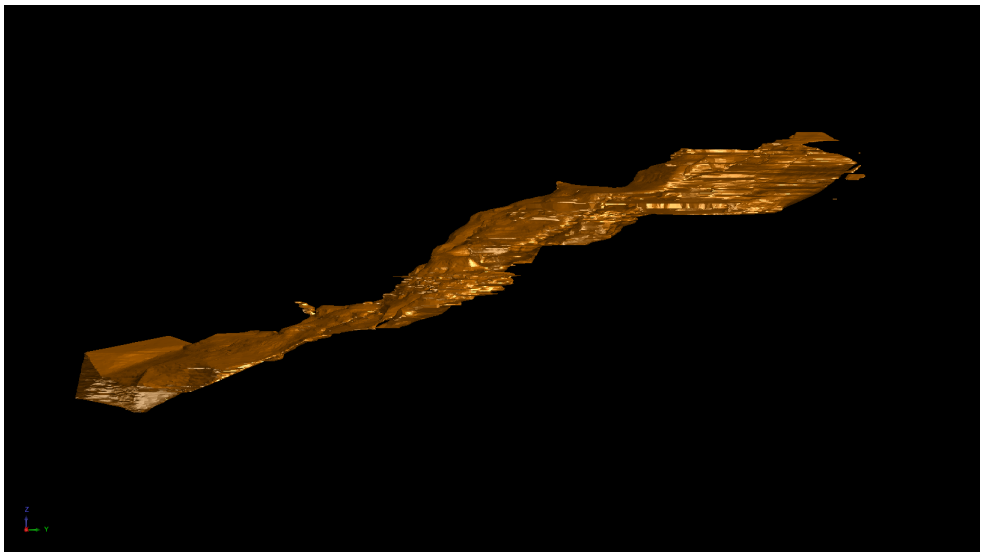

Figure 1.3: The geometry of a non-tabular irregularly shaped deposit

If a TBM is deemed suitable for a mining project, the next step is to choose the most suitable machine type based on the expected geological conditions. Gripper TBMs are the most common type used in underground mines due to their low risk of entrapment and flexibility in turning. They are compatible with versatile rock support systems like bolts, wire mesh, and ribs, making them ideal for mining projects. However, the gripper shoes might face difficulties providing excavation reaction forces in weaker rock types. Dealing with such difficulties together with time-consuming support installation in very soft grounds reduces their utilization rate. Shielded TBMs, on the other hand, use stiff segmental lining supports and are prone to get stuck in squeezing grounds.

In cases where neither option is capable of meeting expectations, it is best to avoid using a TBM. In deep mines, the primary challenges that pose a threat to the safe use of TBMs are squeezing in weak grounds and rock burst hazards in hard brittle rocks. Accurately assessing the extent of these hazards and implementing quick counteracting preventive measures are necessary to combat their consequences.

Rocks that are overstressed and have a brittle behavior are prone to rock bursting and spalling at the excavation face or walls. The abrupt energy release can have a significant impact on the tunnel support installation, damage the cutters and cutterhead, and create gripping and mucking difficulties while also posing risks to

workers. However, high in-situ stresses have a different influence on more ductile materials. The existence of weak rocks can result in high rates of convergence, potentially leading to the jamming of the TBM (Figure 1.4). In TBM excavation case studies in mining, weak ground conditions accounted for the majority of downtimes. These issues are critical in any deep tunneling project for any application, such as the transalpine tunnels with high overburden. In this thesis, the scope of work is limited to investigating the main geological consequences of deep mining/tunneling and their effects on the performance of full-face cutting machines such as TBMs. Other critical limitations of using TBMs in mines require further and broader studies out of the scope of this research.

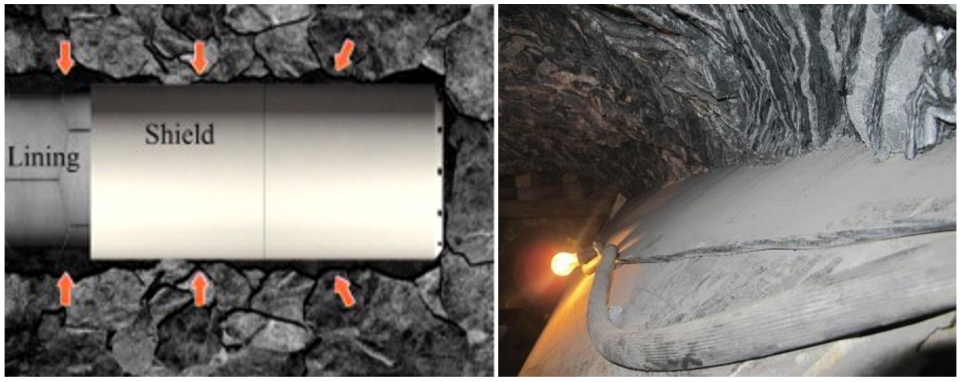

Figure 1.4: Entrapment of a shielded TBM in a squeezed ground [6]

1.1 Research Objectives

To address the aforementioned challenging geological conditions, it is crucial to accurately assess the extent of the hazards and take prompt preventive measures. This is especially vital in deep mines where geological knowledge is limited. According to the ITA Working Group n17, even with a comprehensive geomechanical database and analysis of TBM data, it is still difficult to anticipate risks like rockburst and squeezing. Rockburst and spalling are particularly hard to predict while squeezing, buckling, and face instability are generally very difficult to predict [7]. As stated before, these difficulties stem from the lack of geological knowledge of the formations and the potential consequences. Therefore, a risk assessment procedure is followed in this thesis to develop a quantitative risk assessment index that can be used to

evaluate the suitability of using a Tunnel Boring Machine (TBM) to excavate tunnels through a set of prescribed rock formations. This index can be applied to compare the performance of different TBM types for the purpose of machine selection. The primary emphasis of the risk assessment will be on identifying and mitigating risks that are pertinent to two key types of rock failure: brittle failure (also known as rockburst), and ductile failure in overstressed rocks (commonly referred to as squeezing). In order to develop the risk assessment index, numerical factors are considered, including the geological characteristics of the rock formations, the type of TBM to be used, and the potential impacts or consequences of rockburst or squeezing on the mining/tunneling operation. By evaluating the risks associated with different types of TBMs, more informed decisions can be made regarding machine selection, which can ultimately lead to improved safety and productivity in the mining/tunneling operation. The risk assessment index can also be useful for regulatory bodies and other stakeholders who are involved in the planning and oversight of mining operations, as it provides a standardized framework for evaluating the geological risks associated with TBMs in deep tunneling conditions.

1.2 Approach

This research is planned to devise a cumulative quantitative risk index that can evaluate the risks associated with the application of TBMs in deep mining or tunneling conditions. The system compares the extent of risk of different machine types in the given geotechnical conditions throughout the tunnel path. It eventually concludes which type of TBM involves the minimum risk. Based on the existing mitigation technologies, operational measures to decrease the possible negative impacts can also be investigated. As can be seen in Figure 1.5, primary geotechnical data including the current and possible future stress state in the mine are imported into the system. The system is supposed to also consider the existing technologies that can mitigate the associated risks. By incorporating several rockburst and squeezing prediction methods, the extent of risks for different TBM types in different chainages of the tunnel pathway is evaluated in the system to come up with a cumulative

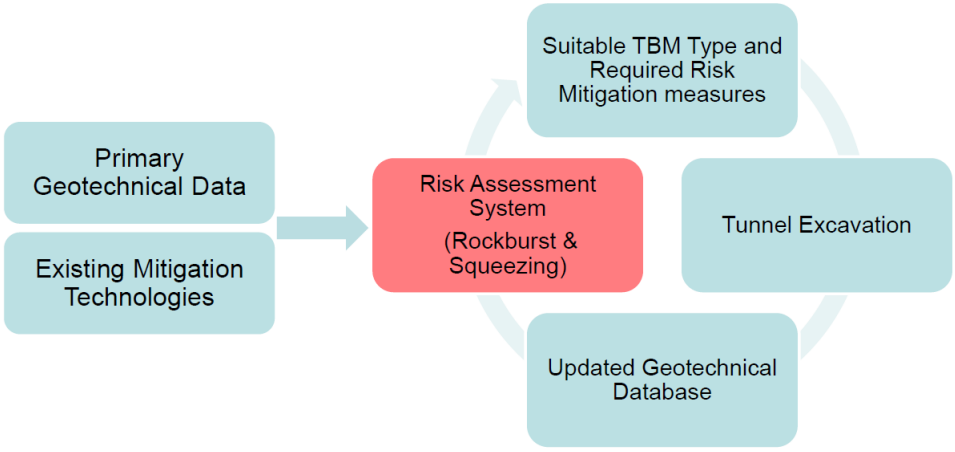

Figure 1.5: A schematic explanation of the risk assessment method

risk quantity. The goal is to include suitable prediction methods for different rock mass conditions and based on the primary data in the system introduce a logic by which the system can opt for the proper methods for certain conditions. In addition, the system can still be applied during the excavation process, as the geotechnical database is improved and can modify the risk extent in the coming chainages of the tunnel. These valuable sources of information could be seismicity measurements in the region, operational data of the TBM, stress state measurements, and advance exploration data gained from probe drilling technologies.

Chapter 2

State of the art

2.1 TBM tunneling

Tunnel Boring Machines (TBMs) are employed for excavating tunnels across a variety of applications, such as transportation, water supply, and mining. There are several types of TBMs that differ in their excavation method, size, and application. They can be broadly classified into two categories based on the type of rock or soil they are designed to excavate: soft ground TBMs and hard rock TBMs. While this classification is helpful in understanding the basic types of TBMs, it is worth noting that some machines are designed to operate in a range of soil or rock types, and that there might be variations within each category of TBM to accommodate specific project requirements. Figure 2.1 shows an overview of different types of TBMs in the two main categories of soft ground and hard rocks [8].

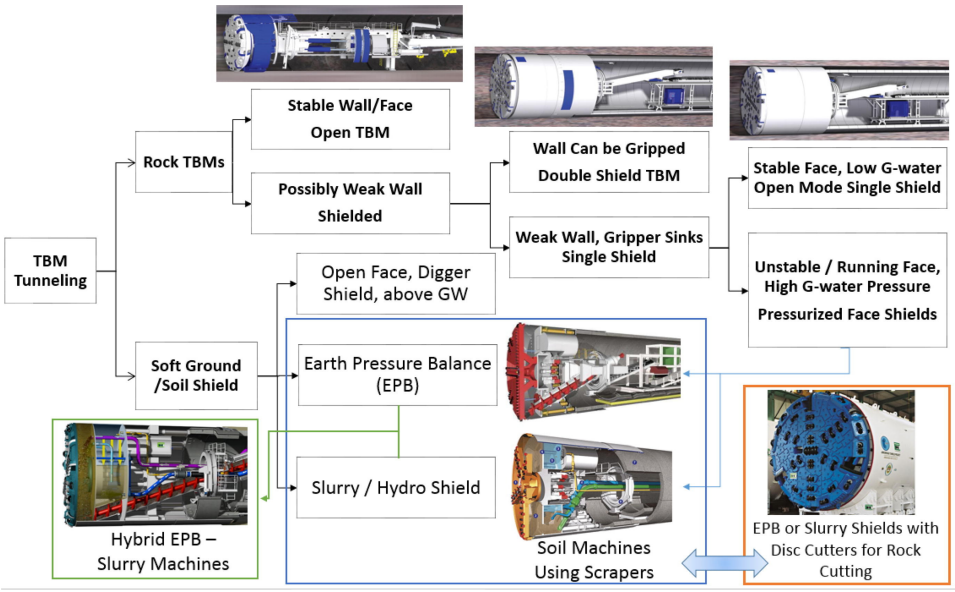

Figure 2.1: Categorization of different types of TBMs according to the ground condition[8]

2.1.1 Soft Ground TBMs

Soft ground TBMs, as the name suggests, are designed to excavate tunnels in soft and unstable soils, such as clay, silt, and sand. These machines typically use a combination of excavation tools and ground support systems, such as cutterheads, augers, and grouting, to excavate and support the tunnel. They can be generally classified into Earth Pressure Balance (EPB) TBMs, Slurry TBMs and Mixshield TBMs [9].

2.1.2 Hard Rock TBMs

Hard rock TBMs, on the other hand, are designed to excavate tunnels in rock formations. These machines typically use disc cutters mounted on the front of the machine to break the rock into smaller pieces, which are then removed by the machine's conveyor system. This study focuses on tunneling in mines and higher depth using hard rock TBMs, where a variety of rock types and strengths are typically encountered. Hence, the research question at hand is to determine the most suitable type of hard rock TBM to use, taking into account the specific ground conditions present. Gripper TBMs (open TBMs), single shielded TBMs and double shielded

TBMs are the three main categories of hard rock TBMs.

- Gripper TBMs:

  When working in rock with medium to long stand-up time, Gripper tunnel boring machines are used without active support for the tunnel face and excavation profile. They use gripper plates to apply contact pressure to the cutterhead, which excavates the rock using disc cutters. It utilizes a shorter shield to protect the cutterhead. The tunnel profile is systematically supported behind the cutterhead shield, with additional support as necessary. In situations with unstable rock conditions, it is suggested to equip the machine with devices for forward probe drilling and rock improvement. Additionally, installing steel arches, shotcrete, spiles or anchors is possible behind the cutterhead for fault zones that consist of less stable rock and carry a risk of rockfall. To prevent contamination of the front section of the machine, the systematic shotcrete lining is usually conducted in the trailing gantry area (L2 area). Anchors should be reinforced in the gantry area to support the rock.

- Single shielded TBMs:

  In stable tunnel conditions, such as in clays with sufficient cohesion or in rock, a single shield is suitable for excavation. This type of shield secures the tunnel profile and allows for the construction of a segmental ring for the lining. A cutterhead equipped with disc cutters excavates the ground, which is removed via conveyor belts. The thrust forces and cutterhead torque are transmitted to the last segmental lining ring via thrust cylinders. In blocky rocks, jacking shields are used to protect against the potentially displaced ground, with a mainly closed cutterhead and shield casing.

- Double shielded TBMs:

  Double shield machines are composed of two telescopic parts and are suitable for stable tunnel faces in solid rock or soils. The front shield holds the cutterhead, the cutterhead drive, and the primary thrust cylinders, while the gripper shield contains the gripper plates and auxiliary thrust cylinders. The segment

placement device and tailskin are connected to the gripper shield. The main thrust cylinders enable the front shield to be extended forwards by a complete ring length, resulting in a telescopic joint, which is closed by the telescopic shield. Within a stable rock mass, the grippers provide the torque and thrust forces for excavation and advance of the machine. This allows parallel construction of the segment ring in the tail skin area while the front shield propels forward. In subsoil where the grippers cannot hold, the advance is supported by the last ring of segments in single-shield mode [9].

Development of a decision aiding tool that can determine the type of TBM with the lowest extent of risk for a specific project is the main goal of this research. This tool can also aid in addressing the specification requirements of the machine and the need for implementing mitigation measures to mitigate risks. There are certain determinative factors that differentiate the above three types of hard rock TBMs: the gripper bracing possibility, the length of the machine shield, the type of support system, the geometrical flexibility of the machine and the advance rate capabilities. The design and selection of these specifications highly depend on the ground condition and the anticipated geological risks in the tunnel path. In the next chapter, the criterion for the assessment of these risks is discussed in detail.

2.2 Risk assessment of TBM tunneling

The process of managing risk in any project starts with establishing the context, identifying, analysis, and evaluating the potential risks. Afterwards, measures are taken to treat, monitor, and control the likelihood or impact of unfavorable events (See Figure 2.2).

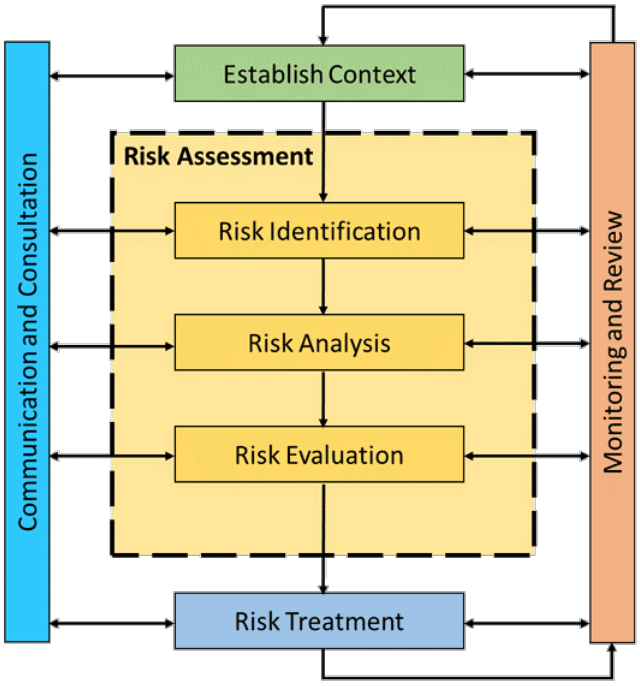

Figure 2.2: A risk management flow chart as described in ISO 31000 standard [10]

The necessity of risk assessment in developing underground excavations results from two main sources of uncertainty: Geology and construction process. The complexity of geological state (geological disturbances) and lack of sufficient information regarding the in-situ stress environment and rock mass properties could lead to unexpected geotechnical hazards. The other source of uncertainty is the extent of success of a specific construction process. In other words, a proper prediction of geology cannot guarantee a successful construction process. The experience of the excavation team, efficient performance of the equipment, and working personnel are of high significance [11]. The mitigating measures taken to alleviate a risk also have specific uncertainties in their degree of success. As for TBMs, which are main focus in this context, their lower adaptability to difficult ground conditions (resulting from high overburden and long excavations) makes their application a real challenge. The main scopes of risks covered in this context are, however, associated with rock engineering design and geological risks. Improper rock engineering design of the excavation method for a deep tunnel results in hazards to the health and safety of personnel, delay in completion of the tunnel, and risks in terms of financial losses:

- Risk to the health and safety

The primary objective in this regard must be to avoid hazards for the personnel and the excavation equipment. In addition, the tunnel must remain stable and operational throughout its designed life.

- Risk in the delay to the completion of the tunnel

  Methods of excavation and the pertaining mitigating measures should be applied in a way that lower downtimes and higher excavation rates can be ensured.

- Risk in terms of financial losses

  And last but not least, the risks must be controlled in a way that financial losses can be minimized. It should be noted that the two terms delay and financial loss pose practically the same consequences. Each day of delay in completion of the tunnel using a TBM means additional costs for the project.

In the context of this study, the decisions to be made include the selection and application of proper construction methods (mainly the type of TBM and its technical features), as well as the application of suitable support system to minimize the negative effects. After the establishment of the context, the important aspect for a successful TBM excavation is to primarily identify the potential risks. This is known to be the most critical component in the risk management process. According to ITA (2017), the most relevant geological risks fall into three main categories: rockburst and spalling, squeezing and buckling, and face instability [7].

2.2.1 Rockburst and spalling

Rockburst is an abrupt failure of rock that is typically marked by the sudden discharge of stored energy within the rock mass, leading to the expulsion of rock fragments and displacement of supporting structures. Spalling, as an outcome of rockburst, refers to a specific type of rock damage caused by high levels of stress, resulting in fracturing into parallel sheets and eventual detachment from the surrounding walls [12]. Figure 2.3 shows an incident of rock spalling taken place above a hard rock TBM.

Figure 2.3: Progressive rock spalling above a TBM excavating in granite [13]

2.2.2 Squeezing and buckling

The time-dependent behavior of rock with high plasticity which can impose high pressures on the ground support is known as squeezing. In extreme cases, high squeezing grounds can lead to the collapse of the tunnel perimeter. Squeezing in tunnel construction is influenced by a number of variables, including rock type, foliation spacing, the orientation of rock structures, stress to intact rock strength ratio, water pressure, the method of construction, and support systems.

The existence of structure and the orientation of the rock structure with respect to the underground excavation have significant impacts on the squeezing behavior, with schistose and foliated rocks being particularly susceptible to it. Buckling belongs to the same category of squeezing and is generated as a result of dominant structural features (schistose layers) being parallel to the tunnel perimeter [14]. Indeed, a higher extent of squeezing is expected to take place, when the foliation is parallel to the tunnel alignment. Numerical models created in UDEC by Schubert and Mendez (2017) show how changing the dip angle can affect the magnitude of deformations in a circular-shaped tunnel (See Figure 2.4)[15]. As can be seen, the maximum displacement is oriented perpendicular to the foliations because of the bending happening in the layers and opening of the joints.

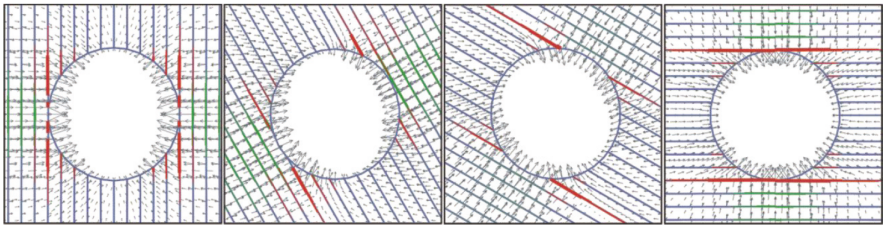

Figure 2.4: Numerical simulation of different dip angles of foliation and their effect on shearing and opening of discontinuities; Foliation strike is parallel to the tunnel axis [15]

2.2.3 Face instability

Face instability in a TBM tunneling project is defined as the potential for the tunnel face to collapse on the cutterhead. In extreme conditions, the cutterhead may be jammed, due to the fact that the adequate toque for the cutterhead to get released from this situation cannot be provided by the machine. Interventions might be necessary to release the cutterhead. Figure 2.5 shows an example of the cutterhead being jammed due to extreme fracturing of rock in a rockburst event.

Figure 2.5: Jamming and damage of the cutterhead due to excessive fracturing of rock in a rockburst event [16]

2.3 Risk analysis

In general, the risk analysis techniques can be categorized as qualitative or quantitative. In qualitative methods, a pre-defined rating scale is employed to prioritize the identified risks. Quantitative techniques, on the other hand, employ numerical scales and enable the establishment of practical and attainable cost and schedule for informed decision-making, when there is uncertainty. Due to the certain advantages

of quantitative methods and the nature of the risk at hand, they are chosen as the main approach in this investigation.

In this section, three of the quantitative risk analysis methods most relevant to the present problem are discussed and applied: Event tree analysis (ETA), Fault tree analysis (FTA), and Probabilistic risk analysis method (PRA). Fault trees and event trees are regarded as structured techniques that pave the way for a better evaluation of the probability of potential risks. A sensitivity analysis of the input data and the recognition of the places where more efforts to design, control, and monitor measures are required, can be conducted using these methods [17].

2.3.1 Fault Tree Analysis (FTA) for the likelihood of hazards

As a top-down deductive method, FTA is a technique introduced to comprehend how certain procedures can malfunction or fail. It is especially applied in safety engineering. In the form of diagrams, the potential failures and faults and their combinations leading to certain events are analyzed. More importantly, strategies for controlling the risk can be investigated using this technique. Other areas of application for this technique include mining, construction, chemical and process, pharmaceutical, and aerospace. FTA is superior to other techniques in depicting the system's resistance to single or multiple initiating faults. However, it can't identify all the potential initiating failures [17].

In this section, each of the aforementioned hazards is studied individually by drawing the fault trees. This can provide a clearer picture of the factors influencing each hazard and its likelihood. Figure 2.6 illustrates the principle factors resulting in squeezing issues. As a general rule of thumb, a soft highly deformable rock together with an existing high-stress state compared to the strength of the rock can contribute to squeezing. Squeezing leads to either too much convergence or in case of a stiff support to high pressures. As for a stiff support like the shield of a TBM, jamming of the shield can become critical. The Squeezing occurrence cannot be avoided, however, the consequences can be controlled.

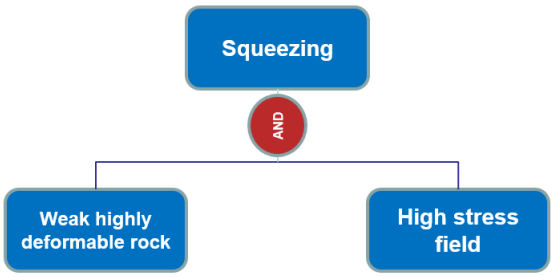

Figure 2.6: The fault tree analysis indicating the factors leading to squeezing risk

Buckling encompasses similar consequences as squeezing, only originating from different mechanisms. As for buckling, the anisotropic foliation exposed to high in-situ stresses would bring about excessive deformations in specific directions. The worst case for the orientation of the foliation in a tunnel is when they are directed parallel to the tunnel axis. As can be seen in Figure 2.7.a, a high-stress field that leads to buckling can be either the result of a high overburden or high anisotropy in an unfavorable direction. According to Figure 2.7.b, the unfavorable direction for the major principle stress is the vertical direction (parallel to the foliation orientation). As squeezing and buckling both have more or less the same implications for a TBM tunneling project, they will be subsequently discussed in the same category of squeezing.

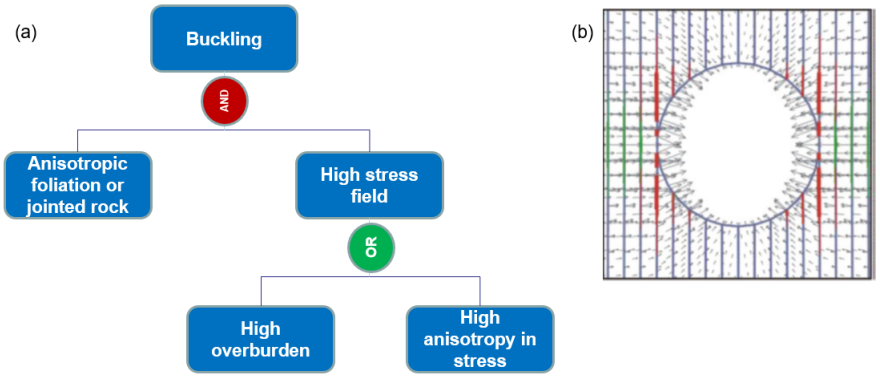

Figure 2.7: (a): The fault tree analysis indicating the factors leading to buckling risk (b): The effect of anisotropic foliation on intensifying the deformations as an indicator of buckling[15]

Rockburst and spalling would occur when a massive hard brittle rock mass undergoes a high stress concentration (See Figure 2.8). The existence of a geological disturbance like a fault, dike, etc. can intensify the situation. As for spalling, it is

worth mentioning that spalling does not necessarily take place in the deepest regions of a tunnel. In the example of Lesotho Highlands water project, rockbursts took place at a depth of 120 m because of higher horizontal stresses than vertical stresses [7].

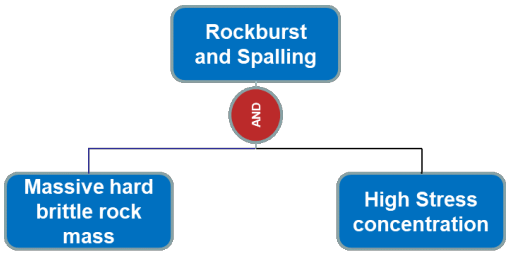

Figure 2.8: The fault tree analysis indicating the factors leading to rockburst and spalling risk

Face instability in a TBM tunneling project, on the other hand, can occur as a result of a wider range of scenarios. Either one of these cases can be the cause: low strength or blocky rock mass on the tunnel face, the unfavorable orientation of discontinuities, and high stress field hazards (squeezing or rockburst) (See Figure 2.9). Low strength or blocky rock mass could occur as a result of faults or hydrothermally altered zones (sandy fault zones, clayey fault zones, blocky rock mass, etc.) and restrict the bearing capacity of the face. An important point to consider is that high water pressure could aggravate the condition and raise the likelihood of face instability occurrence. With regards to squeezing, extreme squeezing can form high plastic zone extension in front of the cutterhead and cause the face to collapse. Closely spaced discontinuities perpendicular or sub-perpendicular to the tunnel axis might lead to the formation of unstable wedges instead of chips. This could cause damage to the cutterhead, cutters, buckets, and belt conveyor. Face instability can frequently occur in large diameter tunnels due to higher appearance of a combination of soft rock, fractures and discontinuities over a large area in the tunnel face (e.g. Niagara Project) [7]. Prediction of the face instability is relatively difficult and complex and as shown in Figure 2.9, depends on a high number of factors. Moreover, when comparing different types of TBMs, face instability will be a potential risk for any type of TBM. Therefore, in a problem where the question is choosing the right type of TBM, face instability is not considered determinative

and will not be included in the following stages of this research.

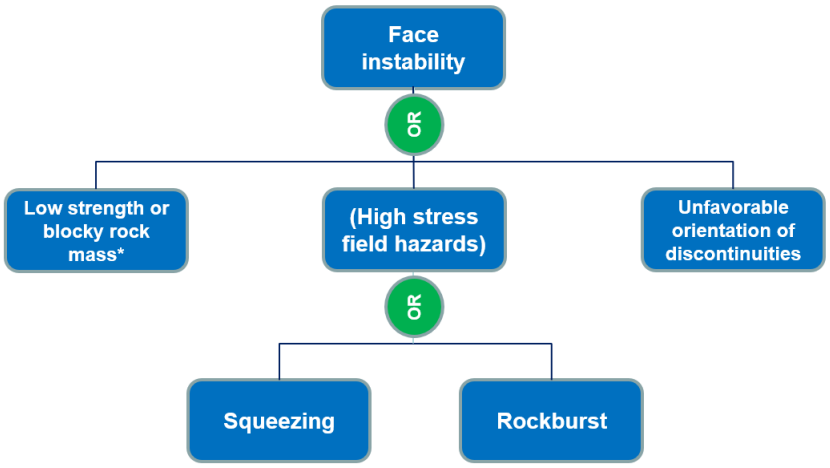

Figure 2.9: The fault tree analysis indicating the factors leading to face instability

2.3.2 Event Tree Analysis (ETA) for investigating the possible consequences

Event Tree Analysis (ETA) is an effective method that enables one to map out plausible event scenarios leading to a major incident. It indicates any system consequences that may happen after an initiating event, in addition to giving numerical estimates of the likelihood of occurrence of the component events and escalated events. Its application areas can be a variety of systems such as manufacturing, chemical plants, and mining.

A comprehensive knowledge of the system is necessary to understand the initiating events followed by intermediate events to be able to create the event tree diagram, starting from the initiating event, subsequent successive events form paths leading to a string of success or failure. The overall probability of occurrence for each path will be finally determined. Fault tree analysis can be employed to compute the probabilities of failures for intermediate events, and the following equation: probability of success (ps) + probability of failure(pf) = 1 can be used to get the probability of success. Figure 2.10 shows an example of an event tree diagram.

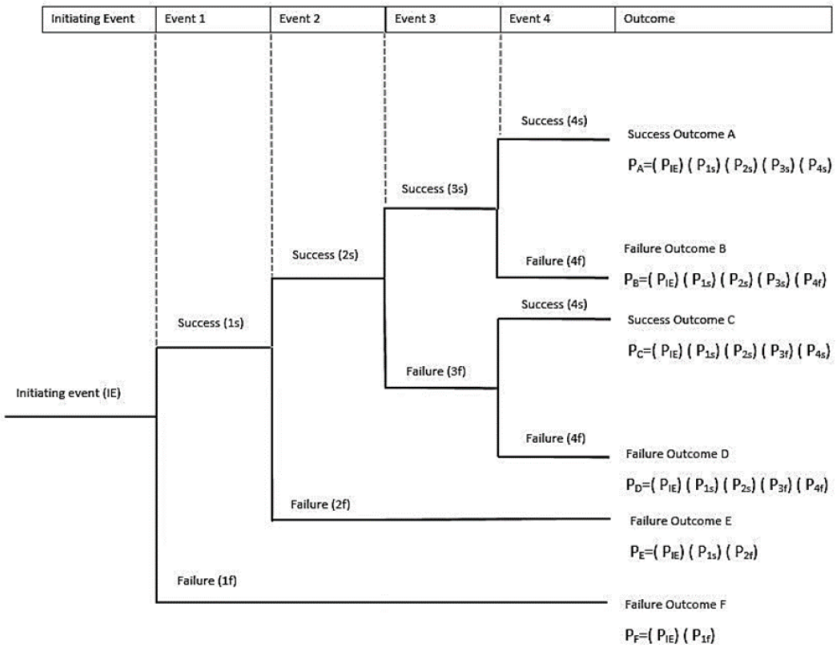

Figure 2.10: An example of an event tree diagram [17]

The event tree analysis for identifying the consequences of squeezing and rockburst for a TBM tunneling project is conducted and diagrams are drawn in Figures 2.11 and 2.12, respectively. Squeezing and buckling are integrated into the single category of squeezing. Rockburst and spalling are also of the same nature and are inserted into one class. A general decision, in the beginning, is to either choose a shielded or an open TBM (gripper TBM). As the implications of a single-shielded and a double-shielded TBM are very similar and only of different extents depending on the geometry of the machine, they are grouped in one class. The next key question is the location of the incident, which have different implications as well. As mentioned before, in this risk assessment, a comparison between the performance of different types of machines against the hazards is conducted, and the incidents occurring in the tunnel face would be the same for all types. Thus, the scope of analysis is limited to the incidents in the sidewalls, to simplify the procedure. The paths leading to the consequences in the sidewalls are highlighted with red color in the figures 2.11 and 2.12. These figures illustrate the most relevant geological risks with their possible consequences. The consequences largely depend on the type of the selected machines, the location of the incident, and the intermediate events in a specific scenario.

The consequences can be devastating, as evidenced by the total destruction of a TBM and seven fatalities in the drainage tunnel of the Jinping II project due to an intensive rockburst (See Figure 2.13). Moreover, Figure 2.14 shows gripper bracing difficulty as a result of severe spalling on the tunnel walls in Jinping II project.

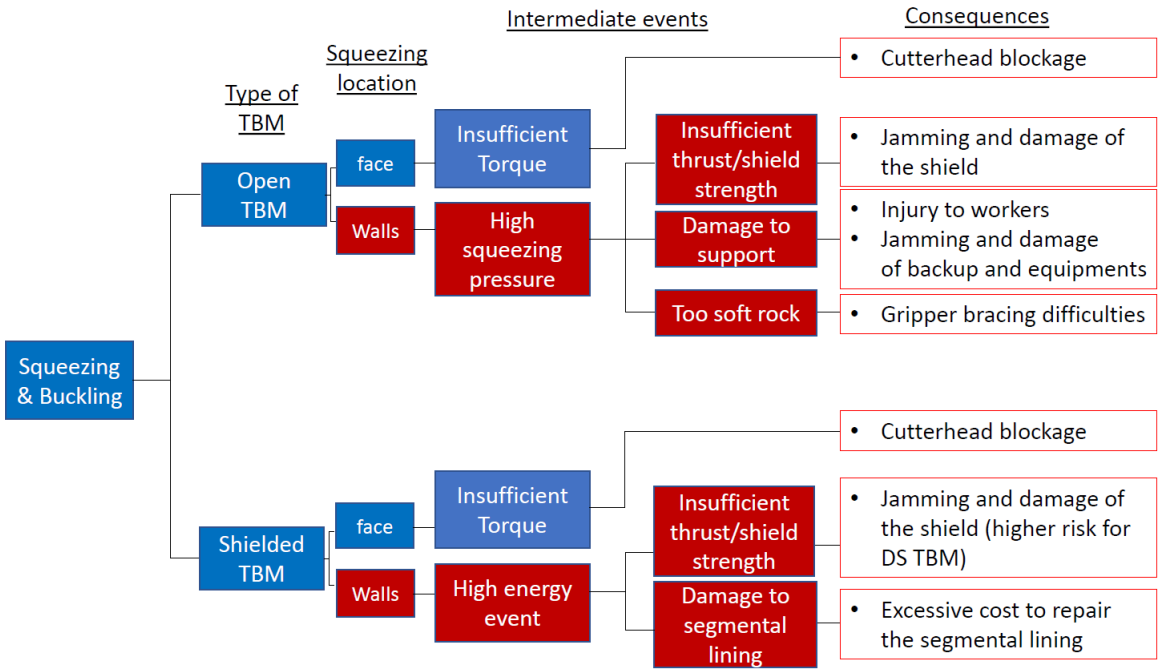

Figure 2.11: An event tree analysis for identifying the consequences of squeezing risk for a TBM tunneling project

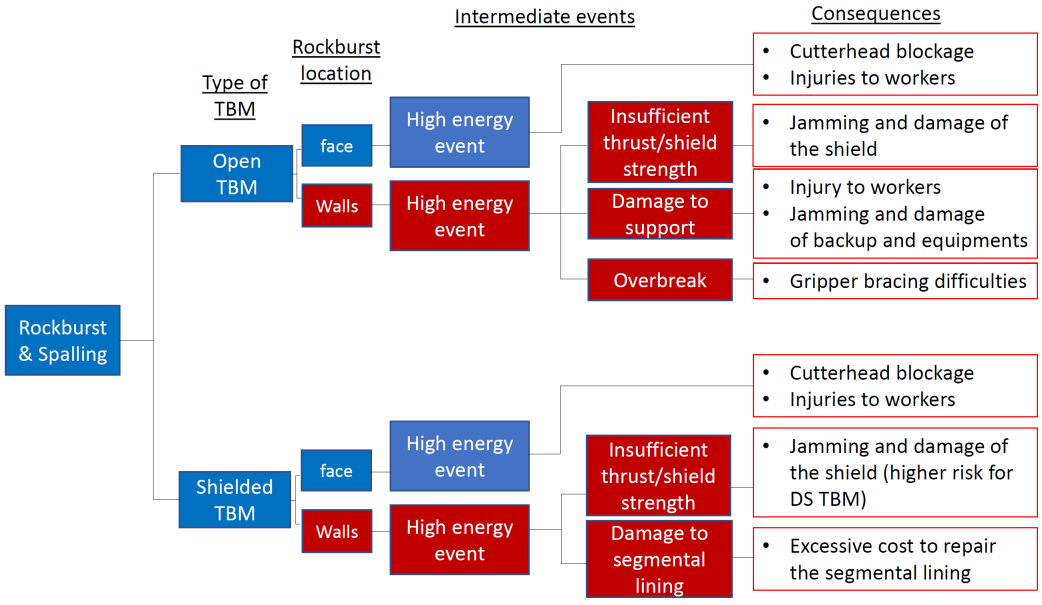

Figure 2.12: An event tree analysis for identifying the consequences of rockburst risk for a TBM tunneling project

Figure 2.13: An extremely intense rockburst in the drainage tunnel of Jinping II hydropower Station project leading to the total destruction of the TBM [18]

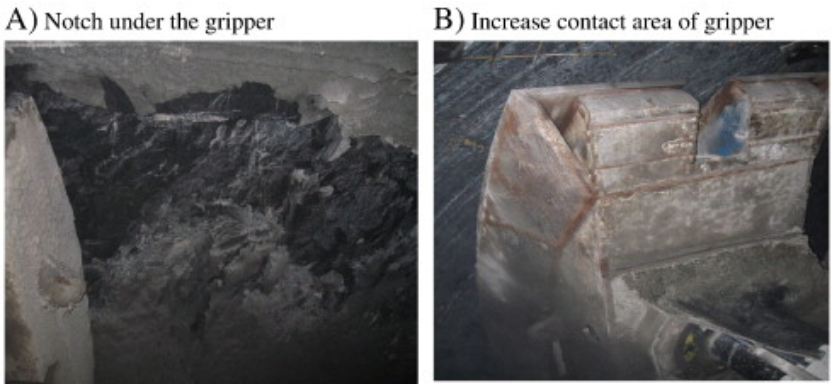

Figure 2.14: Gripper bracing difficulty as a result of severe spalling on the tunnel walls in Jinping II project [16]

2.3.3 Probabilistic risk analysis method (PRA)

Probabilistic analyses offer a wider spectrum of potential outcomes and the associated probability of the events happening, in contrast to deterministic analysis. This approach allows us to evaluate the impact of input parameter variability and uncertainty. To do so, we must first establish a sampling technique. Two widely recognized and frequently used methods are the Point estimate method and the Monte Carlo simulation method, which will be separately outlined as follows:

- Point Estimate Method

  According to Rosenblueth (1975), the Point Estimate Method is a straightforward approach for sampling random variables [19]. As illustrated in Figure

2.15, two values, one standard deviation away from the mean, are randomly selected on either side. These selected values are subsequently employed to compute the measure of risk.

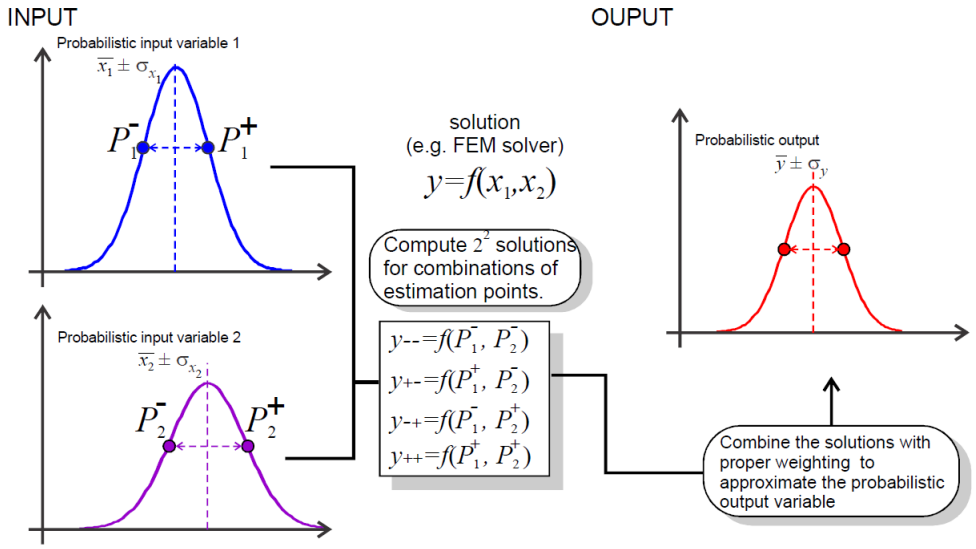

Figure 2.15: The computational principle behind the Two Point Estimate Method utilized in Phase 2 v8.0 [20]

As depicted in Figure 2.15, solutions are computed at different estimation points. These solutions are then combined using appropriate weighting to determine the probabilistic output variable according to equations 2.1 and 2.2.

$$\bar{y} = \sum_{i=1}^{2^n} w f_i \tag{2.1}$$

$$\sigma_y = \sqrt{\sum_{i}^{2^n} w f_i^2 - \left(\sum_{i}^{2^n} w f_i\right)^2} \tag{2.2}$$

- Monte Carlo simulation

  The Monte Carlo technique is widely used in engineering for probabilistic analysis. When there is knowledge about the degree of variability or uncertainty of risk-influencing parameters, Monte Carlo simulation can be employed to determine the distribution of the risk quantity, which is the output parameter. As shown in Figure 2.16, discrete values are randomly generated from

the distribution functions of each influencing parameter. These values are then used as inputs for the geological risk evaluation function or formulation, which calculates the risk quantity. This process is repeated many times to generate randomized data and obtain the distribution of the risk quantity.

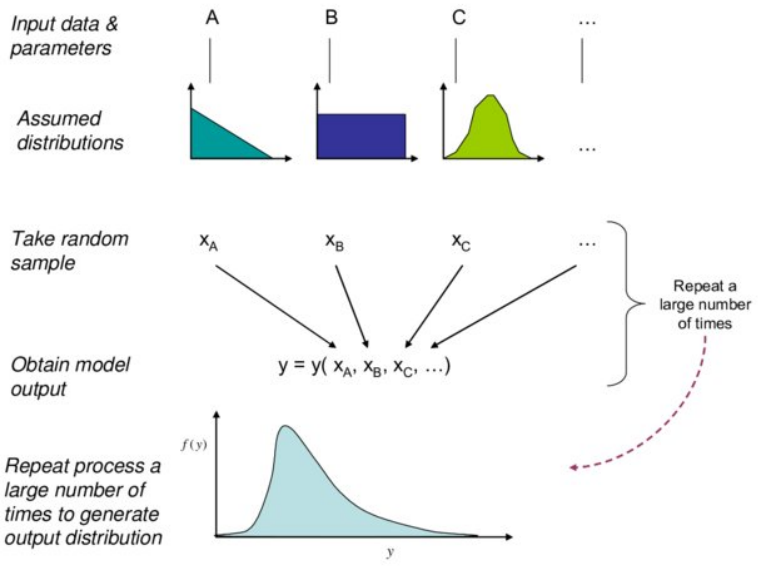

Figure 2.16: A visual representation of the Monte Carlo simulation process [21]

When dealing with over 10 influencing parameters, it is advisable to use the Monte Carlo simulation method instead of the PEM. Furthermore, the Monte Carlo simulation has the advantage of being able to test an infinite number of scenarios, as long as computational time is not a limiting factor.

Considering the significant number of parameters affecting the risk quantities in this study and the high extent of uncertainties involved, the Monte Carlo simulation method is adopted as the main method for risk evaluation. The requirements in this system are, however, the prediction tools or calculation methods. Following the identification of the risks, this can be seen as the most critical stage in such investigations. In this regard, many qualitative and quantitative methods have been introduced for both rockburst and squeezing. In chapter 2.4, the focus is made on rockburst and the required prediction tools for acceptable risk analysis. The very high difficulty existing in the prediction of rockburst hazards necessitates a thorough investigation into the introduced prediction tools in the literature. Subse-

quently, Chapter 2.5 is dedicated to a brief introduction to the most typical squeezing assessment methods.

2.4 Rockburst hazard prediction methods

Rockburst could take place in transportation tunnels, hydroelectric projects, and deep mining areas. Understanding the phenomena associated with rockburst remains a critical issue and needs to be further investigated to avoid or manage the pertaining consequences [22].

Rockburst events normally fall into three main categories: strainbursts, pillar bursts, and fault bursts. Strainbursts take place only under low confinement, i.e., where the confining pressure of the rock mass reduces significantly as a result of excavation. Pillar bursts could occur in a range of low to high confinement pressures. Fault slip rockbursts, on the other hand, are known to take place under high confinement conditions [23].

The development of a risk assessment system for rockburst hazards requires appropriate tools for prediction. For this purpose, we need to initially study the factors affecting the occurrence of a rockburst. Sousa (2010) summarized some main determining factors giving rise to the probability of a rockburst event [11] (See Figure 2.17). The stress state in the excavation region is regarded as the most important parameter leading to a rockburst. A high stress state could originate from high overburdens that increase vertical stresses. The horizontal stresses can also be of a high value due to the topography on the surface and the tectonic regime. The type and rock strength are other very important factors. Strong and competent rocks with especially brittle behavior can potentially absorb high amounts of energy and increase the likelihood of a rockburst. The shape and size of the excavation determine the magnitude of stresses and the locations where high amounts of stress and energy can be concentrated. The size and volume of excavated rock affect the amount of released energy. These parameters are especially of high importance in mining engineering, where versatile excavation geometries are created. As for TBMs, the excavation is usually of a constant circular shape, and localizing the rockbursts

involves less complexity.

Another important factor that needs to be considered for a proper rockburst prediction is the construction method. The support system of regional type can highly affect the intensity and extension of rockburst. Regional and local support systems are topics that are relevant mostly to mining engineering. A regional support system refers mainly to different extraction techniques applied in deep mining regions. Developing pillars in a systematic way in the room and pillar mining method, longwall mining where caving leads to destressing in a largely extended region, and applying backfill to absorb part of the stored energy in the rock mass are all some examples of regional support. Local supports such as rockbolts, shotcrete, and segmental lining, on the other hand, are known to locally reduce the consequences of a rockburst incidence and are not able to control the magnitude of seismic events. As the point of focus here is on TBM excavated tunnels, only local support systems apply, which do not regionally affect the intensity of rockburst and are only regarded as the mitigation measures controlling the risks. The type of construction method also has a determinative effect on the severity of rockburst. Experiences have proved that in the same rock mass conditions, a mechanically excavated tunnel is more prone to strainbursts than a tunnel excavated with drilling and blasting method. This is mainly due to the fact that drilling and blasting create a fractured area in the surroundings of a tunnel, which increases the deformability of the rock mass in that region and leads to some extent of destressing. The mechanical excavation, however, performs quite differently without disturbing the rock mass [11].

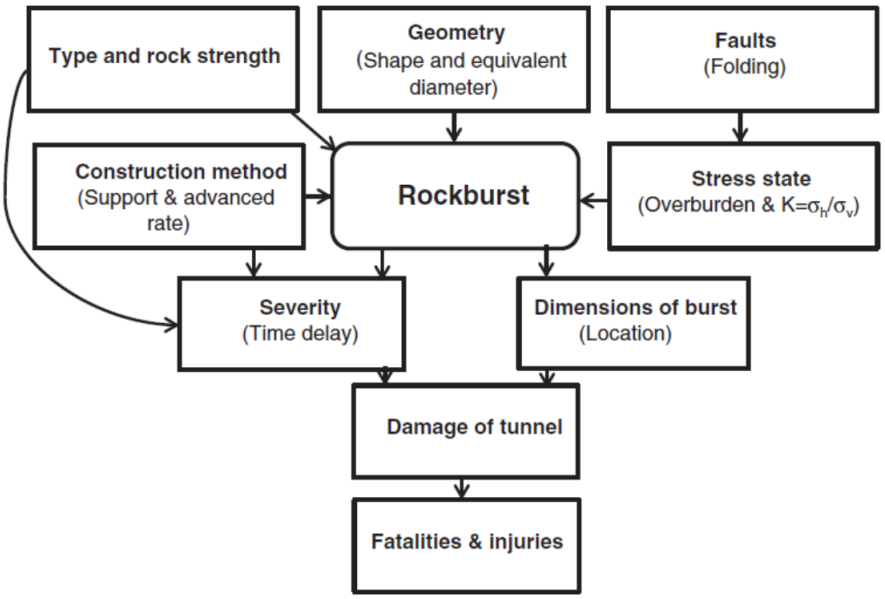

Figure 2.17: Influence diagram of rockburst adapted by Zhou et al. [24]

In this section, an attempt is made to bring a collection of rockburst prediction methods that can give us a quick and reliable evaluation of the rockburst risk. These methods have developed themselves over time. As sufficient information regarding the rock mass condition was not always available, any method could cover some parameters. These methods can be generally categorized based on three main criteria: the surrounding rock stress and rock strength, rock mass lithology and brittleness, and rockburst and energy [24].

2.4.1 The surrounding rock stress and rock strength

The extent of consequences as a result of rockburst depends highly on the strength characteristics of the rock, the amount of stresses, and the orientation of excavation with respect to the main principal stresses in the region. The in-situ stress state of the surrounding rock mass is proved to be closely relevant to the occurrence of a rockburst. In rockburst prediction methods it is either expressed in the form of the overburden stress or the major principle stress surrounding the rock mass (tangential stress) in specific locations of the excavation.

These criteria take into account both the mechanical properties of the rock and the in-situ stress conditions in the rock mass. In this section, a summary of some of the

most prominent methods is introduced in Table 2.1. One main motivation here is also to identify the suitable area of application for each method or where they are recommended to be applied.

Table 2.1: Summary of some rockburst prediction equations using stress state and the strength of rock

Equation	No rockburst	Light rockburst	Medium rockburst	Heavy rockburst	Serious rockburst
$\frac{(\sigma_\theta+\sigma_L)}{\sigma_c}$ [25][1]	≤0.3	0.3−0.5	0.5−0.8	> 0.8	
$\frac{\sigma_\alpha}{\sigma_1}$[26][2]	>10	10−5	5−2.5	<2.5	
$\frac{\sigma_L}{\sigma_1}$		>0.66	0.66−0.33	0.33−0.16	<0.16
Stress Coefficient $\frac{\sigma_\theta}{\sigma_c}$ [27][3]	≤0.2	0.2−0.3	0.3−0.55	>0.55	
Stress Coefficient $\frac{L_\alpha}{\sigma_\theta}$ [27][3]	>0.2	0.15−0.2	0.083−0.15	<0.083	
$\frac{\sigma_\theta}{\sigma_c}$ [28] [4]		0.34	0.42	0.56	≥0.7
$\frac{\sigma_1}{\sigma_c}$ [29] [5]	<0.069	0.069−0.180	0.180−0.400	>0.400	
Competency factor $C_g = \frac{I_\sigma.\sigma_c}{\sigma_\theta} = \frac{RM_i}{\sigma_\theta}$ [30][6]	>2.5	1.0−2.5	0.5−1.0	<0.5	
Normalized deviatoric stress $NDS = \frac{(\sigma_1-\sigma_3)}{\sigma_c}$ [31]	≤0.35	0.35−0.5	0.5−0.8	0.8−1.0	>1.0
$BSR = \frac{(\sigma_1-\sigma_3)}{\sigma_c}$ [23][7]		0.35−0.45	0.45−0.6	0.6−0.7	>0.7

[1] Where σ_L is the longitudinal stress near the outline that is parallel to the longitudinal axis of the excavation.

[2] Some methods such as Barton's criteria take the major principle stress in the rock mass into account for investigations. Their main shortcoming is that the criteria cannot be a good representative for anisotropic stress states. For instance, in the Scandinavian region where very great anisotropy between maximum and minimum principal stresses exists, such methods need to be adapted. For such cases, however, Barton et al. (1974) suggests a modification as follows [26]:
In the case of a highly anisotropic stress field: if $5< \frac{\sigma_1}{\sigma_3} < 10$, reduce σ_c and σ_t to $0.8\sigma_c$ and $0.8\sigma_t$; when $\frac{\sigma_1}{\sigma_3} > 10$, reduce σ_c and σ_t to $0.6\sigma_c$ and $0.6\sigma_t$ where: σ_t = tensile strength (point load), σ_1 and σ_3 = major and minor principal stresses.

[3] Russenes (1974) formulation fits relatively well with the Hoek and Brown (1980) method.

[4] The method by Hoek and Brown (1980) was investigated in various types of massive quartzite rocks of South Africa with a stress ratio of k=0.5 where maximum

tangential stress of the surrounding rock (σ_θ) is 1.4 times the overburden stress[28].
[5] This criterion was introduced based on the experiences of underground construction in China. The range of UCS for the rocks where rockbursting was reported is: 150-200 MPa (igneous rocks) or UCS>60-100 MPa (Sedimentary rocks). Besides, the type of stress-strain curve is important to notice. This criterion is also applying the major principle stress rather than the maximum tangential stress which is an obstacle towards generalizing them for various cases.
[6] Palmström introduced the competency factor expressed as the ratio between rock mass strength and the tangential stress around the excavation. RMi as the rock mass index factor describing the rock mass strength of a continuous rock mass was applied to investigate if the rock is overstressed. This criterion is also mainly based on the Hoek and Brown (1980) equation. Some recommendations for selecting a suitable support system were also derived from experiences in continuous and brittle rocks of Scandinavia (See Figure 2.18).

[7] σ_1 and σ_3 are the major and minor principals induced stresses, respectively. This method is mainly applied to investigate strain burst potential. There are successful experiences with the usage of the concept of stress-strength ratio in deep mining. In deep South African gold mines, the simple rule of thumb was to estimate the critical field stress (σ_{cr}) corresponding to 40% of uniaxial compressive strength of rock. According to those experiences, a typical gold mine was generally stable as long as the vertical stress acting on the tunnel was less than 0.4 σ_c. Later on, Wiseman (1979) extended this criterion to a design tool by considering the major and minor principal stresses and the tunnel support[32]. The following semi-empirical method was suggested:

$$RCF = \frac{(3\sigma_1 - \sigma_3)}{k_c.\sigma_c} \tag{2.3}$$

Where σ_1 and σ_3 denote the maximum and minimum principal stresses in the plane of the excavation cross-section and k_c is a strength reduction factor to include the effect of discontinuities on the rock mass strength. As for a highly discontinuous rock mass, experience has shown that for RCF < 0.7 good conditions with the minimum

required support system are expected. For $0.7 < \text{RCF} < 1.4$ average conditions prevail with typical tendon support in gold mines. When $\text{RCF} > 1.4$ the tunnel condition deteriorates rapidly [33].

The above method is a very valuable tool for studying the general stability of a tunnel but does not contain any more explanation for the rockburst risk and its extent.

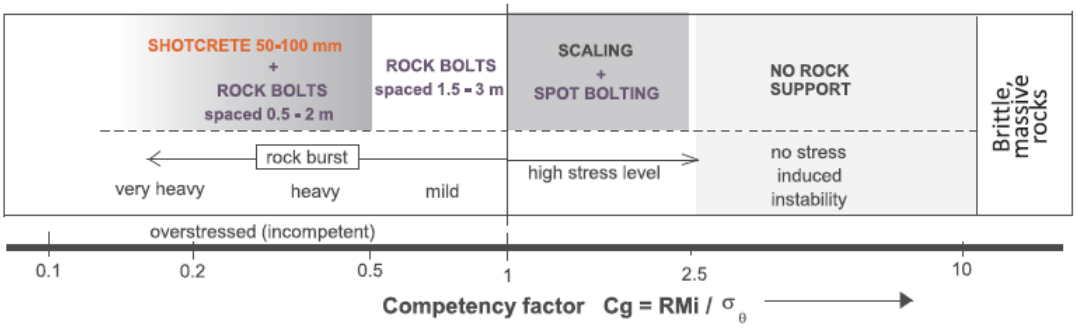

Figure 2.18: Some recommendations introduced by Palmström to select the suitable support system (adapted by Zhou et al. [24])

2.4.2 Rock mass lithology and brittleness

Another very important factor that has been the point of focus of many scholars is the rock mass lithology. Rockburst usually occurs in compact rocks which are highly capable of storing a significant amount of energy. It is mainly characterized by the uniaxial compressive strength and the tensile strength of the rock. Table 2.2 contains some of the well-known equations that can estimate the inherent potential of rock mass in accumulating a significant amount of energy. For more details regarding the formulations refer to [24]. Thus, they measure the physical-mechanical property of the rock. The versatility of the methods based on the brittleness stems from the lack of a universally accepted index to represent this property of rock. Such methods can give a suitable overview of the existing potentials, but they are not recommended to be the single way of determination and better be combined with other methods.

Table 2.2: Summary of some rockburst prediction equations using the brittleness concept [24]

Author/s	Equation	No rockburst	Light rockburst	Medium rockburst	Heavy rockburst
Tan et al. (1991) [34][1]	Brittleness index $K_u = \frac{U}{Ul}$	≤3.5	3.5−5.0	5.0−7.0	>7
Peng et al. (1996) [35]	Rock brittleness coefficient $B_3 = \frac{\sigma_c}{\sigma_t}$	>40	40−26.7	26.7−14.5	<14.5
Feng et al. (2000) [36][2]	$k = \frac{0.1(\sigma_c \times \epsilon_f)}{(\sigma_t \times \epsilon_b)}$	<3	3−5		≥5
Zhang et al. (2003) [37]	Brittleness index $K_u = \frac{U}{Ul}$	≤2	2−6	6−9	>9
Zhang et al. (2003) [38]	$B_3 = \frac{\sigma_c}{\sigma_t}$	<10		10−18	>18

[1] U is the total peak strength of before rock deformation and U_l is the permanent deformation before peak or plastic deformation.

[2] ϵ_f is the strain before peak and ϵ_b is the strain after peak.

2.4.3 Rockburst and energy

Since the introduction of energy theory, many researchers have tried to correlate the damage properties of the surrounding rock mass and the energy changes occurring in the environment giving rise to rockbursts. The main disadvantage of these methods is the more complex set of data required compared to other methods, however, they can provide a better knowledge of the extent of issues.

The main shortcoming of the other categories of methods (rock stress and rock lithology) is the negligence of the effect of loading stiffness (the surrounding rock stiffness), and that such methods do not distinguish between static and dynamic failure. It is proved that the strain energy storage property of rock and stress concentration of the environment directly influences the extent of rockburst [39]. Indeed, the stress state is unable to fully describe the energy release characteristics of the rock mass. However, as evaluation of the rock mass stiffness is not a regular procedure in underground excavations, such empirical criteria are sometimes the only prediction tools, which can bring an acceptable accuracy [23]. In other cases where the stress-strain behavior of the rock can be partially evaluated, the prediction methods based on energy release indices can be extremely helpful. Cook et al. (1966) described the important role of changes in energy during the mining of rock mass in deep under-

ground mines, and how the excess potential energy is linked to the rockburst damage [40]. A very basic parameter that can represent this concept is the Energy Release Rate (ERR). The change of the strain energy as a result of enlarging an excavation normalized by the area of the excavated region ($\frac{\Delta U_m}{\Delta A}$) is known as ERR. As for the fault slip types of rockburst, the other parameter of Excess Shear Stress (ESS) can be defined, which is the difference between the dynamic strength of a fault plane for initiation of rockburst and the prevailing shear stress before the slip occurs [24]. As suggested by Ryder (1988), ESS together with ERR can be efficiently applied to investigations of rockburst in South Africa [41]. In Table 2.3, some of the most common methods based on energy indices are listed.

Table 2.3: Summary of some rockburst prediction equations using the energy release concept

Author/s	Equation	No rockburst	Light rockburst	Medium rockburst	Heavy rockburst	Serious rockburst
Neyman et al. (1972) [42][1]	$W_{et} = \frac{E_e}{E_p}$	<2.0	2.0−3.5	3.5−5.0	>5.0	
Ryder (1988) [41][2]	$ESS = \lvert\tau\rvert - \sigma_n.tan\varphi_d$	<5	5−15	>15		
Cook et al. (1966) [40][3]	$ERR = \frac{\Phi_k}{\Phi_o}$	<3.5%	3.5−4.2%	4.2−4.7%	>4.7%	
Mitri et al. (1999) [43]	$BPI = \frac{ESR}{E}$	<0.25	0.25−0.5	0.5−0.75	0.75−100	>1
Wang and Park (2001) [39]	$PES = \frac{\sigma_c^2}{2E_s}$	≤50	50−100	100−150	150−200	>200
Zhou et al. (2017) [44]	$W_{et} = \frac{E_e}{E_p}$	<2.0	2.0−5.0	5.0−10.0	>10.0	

[1] E_e is the elastic energy stored in the rock through loading up to σ_A and unloading, and E_p is the dissipated energy in the creation of microfracture and plastic deformation of the rock in one cycle of loading.

[2] ESS is called the excess shear stress of a fault with the potential of triggering a seismic activity through exceeding the shear strength. σ_n is the normal stress at the slipping point (MPa), τ is the shear stress at the slippin gpoint and φ_d is the dynamic friction angle of the slipping fault.

[3] Φ_k is the rock kinetic energy with destructive ejection, and Φ_o is the maximum elastic strain energy.

Provided that the necessary input parameters with acceptable accuracy are present, numerical analysis can be applied as a strong tool for evaluating the energy indices.

As explained by Mitri et al. (1999), with a numerical analysis the maximum allowable mining step without seismically induced failure can be estimated [43]. A numerical simulation was conducted to examine the strainburst events by this approach [45]. The following formula is suggested for ERR:

$$ERR_{rm} = \frac{1}{2}\int \Delta\sigma_{ij}\Delta\varepsilon_{ij}dV \tag{2.4}$$

Where $\Delta\sigma_{ij}$ and $\Delta\varepsilon_{ij}$ represent the amount of incremental stress and strain changes as a result of a certain excavation step. The ERR concept was broadly applied in South Africa. Yet, Salamon (1993) states that the failure characteristics of the rock is not considered in this parameter. To address this issue, Mitri et al. (1999) introduced another index called Burst Potential Index (BPI) to evaluate the pillar burst or strainburst type of rockburst. According to this method, the proportion of Energy Storage Rate (ESR) (as the energy accumulated within the rock mass due to excavation) to the maximum strain energy (E_{max}) that the rock mass can withstand before failure is evaluated.

$$ESR = \int \sigma_{ij}\varepsilon_{ij}dV \tag{2.5}$$

Where σ_{ij} and ε_{ij} are the induced stresses and strains. The following formula is also suggested for E_{max} :

$$E_{max} = \int \left[\frac{1}{2}\sigma_p.\varepsilon_p - \int \sigma^0.d\varepsilon\right] dV \tag{2.6}$$

where σ_p and ε_p are the peak strength and strain of rock mass. By knowing the two indices, BPI can be estimated as:

$$BPI = (\frac{ESR}{E_{max}}).100\% \tag{2.7}$$

The effect of mining depth (stress state of rock), the stiffness and the strength of rock mass are all considered in one parameter (BPI), which is quite advantageous. According to Mitri (2007) it seems to be more conservative compared to stress methods and needs to be more studied to be validated for application in mine design.

Many conducted measurements prove that an elastic behavior dominates the regions where rockburst hazard is associated. This assumption is slightly conservative, as a fraction of energy is dissipated during fracturing [43]. According to Figure 2.19, the elastic strain energy accumulated in a unit volume of rock prior to the maximum strength can be estimated as follows [39]:

$$PES = \frac{\sigma_c^2}{2E_s} \tag{2.8}$$

σ_c is the uniaxial compressive strength

E_s is the unloading tangential modulus (MPa)

Among all the introduced methods of rockburst prediction, empirical criteria are the most common due to their simplicity and operability in underground mines, and, the ratio of σ_1 and σ_θ to σ_c are the most widely used parameters. However, the changes in lithology and structure along with the brittleness indices of the rock mass and its energy storage characteristics need to be integrated into the construction process to increase the accuracy of predictions.

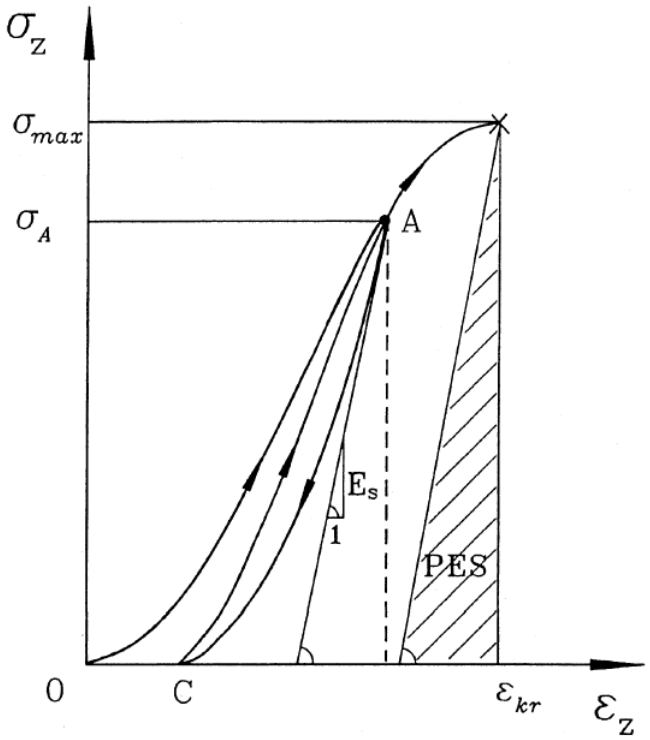

Figure 2.19: Schematic illustration of the calculation of potential elastic strain energy (PES)[39]

2.5 Squeezing hazard prediction methods

There are several factors affecting the occurrence of squeezing in an underground excavation: rock type, stress state, strength and deformability of the rock mass, water pressure, construction method, and the support system as well as the orientation of the geological structures [46]. Based on the importance of these parameters and their relevance in a rock engineering problem, they should be considered in risk assessment methods of squeezing. Several methods are available for evaluating the squeezing extent in underground excavations, including empirical, semi-analytical, analytical, and numerical modeling techniques. Empirical methods, such as those by Singh et al. (1992) [47] and Goel et al. (1995) [48], classify tunnel depth and rock mass quality to identify possible squeezing issues but do not calculate deformation or support pressure. Semi-empirical approaches, such as those by Aydan et al. (1993) [49] and Hoek and Marinos (2000) [50], provide straightforward tools for predicting deformation and squeezing potential in circular tunnels under hydrostatic stress. And lastly, analytical methods that use closed-form solutions involve mathematical equations that can provide insight into the behavior of soil and rock under pressure.

Empirical methods

The empirical methods primarily rely on rock mass classification systems. Two of these approximation methods are discussed in this section:

- Singh et al. (1992) approach

  In order to distinguish between squeezing and non-squeezing circumstances in tunnels, Singh et al. (1992) developed a method that involved sketching a demarcation line using information from 39 case histories [47]. The line is determined by an equation, using the rock mass quality Q and the overburden H:

  $$H = 350Q^{1/3} \tag{2.9}$$

  Squeezing conditions are shown by data points above the line, whereas non-squeezing situations are indicated by data points below the line (See Figure

2.20).

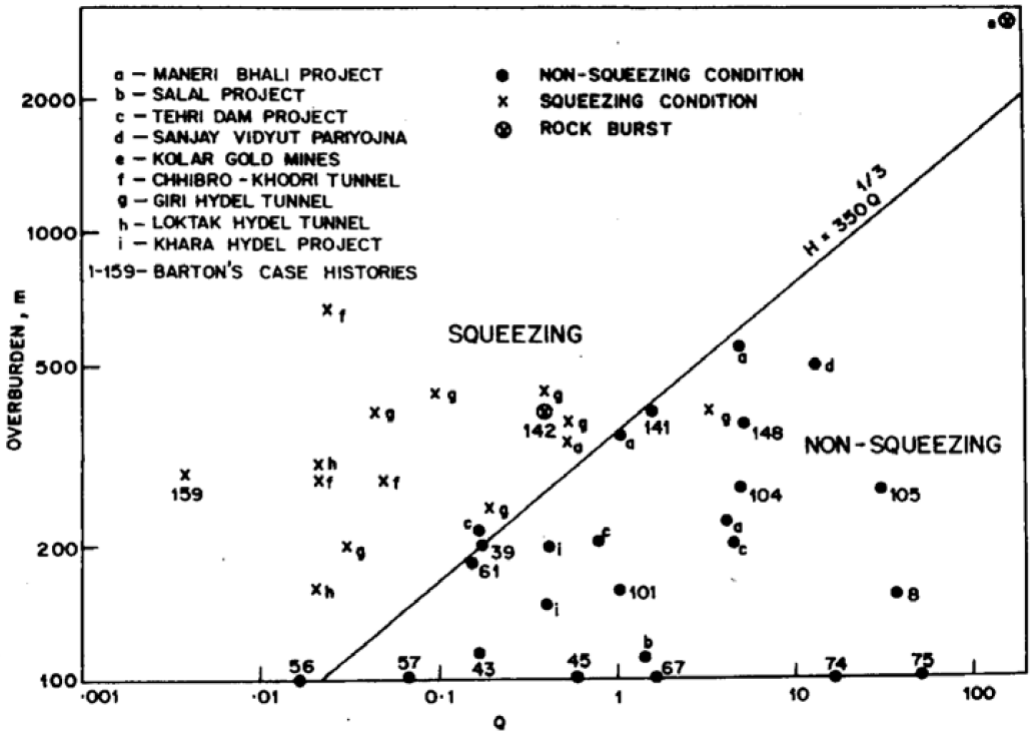

Figure 2.20: Singh et al. (1992) approach to assess the squeezing potential [47]

- Goel et al. (1994) approach

  Using the rock mass number N, which is the ratio of the stress-free Q to the specified roughness factor (SRF) set to 1, Goel et al. (1994) proposed an empirical method for evaluating rock mass behavior [51]. The tunnel depth (H), tunnel span or diameter (B), and rock mass number (N) were all taken into consideration. In the Himalayan region, where all 27 squeezing tunnel sections were examined, 38 of the 60 data sets came from 5 projects. The remaining 72 data sets were from sections that weren't squeezed. The relevant data was displayed by the authors on a log-log diagram between N and $HB^{0.1}$ (See Figure 2.21). Squeezing states are represented by data points above the line AB with the following equation:

$$H = (275N^{0.33})B^{-0.1} \tag{2.10}$$

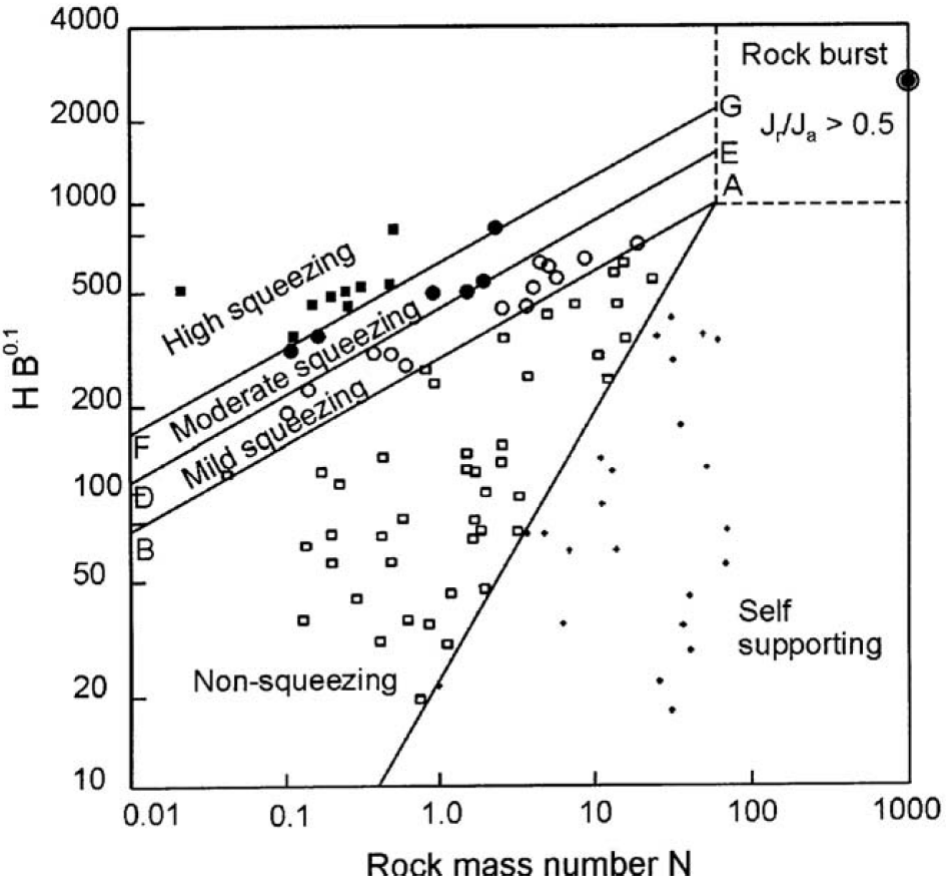

Figure 2.21: Goel et al. (1994) approach for assessing the squeezing potential[51]

The non-squeezing conditions are represented by data points below the line. The tunnel depth H should be significantly more than $(275\mathrm{N}^{0.33})\mathrm{B}^{-0.1}$ in squeezing conditions and much less than $(275\mathrm{N}^{0.33})\mathrm{B}^{-0.1}$ in non-squeezing conditions.

2.5.1 Semi-empirical methods

Semi-empirical techniques offer predictive indicators for squeezing situations to estimate the expected deformation around the tunnel [52]. Some of the most relevant approaches have been introduced by Hoek and Marinos (2000) [50] and Aydan et al. (1993) [49]. Hoek and Marinos (2000) as the most common method is briefly described in the next section.

Hoek and Marinos (2000) approach

Hoek and Marinos (2000) proposed plotting tunnel strain (ϵ) as a function of the ratio of rock mass strength to the in-situ stress (σ_{cm}/P_0) as a means of evaluating tunneling difficulties in squeezing scenarios (see Figure 2.22). While Hoek and Brown's criteria for estimating rock mass strength and deformation characteristics assume isotropic behavior, these criteria can be adapted for heavily fractured rock masses where the continuity of bedding surfaces has been disrupted, resulting in isotropic behavior.

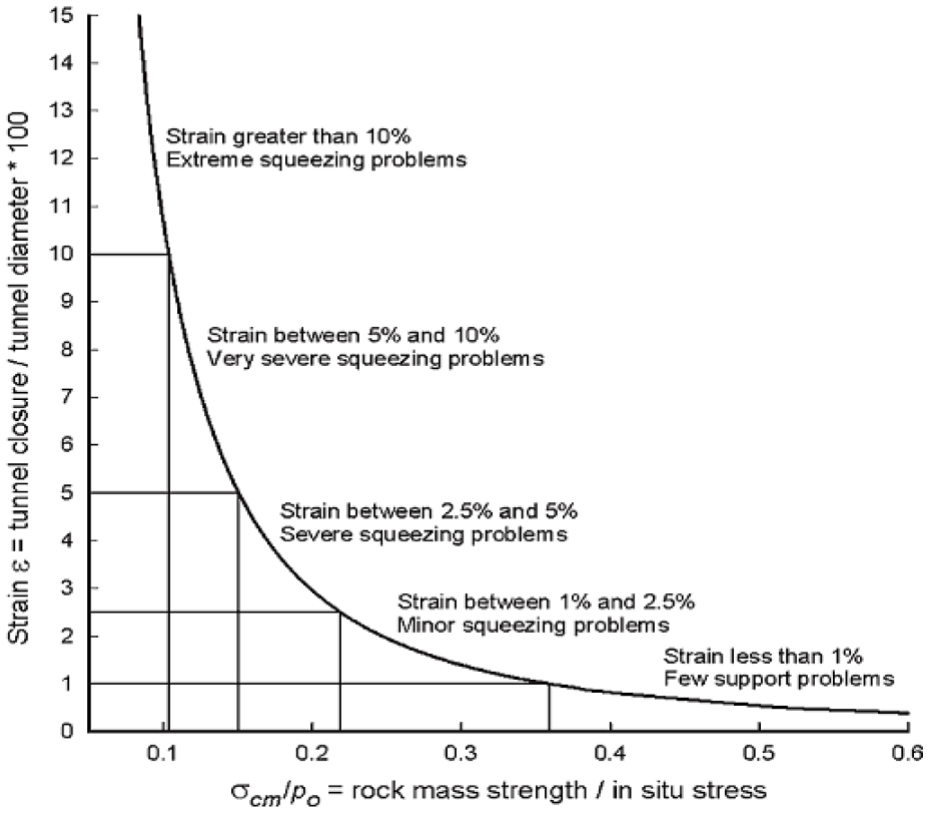

Figure 2.22: Hoek and Marinos (2000) approach for estimation of tunnel deformation [50]

The curve can be constructed using the following equation:

$$\varepsilon = \frac{\delta_i}{d_0} = \left[0.002 - 0.0025\frac{p_i}{p_0}\right]\left(\frac{\sigma_{cm}}{P_0}\right)^{\left(2.4\frac{p_i}{p_0}-2\right)} \tag{2.11}$$

where the support pressure (pi) starts at zero and increases until the strain reaches an acceptable level. P_0 is the in situ stress; δ_i, the tunnel sidewall deformation; and

d_o is the original tunnel diameter measured in meters.

2.5.2 Analytical methods

Analytical approaches contain closed-form solutions that simplify the rock mechanics problem based upon some idealized uniform in-situ stress regime and circular shape of the excavation. In order to analyze the stress-deformation behavior of the rock mass and support system (shield or segmental lining), the Convergence Confinement Method (CCM) is applied.

Convergence Confinement Method (CCM)

The convergence confinement method assumes a two-dimensional plane strain problem instead of the actual three-dimensional condition. Stress (σ) with the value of equation 2.12 is applied to the interior sides of a circular opening.

$$\sigma = (1 - \lambda)\sigma_0 \tag{2.12}$$

σ_0 is the ground in-situ stress, λ is called the confinement loss as the excavation moves further. As can be seen in Figure 2.23, following the loss of confinement, the deformation would rise. Therefore, a support system installed at the face would be more and more under pressure as the face advances and the confinement produced by the face effect decreases.

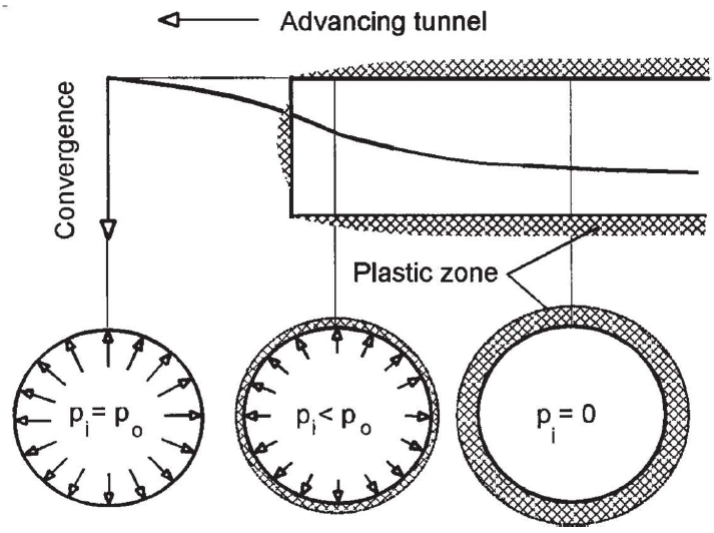

Figure 2.23: Change in confinement loss with the tunnel advance [53]

The CCM consists of three basic components: the Ground Reaction Curve (GRC), the Longitudinal Deformation Profile (LDP), as well as the Support Characteristic Curve (SCC) [54]. Figure 2.24 shows the combination of all these graphs and how they can be integrated to estimate the load acting on the support system. In the beginning stages of excavation, the tunnel face effect or the confinement loss is lower, which means less pressure carried by the installed support system. As the tunnel face moves away, more and more pressure will be absorbed by the support. According to the diagram, the displacement increases from zero to the maximum u_r^M during rock mass excavation. The critical pressure P_{cr} (point E) marks the point where internal stress P_i adjusts from its initial in situ condition of σ_o (point O) and elastic stress ends, making way for plastic stress. Eventually, the stress surrounding the rock mass excavation will decrease to zero (point M). It is critical to apply a confining pressure at a specific point (point D) on the excavation boundary to avoid excessive radial convergence, as determined by the support characteristic line. To ensure compatibility of deformations at the interface between the rock support and the rock wall, the radial displacement of the support should match that of the rock wall after installation.

The CCM is based on certain assumptions. It considers the tunnel as circular, which is always the case for a TBM excavated tunnel. Moreover, a hydrostatic stress

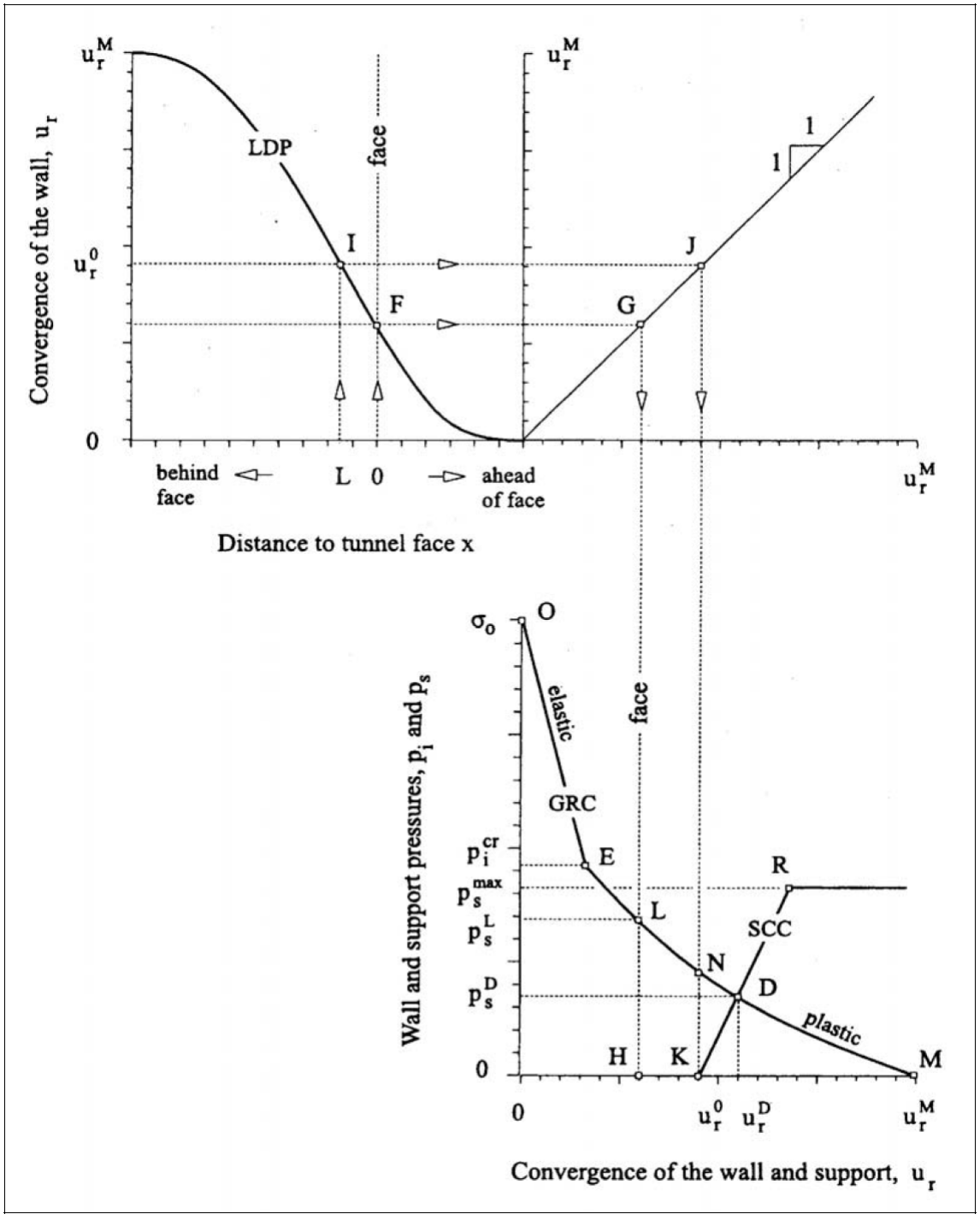

Figure 2.24: Representation of the Ground Reaction Curve, Longitudinal Deformation Profile, and the support characteristic curve
[54]

state is assumed for the region. This assumption however brings a limitation, as in most instances the in-situ stress is not hydrostatic. This is especially critical in shallow conditions (See Figure 2.25). However, as the tunnel gets deeper, which is the subject of this research, the horizontal-to-vertical ratio (k) becomes closer to one. Application of CCM should especially be avoided when k<0.6, otherwise, the average of the vertical and horizontal stresses can be used as σ_0 [46].

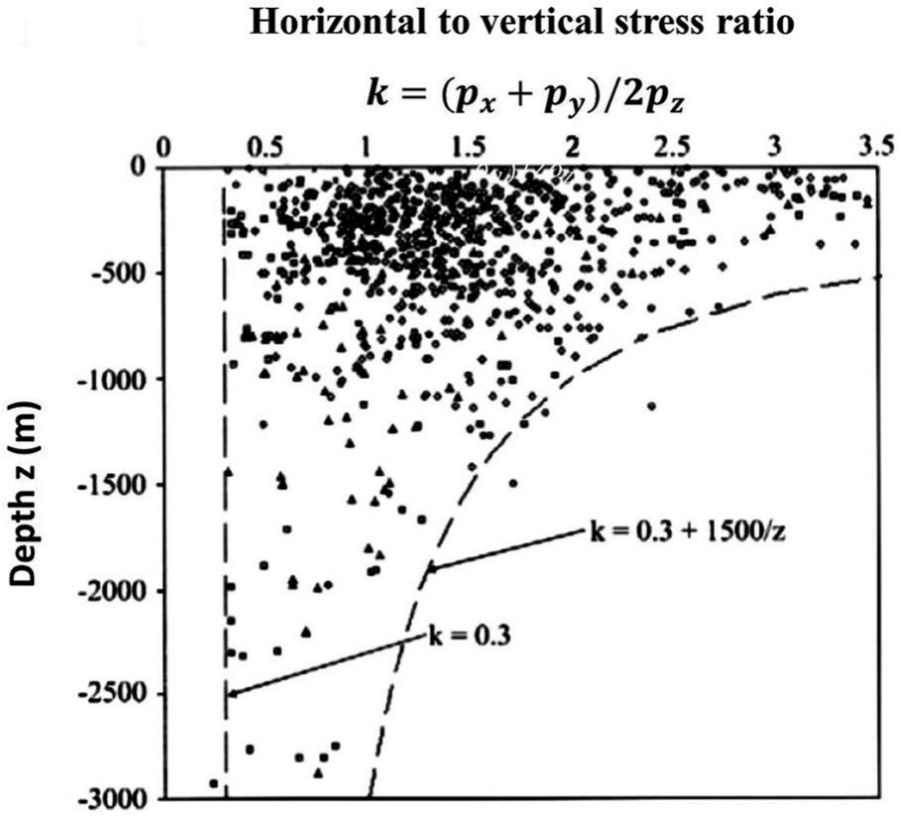

Figure 2.25: Variation of horizontal to vertical stress ratio as a function of the depth [55]

Different solution methods have been suggested for analyzing the rock support interaction with CCM by calculation of the plastic zone extension and the derivation of the Ground Reaction Curve. For instance, Duncan Fama (1993) developed a closed-form solution that applies the Mohr-Coloumb as the failure criteria and is able to calculate small strain deformations with dilation [56]. As for the Hoek-Brown criterion, Carranza-Torres (2004) introduced formulations that can apply this criterion for similar small strain conditions [57]. Another approximation method was developed by Vrakas and Anagnostou (2014) which uses the Mohr-Coloumb

criterion and can be applied also for large strain problems with dilation [58]. In this investigation, the two most commonly applied closed-form solutions for small strains (Duncan Fama (1993) and Carranza Torres (2004)) are introduced and subsequently applied in the system.

Duncan Fama solution (1993)-Mohr Coloumb criterion

The exact solution for determining the plastic zone extension and the radial convergence of a circular opening in a Mohr-Coloumb perfectly plastic material is introduced in this section. Figure 2.26 depicts an infinitely long circular tunnel of radius a with an internal pressure p_i as well as in-situ stresses of σ_0 assuming a plain strain condition. The tunnel wall converges to u_r^a due to the internal pressure p_i being reduced below its starting value σ_0. A failure zone with a radius of R_{pl} forms around the tunnel when the internal pressure p_i drops below the critical value p_i^{cr}.

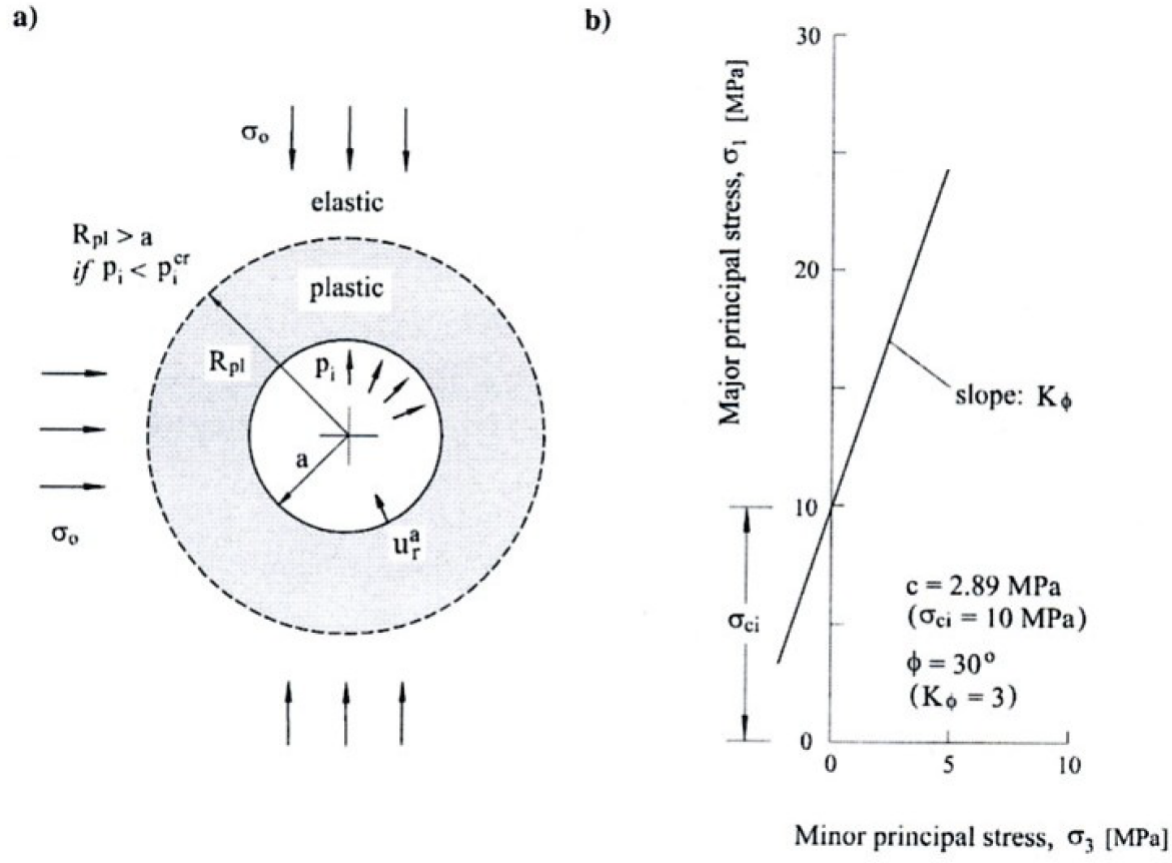

Figure 2.26: The mechanical behaviour of a circular shaped tunnel in a Mohr-Coloumb elasto plastic material for a uniform in-situ stress field [59]

The elastic and plastic behavior of the rock is given by Young's Moulus(E), Cohesion(c), Friction angle(φ), and the dilation angle(ψ). The Shear Modulus of the rock is estimated with the following equation:

$$G = \frac{E}{2(1+\nu)} \tag{2.13}$$

The internal friction angle, cohesiveness, and dilation angle all play a role in the material's plastic behavior. The major and minor principal stresses, denoted by σ_1 and σ_3, are correlated according to the Mohr-Coulomb failure criterion. This relationship can be stated as follows:

$$\sigma_1 = K_\varphi \sigma_3 + \sigma_{ci} \tag{2.14}$$

Based on the internal friction angle, the passive reaction coefficient K_φ is computed.

$$K_\varphi = \frac{1+\sin\varphi}{1-\sin\varphi} \tag{2.15}$$

As shown in Figure 2.26, the Mohr-Coulomb failure criterion uses the intercept of the linear envelope with the vertical axis to represent the unconfined compression strength (σ_{ci}), and the slope of the linear failure envelope, K_φ. The material's volumetric response is affected by the dilation angle, which can either be non-associated or associated (equal to the internal friction angle). In the case of non-associated or associated dilation angles, there will be no volumetric change or expansion during plastic deformation, respectively. The elastoplastic formulation provided here uses the parameter K_ψ, which is similar to K_φ but depends on the dilation angle.

$$K_\psi = \frac{1+\sin\psi}{1-\sin\psi} \tag{2.16}$$

The critical stress level for failure initiation, p_i^{cr}, can be computed using Duncan Fama's analytical method, assuming no plastic volume change in the rock mass, as

shown below:

$$p_i^{cr} = \frac{2\sigma_0 - \sigma_{cm}}{K_\varphi + 1} \tag{2.17}$$

The compressive strength of the rock mass is shown here by the symbol σ_{cm}. The radius of the plastic zone R_{pl} and the inward deformation of the tunnel wall u_r^a can be calculated as follows when the support pressure p_i is smaller than the critical pressure p_i^{cr}:

$$\frac{R_{pl}}{a} = \left[\frac{2(\sigma_0(K_\varphi - 1) + \sigma_{cm})}{(K_\varphi + 1)((K_\varphi - 1)p_i + \sigma_{cm})}\right]^{1/(K_\varphi - 1)} \tag{2.18}$$

$$\frac{u_r^a}{a} = \frac{(1+\upsilon)}{E}\left[2(1-\nu)(\sigma_0 - p_i^{cr})(\frac{R_{pl}}{a})^2 - (1-2\nu)(\sigma_0 - p_i)\right] \tag{2.19}$$

E is a representation of the rock mass's deformation modulus.

Carranza-Torres and Fairhurst (2000)-Hoek-Brown criteria

A solution was put out by Carranza-Torres and Fairhurst (2000) on the basis of the generalized Hoek-Brown failure criteria [54]. As shown in Figure 2.27, the solution takes into account a cylindrical tunnel section with radius R that is subjected to uniform far-field stress σ_o and interior pressure p_i. The unconfined compressive strength of intact rock (σ_{ci}), the intact rock parameter (m_i), and the rock mass parameters (m_b and s) are assumed to determine the behavior of the rock mass under the Hoek-Brown failure criterion specified by Equation 2.20.

$$\sigma_1 = \sigma_3 + \sigma_{ci}\left(m_b\frac{\sigma_3}{\sigma_{ci}} + s\right)^a \tag{2.20}$$

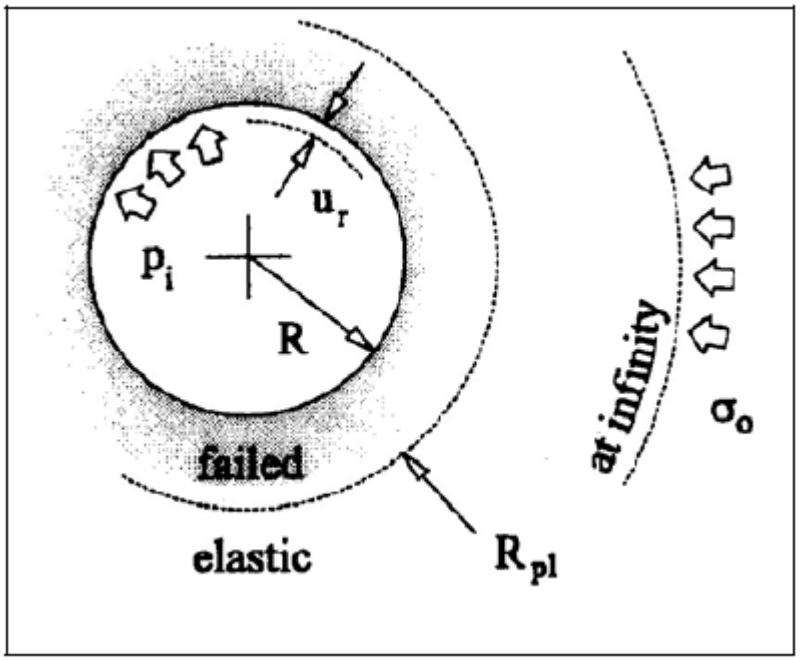

Figure 2.27: The cross-sectional shape of a circular tunnel with a radius R [54]

Internal pressure and far-field stress control the mechanical reaction of rock mass. Scaling these parameters involves converting internal pressure p_i and far-field stress σ_o into scaled versions P_i and S_0, respectively (See equations 2.21 and 2.22).

$$P_i = \frac{p_i}{m_b \sigma_{ci}} + \frac{s}{m_b^2} \tag{2.21}$$

$$S_0 = \frac{\sigma_0}{m_b \sigma_{ci}} + \frac{s}{m_b^2} \tag{2.22}$$

Rock mass exhibits a change in behavior from elastic to plastic at the critical internal pressure p_i, denoted by point E in the GRC of Figure 2.24. When p_i^{cr} is greater than p_i, a plastic area with a radius of R_{pl} forms around the tunnel while the rock remains elastic when p_i^{cr} is smaller than p_i (See Figure 2.27). Equation 2.23 provides the scaled critical (internal) pressure where the elastic limit is reached.

$$p_i^{cr} = \frac{1}{16}\left[1 - \sqrt{1 + 16 S_0}\right]^2 \tag{2.23}$$

The inverse of the equation can be used to determine the real critical pressure

(Equation 2.24).

$$p_i^{cr} = \left[P_i^{cr} - \frac{s}{m_b^2} \right] m_b \sigma_{ci} \tag{2.24}$$

When $p_i \geq p_i^{cr}$, the relationship between radial displacements u_r^{el} and internal pressure p_i in the elastic part of the GRC (i.e., segment OE in Figure 2.24) can be expressed by the following equation, where G_{rm} is the shear modulus of the rock mass.

$$u_r^{el} = \frac{\sigma_0 - p_i}{2G_{rm}} R \tag{2.25}$$

In case of $p_i < p_i^{cr}$, the following equation would give us the plastic zone extension.

$$R_{pl} = R. \exp\left[2(\sqrt{P_i^{cr}} - \sqrt{P_i}) \right] \tag{2.26}$$

To determine the plastic portion of the GRC (EM segment shown in Figure 2.24), a flow rule for the material must be established. This rule specifies the correlation between the strains that result in distortion and those that cause volumetric changes as the material undergoes plastic deformation. A linear flow rule is generally assumed in underground excavation practice, with the magnitude of volumetric change represented by the dilation angle ψ. If $\psi = 0$, no volume change occurs during plastic deformation, while $\psi > 0$ results in an increase in volume. In the present solution, the flow rule is defined by the dilation coefficient K_ψ, calculated from the dilation angle ψ by the equation $K_\psi = (1 + \sin\psi)/(1 - \sin\psi)$. For instance, K_ψ equals 1 when $\psi = 0$, and K_ψ is 3 when $\psi = 30$. Once the dilation coefficient K_ψ is determined, the plastic part of the GRC (EM segment in Figure 2.24) is represented by equation 2.27.

$$\begin{aligned}\frac{u_r^{pl}}{R}\frac{2G_{rm}}{\sigma_0 - p_i^{cr}} &= \frac{K_\psi - 1}{K_\psi + 1} + \frac{2}{K_\psi + 1}\left(\frac{R_{pl}}{R}\right)^{K_\psi + 1} \\ &+ \frac{1 - 2\nu}{4(S_0 - P_i^{cr})}\left[\ln\left(\frac{R_{pl}}{R}\right)\right]^2 \\ &- \left[\frac{1 - 2\nu}{K_\psi + 1}\frac{\sqrt{P_i^{cr}}}{S_0 - P_i^{cr}} + \frac{1 - \nu}{2}\frac{K_\psi - 1}{(K_\psi + 1)^2}\frac{1}{S_0 - P_i^{cr}}\right] \\ &\times \left[(K_\psi + 1)\ln\left(\frac{R_{pl}}{R}\right) - \left(\frac{R_{pl}}{R}\right)^{K_\psi - 1} + 1\right].\end{aligned} \tag{2.27}$$

where ν represents the Poisson's ratio for the rock mass. Assuming no plastic volume change in the rock mass may be more appropriate in some circumstances. For non-dilating rock masses with a coefficient $K_\psi = 1$, equation 2.27 reduces to equation 2.28.

$$\begin{aligned}\frac{u_r^{pl}}{R}\frac{2G_{rm}}{\sigma_0 - p_i^{cr}} &= \left[\frac{1 - 2\nu}{2}\frac{\sqrt{P_i^c r}}{S_0 - P_i^{cr}} + 1\right]\left(\frac{R_{pl}}{R}\right)^2 \\ &+ \frac{1 - 2\nu}{4(S_0 - P_i^{cr})}\left[\ln\left(\frac{R_{pl}}{R}\right)\right]^2 - \frac{1 - 2\nu}{2}\frac{\sqrt{P_i^{cr}}}{S_0 - P_i^{cr}}\left[2\ln\left(\frac{R_{pl}}{R}\right) + 1\right]\end{aligned} \tag{2.28}$$

Support Characteristic curve

One can use the relationship between the applied stress (p_s) and the closure that results (u_r) for a unit length segment of support facing the tunnel to produce the Support Characteristic Curve (SCC), as shown in Figure 2.24. According to the equation $p_s = K_s u_r$, the elastic segment of the SCC, represented by segment KR in Figure 2.24, can be computed. This relationship is based on the elastic stiffness (K_s) of the support. The stiffness K_s is expressed in terms of pressure per length, i.e., MPa/m. The maximum pressure (p_s^{max}) that the support can withstand before collapsing determines the plastic section of the SCC, commencing at point R and extending horizontally in Figure 2.24. For instance, the maximum pressure and the stiffness of concrete lining can be calculated by equations 2.29 and 2.30 [55].

$$p_s^{max} = \frac{\sigma_{cc}}{2}\left[1 - \frac{(R - t_c)^2}{R^2}\right] \tag{2.29}$$

$$K_s = \frac{E_c}{(1-\nu_c)R} \frac{R^2 - (R-t_c)^2}{(1-2\nu_c)R^2 + (R-t_c)^2} \tag{2.30}$$

where E_c is the Young's Modulus of the concrete, ν_c is the Poisson ratio of the concrete, R is the external radius of the concrete or the radius of the tunnel, t_c is the thickness of the concrete, and σ_{cc} is the compressive strength of the concrete (See Figure 2.28).

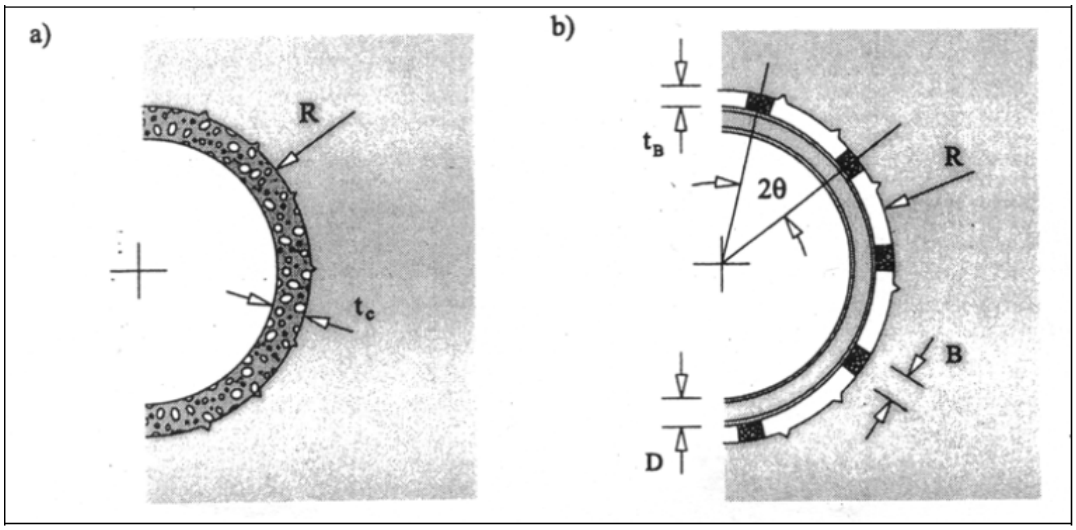

Figure 2.28: Sections of two types of tunnel support systems: (a) shotcrete or concrete rings, and (b) steel sets modified from Brady and Brown (2006) [55]

2.6 Mitigating measures against the consequences of rockburst and squeezing in TBM tunneling

To effectively manage risks in a TBM tunneling project, it is imperative to take measures that can reduce the intensity of potential consequences to an acceptable extent. This section presents a summary of essential measures derived from the literature, specifically focusing on addressing the consequences of rockburst and squeezing in a TBM tunneling project [7].

2.6.1 Mitigating measures against rockburst

The most common measures for reducing the impact of rockbursts in a TBM tunneling project fall into two main categories: efficient support system installation and

proactive measures to avoid exposure of workers to seismic events. Although these measures cannot fully control the consequences, implementing them can reduce the potential consequences and enhance the overall safety of the tunneling operation.

Efficient support system installation

The stability issues for high-stress environments in hard rock masses should be analyzed in two categories of static and dynamic events. In static stress situations, the main focus is on controlling the fracturing around the excavation and preventing hazards related to progressive buckling of the fractured zone. Stiff boundary supports in static average to relatively high-stress situations can be applied. The stiff boundary support could be a layer of shotcrete or a segmental lining system. However, the application of stiff support systems should be done with caution in dynamic stress environments. The fibre-reinforced shotcrete is reported as effective in mild seismic loading situations. As for the high dynamic stress states, the functionality of stiff support systems is questionable. Thus, the load-deformation behavior of support is of crucial importance. The emphasis of support for dynamic events should be on energy absorption rather than on support strength. Inflatable tubular support tendons as well as more energy-absorbing support tendons such as cone bolts, D-bolts are well suited for such states. However, they should be supplemented by boundary support [17].

According to Wagner (2020), different damage mechanisms could take place as a result of seismicity: rock bulking as a result of fracturing, strain bursting, rock ejection, and rockfalls triggered by seismic vibrations [17]. Each of these requires specific characteristics by the support system to be controlled as shown in Figure 2.29. For instance, in the case of rock bulking, high deformability and high strength are necessary for the reinforcement tendons, and high deformability, flexibility, and high tensile strength are required for the retaining support. As for the case of rock ejection due to seismic energy transfer, in addition to high deformability and strength, reinforcement tendons should possess the capacity to absorb significant amounts of energy.

When using Gripper TBMs, there is a higher flexibility in choosing the aforementioned support system. In contrast, the segmental lining is regarded as a stiff support system. The backfilling operation of the annular gap between the segmental lining and the ground needs to be well conducted to stabilize the segmental lining ring as early as possible. This involves selecting the appropriate design of backfill injection methods and conducting on-site testing and calibration to optimize the material's deformability and injection locations. By effectively stabilizing the segmental lining, the risk of rockburst-induced damage can be reduced.

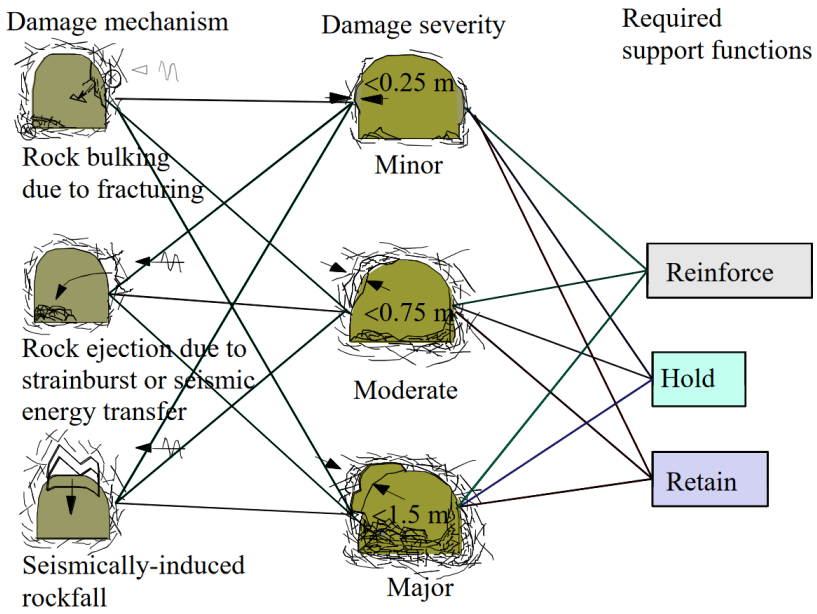

Figure 2.29: Mechanism of Rockburst Damage, Damage severity, and the functions required by the support system [60]

Reducing the exposure of personnel to rockburst events

Ensuring worker safety is of paramount importance when addressing the risks associated with rockbursts. It is necessary to avoid the presence of workers near risky areas, especially new unsupported surfaces in Gripper TBMs, during the initial hours following the excavation. The same applies to entering the cutterhed after excavation. These safety measures allow time for rock-bursting inducing stresses to equilibrate, reducing the risk of injury to personnel.

Another related measure can be implementing alternative technologies, such as face inspection cameras and wear-cutting tool inspectors to avoid the presence of workers

in the cutterhead area, where strainbursts are likely to occur. These technologies provide real-time monitoring and assessment of the tunnel face condition remotely. Additionally, implementing McNally system in Gripper TBMs as an innovative technology provides full protection from the early stages, reducing the risk of injuries and damages. This measure will be explained in detail in the following section.

The development of Mc Nally system in grounds with rockburst risk

A new system invented by C&M McNally Engineering from Toronto, Canada, offers a solution for safeguarding personnel and TBM equipment against seismic events in rock formations prone to bursting [61]. This invention involves equipping the TBM with a shield consisted of a sequence of hollow rectangular tubes arranged in an arc. These tubes are interconnected and installed on a framework of curved beams, running longitudinally along the tunnel axis. The tubes extend from a position just behind the TBM's cutterhead to the point where the tunnel roof support is completed. The attachment of the framework to the TBM enables the shield's curved upper surface, formed by the interconnected tubes, to be firmly held against the tunnel roof. Within specific limits, the height of the shield can be adjusted accordingly. Prior to the TBM's stroke, hollow tubes are preloaded with timber or steel members. The protruding ends of these slats allow them to be securely bolted to the tunnel roof using steel straps. As the TBM progresses, the slats are extracted from the pockets and continuously bolted to the roof using the next straps. This ensures effective support against loose and unstable rocks. Based on the ground conditions, this system can be applied in the roof area and the side walls of the tunnel. Figure 2.30 Shows an overview of the system applied in the Alto Maipo Hydroelectric project (with tunnels of up to 1.5 km depth). As depicted in Figure 2.30, instead of the conventional finger shield, a roof shield was developed to integrate the Robbins-McNally slat-type ground support system. The shield comprised 35 roof fingers positioned to provide protection to the workers from falling rocks within the TBM vicinity.

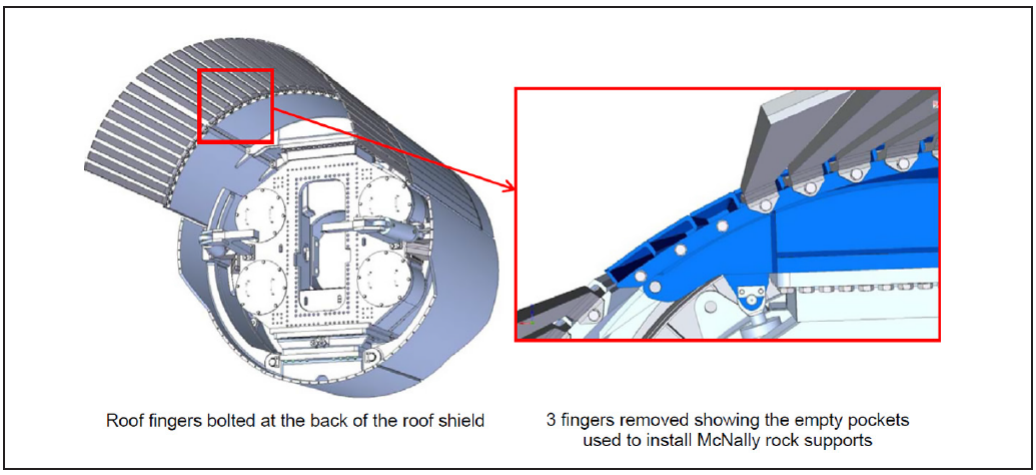

Figure 2.30: Finger shield removal and McNally system installation [62]

The McNally system is compatible with a range of rock support options, including prefabricated rebar, wood/metal slats, and wire mesh, combined with rock straps and rock bolts [63]. A very successful application of the above system was in Peru's Olmos Trans-Andean Tunnel. The tunnel is the second deepest civil work tunnel in the world after AlpTransit, below 2 km of Andean rock. The encountered rock types varied from quartz porphyry to andesite, dacite, and weak rocks. A Robbins open TBM was later in 2006 applied to excavate the remaining 12.8 km of the tunnel. After running into severe rock bursting and squeezing issues, a new plan was devised that involved modifications to the TBM. Specifically, the roof shield fingers, which were under damage from falling rocks and rock bursting, were replaced with the McNally Support System utilizing steel slats. With the implementation of this system, safe progress was achieved even under extreme rock bursting conditions. The TBM successfully completed the breakthrough in December 2011, despite experiencing approximately 16,000 recorded rock bursting events.

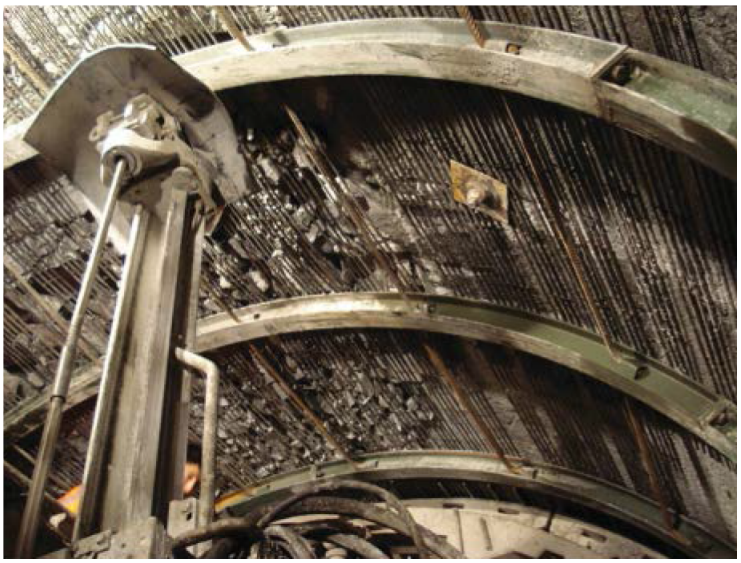

Figure 2.31: Detailed view of the Mc Nally system [63]

2.6.2 Mitigating measures against squeezing

This section introduces the mitigating measures aimed at addressing the three primary consequences associated with squeezing in TBM tunneling: shield jamming, support damage, and difficulties in gripper bracing.

Measures against shield jamming

- Providing sufficient overcutting: A high enough excavation diameter yielding a large shield gap behind the shield has proved to alleviate squeezing risks by providing space for ground movement and reducing stress concentrations (See Figure 2.32).

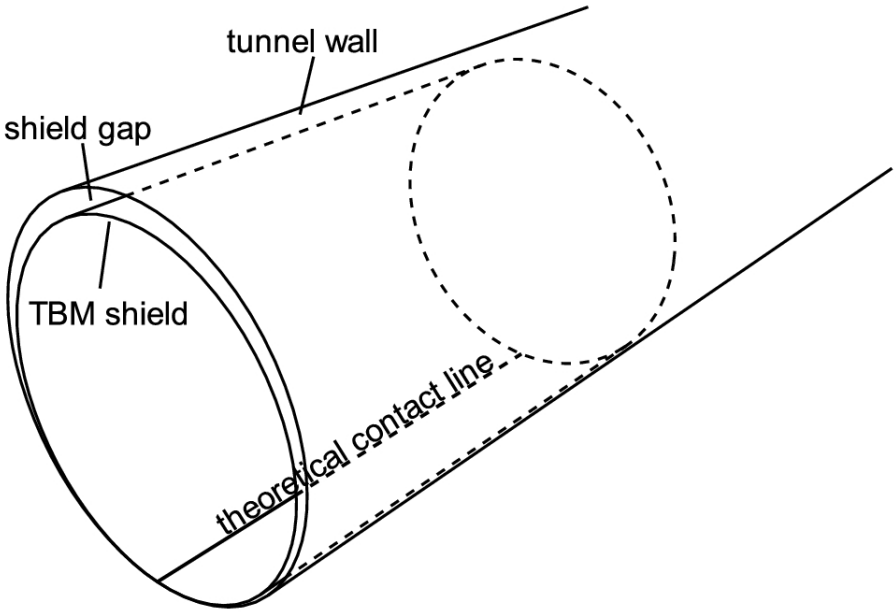

Figure 2.32: Overcutting of the tunnel diameter to provide space for ground deformation [64]

- Shield lubrication is another measure that can reduce the likelihood of jamming by lowering the existing friction between the ground and the shield. Figure 2.33 depicts a system specifically designed for the injection of bentonite, aimed at lubricating the shield of a TBM.

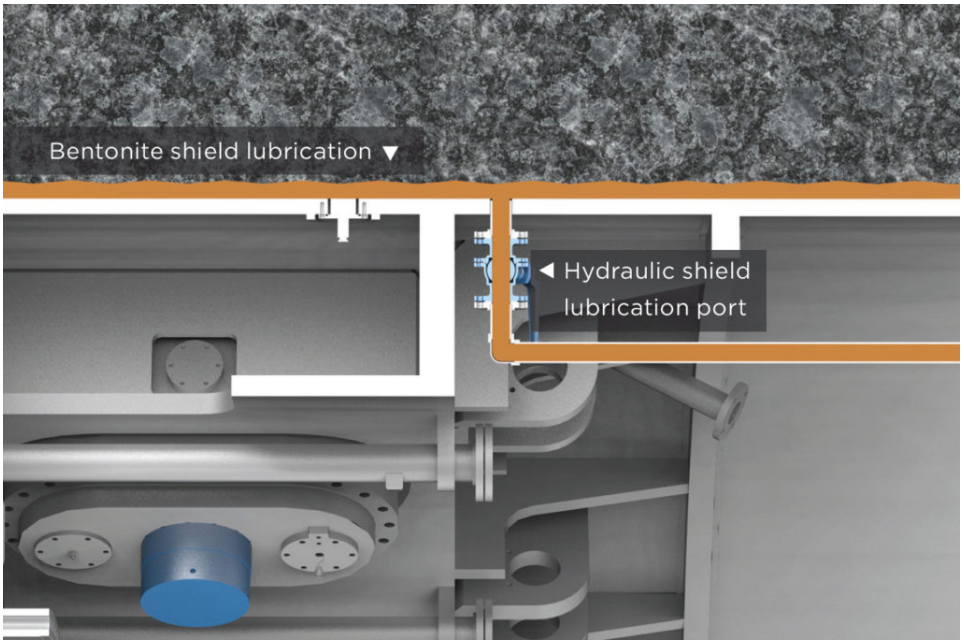

Figure 2.33: The external shield lubrication system to alleviate the jamming risk [65]

- Choosing the appropriate shield geometry is a crucial decision when choosing a

TBM for a project. The shield length plays a significant role, as a shorter shield reduces the potential contact between the ground and the shield, consequently requiring less frictional force to overcome.

- Due to the time-dependent deformations in squeezing grounds, implementing a high advance rate of excavation is another measure to address the jamming risk. However, this may require modifications to the project's shift system, as continuous operation necessitates adequate staffing and increased logistical support.

- Proper anticipation of potential jamming hazards can be achieved through systematic sub-horizontal exploration drilling ahead of the TBM. By gathering geological information and identifying unstable zones, steps can be taken to mitigate the risks associated with squeezing and buckling.

Measures against support damage

- For a gripper TBM, utilizing yielding support systems, such as sliding ribs and openings in shotcrete with compressive elements, is effective in accommodating ground movements. Such flexible support systems allow for controlled deformation and help to avoid subsequent support damage. Figure 2.34 illustrates an example of the application of steel sets with sliding joints for enabling controlled deformation in the Yacambú-Quibor tunnel in Venezuela [66].

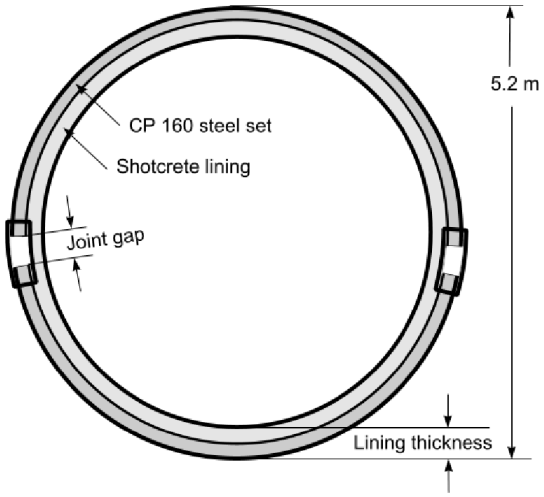

Figure 2.34: Yielding Support Design Details in the Yacambú-Quibor Tunnel [66]

- For Shielded TBMs, using high-strength concrete and a high steel ratio in the segmental lining construction enhances its structural integrity against high squeezing deformations. These measures ensure a high load-bearing capacity for the lining, reducing the risk of support damage.

- In extreme squeezing conditions, utilizing a deformable annular backfill can be beneficial. This measure allows the lining to adjust to ground movements and possibly reduce the support damage.

- An essential aspect to consider in shielded TBMs is the significant thrust forces exerted on the segmental lining when passing through squeezing zones. It is crucial to incorporate the anticipated thrust force into the lining design to guarantee the stability and integrity of the tunnel structure.

- The implementation of the double lining concept can be regarded as a final measure to address the limitations of the existing lining in ensuring tunnel stability. By introducing an additional layer of support, the load is distributed, thereby enhancing the overall stability of the tunnel structure. This measure must be avoided by other mitigating measures due to its low cost and time efficiency.

Measures against gripper bracing difficulties

Gripper bracing difficulties arise in squeezing grounds when the ground is excessively soft, leading to inadequate thrust forces from the gripper shoes, hindering the excavation and advancement of the machine. To mitigate such issues, it is vital to equip the machine with appropriately sized gripper shoes. Alternatively, one effective measure involves installing timbers behind the gripper shoes to increase the pressurizing area. This implementation helps evenly distribute the forces exerted by the gripper shoes, thereby minimizing the risk of bracing-related issues. However, it can interrupt the excavation operation and reduce the advance rate of the machine.

In conclusion, the implementation of the measures introduced above is of utmost importance for the successful execution of the project and the safety of personnel and equipment. Thoroughly considering their potential effects on costs and advancement rates is essential to achieve optimal outcomes. By prioritizing these measures, project teams can mitigate risks effectively and maintain a secure working environment, ultimately leading to successful project completion.

Chapter 3

Methodology

In this chapter, we will explore the process of defining a representative quantity for risk evaluation, building upon the literature review and introduction of prediction tools. By analyzing the information, we aim to establish a logical framework for selecting a suitable index to capture the level of risk in a TBM tunneling project. The following requirements are defined for the framework of this risk assessment index:

- The quantity should be able to integrate the extent of the main geological risks (Rockburst and Squeezing) and enable a decision-making procedure.
- The index is intended to be cumulative and consider the whole length of the excavation.
- Moreover, the system should have the capability of considering the mitigating measures for minimizing the risks.

To fulfill the requirements of this risk assessment system, several relevant prediction tools are tested by the case studies, and employed accordingly in the system. The chosen quantification method for this project is mainly the Monte Carlo simulation approach, which is regarded as the most common probabilistic risk assessment method.

According to the analyses made in Chapter 2, the main consequences to be considered for squeezing and rockburst for different types of TBMs are listed in Tables 3.1

and 3.2 , respectively. It should be noted that the likelihood of shield jamming as a result of a rockburst is low unless an extremely severe rockburst occurs.

Table 3.1: The classification of Squeezing consequences for different types of TBMs

	Injuries to workers	Damage to equipment	Jamming of the shield	Damage to support	Gripper bracing difficulties
Open TBM	*	*	*	*	*
Single Shield TBM	*	*	*	*	-
Double shield TBM	*	*	*	*	*

Table 3.2: The classification of Rockburst consequences for different types of TBMs

	Injuries to workers	Damage to equipment	Damage to support	Gripper bracing difficulties
Open TBM	*	*	*	*
Single Shield TBM	*	*	*	-
Double shield TBM	*	*	*	*

3.1 The quantification procedure for the system

An unexpected event has the potential to cause a range of accidents, with both economic and non-economic consequences. These consequences can often be expressed in monetary terms or described qualitatively to reflect their impact. As previously mentioned, the ideal system for this research should be capable of integrating the two primary risk categories of rockburst and squeezing. To achieve this, a general formulation is adopted, where each consequence is quantified separately for a specific chainage of the tunnel (L_i). The degree of consequences resulting from rockburst and squeezing are quantified using Table 3.3, which assigns a number from

one to five to represent the severity of each consequence, with one indicating an insignificant outcome and five denoting a catastrophic one. These consequences are classified as squeezing risk (SR_{ij}) and rockburst risk (RBR_{ij}) for each formation i and risk category j. To better capture the criticality of each risk in relation to TBM selection, a significance factor (W) is assigned to each consequence. In this research, the author's general knowledge is supplemented with a consultation to provide a rough approximation of the significance factors (See Table 3.4). Furthermore, each consequence is quantified individually for a specific section of the tunnel length (L_i). Figure 3.1 illustrates the longitudinal cross-section of a tunnel with different ground classes and lengths being excavated by a TBM. The total rock mechanical risks associated with a specific TBM's application can be calculated by summing the consequences of all ground classes with different lengths, as described in equation 3.1. The proportion of the tunnel length associated with each ground class ($\frac{L_i}{L_t}$) is used in the index to normalize the risk quantity to the length of each section i. The consequences are preferably evaluated in a probabilistic manner, meaning that at the end a distribution for the TBM Risk index is presented. In the next two sections of this chapter, methodologies for determination of the squeezing risk (SR_{ij}) and rockburst risk (RBR_{ij}) are introduced accordingly.

Table 3.3: Quantification of the consequences in the system based on their extent

The consequence extent	The consequence quantity
Insignificant	1
Minor	2
Moderate	3
Major	4
catastrophic	5

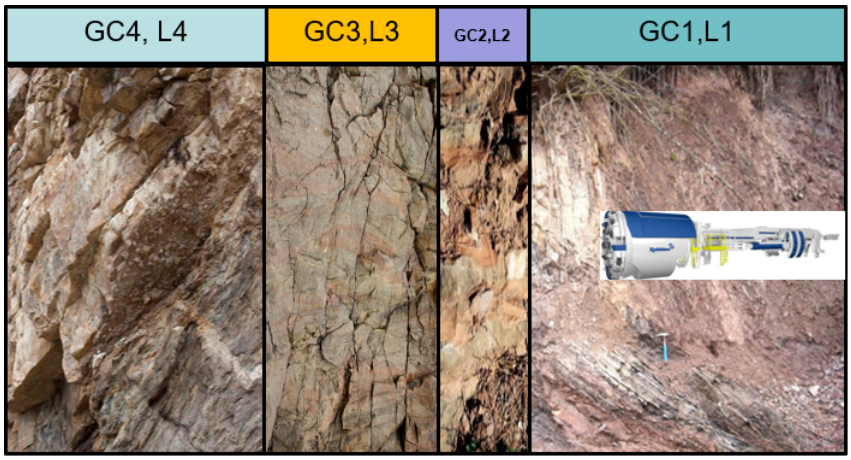

Figure 3.1: The cross-section of a tunnel with different rock characteristics and the corresponding length being driven through by a TBM

$$TBM_{RI} = \sum_{i=1}^{n} \sum_{j=1}^{m} (S_{ij}.W_{S_j} + RB_{ij}.W_{RB_j}).\frac{L_i}{L_t} \tag{3.1}$$

Where

n = number of formations

m = number of risk types

L_i = Length of formation i

L_t = Total length of the tunnel

W_{S_j} = The significance factor of squeezing risk j

W_{RB_j}= The significance factor of Rockburst risk j

S_{ij} = The squeezing risk j for the formation i

RB_{ij} = The rockburst risk j for the formation i

Table 3.4: The quantification of the significance factors for different consequences

Consequence		Significance factor	
		Rockburst	Squeezing
Damage and time-consuming operation	Cutterhead damage	1	-
	Shield damage	1	1
	Shield jamming	-	1
	Other equipment damage	1	1
	Support damage (Gripper TBM)	0.8	0.8
	Support damage (Shielded TBM)	0.8	0.8
	Gripper bracing difficulties	0.2	0.2
Injury or fatality		1	0.2

3.2 Evaluation of the main consequences of squeezing for TBM tunneling

In this section, we will thoroughly examine the potential risks associated with squeezing and propose evaluation methods to incorporate into the risk assessment system. As discussed earlier in Chapter 2, these risks primarily fall into three categories: shield jamming and damage, support damage, and difficulties with gripper bracing.

3.2.1 Shield jamming and damage

When a Tunnel Boring Machine (TBM) operates in soft ground and experiences significant deformations, the primary concern is the potential of the TBM's shield to become jammed. In the event of a jammed TBM, subsequent manual release operations are necessary to resume excavation, which are not only labor-intensive and expensive but also time-consuming and can pose safety risks. Figure 3.2 shows a photo of the jamming of the TBM shield in a faulted zone in Golab tunnel, taken during the rescue operation.

To address the issue of jamming, several researchers have developed methodologies to analyze and predict this risk. These approaches fall into three main categories: analytical methods, numerical simulation methods, and artificial intelligence methods ([67], [68] and [69]). Empirical and semi-analytical methods, which predict squeezing risk based solely on the extent of deformations, are excluded because they do not consider the longitudinal deformation profile of the ground and how displacement evolves throughout the shield length. Indeed, the key issue for evaluating the jamming risk is estimating the required thrust force to counteract the friction forces developed between the shield and ground due to excessive deformations and high pressures. Although artificial intelligence methods are the most innovative, they can be time-consuming and difficult to implement due to the requirement for significant amounts of training data. Since AI is not the focus of this study, we will explain the analytical and numerical approaches that will be applied in the assessment procedure.

Figure 3.2: The jammed shield of the double-shielded TBM in Golab tunnel [6]

Analytical approach for determination of the jamming risk

In Chapter 2, the analytical solution for the determination of the ground reaction curve was explained. In this section, the remaining steps in the calculation process, which involve estimating the potential friction force on the TBM shield are covered. Previous attempts by Jafari et al. (2007) and Farrokh et al. (2006) proved the application of the analytical solution in approximating the frictional force between the shield and the ground [70] and[67]. Farrokh et al. (2006) proposed that the pressure on the tunnel boundary can be classified into two distinct components: the inherent supportive pressure of the ground, and the pressure from the tunnel support system [67]. The natural supporting pressure is the supporting effect of the tunnel face contributing to the stability of the ground. To identify the locations where the shield interacts with the adjacent rock, the longitudinal deformation profile (LDP) of the rock mass can be used to measure the wall displacement at different distances from the tunnel face. Following that, the pressure applied by the ground on the shield can be evaluated at different distances from the tunnel face. This quantity can be calculated by deducting the natural supporting pressure from the final pressure applied to the shield at a distance further from the tunnel face.

In order to provide a clear illustration of the estimation process, an instance of a

Double shielded TBM jamming in the Zagros Tunnel is utilized. This procedure allows for an approximate evaluation of the shield's final pressure. According to Rasouli Maleki et al. (2018), the overcutting of the excavation in this project is limited to a maximum of 65 mm in radius [71]. The GRC is established through the use of discontinuous numerical simulations. Furthermore, the LDP of the ground is calculated based on Vlachopoulos and Diederichs equations [72]. Due to the stiffness of the shield, the support characteristic curve (SCC) is almost a vertical line, as shown in Figure 3.3. As can be seen, a displacement of approximately 65 mm takes place at a distance of around 3.7 m from the tunnel face. This is the first point where the ground touches the shield. Given that the TBM's shield length is 12 m, the final ground pressure acting on the shield can be estimated by the intersection of a vertical line from this location with the GRC. The following equation can be used to estimate the ground pressure acting on the shield at a specific distance of x to the tunnel face $P_i(x)$:

$$P_i(x) = P_u - P_f(x) \tag{3.2}$$

where: P_u is the natural supporting pressure of the ground at the distance where the ground gets in contact with the shield, and $P_f(x)$ represents the natural supporting pressure of the ground at a distance x from the tunnel face. By utilizing this equation at various points (x) on the shield, as shown in Figure 3.4, the relationship between ground pressures exerted on the shield and the distance from the tunnel face can be determined. The magnitude of the frictional forces operating on the shield surface is calculated by summing the TBM weight with the integral of this diagram on the shield surface.

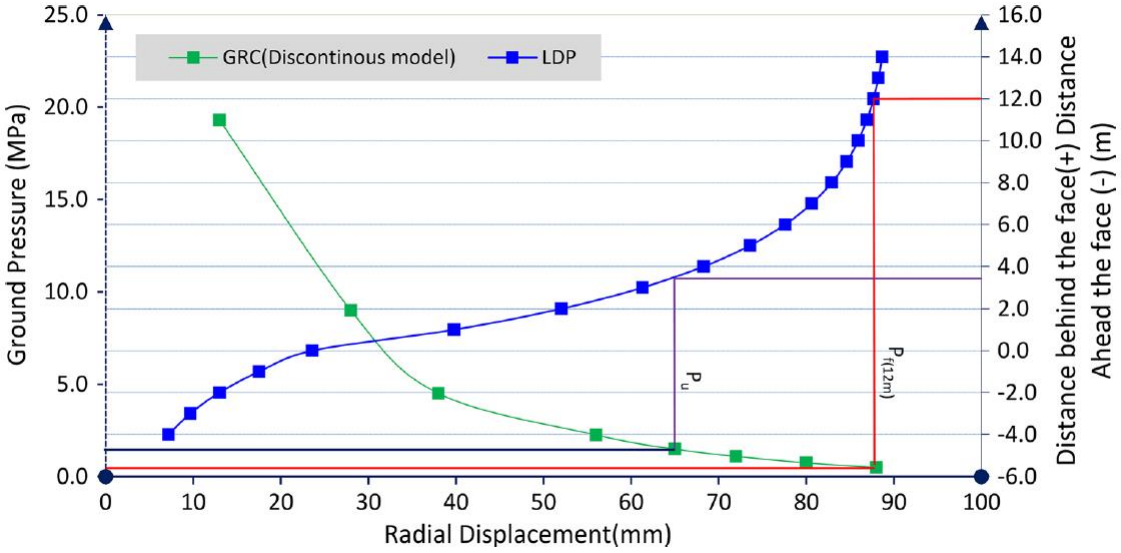

Figure 3.3: A combination of the GRC and LDP diagram for assessing the ground pressure exerted on the TBM shield [71]

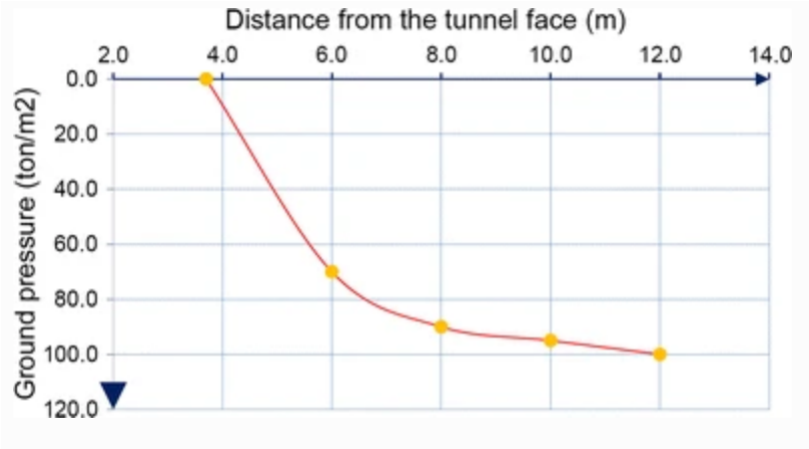

Figure 3.4: Ground pressure variation on the shield in relation to distance from the tunnel face [71]

The main shortcomings of the analytical solution (CCM)

Prior to applying the analytical solution mentioned earlier, it is important to note its limitations. In addition to idealized and simplified assumptions made in the closed-form solutions (hydrostatic stress field, isotropic behavior of the ground, and uniform tunnel support), other main shortcomings are as follows:

- Uncertainties in the assumed pre-deformation before lining installation;
- Neglecting the effect of the backfilling properties;

- Lack of details regarding the longitudinal distribution of rock pressure on the shield and lining [73];

- Failure to consider the influence of stress path on deformations and ground pressures;

  According to Cantieni and Anagnostou (2009), ignoring the impact of the stress path could significantly affect the accuracy of results for heavily squeezing conditions [74]. In practical terms, inaccuracies arising from the assumption of plane strain are not significant for tunneling scenarios where rigid support is installed with just a few meters distance from the face.

- Neglecting the effect of machine advance rate and time-dependent ground deformations, which as previously discussed are beyond the scope of this work.

Amongst the above shortcomings, this study focuses on addressing uncertainties related to pre-deformation, the effect of shield and segmental lining installation, and backfilling. Addressing the inaccuracies arising from the other assumptions requires additional investigation.

The adjusted analytical solution considering the limitations

The analytical solution comprises three key components: the ground reaction curve (GRC), which represents the radial displacement of the rock at the excavation boundary as a function of the support pressure; the support characteristic curve (SCC), which depicts the radial displacement of the lining based on the rock's pressure; and the longitudinal deformation profile (LDP) of the ground. A reasonably accurate estimation of these components is a prerequisite for a proper approximation of the segmental lining load and eventually the shield friction force.
Regarding the GRC, recent 3D numerical simulations conducted by Hasanpour and Schmitt (2016) have demonstrated that the behavior of the ground for shielded TBM tunneling can differ from the traditional excavation methods. This phenomenon is particularly the case when the TBM's shield comes into contact with the rock mass in weak ground conditions and the relaxation takes place [75]. According to Figure

3.5, neglecting this effect would lead to higher values of ground pressures and higher shield friction forces. As this aspect was not considered in the study, the evaluations may be slightly conservative.

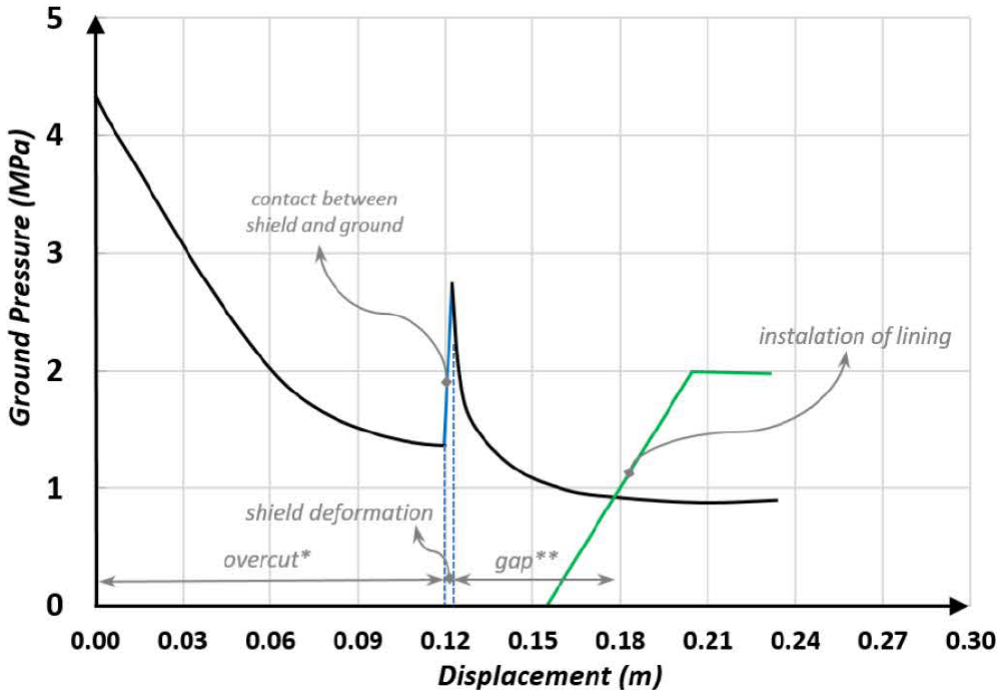

Figure 3.5: Ground Reaction Curve of a TBM excavated tunnel affected by the interaction with the shield [75]

The analysis of the interaction between the support components (segmental lining and backfill) and the ground can be best studied by numerical simulations, however, analytical solutions such as convergence confinement methods can also provide us with a viable alternative, in case the interactions can be well comprehended. There have been attempts to address the limitations outlined above. For instance, a new technique is devised by Aydan and Hasanpour (2019) [76], which integrates a theoretical model based on Aydan et al. (1996) [77]. This technique employs a displacement function that considers face distance, shield type, and rigidity to estimate the contact ground pressure on TBMs during rock squeezing. Oreste (2015) has developed an innovative procedure for the application of the CCM [78]. This new approach was subsequently slightly modified for better consideration of the support system stiffness [79]. The main advantage of this method is that it takes into account the composite stiffness, rather than just the lining stiffness, and

includes a method for estimating pre-deformation. Additionally, adaptations have been made to the LDP of the ground using the Vlachopoulos-Diederichs method to take account of the presence of the TBM shield. These advancements provide a more comprehensive approach for utilizing the CCM. This approach is applied for adaptation of the procedure described in section 3.2.1 in order to evaluate the shield jamming risk and the support damage risk for shielded TBMs.

As depicted in Figure 3.5, the empty space between the segmental lining and the outer radius of the ground (R) is filled with backfill material such as mortar or pea gravel mixed with cement grout. To accurately determine the load on a segmental lining, it is of utmost importance to take into account the properties of the backfill material [80]. Therefore, when analyzing the load on a segmental lining, the entire stiffness of the system comprising the concrete and backfill material should be considered during the calculation process. The following equations are applied for the estimation of the overall stiffness of the support system k_{sys} [79].

$$k_{sys} = \frac{2E_f(1-\nu_f)R[\frac{E_f}{(1+\nu_f)} + (R-t_f)k_c]}{E_f(1-2\nu_f)R^2 + (R-t_f)^2[E_f + (1-2\nu_f)(1+\nu_f)k_c t_f(1+\frac{R}{(R-t_f)})]} - \frac{E_f}{(1+\nu_f)R} \tag{3.3}$$

where:

$$k_c = \frac{E_c}{(1+\nu_c)} \frac{(R-t_f)^2 - (R-t_f-t_c)^2}{(1-2\nu_c)(R-t_f)^2 + (R-t_f-t_c)^2} \frac{1}{(R-t_f)} \tag{3.4}$$

E_f and ν_f are the elastic modulus and Poisson's ratio of the backfill. E_c and ν_c are the Young's modulus and the Poisson's ratio of the segmental lining, respectively. t_f and t_c are the thickness of the backfill and the segmental lining, respectively. k_c is the radial stiffness of the segmental lining and R is the tunnel radius.

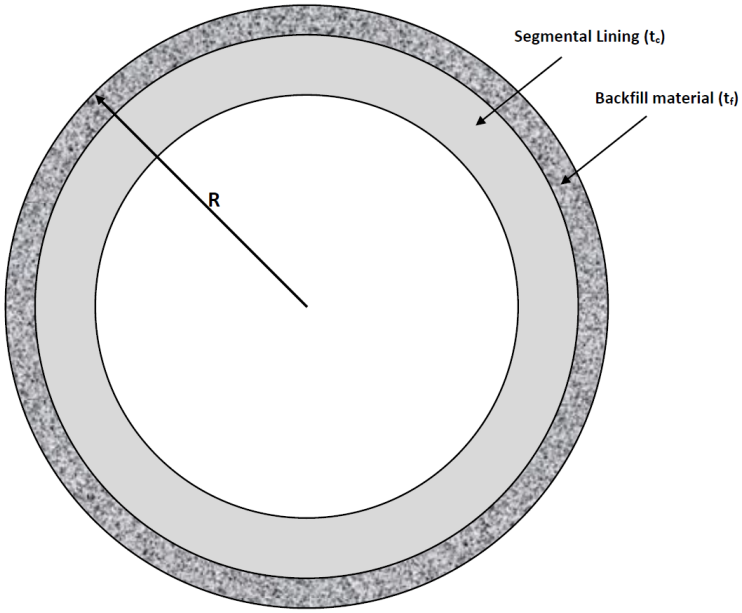

Figure 3.6: The cross section of the tunnel excavated by a shielded TBM considering the over cutting void filled with backfill material (t_f is the thickness of the backfill and t_c is the segmental lining thickness.)

As previously stated, determining the deformation value at the time of lining installation ($u_{R,in}$) is a crucial parameter. Even slight deviations from the correct value can have a big impact on the rock pressure, especially when the ground response is quite non-linear. The Vlachopoulos and Diederichs (2009) formulation for the variation of radial displacement behind the tunnel face will serve as the basis for the determination process [72]:

$$u_R = u_{Rmax}.\left[1-(1-\frac{1}{3}.e^{-0.15.\frac{R_{pl(p_{int})}}{R}}).e^{-\frac{3x}{2.R_{pl(p_{int})}}}\right] \tag{3.5}$$

$R_{pl(p_{int})}$ is the plastic zone radius when the tunnel interior is subjected to an internal pressure p_{int} from the support system. When there is no overcutting, the shield of the TBM prevents radial displacements at the excavation face directly behind the TBM cutterhead. In this case, according to curve 2 in Figure 3.7 , radial displacement of the tunnel along the whole length (SL) of the TBM shield will be constant and equal to the value of $u_{R,in}$ [78]:

$$u_{R,in} = u_{R,max}.\left[\frac{1}{3}.e^{-0.15.\frac{R_{pl(p_{int})}}{R}}\right] \tag{3.6}$$

Beyond x = SL, it is possible to hypothesize that the trend of u_R resembles curve 1, only with a shift of the shield length along the tunnel axis (x).

If there is overcutting of DR , which occurs when the tunnel radius is larger than the shield outer radius, the radial displacement profile will resemble curve 3, as illustrated in Figure 3.7. In this scenario, the following equation is employed to calculate the pre-deformation value $u_{R,in}$:

$$u_{R,in} = u_{R,max} \cdot \left[\frac{1}{3} . e^{-0.15 . \frac{R_{pl(p_{int})}}{R}} \right] + DR \tag{3.7}$$

δ in Figure 3.7 refers to the amount of displacement which is hindered due to the shield existence. Overcutting can both contribute to a reduction of $u_{R,in}$ bringing about lower load on the support and decrease the value of δ leading to less pressure on the shield of the TBM.

Curve 1 in Figure 3.7 represents the case when the DR is larger than the displacement at the end of the shield and leads to no pressure on the shield.

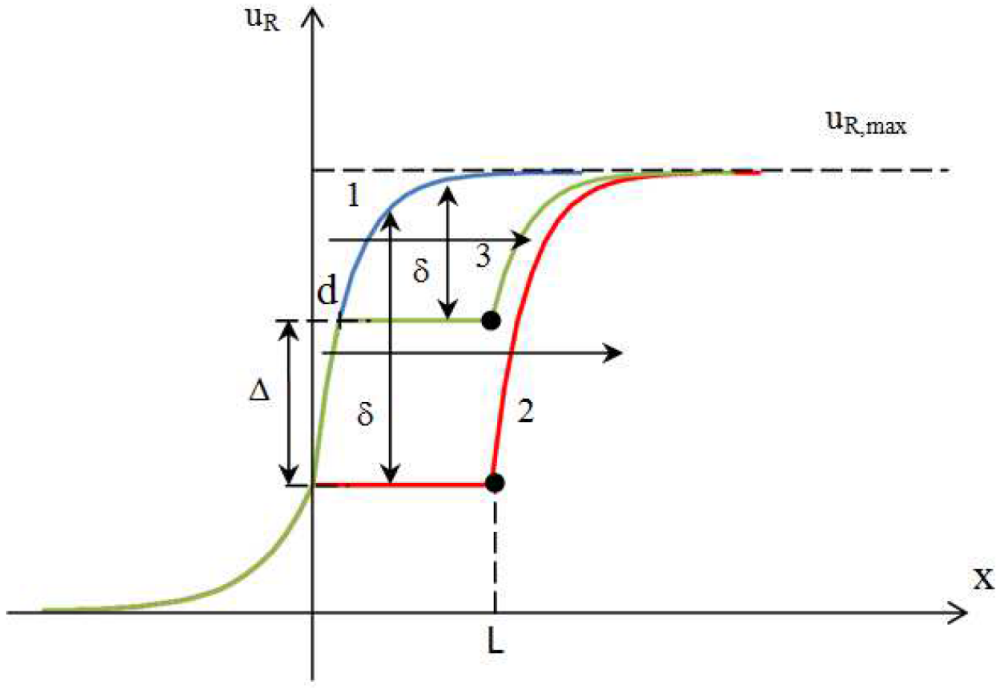

Figure 3.7: The longitudinal profile of radial displacements for different overcutting values. Curve 1: when DR is larger than the displacement at the end of the shield, Curve2: when DR = 0, Curve 3: DR smaller than the displacement at the end of the shield [78]

According to equation 3.5, by inserting the shield length as x, the u_{R0} or the displacement at the time of support installation (assuming that backfilling is immediately applied) would depend on u_{Rmax}. Besides, the intersection of the SCC and the GRC gives us the value of u_{Rmax}. However, SCC itself also depends on the value of u_{R0}. To solve this problem, Oreste et al. (2021) proposed an iterative procedure, which would finally satisfy both of these dependencies [79](See Figure 3.8). Following the determination of the GRC by Duncan Fama or Carrenza Torres formulations, a low initial value of u_{R0} is assumed. Then using this initial value, the backfill void thickness is estimated as follows:

For $u_{R0} <$ DR :

$$t_f = DR - u_{R0} + R_{sh} - R_c \tag{3.8}$$

For $u_{R0} >$ DR :

$$t_f = R_{sh} - R_c \tag{3.9}$$

where: R_{sh} is the radius of the end of the shield. Using the backfill thickness in equation 3.3 , the support system stiffness (k_{sys}) can be evaluated, which together with u_{R0} would give us the SCC of the segmental lining. Subsequently, by intersecting the GRC and the SCC, the maximum final value of support internal pressure (P_{int}) and the maximum radial displacement (u_{Rmax}) are calculated. In the next step, we need to see how much the displacement at the end of the shield ($u_{R,SL}$) is according to the Vlachopoulos equation for LDP (Equation 3.5). In case the displacement is larger than the overcutting value (DR), equation 3.7 is applied to calculate the $u_{R,in}$, otherwise, $u_{R,in}$ would be equal to $u_{R,SL}$. Finally, the estimated value of $u_{R,in}$ is compared to the initial assumed value of u_{R0}. The loop is continued as long as this value is smaller than u_{R0}. When this value equals to $u_{R,in}$ or becomes larger, it means that both states (functions defined by the characteristic curves and the LDP function) are satisfied, and the $u_{R,in}$ and P_{int} can be applied for determination of the jamming risk. Subsequently, these values will also be used for evaluation of the support damage risk.

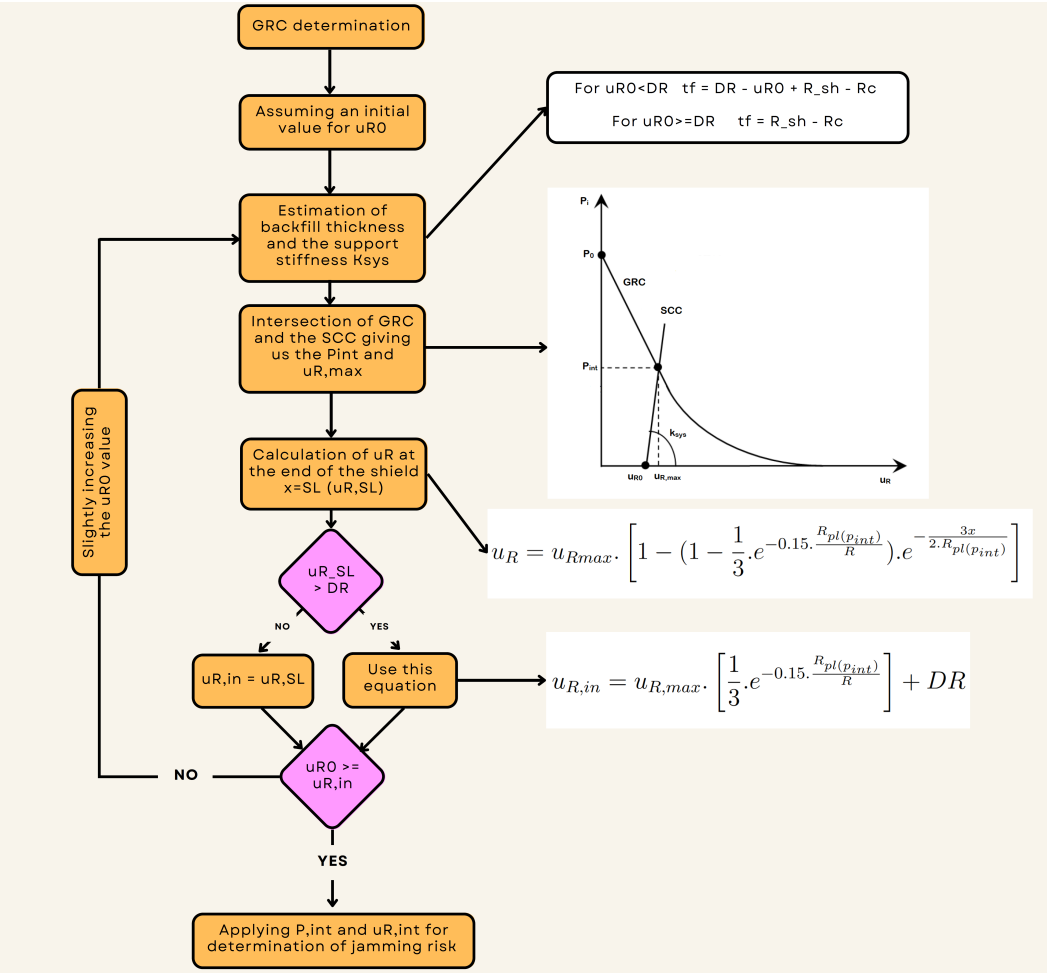

Figure 3.8: The cross section of the tunnel excavated by a shielded TBM considering the over cutting void filled with backfill material (t_f is the thickness of the backfill and t_c is the segmental lining thickness.

The assessments for a shielded machine using the introduced analytical solution are conducted under the assumption that the void area behind the segments is immediately filled with backfill, including pea gravel. However, this assumption may not always align with the actual conditions. In practice, when the immediate injection is not implemented, a certain degree of deformation is permitted, resulting in lower final loads being exerted on the segmental lining.

It should be noted that Gripper TBMs differ from shielded TBMs in that the support system is selected locally based on the specific ground conditions encountered during excavation. Thus, the stiffness of the support system and the extent of predeformation at the time of installation will vary depending on the type and location of the support system [81]. Therefore, it is critical to accurately approximate these

factors in order to effectively model the behavior of the ground in Gripper TBM tunneling.

Parametric investigations based on pre-conducted numerical simulations

Numerical simulations have the advantage that they can consider the ground and TBM components, providing a better approximation of the interaction mechanisms between the ground and different parts of the machine. Furthermore, numerical models can incorporate the time-dependent behavior of the ground and the excavation's advance rate, improving the accuracy of the mechanical behavior of the material. Previous studies have employed various computational methods to simulate TBM excavation in challenging geological conditions [82], [83], [84] and [85]. More recent studies by Zhao et al. (2012) [86] and Hasanpour et al. ([68] and [75]) have demonstrated the capabilities of 3D finite difference in modeling the excavation process using TBMs. These models are primarily applied to calculate the pressure on the shield and the segmental lining load.

Generating a numerical model incorporating the machine and the ground can be time-intensive, and each project necessitates individual and expert modeling. However, the primary objective of this research is to develop a risk assessment method that can be promptly utilized for initial investigations. Therefore, the modeling procedure is not integrated into the system. Instead, the system employs pre-conducted numerical simulations from past research. Hasanpour et al. (2018) performed a parametric study to evaluate the impact of various factors on the required thrust force for avoiding shield jamming [87]. This was achieved by conducting 200 3D finite difference numerical simulations, identifying the most effective parameters, and performing a nonlinear regression analysis to establish a correlation between the machine performance and rock mass parameters (See Figure 3.9). Table 3.5 contains the range of the input data chosen for the conducted numerical simulations. A correlation between contact loads and numerous independent variables, including geomechanical and TBM parameters was found using the MVR approach. This led to the creation of a predictive model for calculating the necessary thrust force

depending on particular machine and ground circumstances.

$$S_{TBM} = \frac{J_{TBM}}{6.35UCS + 12.65GSI + 7.55m_i + 32.85E_i + 9.5DR} \tag{3.10}$$

$$F_f = \mu.F_{sh} = 228\mu\,(S_{TBM})^{1.30} \tag{3.11}$$

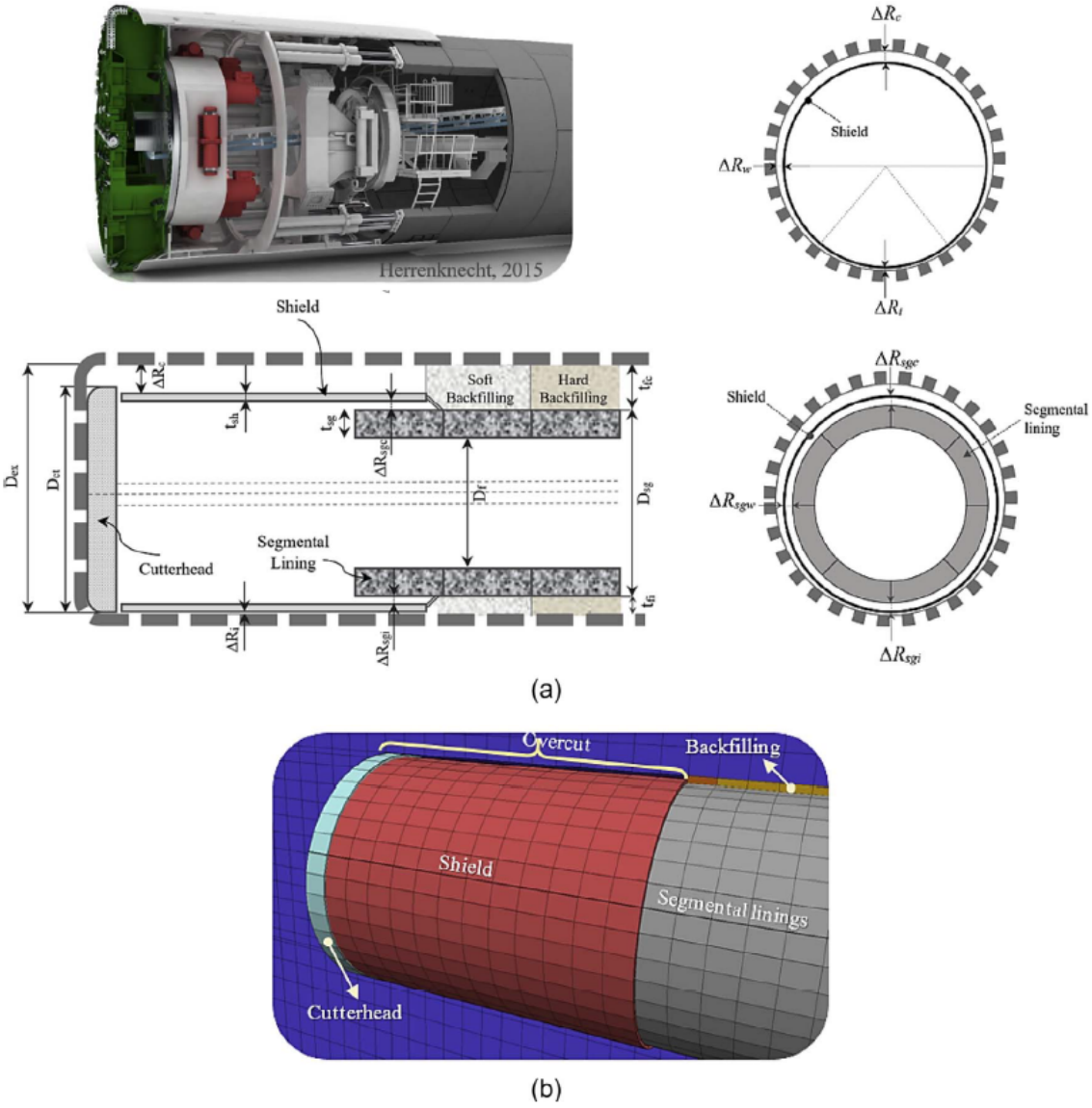

Figure 3.9: (a) Illustration depicting the configuration of a single shielded TBM suitable for use in squeezing conditions. (b) Representation of the 3D model in FLAC3D [87].

Table 3.5: The range of parameters assumed for the set of numerical simulations [87]

Ground properties, tunnel parameters and SS-TBM components	Unit	Value
Geological Strength Index (GSI)	-	20–60
Hoek-Brown material constant (m_i)	-	4–20
Uniaxial compressive strength (UCS)	MPa	5–75
Elastic modulus of the intact rock (E_i)	GPa	5–40
In-situ stress (P0)	MPa	2–20
Tunnel outer radius (R)	m	2–9
Overcutting (DR)	mm	20–200
Shield length (SL)	m	8–12

The expression for calculating F_f involves several parameters, including the UCS (uniaxial compressive strength) of the intact rock in MPa, the GSI (geological strength index), m_i (material constant based on the Hoek-Brown failure criterion), E_i (elastic modulus of the intact rock in GPa), and DR (overcutting in cm). When using J_{TBM} to calculate F_f, the values of P_0, R, and L should be entered in MPa and meters, respectively.

Similar investigations through several thousands of 2D simulation models provided dimensionless design nomograms for analyzing the particular challenges of mechanized tunneling in squeezing ground, the occurrence of shield jamming and the effects of counter measures for different types of TBMs [73]. Figure 3.10 shows two of the nomograms out of dozens of nomograms developed by Ramoni and Anagnostou (2010) [73]. F_f in the graph is the frictional force in the front shield, φ is the friction angle of the rock mass, and ψ is the dilatancy angle of the ground.

It should be noted that the nomograms were developed with the assumption of a uniform ground condition. However, it is important to consider that the degree of squeezing can fluctuate significantly over short distances along the tunnel's path. For instance, in the event of a fault section with squeezing potential for a short length, the assumption of the weak ground over a long enough section leads to an overestimation of the squeezing hazard. This is an assumption that is made for all the methods introduced in this research including the 3D parametric method as well as the adjusted CCM analytical solution.

In contrast to the formulation presented by Hasanpour et al. (2018) [87], the nomograms developed by Ramoni and Anagnostou (2010) [73] are less conducive to adoption in a risk assessment system due to the large number of nomograms involved. To facilitate the application of these nomograms in the risk assessment, the 2D nomograms were converted into a smaller number of 3D nomograms, and curve fitting using interpolation was automated by coding in Matlab (See Figure 3.11).

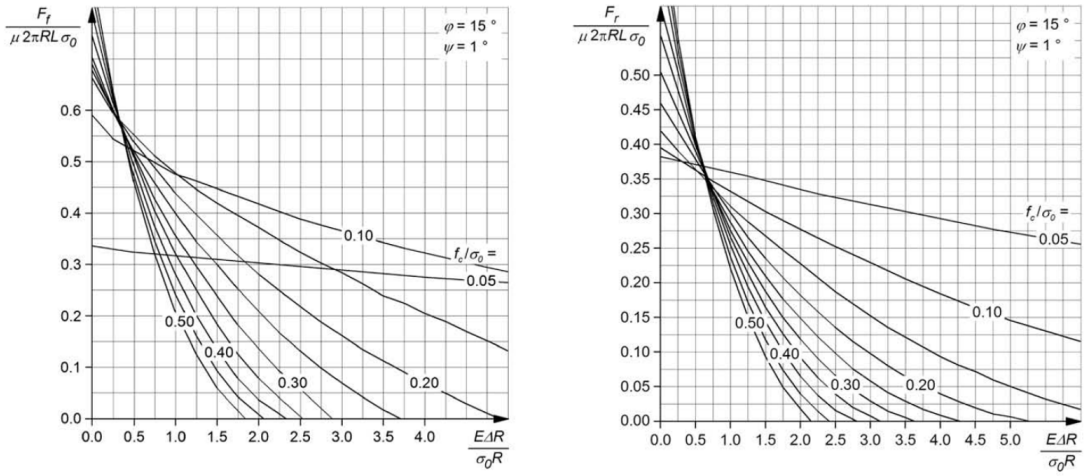

Figure 3.10: Two of the dimensionless diagrams developed for estimation of the rear and forward frictional force of the shield in squeezing grounds [73]

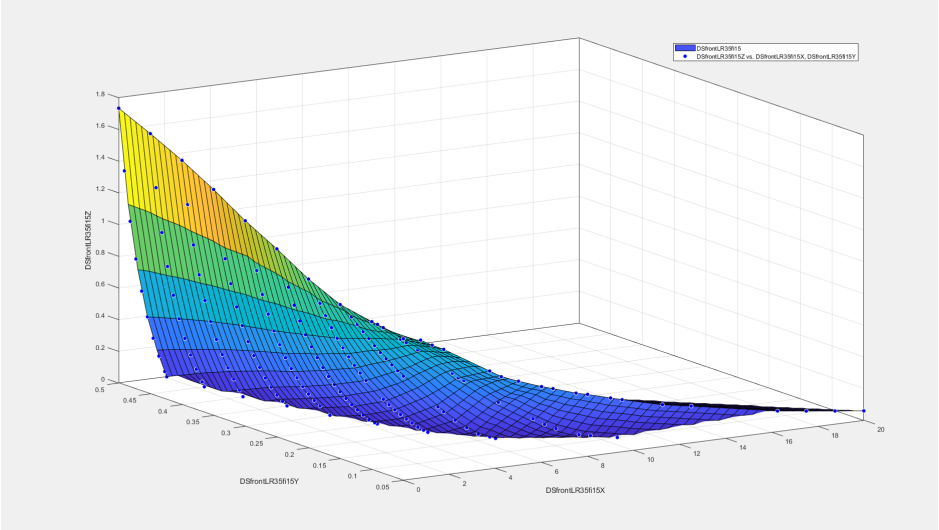

Figure 3.11: A 3D nomogram for estimation of the frictional force on the front shield of a Double shielded TBM.

Jamming risk level determination

Once an estimate of the shield frictional force has been obtained, the next step is to assess the risk of the shield jamming both qualitatively and quantitatively. This is essential in order to effectively integrate this risk with other potential risks within the system. To accomplish this, the ratio of the shield frictional force to the available thrust force for pushing the shield and cutterhead forward is defined as the shield jamming riks (JR) using equation 3.12.

$$JR = \frac{F_f}{F_a} = \frac{F_f}{F_{th} - F_e} \tag{3.12}$$

Where F_a is the available thrust force that can be applied for pushing the shield through the squeezing zone, calculated by subtracting the thrust force required for the excavation of the rock (F_e) from the maximum thrust force (F_{th}) that the thrust cylinders or the auxiliary thrust cylinders (in the case of single shield or double shield TBMs) can provide. Hou et al. (2023) applied the same ratio and developed a classification rule for the shield jamming risk as follows [88]:

$JR \geq 1$ Very high jamming risk

$0.8 \leq JR < 1$ High jamming risk

$0.5 \leq JR < 0.8$ Medium jamming risk

$0.3 \leq JR < 0.5$ Low jamming risk

$JR < 0.3$ Very low jamming risk

The same criterion is also applied in this research.

Analysis of some case studies for the jamming risk

To assess the reliability of the the aforementioned methods for the estimation of the shield friction forces, three case studies where TBMs of different types (gripper, single shield, and double shield) were jammed are chosen. Each case study will be shortly described and the calculation results are presented accordingly.

Uluabat tunnel-single shielded TBM

The Uluabat tunnel in Turkey experienced several shield jamming events when the 5.05 m diameter single-shielded EPB-TBM encountered claystone with intense shear and squeezing conditions. Figure 3.12 shows a view of the end of the shield and the beginning of the segmental lining installed in a squeezing zone, well indicating how the over-excavation gap is filled with deformed rock. It is reported in the project that excessive cylinder pressure caused damage to the segmental lining. To analyze the excavation at three different chainages with varying overburdens in similar geological conditions, three sets of evaluations were carried out for 125 m, 250 m, and 300 m of overburden. These evaluations involved taking the vertical stress and treating it as a hydrostatic stress state across the region. Consequently, stress magnitudes of 3.06 MPa, 6.125 MPa, and 7.35 MPa were determined as part of the evaluation process (assuming a density of 2450 kg/m^3). Geotechnical and performance parameters, along with segmental lining properties, are included in Tables 3.6, 3.7 and 3.8 taken from Hasanpour et al. (2017) [89]. To incorporate variability in the parameters, a normal distribution is used in a probabilistic approach using Monte Carlo simulation. The Empirical Rule, stating that 95 percent of the data lies within two standard deviations, is applied to set a range of acceptable values between μ-2σ and μ+2σ (μ is the mean and σ denotes the standard deviation),

beyond which values are discarded to avoid unrealistic random selection.

The resources which were referred to for the determination of ground properties did not well distinguish between the two failure criteria of Hoek-Brown and Mohr-Coloumb and converting the parameters from one criterion to another did not produce the anticipated values. Therefore, a comparison between the 2D parametric modeling method, which takes Mohr-Coloumb parameters as the input, and the 3D parametric modeling method which takes Hoek-Brown criterion parameters was not possible.

Figure 3.12: The jamming of the shield in Uluabat tunnel [90].

Table 3.6: The geotechnical parameters of the jamming zone in Uluabat tunnel

Statistical measures	Geotechnical Parameters				
	m_i	E_i (MPa)	ν	σ_{ci} (MPa)	GSI
Mean	6	535	0.275	0.7	19.5
Standard Deviation	0.66	232	0.087	0.25	2.75

Table 3.7: The performance parameters of the TBM in Uluabat tunnel

Radius (m)	Overcutting-DR (cm)	Shield friction (μ)	Shield Length (m)	Max. thrust force (MN)
2.525	3	0.45	12	28

Table 3.8: The segmental lining and backfill properties in Uluabat tunnel

	Segmental Lining				Backfill	
	Thickness(m)	UCS (MPa)	E_c(MPa)	ν_c	E_f(MPa)	ν_f
Mean	0.3	27.5	36000	0.2	500	0.4
Standard Deviation	0	1.25	0	0	0	0

A primary deterministic approach is adopted using the Convergence Confinement method based on Carrenza Torres closed form solution (CC-CT) and the 3D modeling formulation by Hasanpour et al. (2018) [87]. Some actual data acquired from the measurements in the project are also employed for validation of the estimation results. The actual data for zones z1, z2 and z3 (H=125m, H=250m, and H=300m) are the maximum thrust forces which are taken by deducting the cutting forces and assumed to be purely consumed for the shield frictional forces [91]. Figure 3.13 shows the summary of the results. As can be seen, the analytical results either underestimate or highly overestimate the shield frictional forces, whereas the 3D modelling approach results are closer to the actual data.

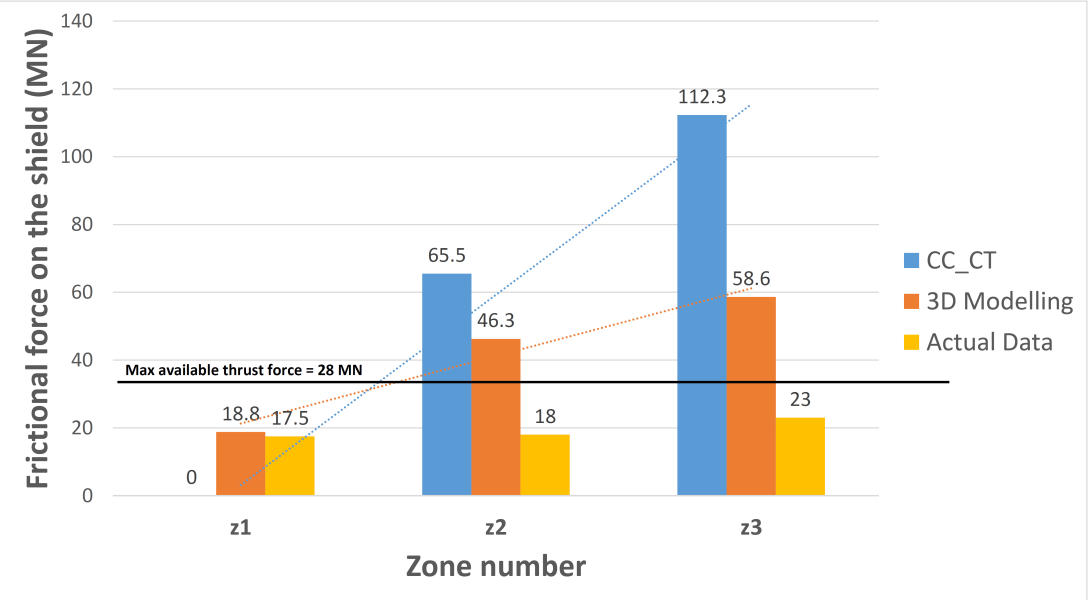

Figure 3.13: The deterministic approach for evaluation of the shield frictional force in three zones of Uluabat tunnel.

In order to consider the variability of input parameters, a probabilistic approach incorporating 40 iterations (randomized selection of parameters) is also implemented and the results are presented in Figure 3.14 and Table 3.9. Since there were not a variety of existing measurement data on-site in each region, the actual data could not be compared in this case.

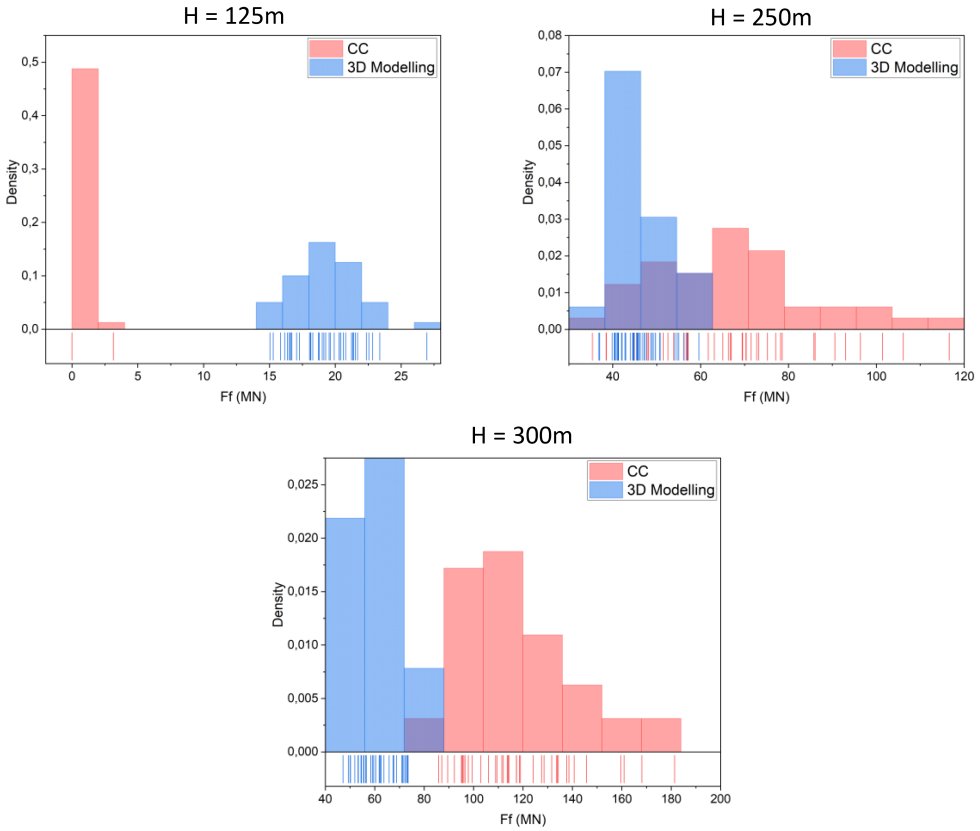

Figure 3.14: The probabilistic approach for evaluation of the shield frictional force in three zones of Uluabat tunnel.

Table 3.9: The mean and standard deviation of shield frictional force using different methods and in different overburdens in Uluabat tunnel

Overburden	3D Modelling		CC Carrenza Torres	
	Mean	Standard Deviation	Mean	Standard Deviation
H=125m	19.2	2.6	0	0.5
H=250m	46.1	5.5	67.6	19.1
H=300m	60.8	7.7	118.5	23.3

Gothard base tunnel - Lot Bodio-gripper TBM

During the construction of the Bodio lot of the Gotthard Base Tunnel in Switzerland, the excavation using two gripper TBMs encountered unexpected squeezing ground

conditions in the western tunnel that caused problems. Specifically, the shield of the western TBM became jammed, resulting in the convergence of the bored profile and damage to the tunnel support. Tables 3.10 and 3.11 contain the geotechnical and performance parameters used for the estimation of the shield friction force. It is important to note that the squeezing zone has a depth of 1000 m.

The western TBM was jammed and the shield was damaged, whereas the eastern TBM could pass the same region without much difficulty. The uncertainty in the ground conditions was recognized as the main cause for these two different outcomes [73]. Vicenzi et al. (2007) reported that at chainage 13+698 m, the shield jack pressure reached a maximum of 300 bar, resulting in the machine getting jammed [92] (refer to Figure 3.15). Assuming that 300 bar corresponds to a maximum thrust force of 27000 KN on the machine, we estimate that the rise in the cylinder thrust force due to excessive pressure would be around 23.5 MN, based on Figure 3.15.

Table 3.10: The geotechnical parameters of the Micaceous gneiss in the Bodio section of Gotthard Base tunnel

Statistical Measures	Geotechnical Parameters							
	m_i	E_i (MPa)	ν	σ_{ci} (MPa)	GSI	E (MPa)	φ	σc (MPa)
Mean	28	10000	0.25	20	57	6568	33.7	6.6
Standard Deviation	1.67	0	0	7.5	0	1278	3.2	2.5

Table 3.11: The performance parameters of the TBM in the Bodio section of Gotthard tunnel

Radius (m)	Overcutting-DR (cm)	Shield friction (μ)	Shield Length (m)	Max. thrust force (MN)
4.465	5	0.45	4.3	27.5

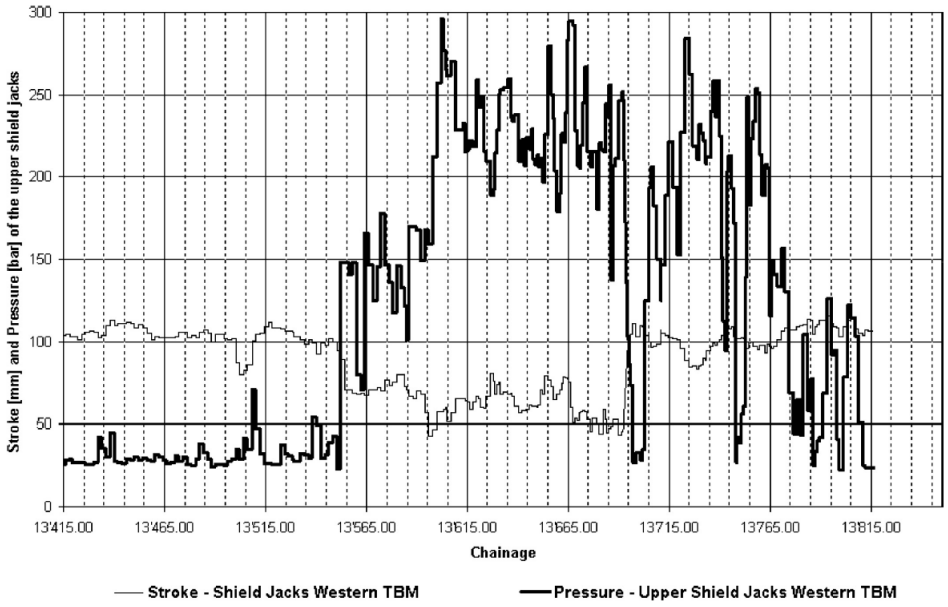

Figure 3.15: The variation of Pressure of the upper shield jacks in the western TBM of Gotthard tunnel-Bodio section [92].

According to Hasanpour et al. (2018) [87], the 3D modelling method is specifically designed for shielded machines, as it assumes a predefined segmental lining installation. Hence, in this research, the 2D modelling and the CC method are used for gripper TBMs. It should be noted that if a support system is positioned near the tunnel face in gripper TBM, its influence in controlling the plastic zone extension and the final deformation of the ground should be considered. Ramoni and Anagnostou's simulations conservatively disregard the effect of the support system. In contrast, the CC method (based on Carrenza Torres or Duncan Fama solution) developed in this study can account for the support system if there is sufficient data on its location and mechanical properties. Alternatively, we could choose to be cautious and neglect its influence. In the case of the Bodio section of the Gotthard tunnel, due to a lack of information in this regard, the support system is ignored, and a probabilistic analysis using Monte Carlo simulation is conducted for 100 iterations, with the results presented as histograms in Figure 3.16. The summary of the statistical parameters gained from the analysis is also inserted in Table 3.12. The results reveal that the 2D modelling method displays an extensive range of values from 0 to 343 MN, indicating a higher likelihood of jamming. In contrast, the CC method utilizing Duncan Fama solution demonstrates a more focused range between

0-76 MN. In this case study, the values obtained from the CC method appear to be more realistic, as one of the two gripper machines excavating in the area became stuck, while the other did not face any jamming issues. We have chosen to present only the Duncan Fama solution since they generate higher values than the Carrenza Torres method, which would provide a more secure margin for decision-making.

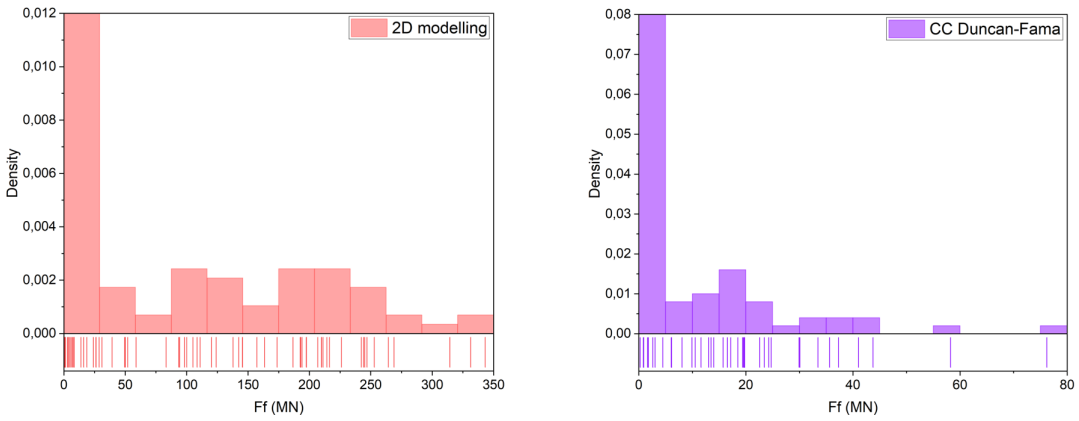

Figure 3.16: The probabilistic approach for evaluation of the shield frictional force in three zones of Uluabat tunnel.

Table 3.12: The mean and standard deviation of shield frictional force using different methods for the Micaceous gneiss in Bodio section of Gotthard tunnel

No. of iterations	2D Modelling				CC Duncan-Fama			
100	Mean	Standard Deviation	Min	Max	Mean	Standard Deviation	Min	Max
	83	99	0	343	7.4	13.8	0	76

Guadarrama tunnel-Double shielded TBM

Four double-shielded TBMs, with a diameter of 9.46 m and 9.51 m, were used to excavate the tunnel of Guadarrama. The 600 m long fault zone known as La Umbria, which is located 300 m beneath the surface, was expected to have squeezing ground conditions during construction. However, these circumstances did not arise during the excavation process and the machine could pass the region without jamming issues.

In this section, the CC method together with the 2D modelling method are applied to investigate the jamming risk. Since there was no information regarding the seg-

mental lining in this project, certain characteristics had to be assumed to facilitate a comparison between the analytical method and the 2D numerical modelling method. Tables 3.13 and 3.14 contain the geotechnical and performance parameters pertaining to the squeezing region. Based on the existing data, the 3D modelling method which requires the Hoek-Brown criterion parameters is not applied. It is important to mention that a friction coefficient of 0.25, recommended by Ramoni and Anagnostou (2010), was assumed to account for the impact of lubrication applied during the excavation process [73].

Table 3.13: The geotechnical parameters of rock mass in the faulted region with squeezing potential in the Guadarrama tunnel

Statistical Measures	Geotechnical Parameters			
	ν	E (MPa)	φ	σc (MPa)
Mean	0.25	500	20	4
Standard Deviation	0	100	0	1.75

Table 3.14: The performance parameters of the TBM in the Guadarrama tunnel

Radius (m)	DR (cm)	Shield friction (μ)	Total Shield Length (m)	Forward Shield Length (m)	Max. Thrust Force (MN)
4.73	4.5	0.25	15.24	5.04	125

The graphs in Figures 3.17, 3.18, and 3.19 illustrate the Monte Carlo analysis results using 2D modelling and the CC method obtained from 100 iterations. The machine can provide 89 MN by the main system of cylinders to push the cutterhead and the front shield forward [73]. A large proportion of the data from 2D modelling exceed this limit, whereas, the CC method gives a mean value of 5.2 MN and a standard deviation of 5.3 MN considerably lower than the max. available force (refer to

table3.15). The results in the other graphs (Figure 3.18 and 3.19) and their comparison to the available thrust forces of the auxiliary cylinders in single and double mode (108 MN and 125 MN, respectively) imply the same conclusion that the 2D modelling method highly overestimates the frictional forces. Due to limitations in the number of available numerical simulations, certain assumptions had to be made regarding the stiffness of the lining, backfill, and shield, as well as the geometrical features of the shield etc. that were established by the developers of this method [73]. The main advantage is that in almost all cases the designer can ensure a safe margin against the risks.

Drawing upon the results obtained from the last three case studies, it can be concluded that the parametric 3D modelling method and the convergence confinement (CC) methods offer values that are more closely aligned with the actual outcomes observed in the projects. The assumptions defined in the 2D parametric method lead to high overestimation in the shield frictional force values.

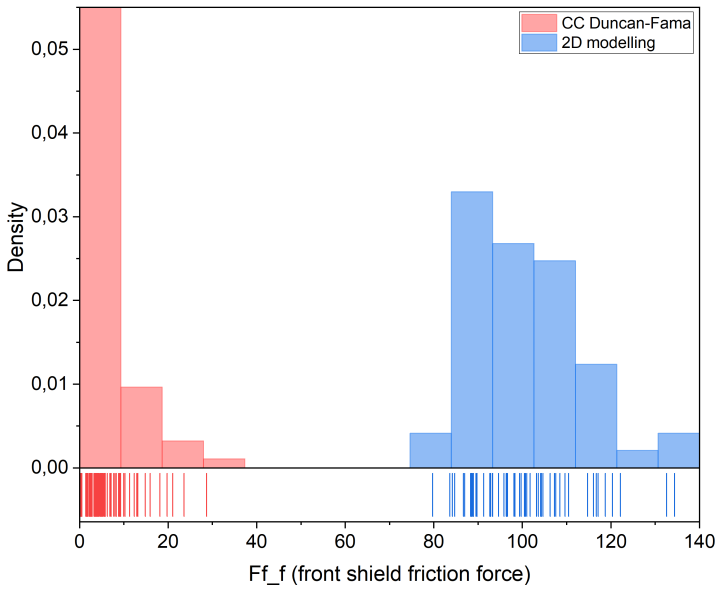

Figure 3.17: The variation of shield frictional forces on the front shield of the DS TBM in Guadarrama.

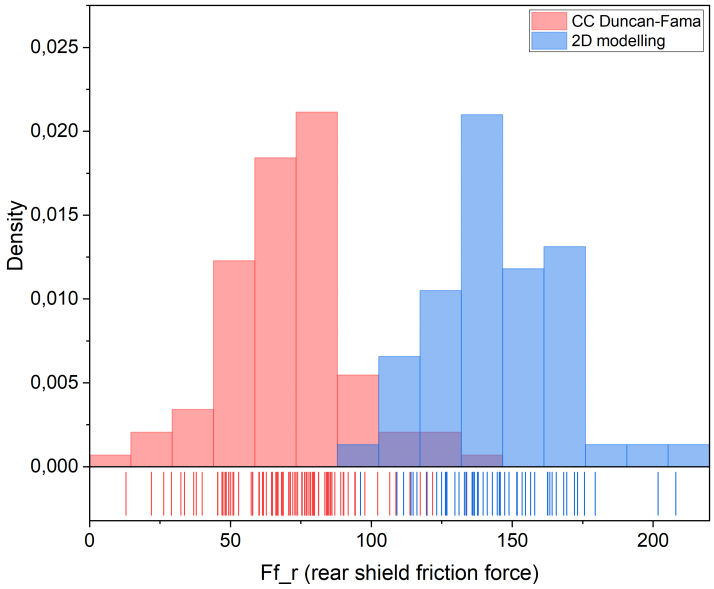

Figure 3.18: The variation of shield frictional forces on the rear shield of the DS TBM in Guadarrama.

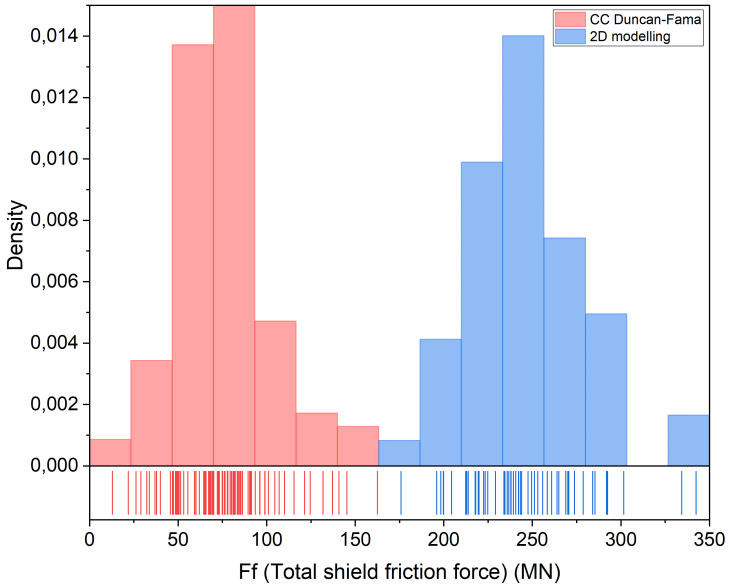

Figure 3.19: The variation of total shield frictional forces on the whole shield of the DS TBM in Guadarrama.

Table 3.15: The mean and standard deviation of shield frictional force using different methods for the jamming zone in Guadarrama tunnel

	Method	No. of iterations	Mean	Standard Deviation
Total shield friction force (MN)	CC Duncan Fama	100	75.3	26.6
	2D Modelling	52	245.5	34.2
Front shield friction force(MN)	CC Duncan Fama	100	5.2	5.3
	2D Modelling	52	100.7	12.3
Rear shield friction force(MN)	CC Duncan Fama	100	70	21.8
	2D Modelling	52	144.7	22.4

3.2.2 Support damage of shielded TBMs

This section is dedicated to addressing the issue of overstressing the support system for shielded TBMs and proposing methodologies to evaluate the associated risks. In the case of a gripper TBM, the support system can consist of various elements such as shotcrete, rockbolts, steel sets, etc. Depending on the distance of the support installation from the tunnel face, the support system may be subjected to specific loads. It is worth noting that if the type and location of the support system are known, the methodology introduced in this section can be adapted for gripper TBMs as well.

When constructing deep tunnels, the interaction between low rock mass quality and excessive or unfavorably oriented in-situ stress is often responsible for extreme deformations of unsupported tunnels or overstressing of support systems. These problems can arise not only during TBM excavation, which can lead to TBM shield jamming but also after the machine has passed through severe squeezing grounds. In such cases, the advance of the TBM shield through squeezing grounds requires excessive thrust force on the segmental lining, potentially causing damage to the segments. To prevent this, thrust forces should be limited to below the strength of the segmental lining, or preventive measures should be implemented to reduce the

required thrust forces for advancing through the squeezing grounds.
Understanding the factors that contribute to damage to the support systems of shielded TBMs in squeezing grounds is crucial for ensuring safe and efficient tunneling operations. It has the potential to increase costs, cause construction delays, and pose safety risks. In order to achieve secure and effective tunneling operations, it is necessary to comprehend the factors and elements that lead to damage to the support systems. There are two main mechanisms that can cause damage to the support system of shielded TBMs: excessive radial deformation on the exterior side of the support system, and longitudinal cracks on the segmental lining resulting from excessive thrust forces by the cylinders. These mechanisms are individually discussed in the following two chapters.

Damage to the exterior side of the support system

This type of damage is a direct result of excessive isotropic or anisotropic deformations of the ground with the segmental lining. Such deformations can create pressures that exceed the compressive or tensile strength of the segmental lining. Researchers have developed empirical correlations to evaluate the load on the support system based on rock mass classifications such as Q and N [51], [47]. However, the main limitation of these methods is that they do not consider factors such as the interaction of the shield and ground, the distance between the tunnel face and the installed support, the backfill characteristics, the longitudinal deformation of the ground, etc. As a result, these methods will not be included in this study. Instead, two categories of methods of analytical and parametric studies based on pre-conducted numerical simulations will be studied individually. These investigations also have certain disadvantages such as the inability to capture damages caused by anisotropic ground deformations. Furthermore, they only consider compressive failure and not tensile failure, which is often the case.

The analytical method based on the Convergence Confinement approach

The analytical approach introduced in section 3.2.1 can take into account several important factors including the longitudinal deformations of the ground, the influence of the shield, and the initial deformation before support installation. By considering these factors, this approach enables the determination of the load acting on the support system (P_{int}) using the procedure described in Figure 3.8. With this determined value, the maximum circumferential principal stress on the segmental lining can be evaluated using the following formulation:

$$sig1_{max_{CC}} = \frac{2.P_{int}}{\left[1 - \frac{(R_c - t_c)^2}{R_c^2}\right]} \tag{3.13}$$

Parametric study based on pre-conducted 2D axisymmetric numerical simulations

It is generally recommended to employ numerical modeling for the cases where significant squeezing potential exists. But as mentioned before, the risk assessment procedure in this study is supposed to put forward a quick preliminary evaluation of the risks, because every numerical investigation requires a thorough modeling of different components. Therefore, pre-conducted numerical simulations with a certain range of parameters are more suitable for this system.

Following up on their previous studies on the assessment of squeezing risks of TBM excavation, Ramoni et al. (2011) dealt with lining overstressing as the other key consequence arising from extreme squeezing [80]. The main focus is on the evaluation of the ground pressure acting on the segmental lining in a shielded TBM. According to their findings, discarding the type, location, and thickness of the backfilling can significantly affect the ground pressure acting on the segmental lining. To conduct numerical calculations, they utilized the finite element code HYDMEC from ETH Zurich with certain simplifications. The numerical coding is based upon the axially symmetric model shown in Figure 3.20. It is assumed that the tunnel is cylindrical, deep-seated, and excavated in a homogeneous and isotropic ground with a uniform in-situ stress state. Moreover, the size of the void between the shield and ground

and between the segmental lining and ground is assumed as constant and the TBM weight is not included. Another very important simplification is that bending of the segmental lining is neglected and only normal forces are assumed to develop in the segments. Furthermore, the model assumes the material to be linearly elastic, perfectly plastic, adhering to the Mohr-Coulomb yield criterion with a non-associated flow rule.

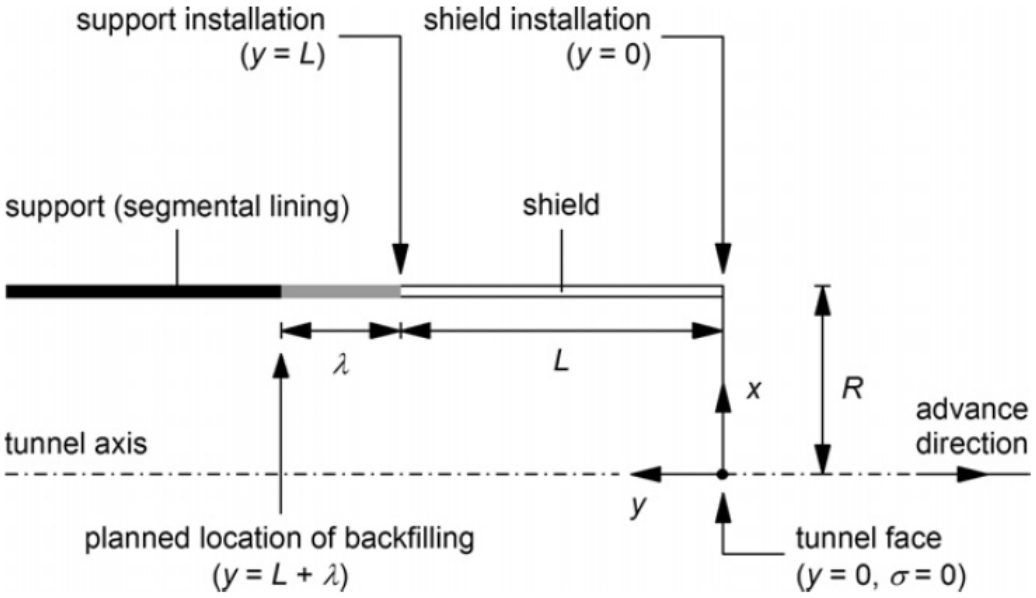

Figure 3.20: The axially symmetric model proposed for simulation of interactions between the ground and machine features by Ramoni et al. (2011)[80].

Ramoni et al. (2011) conducted a parametric study on the results of the simulations to facilitate the support damage assessment. Several ground properties and in-situ stress conditions, as well as different machine parameters, lining, and backfilling, were assumed in the simulations to come up with nomograms that can enable a quick preliminary assessment of the loads acting on the segmental lining (P_{2D}) (See Figure 3.21). Similar to the nomograms developed for jamming consequences, the 2D nomograms are converted in this research to 3D graphs for an easier estimation process. Subsequently, through the utilization of Matlab coding, the process of curve fitting and interpolation is automated to evaluate the load that impacts the segmental lining.

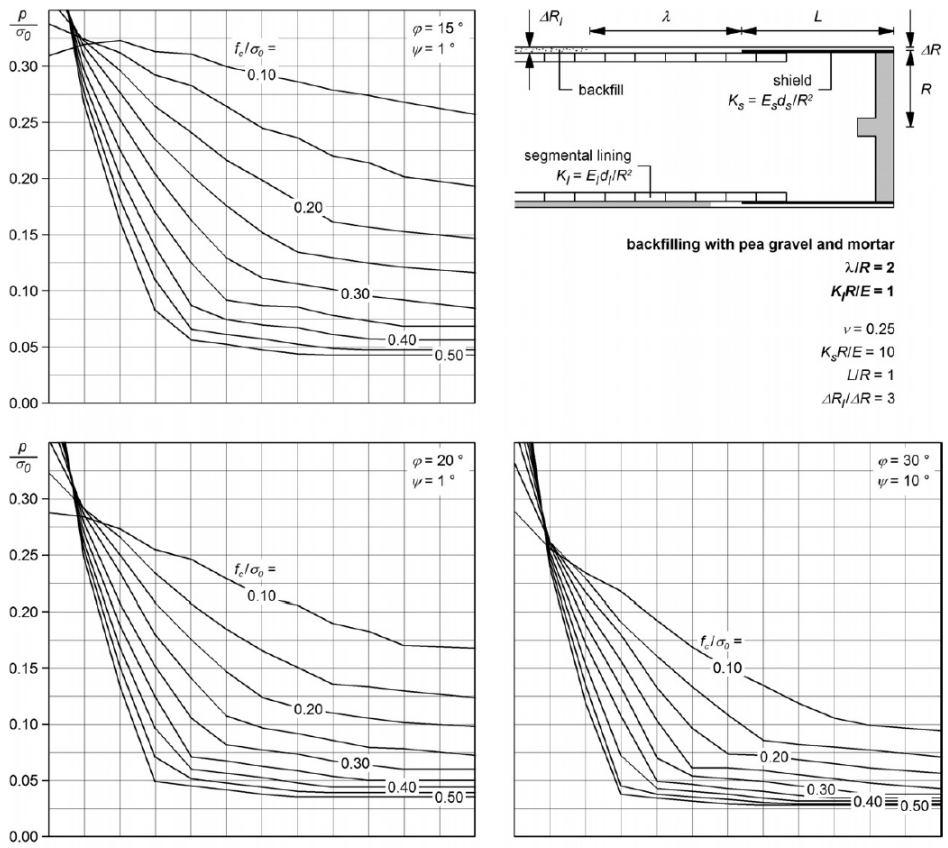

Figure 3.21: One example of nomograms developed for assessment of the final load on the segmental lining by Ramoni et al. (2011) [80].

This time the support pressure calculated by the parametric study (P_{2D}) is employed to obtain the maximum circumferential principal stress on the segmental lining as follows:

$$sig1_{max_{2D}} = \frac{2.P_{2D}}{\left[1 - \frac{(R_c - t_c)^2}{R_c^2}\right]} \tag{3.14}$$

A major drawback of both the analytical method and the 2D pre-conducted modelling method is that they only consider the compressive strength of the support system, while neglecting its tensile strength. In many cases, the failure of the support system is due to bending moments stemming from anisotropy in the stress state and inhomogeneity of the rock mass. To address this shortcoming, Ramoni et al. (2011) recommended employing a higher safety factor while evaluating the structural integrity of the segmental lining to consider the bending moments [80]. To give an example, they state that a lining with a 10-meter diameter, 50-cm thickness, and 0.4 percent reinforcement content may withstand around 45 percent less stress if

the loading is not uniform and has a ratio of 1.2 (highest to lowest radial pressure). Thus, considering a safety factor of around 2 can include this effect. The damage risk quantity will be evaluated by dividing the product of $sig1_{max}$ and a safety factor of SF_{sig1} by the compressive strength of concrete (f_c) (Equation 3.15). $sig1_{max}$ is chosen as the maximum value of the pre-conducted 2D numerical simulations ($sig1_{max_{2D}}$) as well as the analytical solution ($sig1_{max_{CC}}$).

$$DR_{sig1} = \frac{SF_{sig1}.\max\left[sig1_{max_{2D}}, sig1_{max_{CC}}\right]}{f_c} \tag{3.15}$$

Damage to the segments as a result of the jack load

In addition to the damages pertaining to the ground pressure acting directly upon the segmental lining, another consequence for the support in a shielded TBM is indirect damage caused by excessive pressures from the jacks attached to the segments. The term "indirect" is used because these high thrust forces leading to damage originate from the elevated ground pressures exerted on the TBM shield. To prevent the shield from getting stuck, high thrust forces are applied to the segments.
The mechanisms influencing the magnitude of forces on the segmental lining differ between single-shielded and double-shielded TBMs. In a single-shielded TBM, the thrust cylinders are responsible for both excavating the rock and pushing the machine forward (See Figure 3.22). When the ground has a high degree of squeezing, the shield could get subjected to high pressures, meaning that the shield friction forces will be dominantly controlling the total thrust forces.

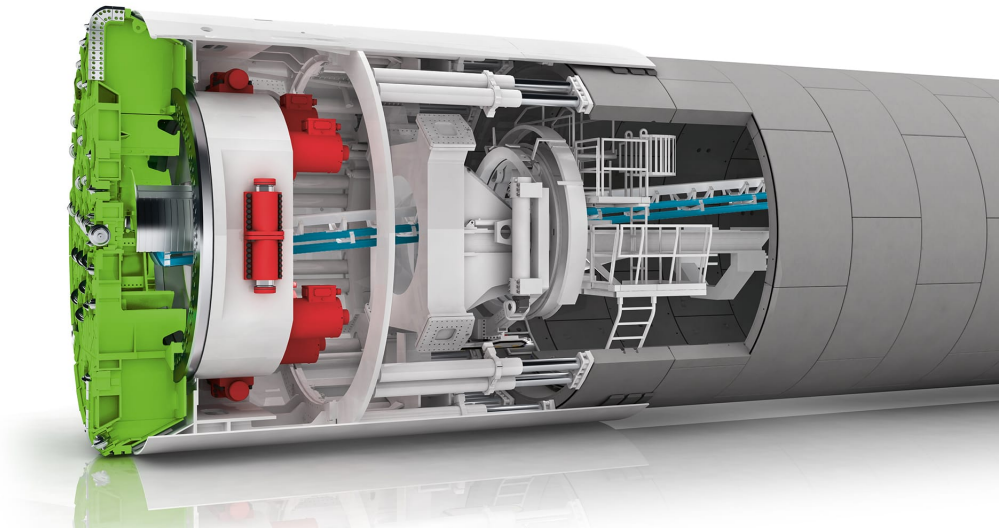

Figure 3.22: The configuration of a single-shielded TBM [93].

As for double shield TBMs, the machine can be operated in two modes: double mode and single mode. In the double mode, two stages are taken for a full stroke advance. Initially, the machine provides the reaction forces needed for excavation and pushing the front shield forward through gripping (by the gripper jacks) (see figure 3.23). Following this stage, the gripper shoes are de-activated and the rest of the machine including the rear shield is pushed forward through the so-called re-gripping mode by dint of the cylinders attached to the segmental lining (See Figure 3.24). In case the pressure acting on the rear shield is high, the thrust forces could be high enough to damage the segmental lining. In certain conditions, where the ground is rather soft, the gripping must be avoided to prevent too much disturbance to the ground. Besides, it is sometimes the case that the ground fails to provide adequate reaction forces by the gripper shoes for the excavation process. Therefore, the machine is alternatively operated in single mode similar to the single shield TBMs. The single-mode excavation technique is introduced as one of the principal pragmatic approaches for passing through squeezing regions. In this technique, two main procedures are followed. Thrust jacks are completely deactivated, and the telescopic shield part of the machine gets closed. Consequently, the excavation process is conducted discontinuously with intermittent excavation and segment installation processes. Under these circumstances, the TBM advances only by means of auxiliary

jacks (See Figure 3.25). Due to the capability of single-mode excavation in reducing the contact area between the machine and the squeezing ground, this technique is regarded as an efficient method for passing through the squeezing regions [71]. In such cases, the auxiliary cylinders could impose excessive pressures on the segmental lining causing damages.

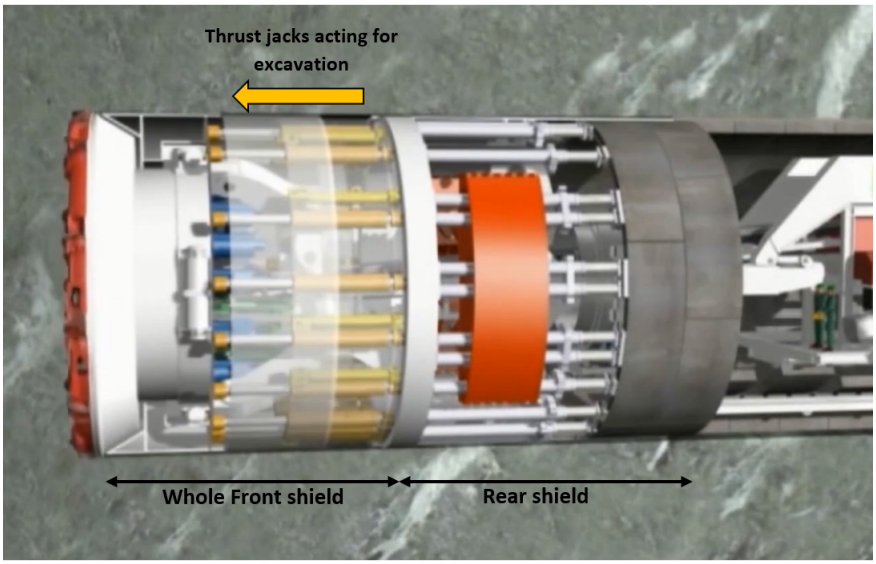

Figure 3.23: The initial stage of excavation using double shielded TBMs in double mode by gripper shoes for providing the reaction forces (red colored means activated gripper shoes.)[94].

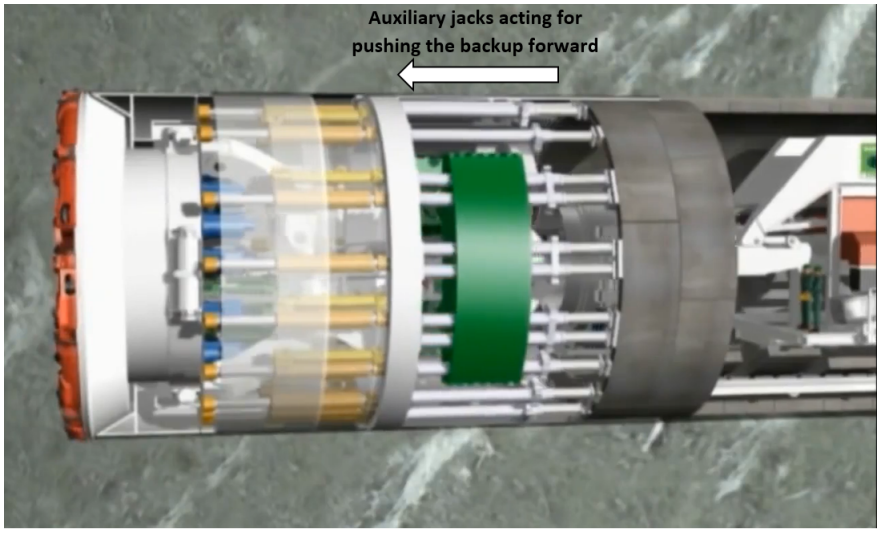

Figure 3.24: The secondary stage of excavation using double shielded TBMs in double mode by the auxiliary cylinders attached to the segments (green colored means deactivated gripper shoes.[94].

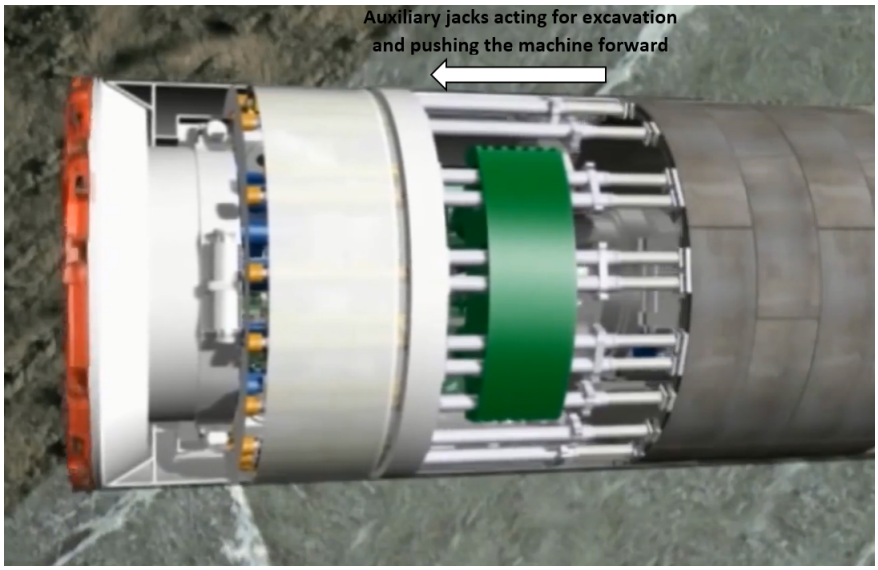

Figure 3.25: Excavation using Double Shield TBMs in the so-called single mode (green colored gripper shoes means deactivated grippers)[94].

In order to estimate these consequences, we need to have an approximation of the thrust forces acting on the segmental lining. The same procedure adopted for the assessment of the jamming risk is applied to calculate the indirect squeezing pressure acting on the segments. Different scenarios can take place, whether the single mode or double mode is employed for excavation. Moreover, the forces needed to be provided by the cutterhead for excavation can be calculated according to the tunnel face rock strength and the cutterhead characteristics and added to the shield friction forces.

As indicated in Figure 3.26, depending on their number, jacks will be pushing against the segments at certain distances. As a result, high compressive stresses might develop underneath the jack pads leading to compressive failure. In addition, high bursting stresses leading to tensile failure are also likely to occur deep into the segment. Each of these events will be discussed accordingly in the next section.

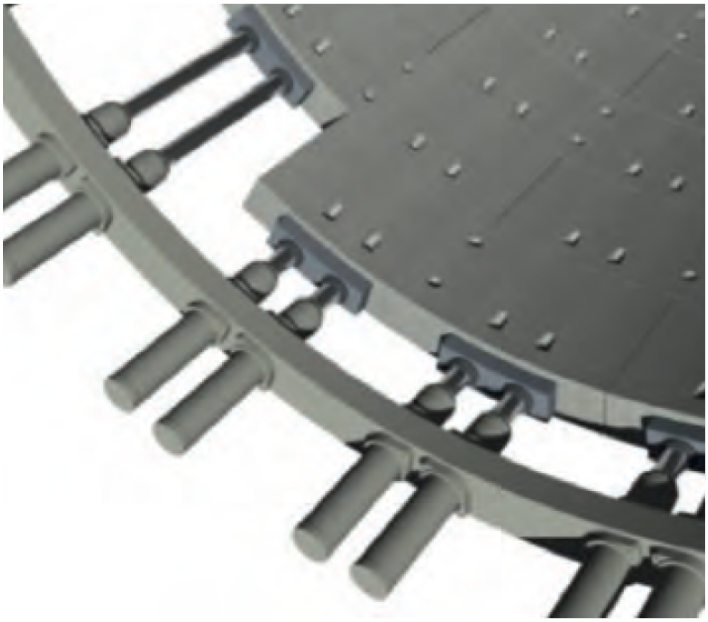

Figure 3.26: Thrust jacks of a shielded TBM pushing on circumferential joints [95].

The compressive stresses on the point load of the jacks

Primarily, the nominal bearing strength of the segments needs to be compared with the maximum compressive stresses from the jacks. ACI 318 puts forward some recommendations to calculate the nominal bearing strength of the segments depending on the geometry of the bearing area [96]. According to Figure 3.27, in case the supporting surface (A2) is wider compared to the jack load surface (A1) on all sides, the lowest value of the equations 3.16 and 3.17 should be used to evaluate the nominal bearing strength of the concrete (B_n) against compressive stresses.

$$B_n = \sqrt{A_2/A_1}\,(0.85 f_c) \tag{3.16}$$

$$B_n = 2\,(0.85 f_c) \tag{3.17}$$

where f_c is the compressive strength of the concrete.
In other cases, the nominal bearing strength (B_n) would be calculated by the following equation:

$$B_n = 0.85 f_c \tag{3.18}$$

Parameter A_2 as the lower base of the largest frustum of the pyramid in Figure

3.27 is calculated using the following formula:

$$A_2 = A_1 + \frac{(L_1 + L_2)C}{2} \tag{3.19}$$

where L1 and L2 are the perimeters of the upper and lower bases, respectively and C is the slant height of the frustum.

In order to evaluate the maximum compressive stress resulting from the jacks on the segments (JC), the shield frictional force as the main portion of the force is divided by the number of jacks and the effective area of the shields as in equation 3.20. Finally, equation 3.21 is used to determine the damage risk quantity due to the compressive stress of jacks. Note that the concrete cover (c_t) on both sides needs to be subtracted from the jack's width (J_W).

$$JC = \frac{F_f}{J_{no}.J_L.(J_W - 2c_t)} \tag{3.20}$$

$$DR_{JC} = \frac{JC}{B_n} \tag{3.21}$$

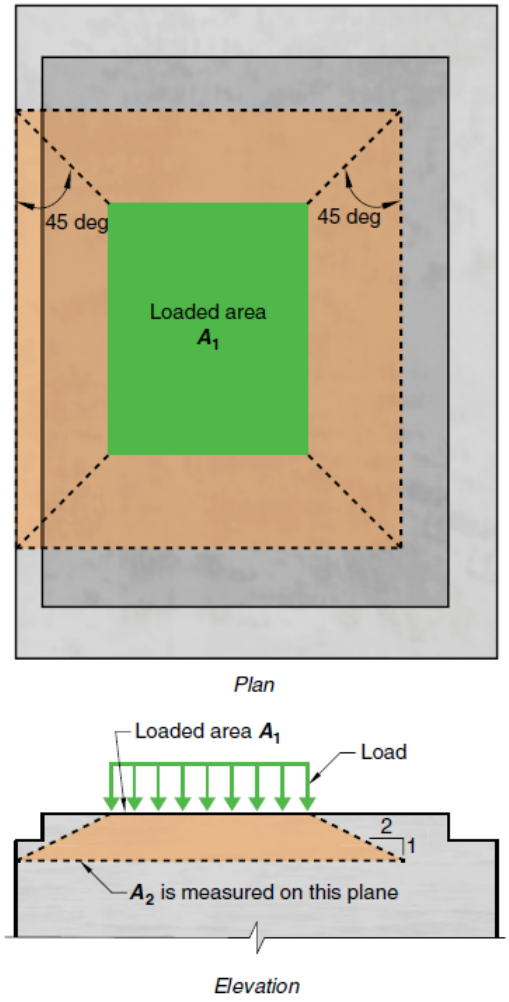

Figure 3.27: Using frustum to calculate A_2 in a concrete segment [96].

Deep-seated bursting tensile stresses in the segment

As previously mentioned, the presence of high compressive stresses can result in considerable bursting tensile stresses deep into the segments. Equation 3.22 can be utilized to estimate the bursting force (T_{burst}). For a better recognition of the parameters and their corresponding relevance, refer to Figure 3.28.

$$T_{burst} = 0.25 P_{pu} \left(1 - \frac{h_{anc}}{h}\right) \tag{3.22}$$

P_{pu} is the force from an individual jack; h_{anc} is equivalent to the length of the jack; and h is the effective length of the segment or the depth of the prism.

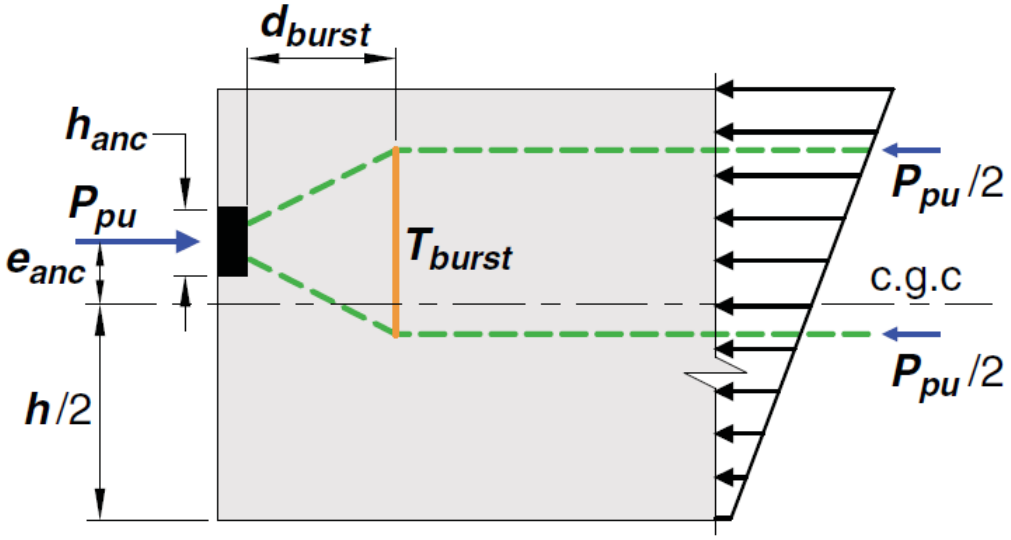

Figure 3.28: The parameters used for calculation of the bursting stresses from a concentrated load on a concrete [96].

To prevent transverse tensile cracking in concrete, sufficient reinforcing rebar needs to be provided in the segments. The longitudinal tensile strength ($T_{b_{max}}$) with the existing reinforcements in the segments can be calculated by the allowed steel tensile stress (σ_s) as shown in equation 3.23.

$$T_{b_{max}} = \frac{\sigma_s . A_{sb}}{SF_{T_b}} \tag{3.23}$$

where A_{sb} is the cross-section of the rebar reinforcements and SF_{T_b} is a safety factor. Reinforcing rebars in this method are placed in horizontal and vertical directions. The transversal rebar calculated through this method needs to be placed in all the zones where there are cracking potentials. Thus, the cross-section of the steel A_{sb} must be uniformly distributed at a distance of $0.2D_e$ to D_e from the end of the loading surface.

Eventually, the damage risk pertaining to bursting tensile stresses can be calculated as follows:

$$DR_{T_b} = \frac{T_{burst}}{T_{b_{max}}} \tag{3.24}$$

Categorization of the extent of the damage to the support system

To simplify the final risk evaluation procedure, the maximum value of the three damage risk indices introduced in this section (DR_{sig1}, DR_{JC}, and DR_{T_b}) will be selected as a conservative estimate for the damage risk (See equation 3.25).

$$DR = max\left[DR_{sig1}, DR_{JC}, DR_{T_b}\right] \tag{3.25}$$

Similar to the jamming risk, a classification rule for the support damage risk is also developed as follows:

$DR \geq 1$ Very high support damage risk

$0.8 \leq DR < 1$ High support damage risk

$0.5 \leq DR < 0.8$ Medium support damage risk

$0.3 \leq DR < 0.5$ Low support damage risk

$DR < 0.3$ Very low support damage risk

3.2.3 The gripper bracing difficulties

Another consequence of TBM tunneling in squeezing grounds, specifically affecting TBMs equipped with gripper shoes, is their inability to generate the necessary reaction forces for propelling the machine forward. Gripper TBMs rely on bracing the grippers against the ground to supply the essential thrust forces for cutting the rock, overcoming possible frictional forces between the ground and the shield and also pushing the machine components forward. Double shield TBMs are also equipped with gripper shoes that are preferably applied most of the time to take advantage of the double shield excavation mode with higher advance rates. The gripper bracing issues emerge when the rock is too weak and is unable to provide the required reaction forces in the gripper shoes. Furthermore, as mentioned by Wittke (2007), in fractured rock masses, the application of gripper forces induces transverse tension leading to a reduction in the tangential forces in the surrounding rock mass and possible loosening of rock blocks on the roof of the tunnel [97].

In this section, the methodology to estimate the gripper shoes' reaction forces based on the rock mass properties and the machine characteristics is explained. By comparing these values to the excavation requirements, another index for quantifying the gripper bracing difficulties can be introduced. Figure 3.29 illustrates how the gripper shoes of a TBM act as an abutment for the summation of the thrust forces and the torque generated by the excavation by pressing against the ground. The excavation thrust and torque values depend on the disc cutter forces and can be evaluated according to the rock mass conditions and the machine characteristics. Figure 3.30 shows different types of forces exerted on one disc cutter. One of the most frequently used formulas for the estimation of cutting forces acting on CCS (Constant Cross Section) disc cutters is the Colorado School of Mines (CSM) model, which estimates cutting forces using the following equations [98]:

$$\varphi = cos^{-1}\left(\frac{R-p}{R}\right) \tag{3.26}$$

$$P_0 = C.\sqrt[3]{\frac{s}{\varphi\sqrt{R.T}}.\sigma_c^2.\sigma_T} \tag{3.27}$$

$$F_t = \frac{P_0.\varphi.R.T}{1+\psi} \tag{3.28}$$

$$F_N = F_t.\cos(\varphi/2) \tag{3.29}$$

$$F_R = F_t.\sin(\varphi/2) \tag{3.30}$$

where F_t is the total resultant force (kgf); R is the radius of cutter (cm); T is the width of disc cutter (cm); ψ is the constant for pressure distribution function which for CCS disc cutters is closer to zero; φ is the angle of contact area between the rock and disk cutter in radian; p is the penetration per revolution (cm); The pressure of the crushed zone, denoted as P_0, is an estimation derived from the rock strength and the cutting geometry (kg/cm2); σ_c is the uniaxial compressive strength of the rock (kg/cm2); c = 2.12; σ_t denotes the tensile strength of the rock (kg/cm2); and s represents the spacing between the cutters (cm).

Figure 3.31 illustrates the involved geometrical parameters of a disc cutter.

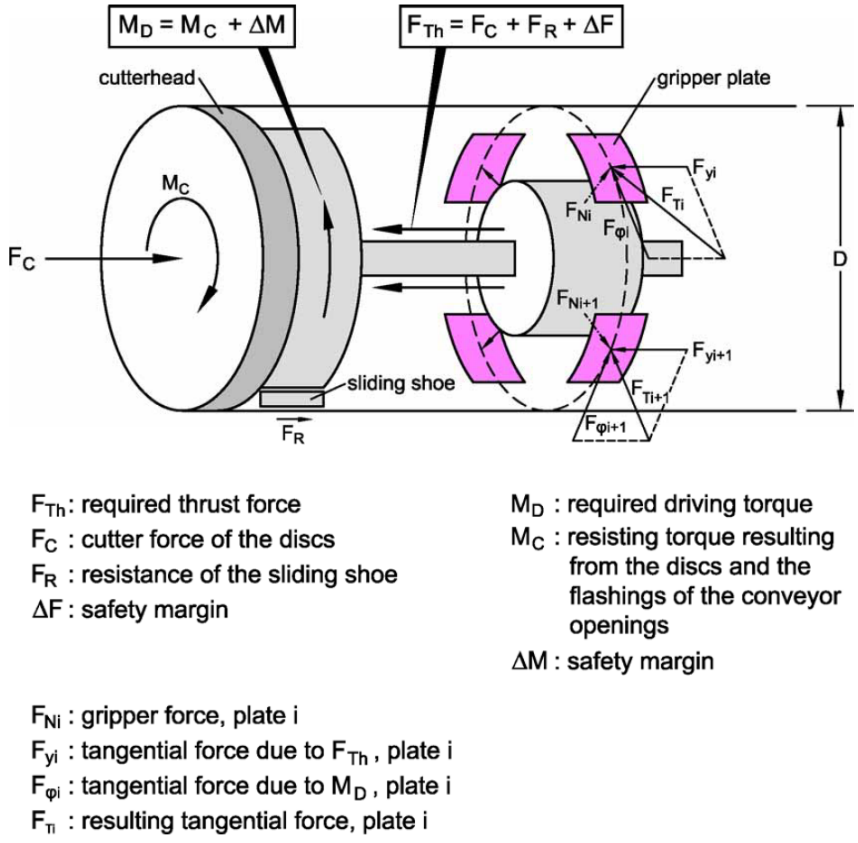

Figure 3.29: The required thrust force, torque as well as gripper bracing force in a gripper TBM [97].

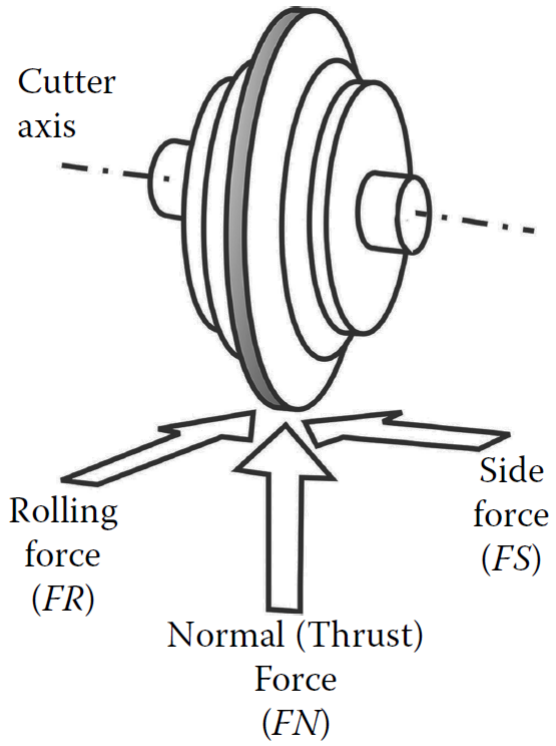

Figure 3.30: Different types of forces on a disc cutter [98]

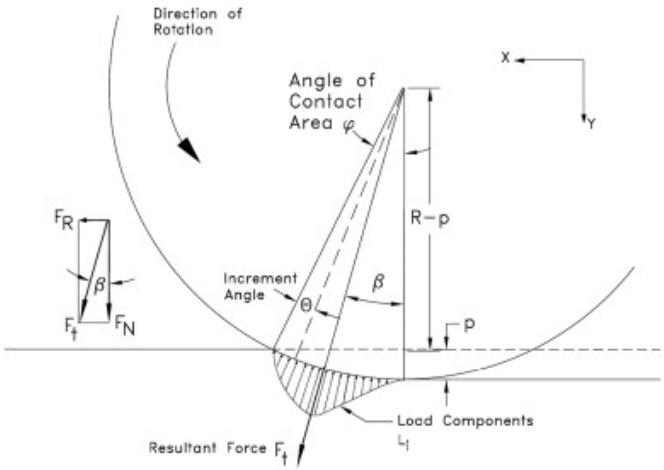

Figure 3.31: Illustration of geometrical features of disc cutters affecting the pressure distribution [99]

The excavation thrust force can be determined by multiplying the number of disc cutters by the average normal force on each disc cutter (F_N). As mentioned earlier, depending on the type of the TBM, the excavation thrust force and the shield frictional force are applied to estimate the required thrust force to be provided by the gripper shoes. The cutterhead torque value can also be estimated by the following

equation:

$$\text{Torque } = \sum_{i=1}^{n} r_i \cdot F_R \tag{3.31}$$

Where r_i is the distance of a cutter to the center of the cutterhead and F_R is the rolling force value of a cutter. The total thrust force and torque bring about tangential forces in the gripper plates. By knowing the tangential force and the extent of friction between the gripper shoe and the ground, a preliminary estimation of the required gripping force can be carried out.

According to Figure 3.29, the amount of thrust force per gripper shoe (F_{yi}) representing the longitudinal component of tangential force can be evaluated by dividing the total required thrust force by the number of gripper shoes as follows:

$$F_{yi} = \frac{F_{Th}}{k} \tag{3.32}$$

where k is the number of gripper plates. The circumferential component of the tangential force caused by the driving torque is calculated according to the following equation:

$$\mathrm{F}_{\varphi i} = \frac{M_D}{\mathrm{k} \cdot \mathrm{R}} \tag{3.33}$$

where R is the tunnel excavated radius. The total tangential forces generated in each gripper shoe will be estimated as follows:

$$\mathrm{F_{Ti}} = \sqrt{\mathrm{F_{yi}}^2 + \mathrm{F}_{\varphi i}{}^2} \tag{3.34}$$

The gripper shoes will be acting against the ground with a pushing force of F_{Ni} to overcome the total thrust force together with the friction between the gripper shoe and the ground. The following equation can be used for this purpose to calculate the necessary gripping force in each gripper shoe.

$$F_{Ni} = \frac{\eta_p . F_{Ti}}{\mu_A} \tag{3.35}$$

where η_P is the safety factor and μ_A is the friction coefficient between the rock mass

and steel.

In order to evaluate the extent of the gripper bracing difficulties in weak grounds, we need to answer the following questions:

1. Is the rock underneath the gripper shoe strong enough to provide a reaction force equivalent to F_{Ni}?

2. Can a high gripper shoe force trigger instabilities on the roof by loosening the wedges?

A numerical investigation, due to its capabilities in computing the stress redistribution following the excavation and the gripper shoe force exertion, as well as the introduction of geological boundaries and discontinuities (mainly for the second question), is highly preferred for this purpose. However, due to the nature of this study in providing a quick and more straightforward procedure, we will be focusing on answering the more critical first question through an analytical process. The strength of the rock in the immediate vicinity of the gripper shoes depends on the residual strength of the rock and the extent of confining pressure. By assuming a certain failure criterion (Mohr-Coloumb or Hoek-Brown), we can estimate the gripper bracing strength of the rock mass (σ_{gs}) using equations 3.36 and 3.37, respectively.

$$\sigma_{gs} = \sigma_{c_{res}} + \sigma_3 \frac{1 + sin(\varphi_{res})}{1 - sin(\varphi_{res})} \tag{3.36}$$

$$\sigma_{gs} = \sigma_3 + \sigma_{ci}(m_{b_{res}} \frac{\sigma_3}{\sigma_{ci}} + s_{res})^{a_{res}} \tag{3.37}$$

Following the excavation of a certain length of the tunnel by the TBM, stress is redistributed and the immediate rock where the gripper shoes are going to pressurize has already failed. Therefore, the residual strength parameters of the rock mass are taken in the above formulations. The variable σ_3 in the above formulations is the confining pressure of the rock mass i.e., the residual tangential stress of the immediate vicinity of the tunnel following excavation. One simplification in the process can be assuming that the rock exhibits perfectly plastic behavior, meaning that the residual and peak parameters are the same values. In this case, the confining

pressure of the rock can be assumed as equal to the compressive strength. This assumption needs to be made with caution as it can underestimate the consequence extent eventually. Thus, it makes sense to add a certain factor of safety or use numerical analysis where there is a significant concern. To be conservative we can ultimately ignore σ_3 in the above formulations and assume unconfined strength of the rock mass as the gripper bracing strength. Figure 3.32 shows the interaction of the gripping pressure and the confining pressure in the ground.

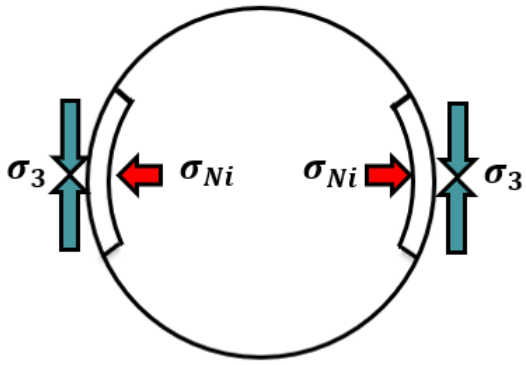

Figure 3.32: The interaction of the gripping pressure from gripper shoes (σ_{Ni}) and the existing ground confining pressure (σ_3)

Once the triaxial strength of the rock mass is determined, the ratio of the required gripper shoe force pressure (σ_{Ni}) (Equation 3.38) to the gripper bracing strength of the rock mass can be calculated to define a new factor called here the gripper bracing difficulty extent (GR). This factor quantifies the severity of gripper bracing difficulties, according to Equation 3.39, and provides a measure of the impact caused by the challenges in gripper bracing.

$$\sigma_{Ni} = \frac{F_{Ni}}{A} \tag{3.38}$$

where A is the area of the gripper shoe.

$$GR = \frac{\sigma_{Ni}}{\sigma_{gs}} \tag{3.39}$$

Based on the following approach, the resulting GR values can be qualitatively cat-

egorized.

$GR \geq 1$ Very high gripper bracing risk

$0.8 \leq GR < 1$ High gripper bracing risk

$0.5 \leq GR < 0.8$ Medium gripper bracing risk

$0.3 \leq GR < 0.5$ Low gripper bracing risk

$GR < 0.3$ Very low gripper bracing risk

3.3 Evaluation of the consequences of rockburst for TBM tunneling

Estimation of the rockburst risk according to the methodology explained in Chapter 2 requires an initial identification of the potential consequences based on the type of TBM, prioritizing the consequences based on their significance according to Table 3.4, and estimation of the extent of the consequences. Due to the high complexity of rockburst and the dependence of its occurrence on many parameters, the quantification of the consequences will be different compared to the squeezing risk. The rockburst degree or intensity needs to be primarily estimated using methods introduced in Chapter 2. Subsequently, the criterion in Table 3.16 is employed to offer a quantity to each consequence j (RB_j). Each rockburst consequence j also needs a significance factor (W_{RB_j}) to take into account the relevance of that consequence to the specific TBM used.

Table 3.16: The categorization of rockburst consequence extent based on the rockburst degree

Rockburst degree	The Consequence extent	The consequence quantity RB_j
No Rockburst	Insignificant	1
Light Rockburst	Minor	2
Medium Rockburst	Moderate	3
Heavy Rockburst	Major	4
Serious Rockburst	catastrophic	5

An important objective of this study from the beginning was to comprehend the mutual correlation between the use of a TBM as the excavation method and the resulting consequences. With regards to the rockburst consequences, the mechanical method of excavation using a TBM would cause the minimum disturbance in the rock mass which consequently affects the extent of rockburst intensity. Be-

sides, the specific features of a certain type of TBM e.g., the shield geometry, the support system type and characteristics, etc., and their relevance to the location and intensity of rockbursts need to also be considered when assessing the extent of the consequences. The place where the rockburst takes place and its interactions with different components of the machine, and the susceptibility of equipment and personnel to the incidents are among others, important indicators for the evaluation of the rockburst consequences.

3.3.1 Considering the effect of the excavation method on the consequences of rockburst

Among the explained methodologies for rockburst prediction in Chapter 2, the first group of empirical methods accounting for the stress state and the rock strength are considered the most frequently utilized ones. They are especially suitable for the first stages of design and the risk assessment process before the onset of excavation, as the effective parameters are simpler to gather and the calculation process is more straightforward to conduct. The second set of methods that calculate the brittleness characteristics of the rock can also act as a side method for the determination of the potentiality of the rock to gain significant amounts of energy. A combination of the first two sets of methods is, therefore, both simpler and helpful.

The third set of methods related to energy release characteristics of an excavation usually requires higher amounts of data with higher accuracy. These data are usually more feasible to access after the onset of excavation. Therefore, in a risk assessment process, they can be quite helpful in updating the assessment results and modifying the extent of risks in the next design stages.

It is important to acknowledge that many of these formulations and methodologies were developed from case studies where drilling and blasting was the main excavation technique. Consequently, it is necessary to recognize the potential limitations when applying these methodologies to mechanically excavated tunnels. In the following sections, some of the most important impacts including the minimal disturbance to the rock mass due to mechanical excavation, the continuity of mechanical excavation

as opposed to the sequential nature of drilling and blasting, and the influence of tunnel shape as the key differences between the two excavation methods are elaborated upon [100].

The effect of disturbance and damage caused by blasting

The degree of disturbance in the rock mass brought about by the drilling and blasting technique distinguishes it from mechanical excavation. Mechanical excavation is known for causing little disturbance in the surrounding rock mass, in contrast to blasting. The stability of the structure could be negatively impacted. However, this disturbance can have even a beneficial effect in deep excavations with high-pressure hazards by releasing stored strain energy in the tunnel wall and face, lowering local stresses, or moving high stresses away from the tunnel face and walls. A forced change in the strength and stiffness of the nearby rock mass has a positive effect as well by lessening its capacity to store elastic strain energy and reducing the likelihood of rockburst.

The disturbance factor in the Hoek-Brown criterion (D) represents the degree of disturbance made by blasting, excavation, or stress relaxation in a rock mass (Carranza-Torres et al. 2002). This factor is used to calculate the m_b, s, and a parameters of rock mass strength and deformability characterization. The disturbance factor (D) ranges from 0 to 1, with D = 0 indicating undisturbed rock and D = 1 representing a highly disturbed rock mass. The effect can be significant in some cases for the rock mass in the immediate proximity of the tunnel. For instance, for a competent rock mass with GSI = 70, the Young's Modulus of a poorly blasted tunnel (with a high disturbance factor of 0.8) might decrease by more than two times compared to a TBM-excavated tunnel (with zero disturbance). According to the Hoek-Brown criterion (2002), for a 10-meter diameter tunnel, this disturbed zone could extend up to 2-3 meters inside the surrounding rock mass. When a deep tunnel is excavated by blasting, the pre-fractured zone of rock can be beneficial by releasing part of the stored strain energy in the rock mass before personnel enters the mining area.

The continuity of mechanical excavation

Another effect that differentiates mechanical excavation from drilling and blasting is the continuity of mechanical excavation. In drilling and blasting operations, excavation advances in rounds and intermittently, while mechanical excavation proceeds in a continuous manner. In contrast to mechanical excavation, each blasting round can eliminate roof support over a larger area, possibly going beyond the immediate roof's capacity and leading to relaxation. This situation could also trigger high-energy seismic events in extreme cases. However, the absence of working personnel during these events decreases the exposure of workers and equipment to hazards and leads to fewer hazards.

The tunnel shape effect

The shape of the excavation is another important feature when using prediction tools for rockburst prediction. While some drilling and blasting operations especially in mining produce square-shaped tunnels, TBM excavations are naturally circular. The development of plastic zones around the tunnels is affected differently by the two shapes. The higher extent of plasticity around a square-shaped tunnel can be slightly beneficial, as this can result in a greater degree of plastic strain and the release of stored energy following a single excavation round.

Numerical simulation for representing the effects

This section involves a number of preliminary numerical simulations aimed at quantifying the aforementioned impacts. Two 3D elastoplastic FDM models were generated using FLAC3D to examine stress redistributions brought on by mechanical excavation as well as drilling and blasting for a 20-meter tunnel length with 3m of radius in a depth of 2000 m. Initially, 15 meters of the whole length were dug out at once to avoid the effect of confinement of the tunnel face. The first simulation involved continuous progress in a tunnel that was mechanically excavated at intervals of 50 cm for the remaining 5 meters length of the tunnel (see Figure 3.33-a). In the other model representing the blasting approach, the remaining 5 meters were exca-

vated in one stage. Moreover, a disturbed zone with lower rock mass characteristics and a thickness of 1.6 m was presumed to surround the whole blasted tunnel except for the tunnel face (See Figure 3.33-b). The characteristics of the undisturbed and disturbed rock mass are inserted in table 3.17. Upon completion of simulations, the major principal stresses in the middle of the second stage (at +17.5 meters of the total 20-meter length) were measured towards the outer side of the tunnel.

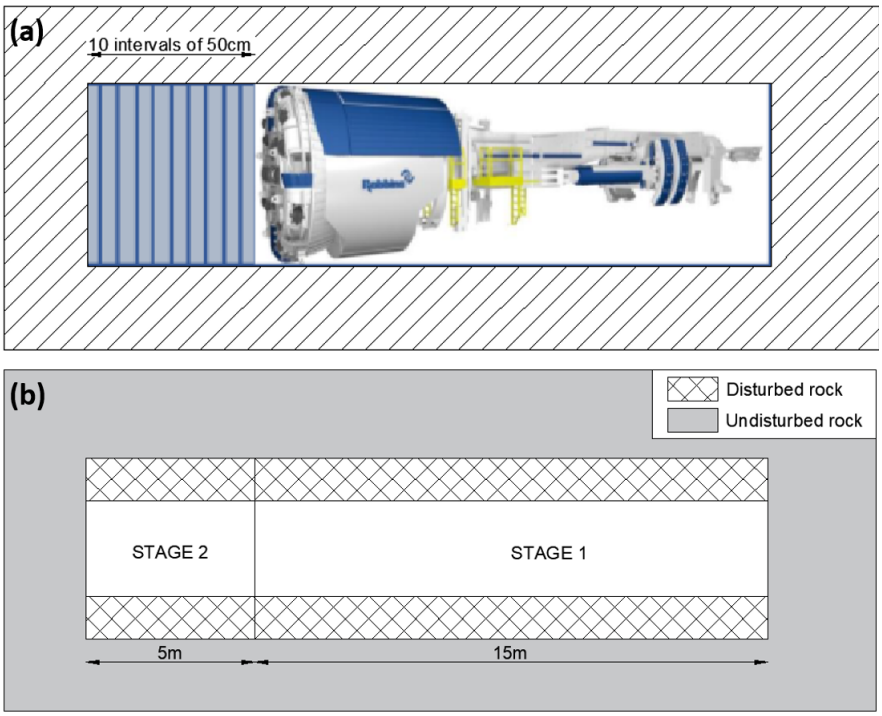

Figure 3.33: The configuration of numerical simulations : a) the TBM-excavated tunnel b) the tunnel excavated using drilling and blasting [100]

Table 3.17: The rock mass properties used for simulation based on the Generalized Hoek-Brown Criterion

Rock condition	GSI	UCS (MPa)	E (Gpa)	Global Strength (Mpa)	m_b	s	a
undisturbed	70	200	44	82	8.563	0.036	0.501
disturbed	70	200	18	56	4.192	0.011	0.501

The major principal stress in the surrounding rock mass as a result of both excavation techniques is shown in Figure 3.34. In the blasting example, the measuring line, which is 1.5 meters long, is totally contained inside the disturbed zone.

The graphs show that the blasted tunnel has much lower stresses than the TBM-excavated tunnel. In particular, the blasted tunnel has a 38% lower stress magnitude in the first 40 cm of the immediate tunnel wall. A 20% average stress decrease can also be seen in the last 1-meter length. It is crucial to keep in mind that this numerical analysis is only a rough estimate and might not adequately account for various phenomena that emerge during the initial fracturing of the rock mass in the disturbed area. Furthermore, in this particular instance, the tunnel environment was assumed to be very poorly blasted. Nevertheless, it provides designers with insight into the potential differences in stress magnitude between the two excavation methods.

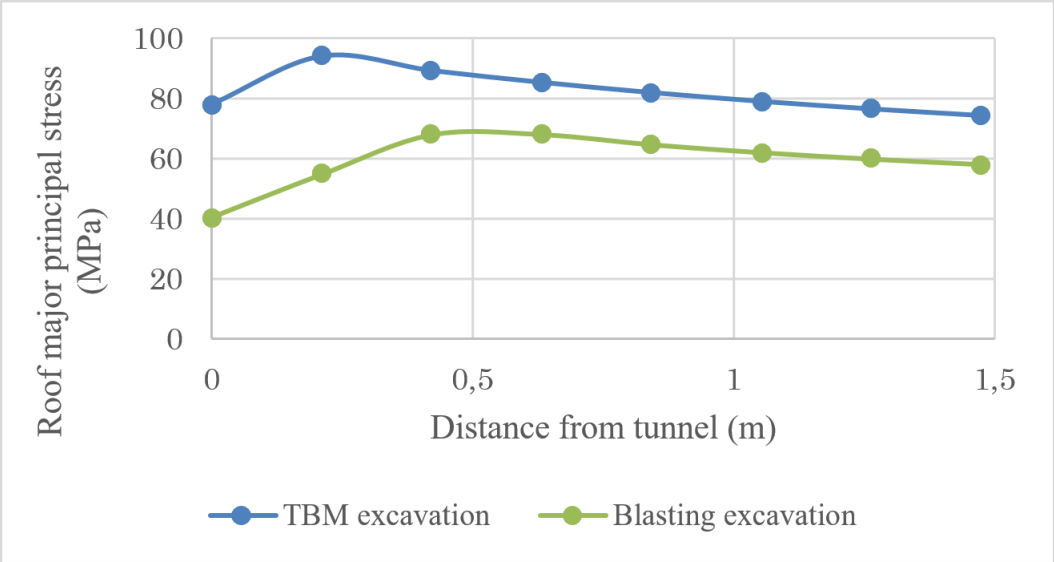

Figure 3.34: Comparison of principal stress variation with respect to the radial distance to the tunnel wall for mechanical and blasting excavation methods [100]

As for the tunnel shape effect, two simplified 2D elastoplastic simulations using FLAC2D (FDM solution) were also conducted. A square and a circular-shaped tunnel were also created in order to better explain how tunnel shape affects the potential release of strain energy. As depicted in Figure 3.35, the sidewalls of a square-shaped tunnel exhibit a greater expansion of the plastic zone than a circular-shaped tunnel.

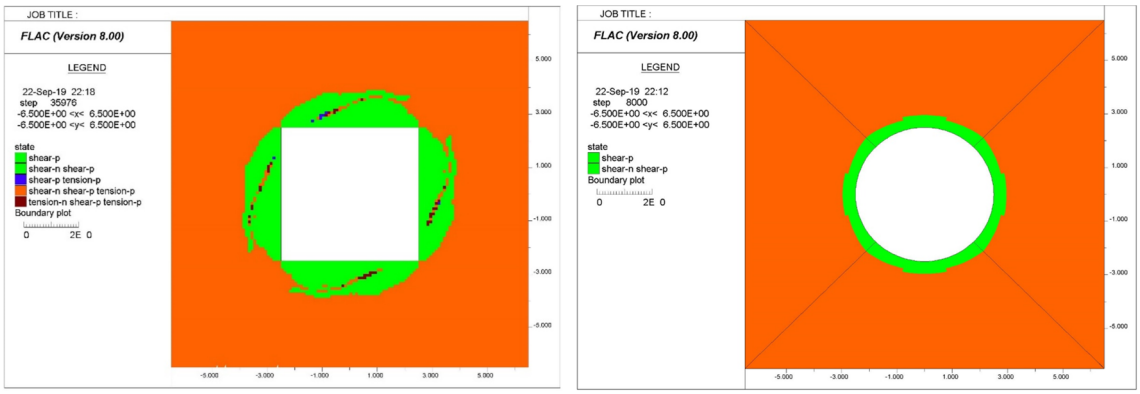

Figure 3.35: The comparison of plastic zone extension for a square-shaped vs. a circular-shaped tunnel [100]

According to the above investigation, the excavation method can have considerable effects on the extent of energy storage around a tunnel. This has different implications for the tunnels coping with rockburst risk. Statistical results derived from the tunnels in the Jinping II hydropower project excavated by TBM and blasting as excavation methods verify this fact [101]. As it is shown in Figure 3.36, the frequency of immediate rockbursts in the No. 2 diversion tunnel excavated by blasting is considerably higher than that in the No. 1 diversion tunnel excavated by TBM. Conversely, the frequency of time-delayed rockbursts displays the opposite characteristics. Most of the rockbursts have taken place in the immediate stage of excavation when there is less exposure of equipment and people for a blasting tunnel. In contrast, time-delayed rockbursts occurring in a TBM excavated tunnel where there is more exposure make rockburst a more critical risk. To conclude, when it comes to a TBM-excavated tunnel, using conventional prediction tools that are largely based on databases of drilling and blasting, it is advisable to err on the side of caution with the predicted results.

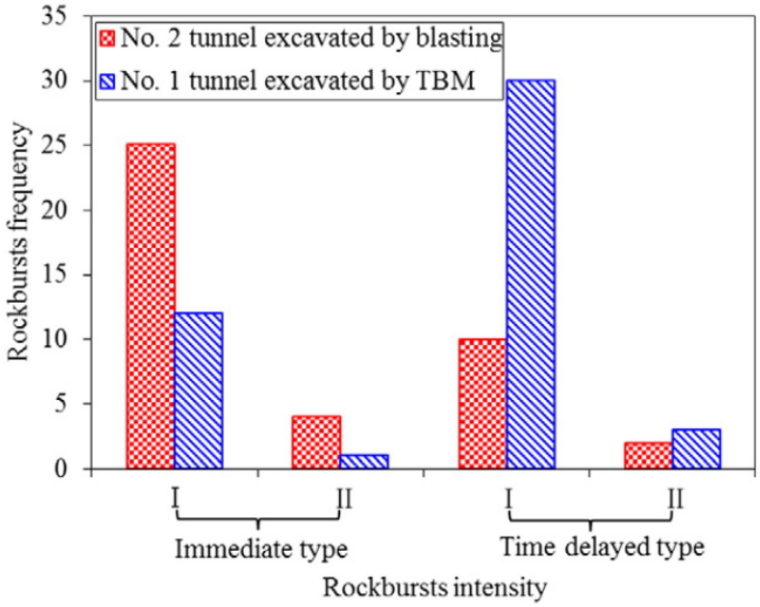

Figure 3.36: The intensity and timing of rockbursts occurring in TBM and blasting excavated tunnels in Jinping II hydropower project [101]

As mentioned before, another very important point to consider for a TBM excavated tunnel is the knowledge of the potential location of rockbursts. Some statistics gained from a TBM excavated tunnel in Neelum–Jhelum Hydroelectric Project has shown that 6.6% of rockbursts occurred on the tunnel face, 37.9% in the first 6m length, 49.5% in the next 4m, and 6% were concerned with the remaining chainages [102]. Figure 3.37 shows an illustration of the gripper TBM applied in the project. The headrace tunnel of the Neelum-Jhelum hydropower was hit by a highly intense rockburst, resulting in three fatalities, 17 injuries, and severe harm to the TBM. As a consequence, the recovery took more than six months before construction could resume. This shows the significance of a risk assessment method that can address or avoid severe consequences.

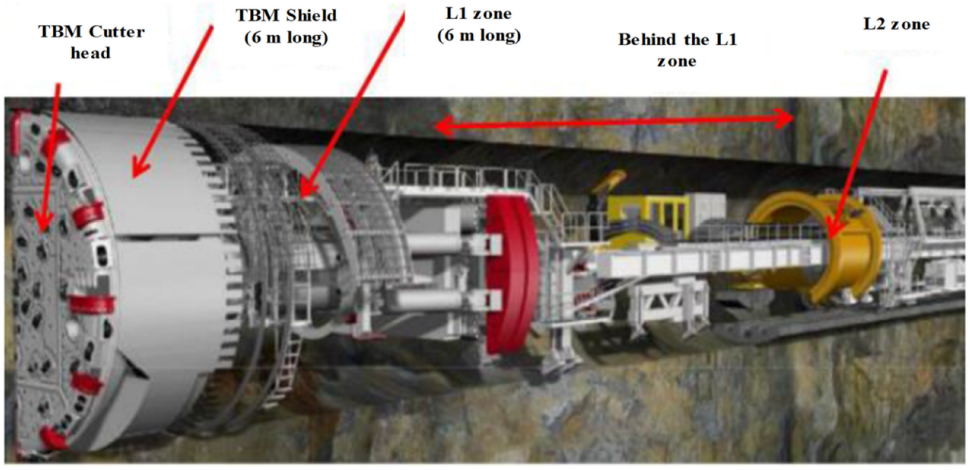

Figure 3.37: An illustration of the gripper TBM used in Neelum–Jhelum tunnel [103]

Rockbursts occurrence at different distances from the tunnel face can have certain consequences ranging from injuries and fatalities to TBM damages. In order to facilitate the quantification process in this probabilistic study, one way can be referring to the statistics data and defining a distribution function that can be applied in a Monte Carlo simulation by a randomized selection of the location of the potential rockbursts. For this purpose, the introduced data in this project is used as a reference and a probability distribution function is fit to the data as shown in Figure 3.38 . Based on the location of the rockbursts predicted through the probabilistic approach, the impacts on the equipment or personnel can be evaluated.

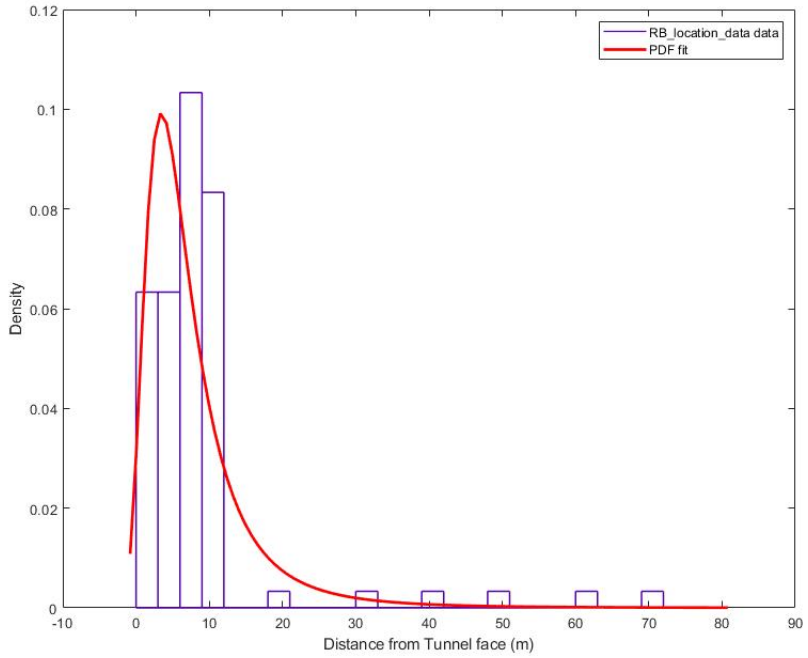

Figure 3.38: The probabilistic distribution function for the rockburst location data from Neelum-Jhelum tunnel

3.3.2 The methodology for obtaining the TBM Rockburst Risk Index

In this section, we will explain the three-step methodology used to evaluate the TBM Rockburst Risk Index.

1. Firstly, based on the existing input parameters, suitable prediction tools are applied for the assessment of the intensity of potential rockbursts. Based on Table 3.4 , the intensity of rockbursts would define the consequence extent.

2. Subsequently, according to an assumed probability distribution function for the possible location of the rockbursts, a Monte Carlo simulation is used for a randomized selection of the distance of the incidence to the tunnel face. The possible location of the rockburst could have certain implications depending on the type of machine and its features e.g., the shield length, and type of support which would determine the extent of exposure of equipment and personnel to hazards. The significance factors of rockburst consequences introduced

in Table 3.4 are once again summarized in Table 3.18 with each numbering representing certain consequences.

Table 3.18: The quantification of the significance factors of rockburst for different consequences

Consequence	Significance (weight factor)
Cutterhead damage (RB_1)	$W_1 = 1$
Shield damage (RB_2)	$W_2 = 1$
Support damage (GTBM) (RB_{3G})	W_{3G}=0.8
Support damage (STBM) (RB_{3S})	W_{3S}=0.8
Equipment damage (RB_4)	W_4=1
Gripper bracing difficulties and cleaning efforts for spalling (RB_{6G})	W_{6G}=0.2
Injury or fatality (RB_5)	W_5=1

In addition to the significance factors, a coefficient is defined to take into account the effectivity of the support system in controlling the rockburst damage. This coefficient called the support mitigation factor (SM) is also between 0 and 1, zero being the most extent of effectiveness, which indicates that support damage would omit the risk. A SM of 1, on the other hand, means the support system would have the lowest effectiveness against damages coming from a rockburst. The magnitude of this factor highly depends on the intensity of the rockburst. For instance, if a heavy rockburst with a consequence quantity is anticipated, stiff segmental lining support would have the poorest performance against controlling the damages and we can assume an SM of 1. The segmental lining as a fixed stiff type of support in a shielded TBM has very low energy absorption characteristics. In fact, the energy absorption

characteristics of stiff and soft support systems differ significantly. Stiff support systems tend to have higher initial stiffness, which means that they can support greater loads without deforming. However, they also have a higher ultimate strength, which means that once they reach their maximum load capacity, they fail suddenly and catastrophically. In contrast, energy-absorbing support systems, such as yielding bolts, cable bolts, or mesh, have lower initial stiffness but greater energy-absorbing capacity, which means that they can deform more readily under load and absorb more energy before reaching failure. This makes them more suitable for use in situations where sudden rockbursts are predicted. An example of a support suitable rockburst prone zones can be a combination of swellex anchors and steel meshes which are finally covered by shotcrete layers.

3. Following the determination of the rockburst location (RB_l), a general criterion is applied by which depending on the type of TBM and its geometrical features and where the rockburst is anticipated, the rockburst consequences can be evaluated. Table 3.19 indicates the criterion and its logic. The consequences for each type of TBM are classified into two groups of damage and time-consuming operations as well as injuries. Since the damages pertaining to the cutterhead (RB_1) exists for any type of machine, it is not included in the logic of this criterion which is based on comparison of the extent of the consequences.

The main parameters inserted in Table 3.19 are described in the following bullet points:

- SL_G, SL_{SS} and SL_{DS} represent the shield length for gripper TBMs, single-shielded TBMs and double-shielded TBMs, respectively.
- Each consequence can be given a mitigating coefficient as a result of the mea-

sures taken to control the consequences. These coefficients are also in the range of 0 and 1, with zero as the highest effect in fully controlling the hazard consequences, and 1 meaning that the measure has no effect in controlling the consequence extent.

- SM_{3G} is the functionality of the support system in a gripper TBM against high-energy events.

- SM_{4G} is the mitigating effect of the support system in a gripper TBM against damages to the machine equipment. This factor is also changing as the support system develops its final characteristics in a gripper TBM.

- SM_{5G} is the mitigating effect of a support system in a gripper TBM against injuries and fatalities.

- It must be noted that the coefficients related to the support system in a gripper TBM (SM_{3G}, SM_{4G} and SM_{5G}) can change as the support system is gradually realized. Therefore, they are not constant.

- Similar parameters are also attributed to single and double-shield TBMs. SM_{3S}, SM_{4S} and SM_{5S} indicate the functionality of segmental lining, the mitigating effect of segmental lining against equipment damage, and injuries and fatalities, respectively. Unlike the support system in a gripper TBM, segmental linings in a shielded TBM are rather fixed structures, meaning that the aforementioned mitigating parameters stay constant. The only thing that might cause changes in their functionality is the time of grouting behind the segmental lining.

Table 3.19: The criterion for evaluation of the TBM rockburst consequences according to the location of the rockburst, TBM type, features and the defined significance factors

The distance of rockburst event (RB_l) (m)	Gripper TBM		SS TBM		DS TBM	
	Damage and time-consuming operation	Injury or fatality	Damage and time-consuming operation	Injury or fatality	Damage and time-consuming operation	Injury or fatality
$0.2 < RB_l \leq SL_G$	$RB_2 + RB_{6G}$	-	RB_2	-	RB_2	-
$SL_G < RB_l \leq SL_{SS}$	$(SM_{3G} \cdot RB_{3G}) + (SM_{4G} \cdot RB_4) + RB_{6G}$	$(SM_{5G} \cdot RB_5)$	RB_2	-	RB_2	-
$SL_{SS} < RB_l \leq SL_{DS}$	$(SM_{3G} \cdot RB_{3G}) + (SM_{4G} \cdot RB_4) + RB_{6G}$	$(SM_{5G} \cdot RB_5)$	$(SM_{3S} \cdot RB_{3S}) + (SM_{4S} \cdot RB_4)$	$(SM_{5S} \cdot RB_5)$	RB_2	-
$SL_{DS} < RB_l \leq 70m$	$(SM_{3G} \cdot RB_{3G}) + (SM_{4G} \cdot RB_4) + RB_{6G}$	$(SM_{5G} \cdot RB_5)$	$(SM_{3S} \cdot RB_{3S}) + (SM_{4S} \cdot RB_4)$	$(SM_{5S} \cdot RB_5)$	$(SM_{3S} \cdot RB_{3S}) + (SM_{4S} \cdot RB_4)$	$(SM_{5S} \cdot RB_5)$

Chapter 4

Introduction of case studies for squeezing and rockburst risks

In the first two sections of this chapter, two separate case studies in which squeezing and rockburst were regarded as the main dominant hazards are studied. The methodologies explained in Chapter 3 for evaluation of the risks are employed for the analyses. Subsequently, several scenarios where both of these sources of risk hold prominence are presented, allowing for an exploration of the suitability and applicability of various types of TBMs in such conditions.

4.1 Introduction of a case study for the squeezing risk assessment

The approximately 10-km-long Golab Water transfer Tunnel (Lot 1) is situated in the western part of the city of Isfahan and its objective is to transfer water from the Zayandehrud river to Kashan. Figure 4.1 shows the roughly 11.5 km long project, which consists of a main tunnel, an access tunnel, a tunnel for water intake, and a cavern for the pumping station. A Wirth 4.5 m diameter Double Shield TBM with the specifications in Table 4.1 was used to excavate the tunnel. Jurassic metamorphic rock units, mostly made up of Phyllite, Slate, and Shale, constituted the majority of the excavation effort. The tunnel faced six shield jamming incidents and partial

lining damage as a result of severe convergences because of the low rock mass quality and high overburden.

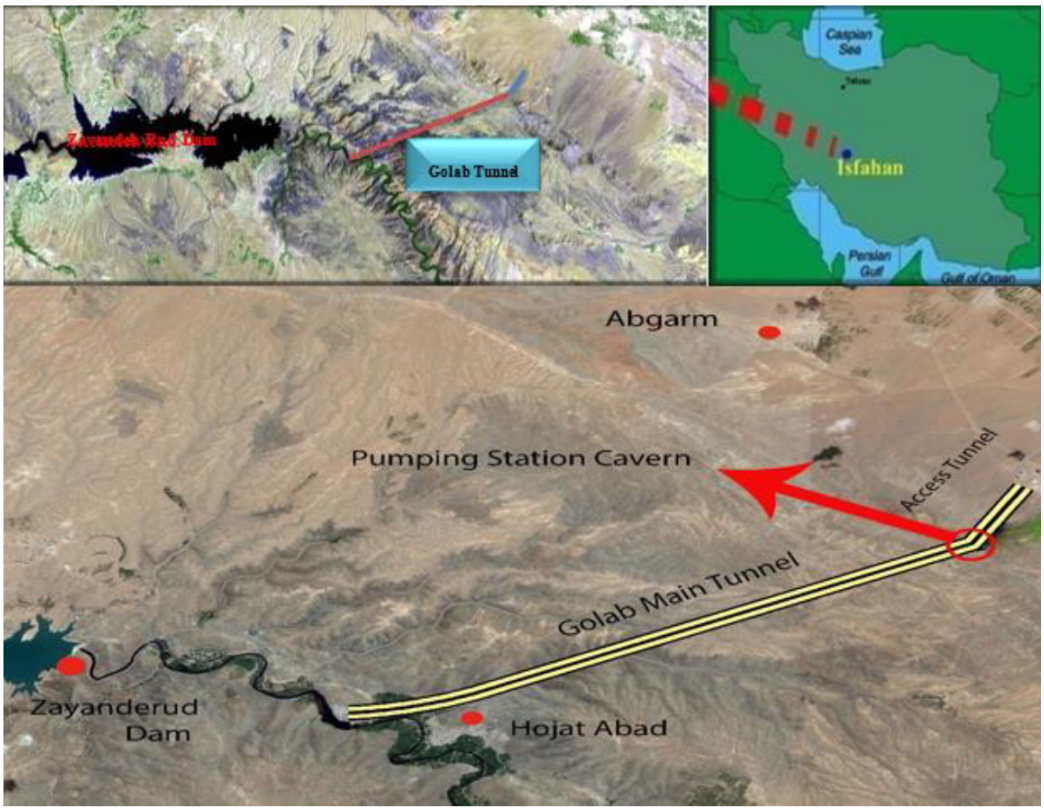

Figure 4.1: An illustration of the different components of Golab project [6]

Table 4.1: The technical specifications of the Wirth TBM - TB 458 E/TS

Parameter	Value
Excavation Diameter	4.53 m
Number of disc cutters	35
Disc cutter Diameter	432 mm
Average Disc Cutter Spacing	75 mm
Max. Cutterhead rotational speed	12 rpm
Max. Cutterhead Torque	802 KNm
Max. Thrust Force	20000 KN
Total Power	1750 KW
Cutterhead Power	1120 KW

The Sanandaj-Sirjan metamorphosed zone, through which the Golab main tunnel is excavated, consists a variety of Schists and igneous rocks at the beginning, slightly metamorphic argillaceous shales in the middle, and limestone and conglomerate at the end of the tunnel (See Figure 4.2). Table 4.2 contains an overall description of the rock characteristics and lithology as determined by field measurements and laboratory tests.

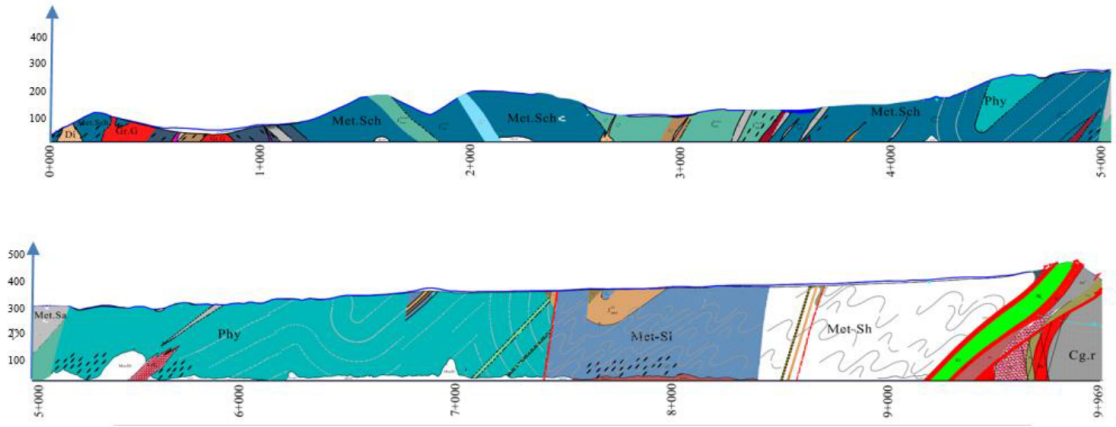

Figure 4.2: The geological profile of Golab main tunnel [6]

Table 4.2: Description of the main formations encountered in Golab tunnel

Lithology description	Lithology	UCS(MPa)	RMR	GSI
Different types of Schists	Met-Sch	20-37	38-40	35-40
Very soft Phyllites	Met-Phy	15-25	30-35	30-35
Very weak and very fine grain Slate with quartz veins	Met-Sl	7-12	29-34	28-34
Greenish gray to dark gray , Schistose meta-sandstone	Met-Sa	25-30	45-47	45-49
Fine to medium grain Microdiorite	Ig-Di	60-65	68-74	62-65
Very low metamorphosed Shale and Sandstone	Met-Sh	9-16	23-30	25-30
Crystallized Limestone and Dolomite	Li	50-60	44-50	44-52
Conglomerate with intercalations of sandstone	Cg.r	70-85	55-62	48-54
Faulty and Crushed zones	FZ , CZ	1-15	10-17	10-20

Primary investigations identified tough squeezing conditions for Slates and Shales located in regions with overburden exceeding 400 meters. Following the excavation in Slates, excessive ground convergences led to shield jamming in various chainages (7+686 km, 7+786 km, 7+819 km, 7+882 km, and 7+920 km). Subsequently, the TBM became also stuck in chainage 8+570 km in the Shales fault zone. Figure 4.3 shows the jamming section in the fault zone of shales and the application of

two-component foams to release the machine. Another consequence of the high convergences was the initiation of cracks in the segmental linings at shield jamming zones, indicating severe squeezing (See Figure 4.4). In the squeezing regions, a combination of ground pressure and regripping pressure from segment jacks was experienced while the shield was being pushed through areas with squeezing potential. During the tunnel excavation, two main mitigating measures were taken to avoid shield jamming: overcutting and increasing the excavation rate. Overcutting can cause stress relaxation before the ground touches the shield leading to lower pressures on the shield. On the other hand, convergence rates in places close to the tunnel face can be decreased by increasing the advance rate. The best progress rate without jamming was fulfilled in weak Phyllites with the potential for squeezing, highlighting the effectiveness of a high excavation rate in avoiding shield jamming. Assuming an average radius of 2.21 m for the shield, an average maximum overcutting of 6cm in radius throughout the shields of the machine could avoid jamming in several sections. Nevertheless, the necessary thrust force was insufficient in a few crucial sections. The most important chainages with harsh consequences of squeezing in Golab tunnel are inserted in Table 4.3 .

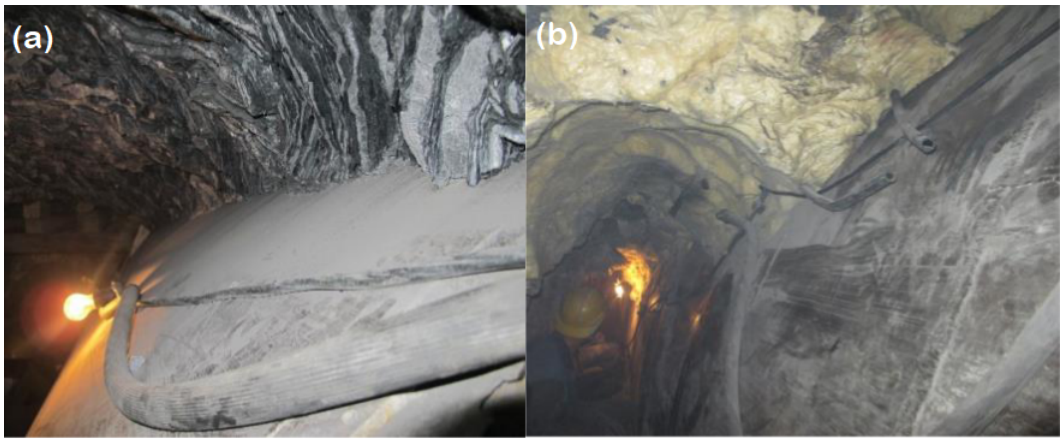

Figure 4.3: The jamming of the shield in Golab tunnel in the fault zone of shales: a) a figure of the squeezed ground; b) Injection of two-component foams for releasing the machine [6]

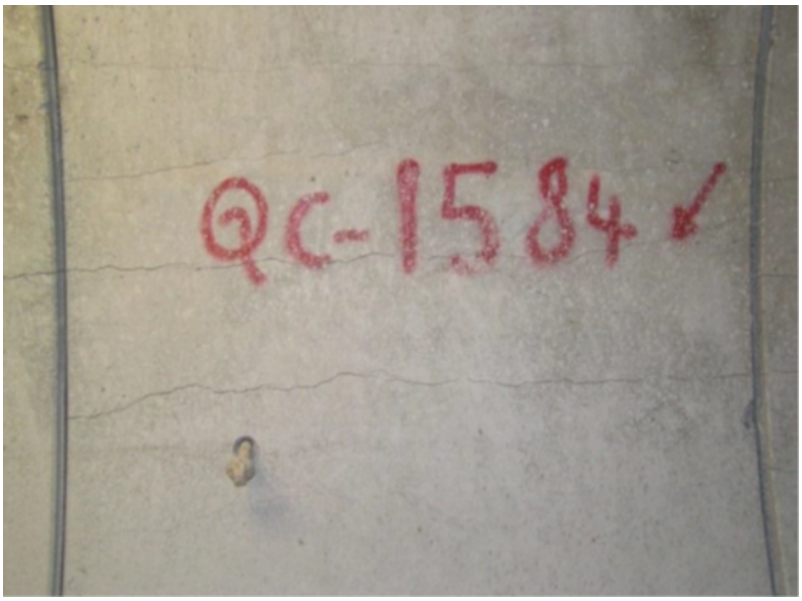

Figure 4.4: The cracking of segments in Golab tunnel due to excessive ground convergences

Table 4.3: A summary of the main chainages encountering consequences of squeezing

Formation	Chainage (m)	Overburden (m)	Squeezing extent	Consequence
Graphite Schist	4500-4800	209-290	Moderate to High squeezing	High regripping pressure and cracking of segments
Phyllite	5235-5340 5470-5480 5713-5720	300-318 320 322	Moderate to High squeezing (more than 10cm)	-
Phyllites and Monzodiorites	6561-6895	367-400		High regripping presssure and cracking of segments
Phillite	7148	385	High squeezing	-
Slate	From 7400 onwards	390-397	High squeezing	Difficulties through passing this region
Slates with graphitic Lense	7694 7786 7819 7882 7920	394-397	High squeezing	5 stoppage of the machine due to jamming 15 to 20 cm of convergence
Fault zone in Shale	8570	416	High squeezing	Jamming of the machine
Fault F.m 38	8942	425	High squeezing	Regripping pressure until 150 bar and passing the region

Following the introduction of the project and the incidents, the methodology for assessment of the squeezing main risks is applied for Golab tunnel. According to the rock mass properties in different sections of the tunnel as well as the stress state (overburden), an approximate length of 6400 m of the whole tunnel where there is sufficient operational data and rock mass characteristics is included in the investigation. In the remaining parts of the tunnel, no squeezing risk was expected. In order to consider the effect of the tunnel depth and stress state, the whole length

was divided into 36 zones consisting of individual rock mass properties and stress states. An example of the rock mass properties from zone 25 (the Slate with graphitic lense) and zone 29 (Meta Shale) where jamming took place is summarized in Table 4.4.

Table 4.4: The rock mass properties for two of the zones where jamming occurred in Golab tunnel

Main Lithology	Statistical parameter	Geotechnical parameters							
		mi	E_i(Mpa)	ν	σ_{ci} (Mpa)	E (Mpa)	GSI	φ	σ_c (Mpa)
Met-Slate (Z25)	Mean (μ)	7	4750	0.35	9.5	1034	31	18	0.88
	Standard Deviation (σ)	1.3	787.5	0.025	1.25	112.4	1.5	2	0.18
Met-Shale (Z29)	Mean (μ)	6	2500	0.34	12.5	968	27.5	17.4	1
	Standard Deviation (σ)	0.67	471	0.017	1.75	97	1.25	1.36	0.16

Tables 4.5 and 4.6 contain the properties concerning the machine performance parameters and the segmental lining, respectively. The average values of these parameters together with the average values of the rock mass properties are initially applied to quickly identify the critical zones for each type of consequence. Subsequently, the probabilistic analysis is conducted in the critical zones to provide a wider and more realistic range of risk quantities for decision-making purposes.

Table 4.5: The machine performance parameters

Radius(m)	L_f (m)	L_r (m)	R_{fsh}(m)	R_{rsh}	μ	Max. Thrust Force (MN)
2.255-2.27	4.4	7.6	2.23	2.19	0.45	20

Table 4.6: The segmental lining poperties in Golab tunnel

		Segmental lining				Backfill	
		Thickness (m)	f_c (MPa)	E_c (MPa)	ν_c	E_f (MPa)	ν_f
Normal segments	Mean (μ)	0.25	35	28200	0.2	90	0.2
	Standard Deviation (σ)	-	0	0	0	30	0
Special segments	Mean (μ)	0.25	40	30200	0.2	90	0.4
	Standard Deviation (σ)	-	0	0	0	30	0

4.1.1 The deterministic analysis of squeezing risks

The primary deterministic analysis is conducted for evaluation of the three main consequences of the squeezing risk: shield jamming, support damage, and gripper bracing difficulties.

Shield jamming risk

To estimate the required frictional forces for preventing shield jamming and the associated risk, two primary methods of analytical and parametric based on pre-conducted 3D numerical simulations are applied. Since the range of values for rock mass properties associated with both Hoek-Brown and Mohr-Coloumb criteria are present, the developed analytical solution using the Carrenza-Torres and the Dancan-Fama closed-form solutions is employed. Figures 4.5, 4.6, and 4.7 show the estimated values of frictional force (F_f) for all the 36 zones by using the aforementioned methods. As can be seen, according to the analytical solution (CC-CT and CC-DF), only for the zones z24, z25, z27, z28, and z29, the ground gets in touch with the shield and frictional forces are evaluated. In contrast, the 3D modeling approach approximates values for all the zones, despite the fact that some of the zones are quite competent and do not develop plastic zones. This shortcoming stems from the developed formulation [87]. This means that the method should be only used for the cases where significant squeezing is anticipated. Therefore, an initial indicator needs to primarily prove the possibility of the risk. The values pertaining

to estimations for the anticipated zones with squeezing are compared to the maximum recorded rear shield friction of the TBM in each zone. As far as the author is informed, the machine was always applied in double shield mode. It should be noted that the regripping pressure encompasses the sum of the shield friction force and the force required to push the backup forward. The amount of pushing force of the backup is assumed to be approx. 20 bar. Therefore, by deducting this value from the regripping pressure, the rear shield friction force is calculated. The maximum recorded rear shield friction forces in each zone are compared to the estimated values and plotted in Figure 4.8. Another important note is that the 3D modeling approach cannot distinguish between the rear shield and forward shield in the case of a double shield TBM, because it is initially developed for a single shielded TBM. Therefore, it considers the whole length of the shield or assumes that the double shield TBM is functioning in single mode, which certainly leads to an overestimation in the values for this case. Since the maximum values are chosen for the recorded actual values, it will be hard to compare the precision of each method with the real condition. This fact can be clearly seen in Figure 4.9, where several times the rear shield friction forces rose and dropped afterward. The red circles in this graph show the spots where the machine was stuck due to jamming. One of the main reasons for this extent of variability is the changes in the ground conditions, which can partially be considered by using a probabilistic analysis through variations in the mechanical properties of the rock. This will be done in the next section of this chapter. Another principal reason could be the changes in the excavation rate which can affect the influence of time-dependent deformations on the shield jamming. This phenomenon is beyond the scope of this research and is not considered.

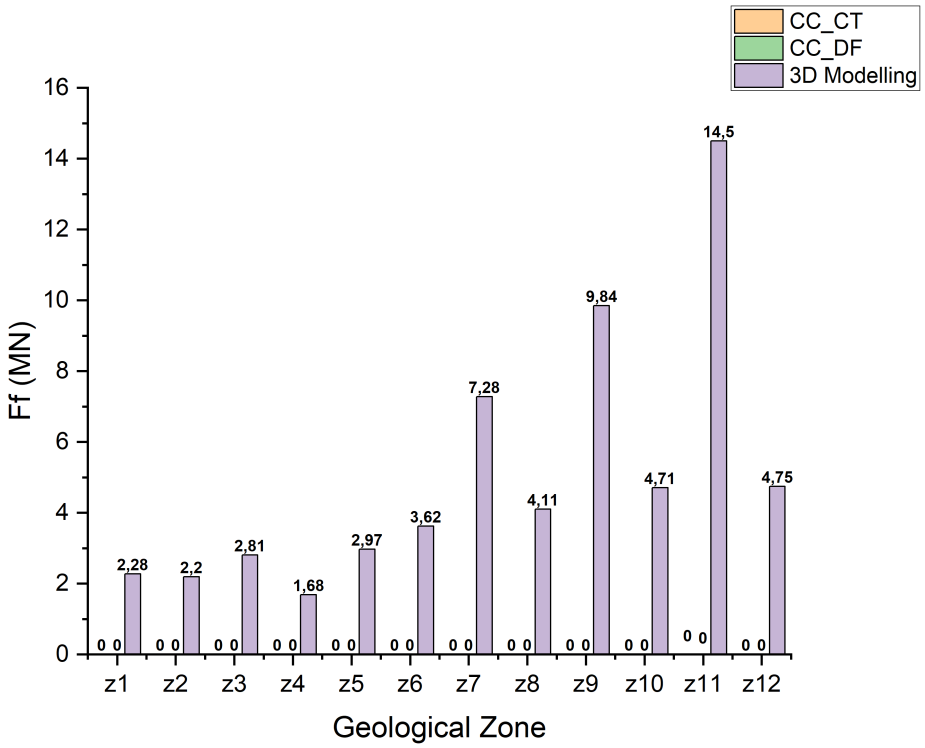

Figure 4.5: The estimated shield frictional force for the zones z1 to z12 using the introduced methods

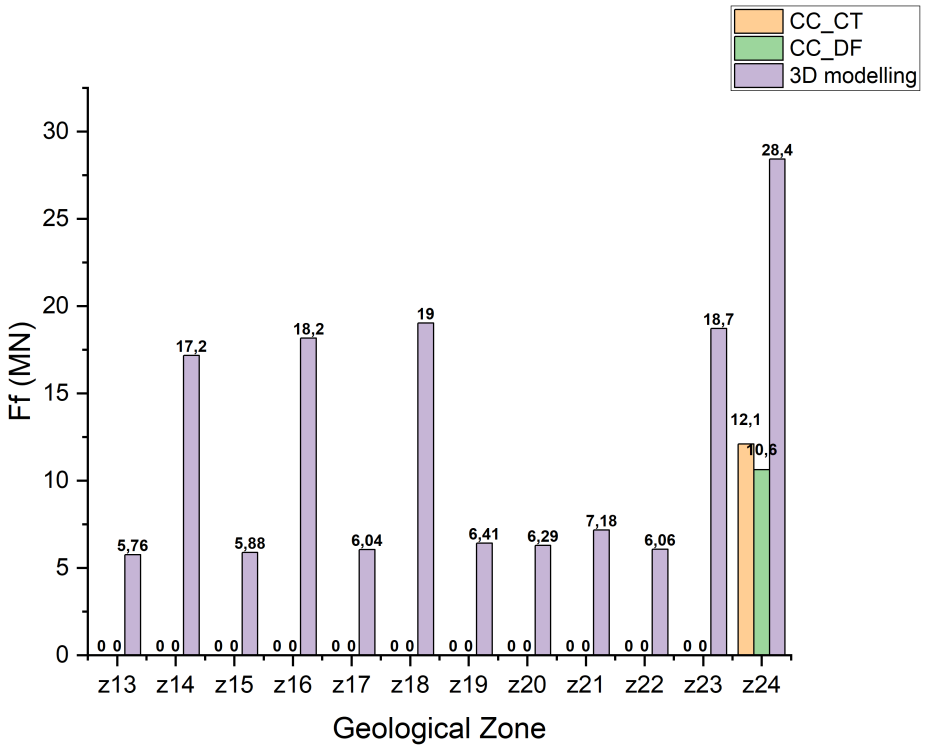

Figure 4.6: The estimated shield frictional force for the zones z13 to z24 using the introduced methods

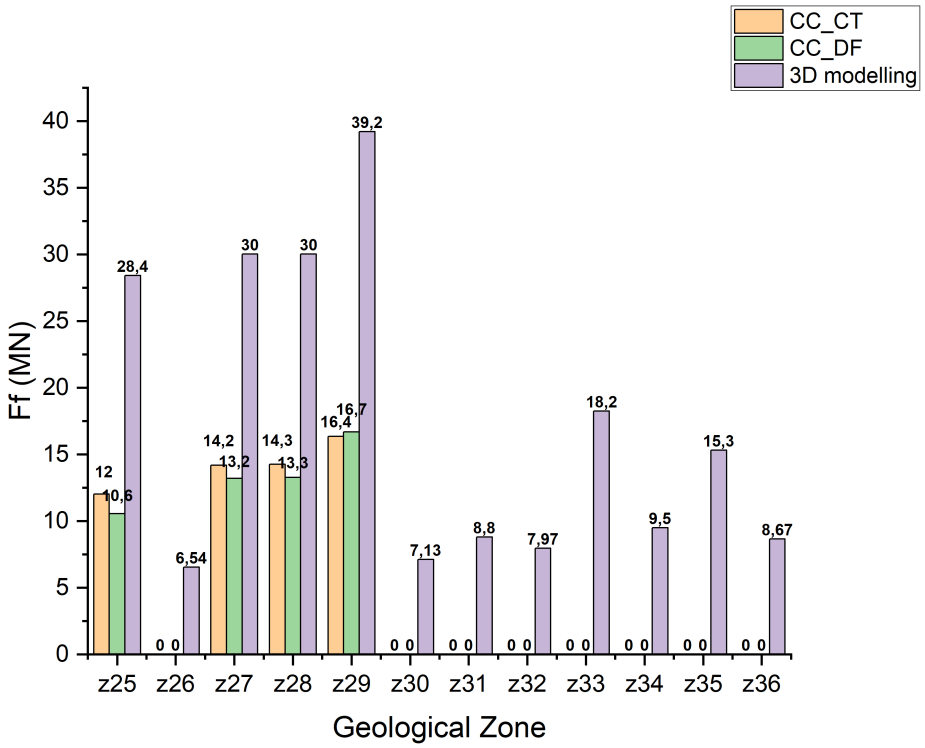

Figure 4.7: The estimated shield frictional force for the zones z25 to z36 using the introduced methods

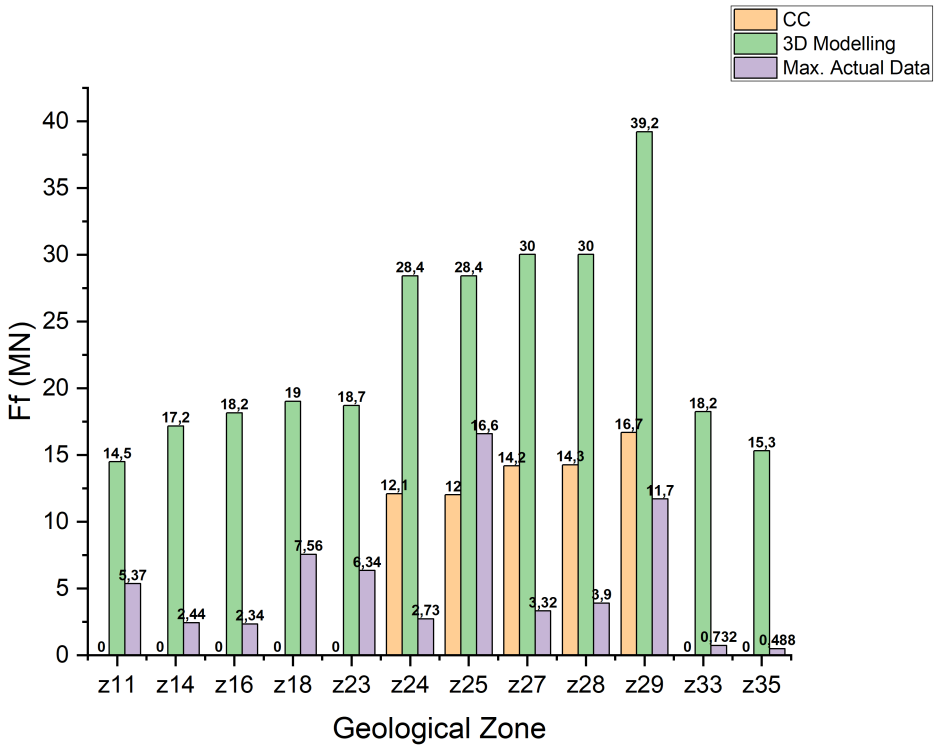

Figure 4.8: Comparison of the estimated shield friction forces and the max. recorded data in the project

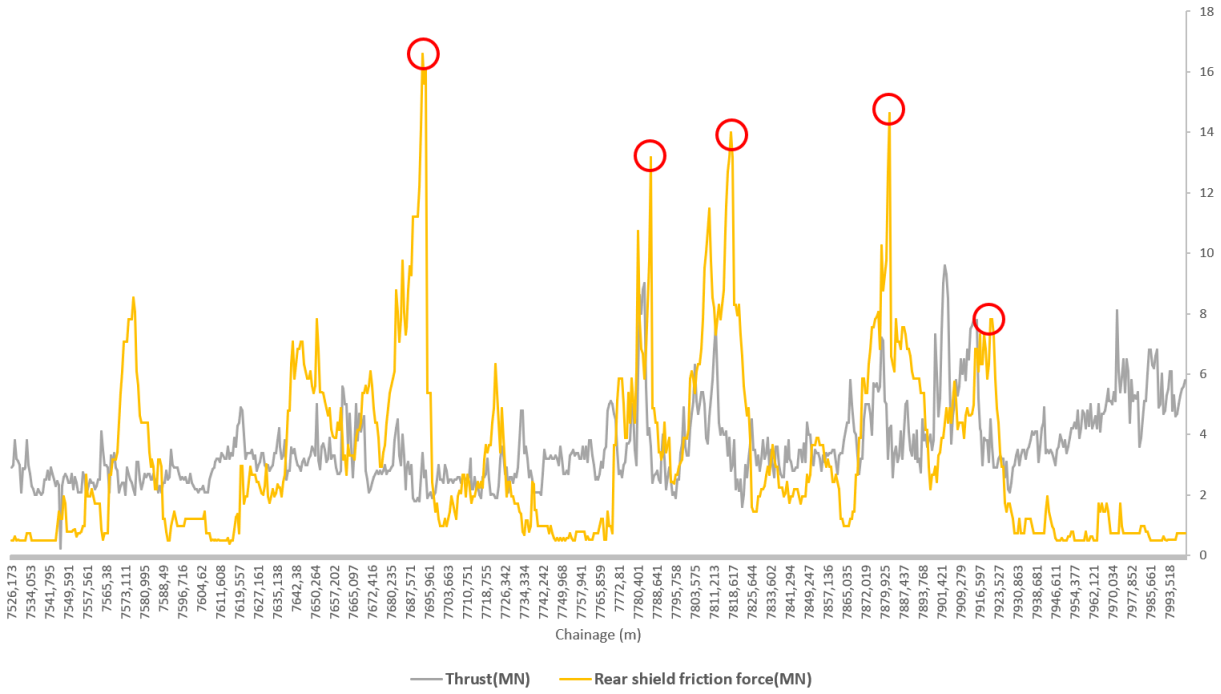

Figure 4.9: The variation of thrust force and the rear shield friction force in the Slate formation (z25)

To err on the side of caution, we will utilize the highest values of frictional force obtained from all approaches, which typically correspond to the 3D modeling method, in this study. Using the maximum values and the aforementioned categorization rule, the zones with the highest risk of jamming are identified as shown in Figure 4.10. As can be seen, according to the values of the jamming risk ratio, z11, and z35 possess a medium level of jamming risk. Zones z14, z16, z18, z23, and z33 have a high level of risk, and zones z24, z25, z27, z28, and z29 contain very high levels of jamming risk. In order to address the risks in these zones, different alternatives and/or mitigating measures are applied in the system: higher overcutting up to 8 cm in radius, shield lubrication, a single shield TBM, a single shielded TBM with lubrication applied on the shield. The last two measures are primary decisions that must have been made ahead of the beginning of the project. The effect of all measures together on the jamming risk level for the critical geological zones is presented in Figure 4.11. According to the results, the overcutting of max. 8 cm does not practically change the extent of risk, whereas lubrication can highly reduce the jamming risk ratio. The usage of a single shielded TBM with a shield

length to the radius (LR) of 3.5 (shield length = 8m) can also significantly reduce the risks. However, the highest mitigation in the jamming risk can be brought about by adding lubrication in the shield of a single shielded TBM, as the extent of risk in all zones will be brought to low to medium.

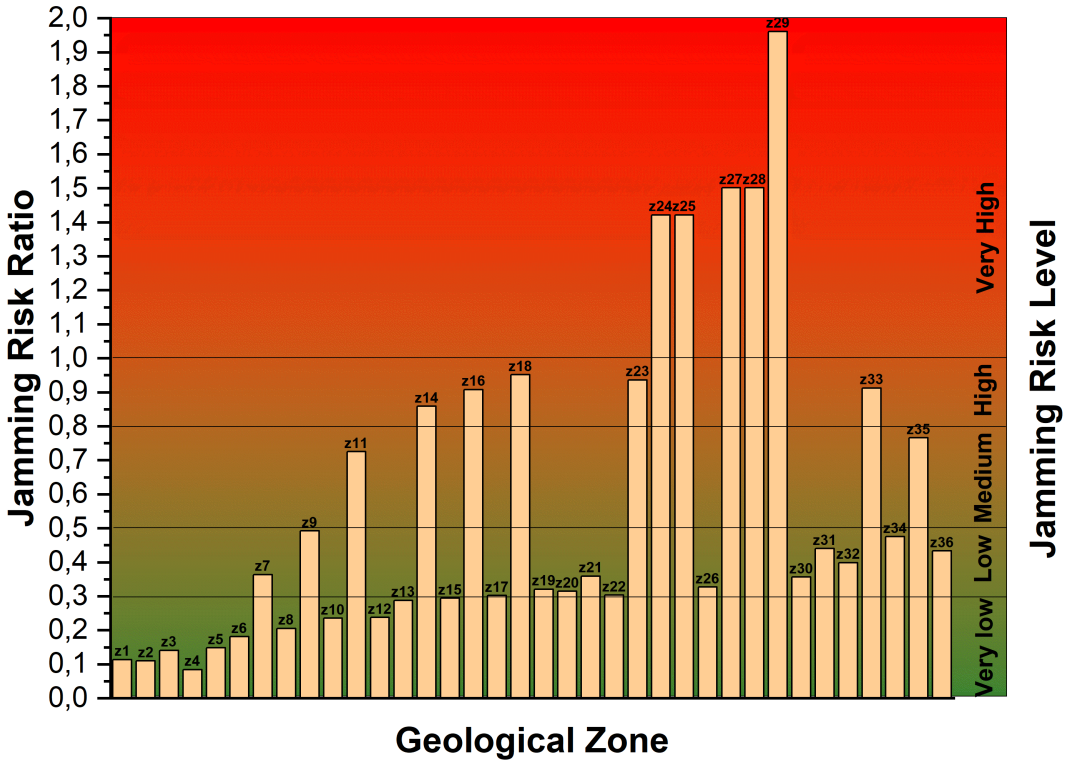

Figure 4.10: The extent of jamming risk level in all the geological zones of Golab tunnel

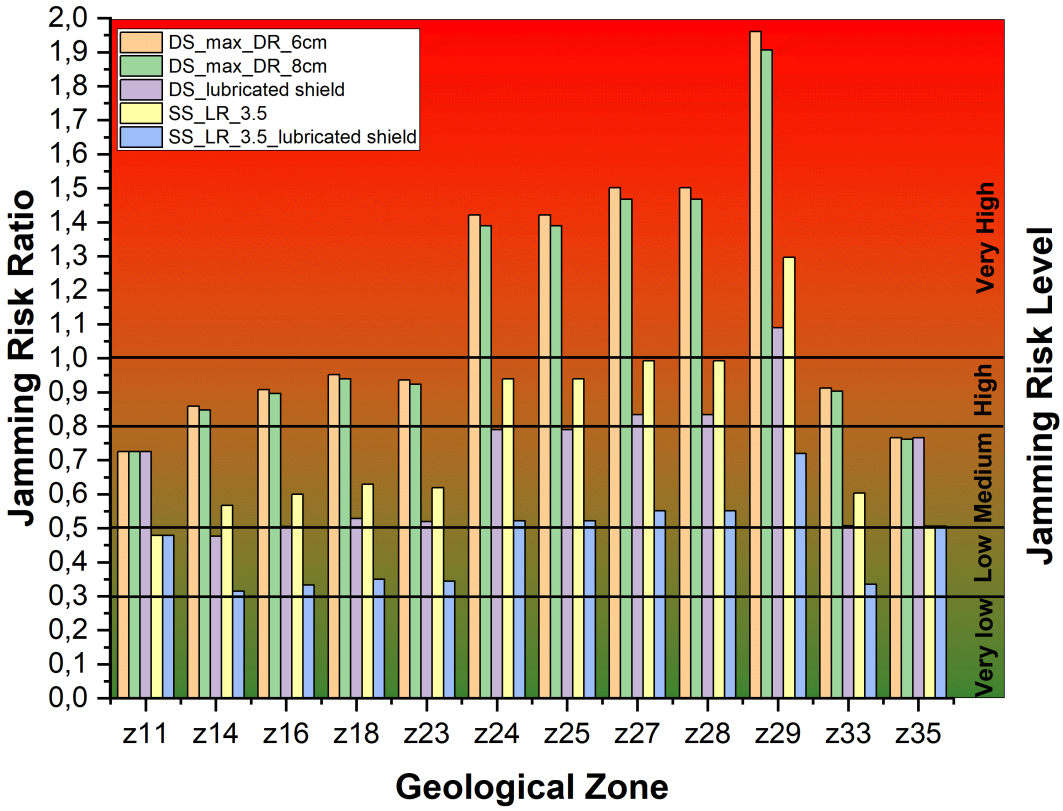

Figure 4.11: The effect of all mitigating measures and different machine types on the jamming risk level for the critical geological zones of Golab tunnel

Figure 4.11 only shows the level of risk in each geological zone without considering the effect of the length and proportion of each zone. Therefore, a better way to show the effect of the different mitigation measures would be through the categorization of the percentage of each level of risk throughout the approx. 6400 m length of the study area in the tunnel. Figure 4.12 indicates the effect of the two measures of lubrication and higher overcutting in comparison to what was applied in practice. As can be seen, a noteworthy decrease in the proportion of the very high and high jamming risk can be expected when using lubrication behind the shield. As for the other case in Figure 4.13 where instead of the double shielded TBM, a single shielded TBM is presumed, around 14 percent of the very high level category is reduced. In case lubrication is also applied, there will be only a 27.3 percent of medium level of jamming risk throughout the tunnel.

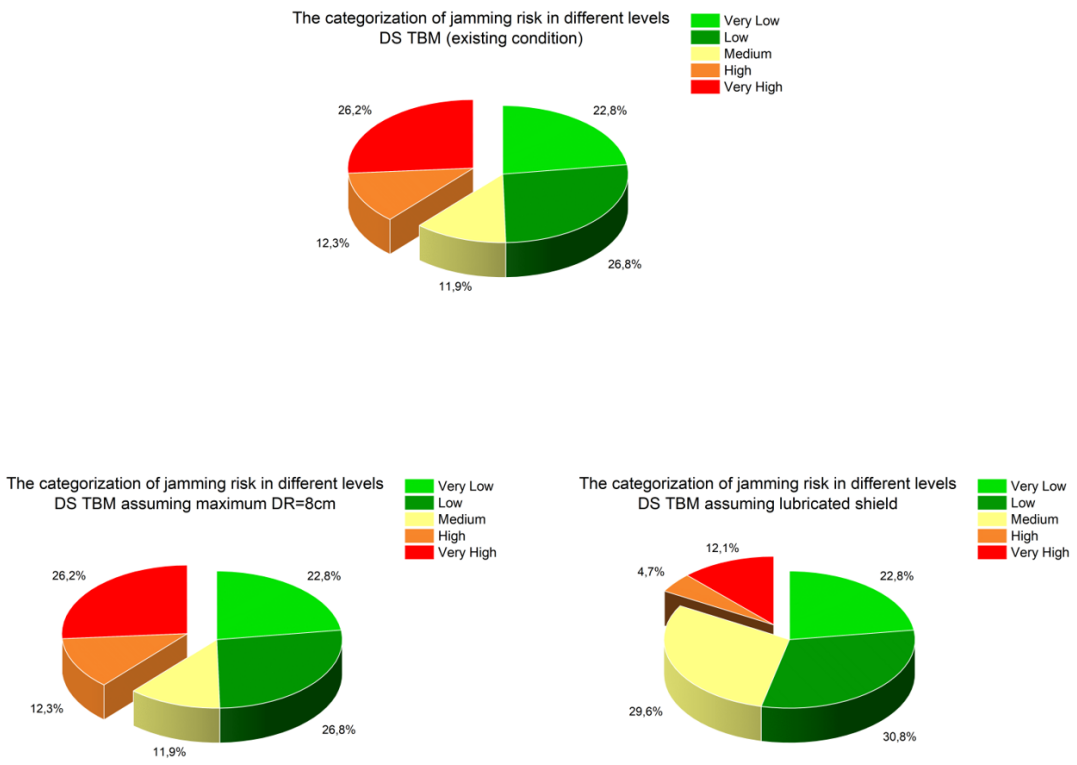

Figure 4.12: Comparison of the proportion of each level of jamming risk throughout the tunnel length by using mitigation measures of higher overcutting and application of shield lubrication

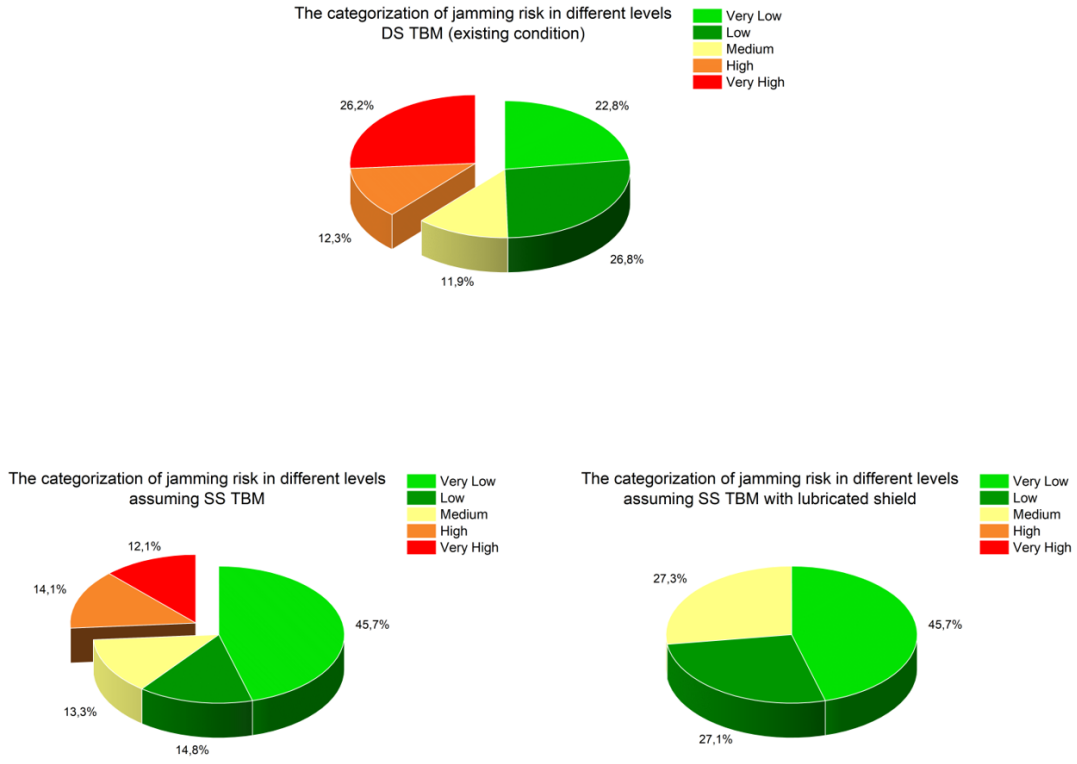

Figure 4.13: Comparison of the proportion of each level of jamming risk throughout the tunnel length by using a single shielded TBM with and without lubrication

Support damage risk

As for the support damage risk, three main sources of damage are studied: damage due to the loads imposed on the exterior side of the support, the damage due to compressive stresses on the point load of the jacks, and the tensile cracks as a result of the bursting tensile stresses.

- Damage due to loads on the exterior side of the support

  As stated before, two types of segments were installed in Golab tunnel: normal and special. The maximum load the normal and special segments can withstand are calculated as 3.83 MPa and 4.28 MPa, respectively. Figure 4.14 shows the estimated maximum lining load in each geological zone compared to the max. allowable load for normal and special segments. It should be noted that based on equation 3.15, $SF_{sig1} = 2$ was considered to take account of the anisotropy in the deformation because of the schistosity of the rock mass. Observations proved that the existing anisotropy was identified as one of the reasons for the damage to the segmental lining in Golab tunnel. The special segments were installed in zones : z25, z26, z27, z29, z30, z31, z32, z33, z34, z35 and z36. This means that in all cases the segmental lining load is not exceeded.

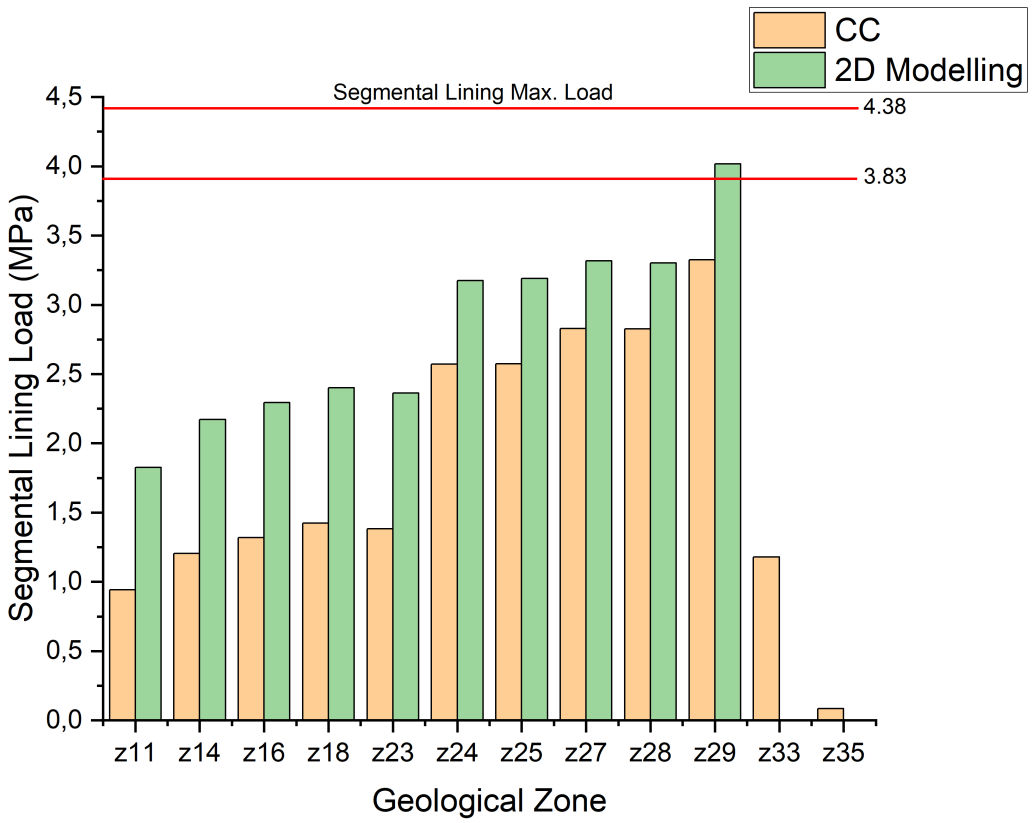

Figure 4.14: The comparison of the segmental lining load compared to the maximum tolerable load using the analytical method(CC) and the 2D modelling parametric method

- The damage due to compressive stresses on the point load of the jacks

  Following the calculation of the nominal bearing strength of the lining, the maximum frictional force on the shield by the analytical solution and the parametric 3D modeling is used to compute the compressive stress on the point load of jacks. The values pertaining to each geological zone are shown in Figure 4.15. The values estimated by the 3D modeling are very close to the maximum allowable strength for both types of segments.

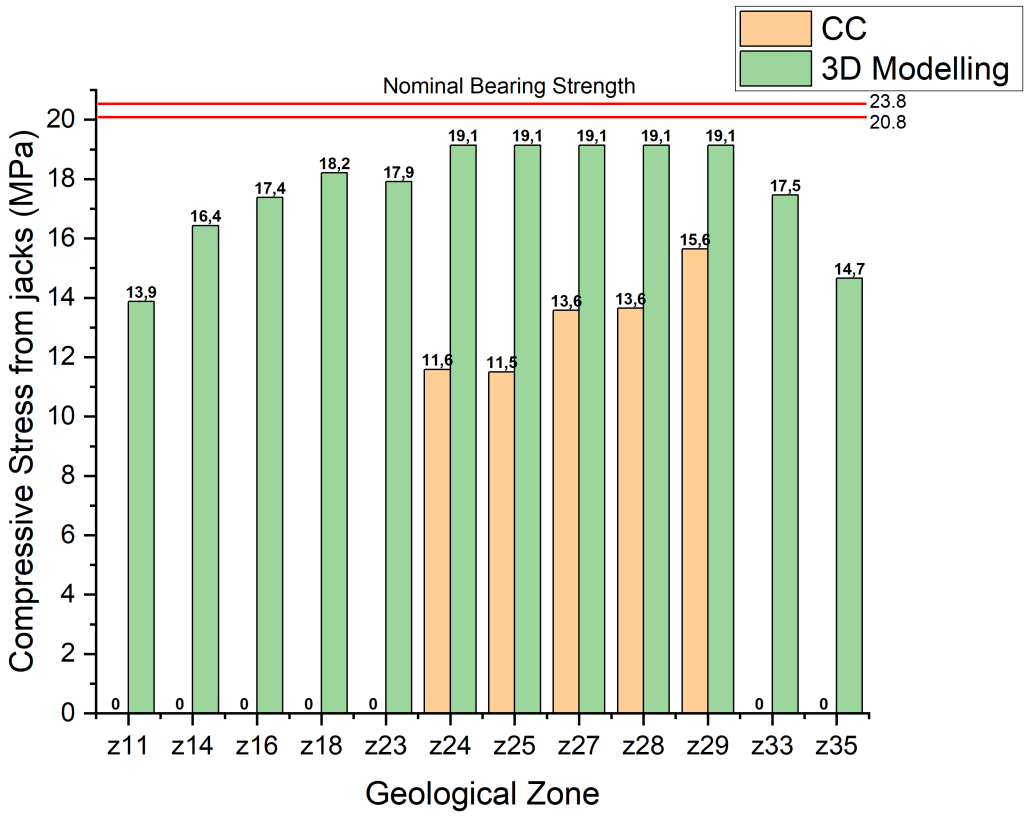

Figure 4.15: The comparison of the segmental lining compressive stress from the jacks to the maximum tolerable nominal bearing strength using the analytical method(CC) and the 3D modelling parametric method

- Tensile cracking as a result of the bursting tensile stresses

  Similar to other cases, the bursting tensile force resulting from the application of jack load is also estimated in critical geological zones. The results presented in Figure 4.16 using both the analytical and the 3D modeling methods are lower than the maximum tolerable bursting force of 39600 kg and 77580 kg for the normal and special segments, respectively.

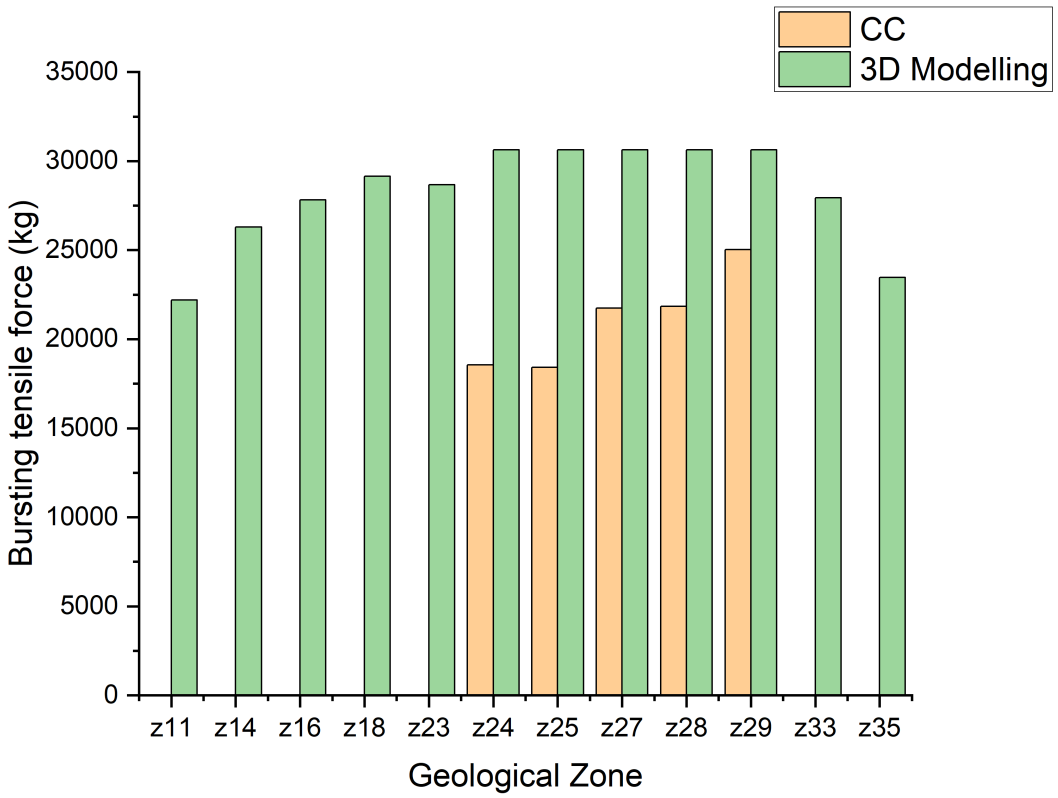

Figure 4.16: The segmental lining bursting tensile force in different geological zones using the analytical method(CC) and the 3D modelling parametric method

Based on the described methodology, the support damage risk level is estimated by considering the maximum level of the above three consequences. The results are presented in Figure 4.17. Considering the risk level of high and very high as critical, the effect of mitigation measures on the zones corresponding to these levels of risk are investigated. The effect of mitigation measures and alternatives for addressing the jamming risk is also investigated for the support damage risk. According to the results presented in Figure 4.18, increasing the overcutting had the highest effect, although it could not mitigate the support damage risk in most of the zones. This can be verified in Figures 4.19 and 4.20, where overcutting in a double-shielded TBM could shift a part of the zones with a very high level of support damage risk to high and medium levels.

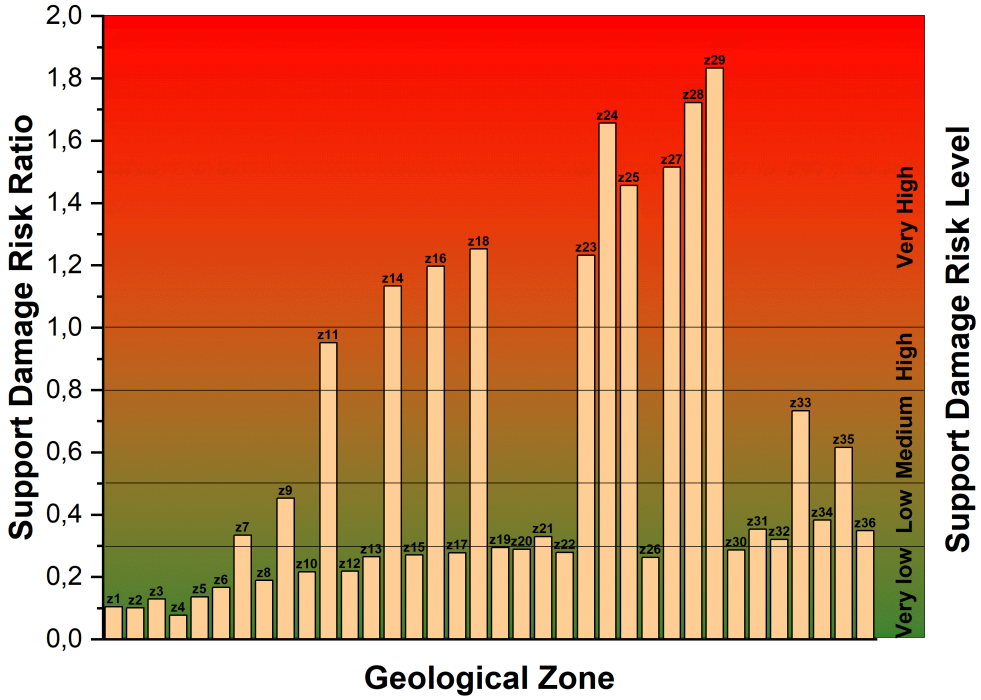

Figure 4.17: The extent of support damage risk level in all the geological zones of Golab tunnel

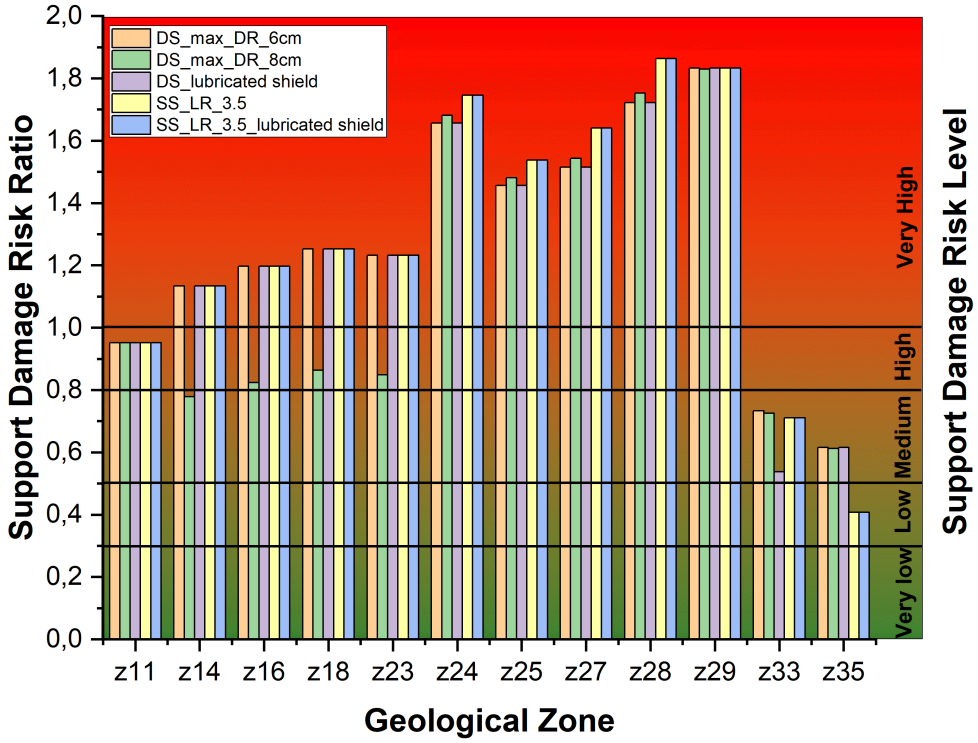

Figure 4.18: The extent of support damage risk level in the critical zones of Golab tunnel by considering the four mitigating measures

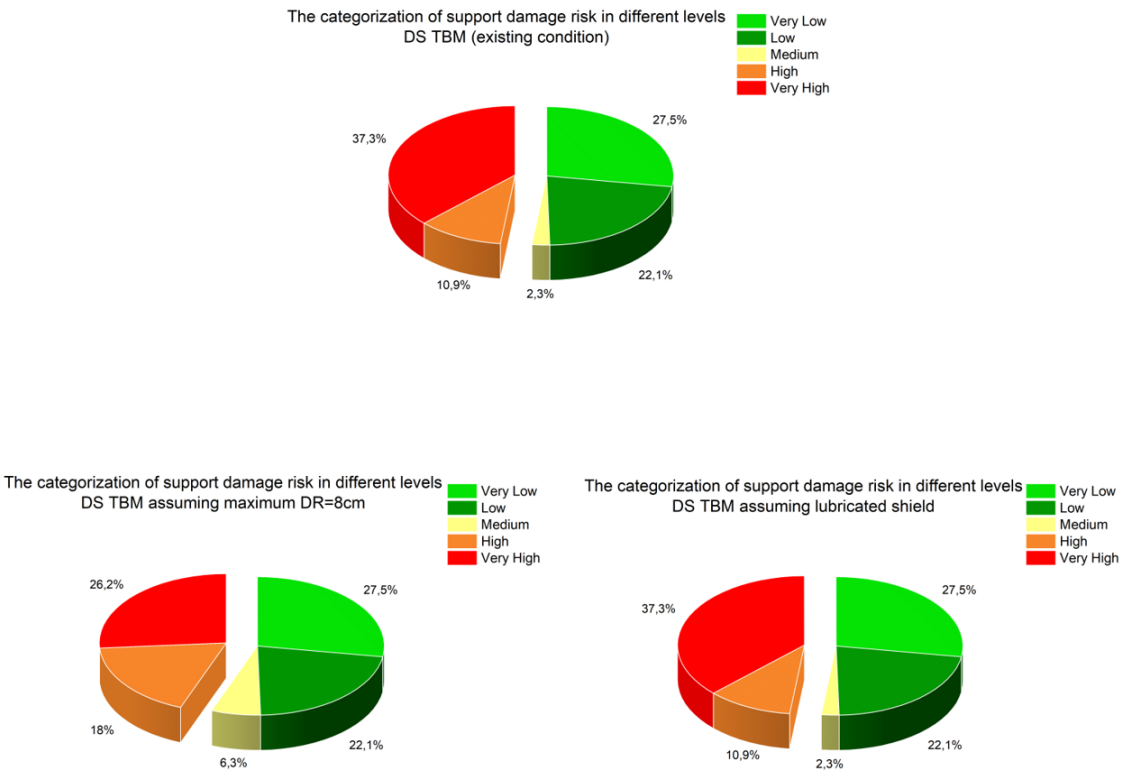

Figure 4.19: Comparison of the proportion of each level of support damage risk throughout the tunnel length by using mitigation measures of higher overcutting and application of shield lubrication

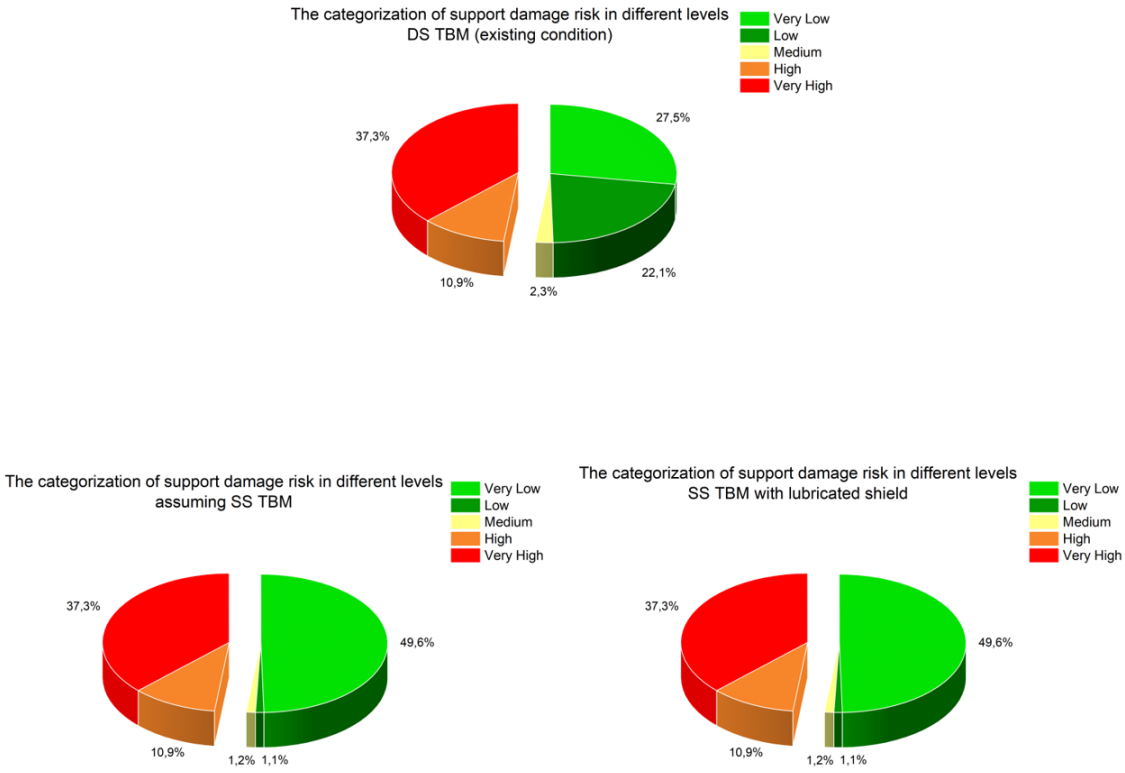

Figure 4.20: Comparison of the proportion of each level of support damage risk throughout the tunnel length by using a single shielded TBM with and without lubrication

It can be concluded that the aforementioned mitigating measures which could alleviate the jamming risk are not equally effective against the support damage risk. Indeed, these measures can reduce the shield frictional forces causing the first two types of damages i.e., the excessive compressive stresses and the bursting tensile stresses due to the high rear friction forces imposed through the jacks to the segment. However, it is important to note that these measures are primarily focused on mitigating the jamming risk and may not effectively address the support damage caused by external forces exerted on the segments. To validate this conclusion and relate it to the observations made on-site, a comprehensive analysis of a valuable database containing information on the type and severity of cracks observed on the segments after excavation has been conducted. The database contains all of the critical damages to the segments including the cracks with a minimum aperture of 0.2 mm.

A closer look at the damage to the support system in Golab main tunnel shows that the damages can be divided into three main groups:

1. 15% of the damages are known as the ones already taken place before the installation of the segments, which is certainly irrelevant to the squeezing (See Figure 4.21).

Figure 4.21: One example of the damages to the segments taken place before the installation of the segmental lining

2. The second type of cracks shown in Figure 4.22 are those which are identified as shear cracks near the connection to the next segment and are assumed to be the result of excessive loads coming from auxiliary cylinders. They are another approx. 15% of the cases.

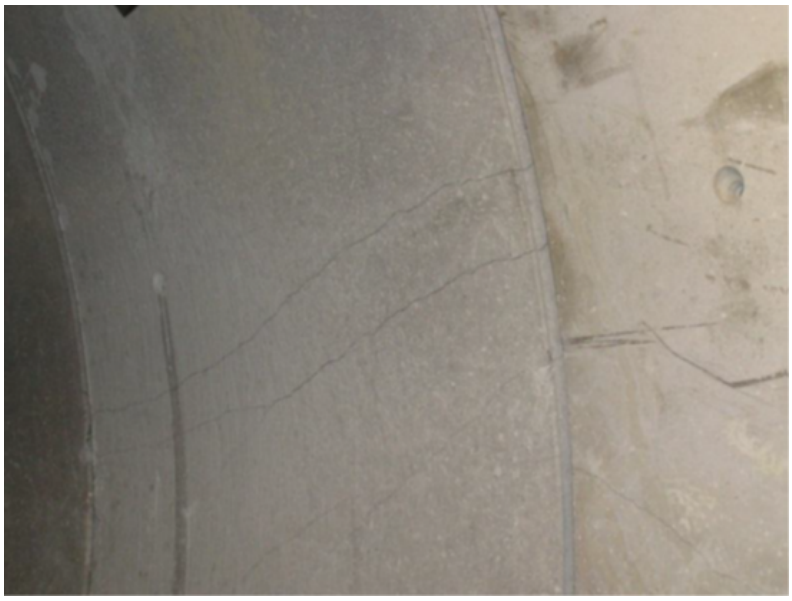

Figure 4.22: Shear cracks in proximity to the adjacent segment junction

3. The majority of damages (approx. 70%) are axial cracks that are known to be caused by the bending of the segments as shown in Figure 4.23. The configuration of these cracks can fall into two categories:

    - axial cracks which are limited to the width of one segment, and are assumed to be formed during the storage of segments or simply formed when the segments are situated in the tail shield of the TBM;
    - axial cracks extended to the nearby segments known to be directly caused by the ground deformations.

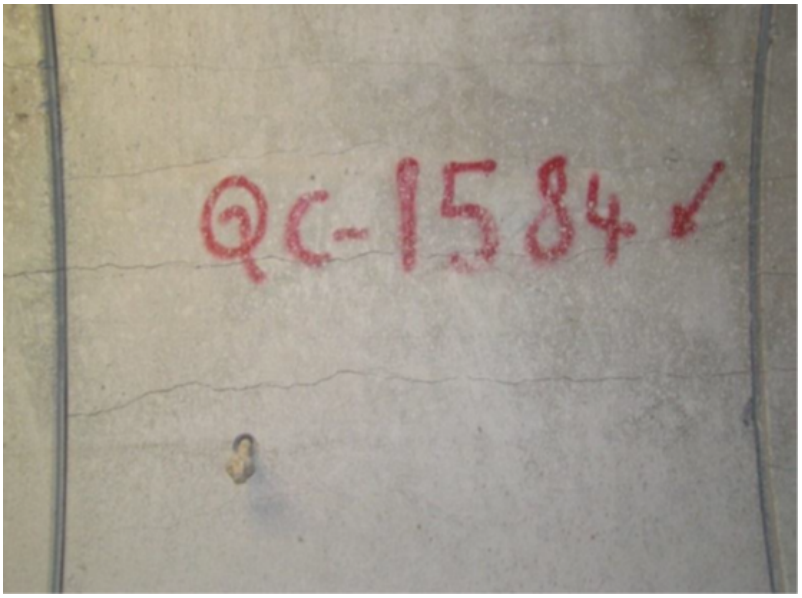

Figure 4.23: Cracks attributed to the bending of the segment

The investigations conducted on the distribution of cracks focused on a few main parameters: the number of cracks in each segment (N), the persistence of the cracks (L), and their maximum aperture (d) (See Figure 4.24). To observe the impact of shield friction force on the extent of cracks, a parameter called the Cracks Max. area (C_A) was defined that would encompass all these geometrical features of the cracks. The calculation of this parameter can be determined using the straightforward formulation in Equation 4.1. A more precise description could even consider the third dimension of a crack to calculate the max. volume of the cracks, which

was not possible due to difficulties in conducting such measurements.

$$C_A = N \times d \times L \tag{4.1}$$

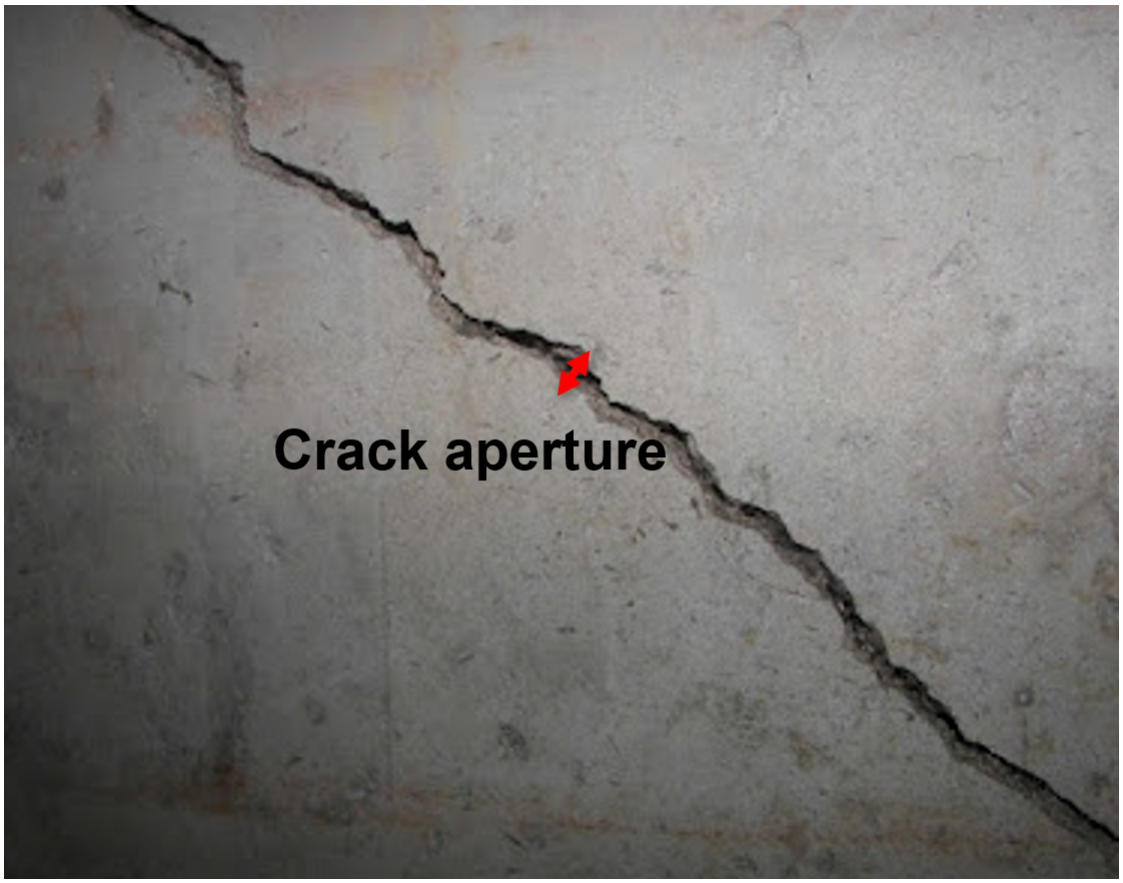

Figure 4.24: A magnified photo associated with intense cracking of a segment in Golab tunnel

The slate formation in z25 where the machine was jammed 5 times was selected for the analysis. The computed maximum area of cracks was drawn together with the magnitude of the recorded rear shield friction force at the chainage where the segments were installed. The whole database was plotted in 5 graphs in figures 4.25, 4.26, 4.27, 4.28 and 4.29. The chainages where the machine was jammed are indicated with red circles. Figures 4.26 and 4.27 demonstrate a clear correlation between the high level of shield friction force and the maximum area of cracks, particularly in areas where the TBM experienced jamming. At the end of the chainages in Figure 4.29 where the shield friction forces are considerably lower, the cracks' maximum area also significantly dropped and became more stable. However, trends seen in

other chainages such as in Figures 4.25 and 4.28 do not necessarily indicate a direct correlation. It can be inferred that the high shield friction force cannot be the only reason for the damages in segments, and other reasons could be the direct pressurization of the segments due to high external loads. Besides, the excavation rate and the time-dependent deformation of the ground can be another important reason that the values are not compatible in all chainages. These results would somewhat justify the ineffectiveness of the mitigating measures introduced in Figure 4.18 towards controlling the support damage risk. As these measures are mainly effective against the shield frictional, it seems that for controlling the support damage, a change in the support system design might have been necessary. It is apparent that such analysis of the interaction between the ground and the support system requires more sophisticated investigations such as numerical modeling. Therefore, considering the integrated effect of direct and indirect pressures on the segmental lining, considering the anisotropies in the direction of ground pressure, and studying other solutions such as using deformable segmental lining that can withstand more deformation need further investigation.

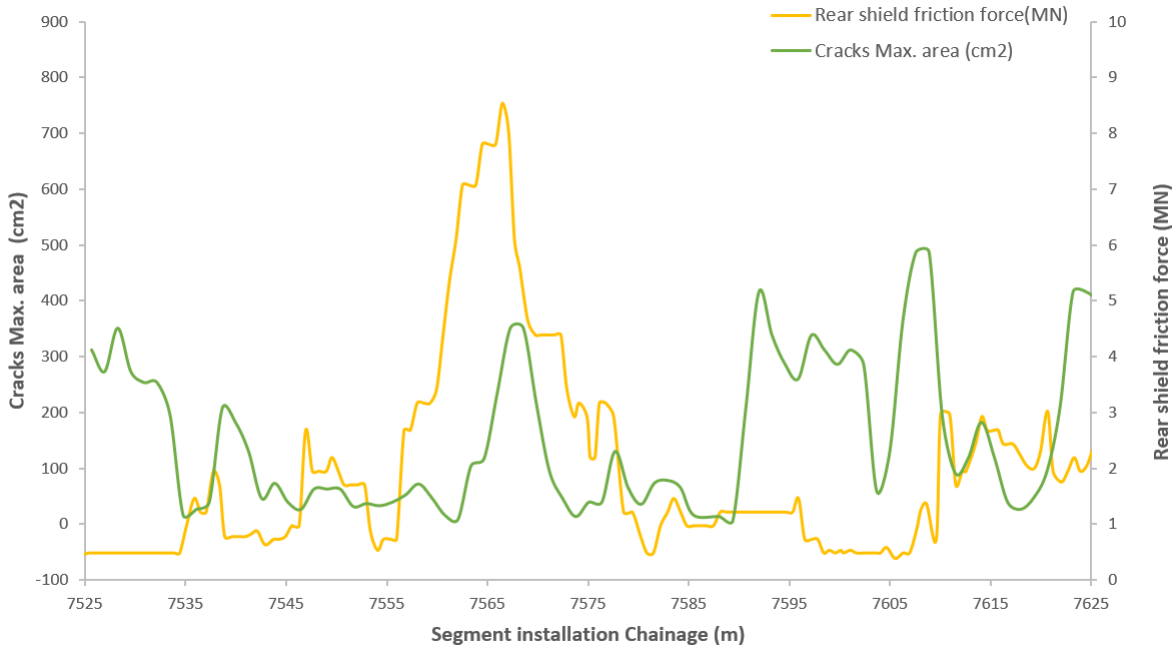

Figure 4.25: Comparison of the trend of the cracks max. area and the rear shield friction force in z25 (slate formation) Chainage 7+525 km to 7+625 km

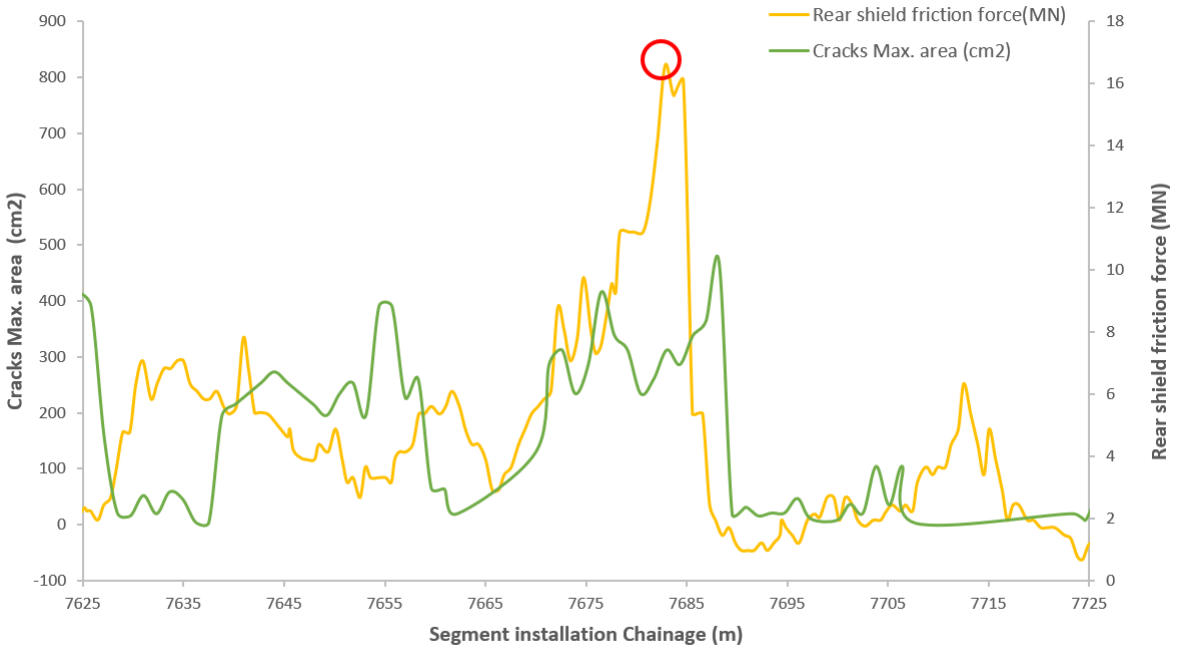

Figure 4.26: Comparison of the trend of the cracks max. area and the rear shield friction force in z25 (slate formation) Chainage 7+625 km to 7+725 km

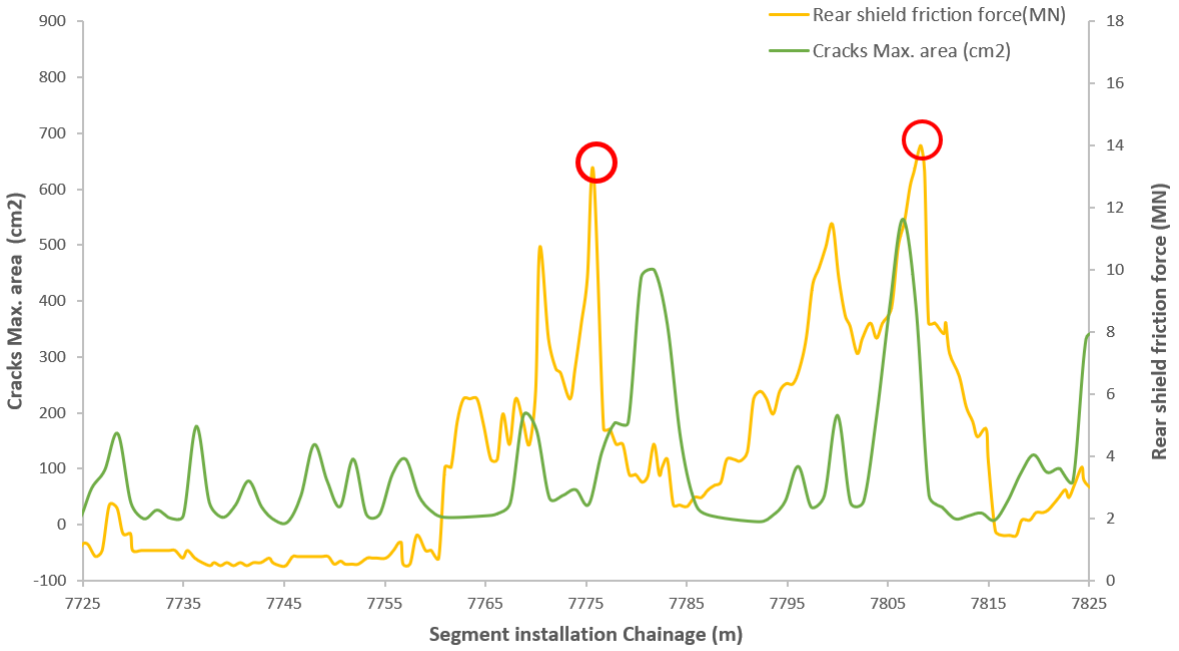

Figure 4.27: Comparison of the trend of the cracks max. area and the rear shield friction force in z25 (slate formation) Chainage 7+725 km to 7+825 km

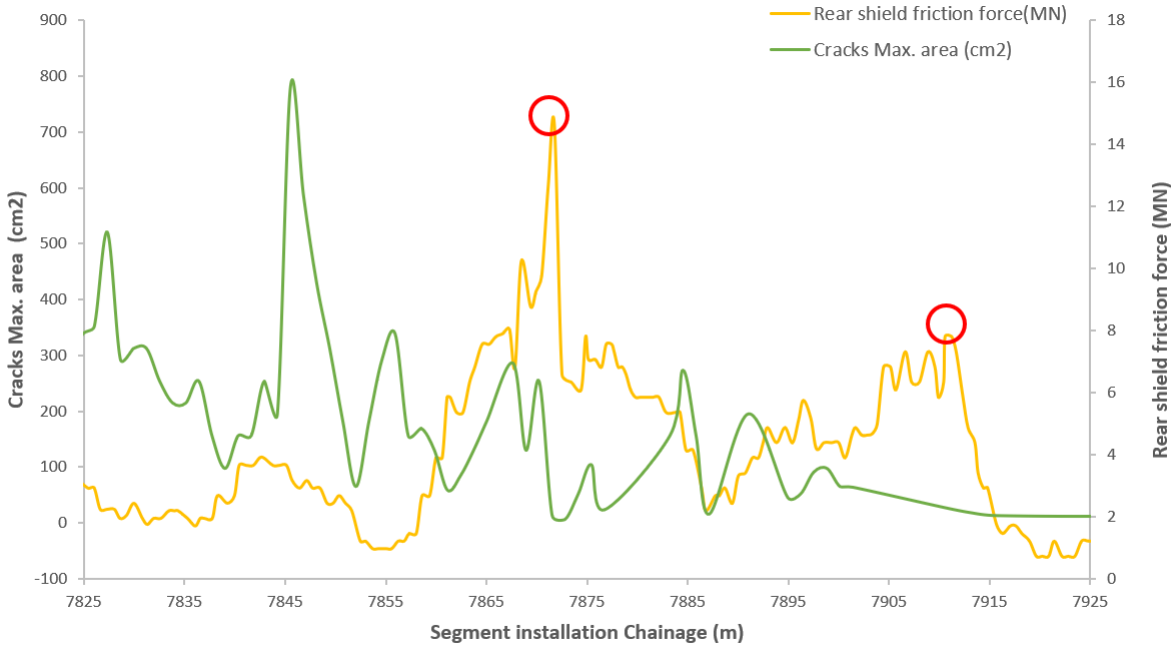

Figure 4.28: Comparison of the trend of the cracks max. area and the rear shield friction force in z25 (slate formation) Chainage 7+825 km to 7+925 km

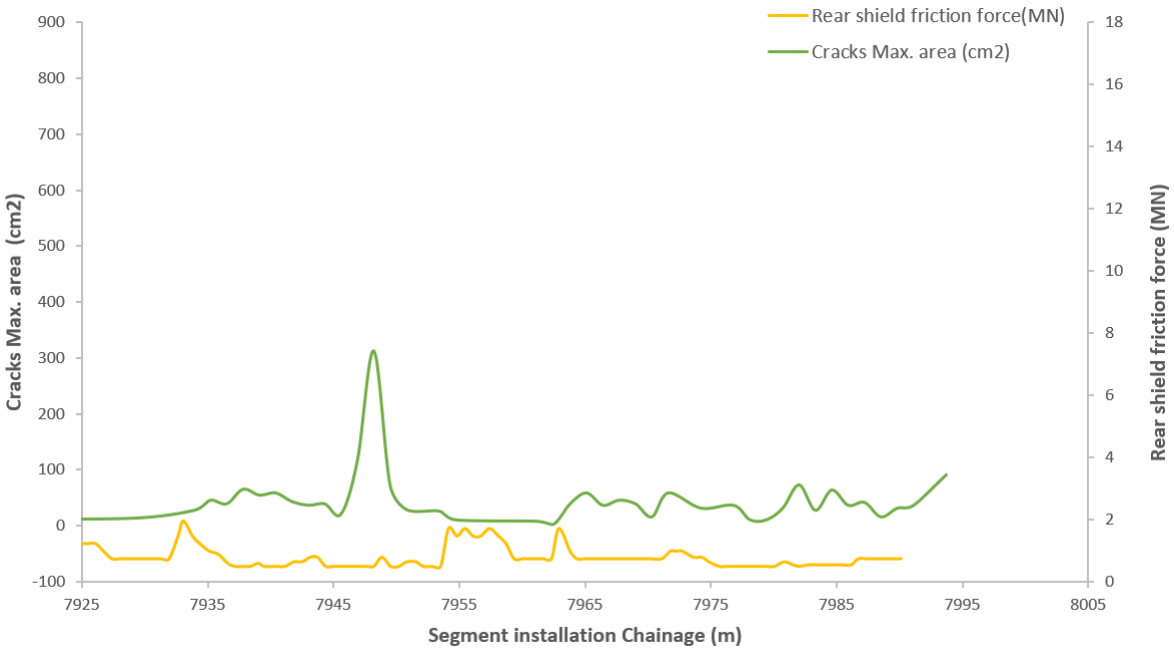

Figure 4.29: Comparison of the trend of the cracks max. area and the rear shield friction force in z25 (slate formation) Chainage 7+925 km to 8+000 km

Gripper bracing difficulties

Based on the aforementioned methodology in Chapter 3, the gripper bracing risk is also evaluated for all the zones in the tunnel. The results presented in Figure 4.30 indicate that the extent of the gripper bracing risk for all the zones is situated at a very low level.

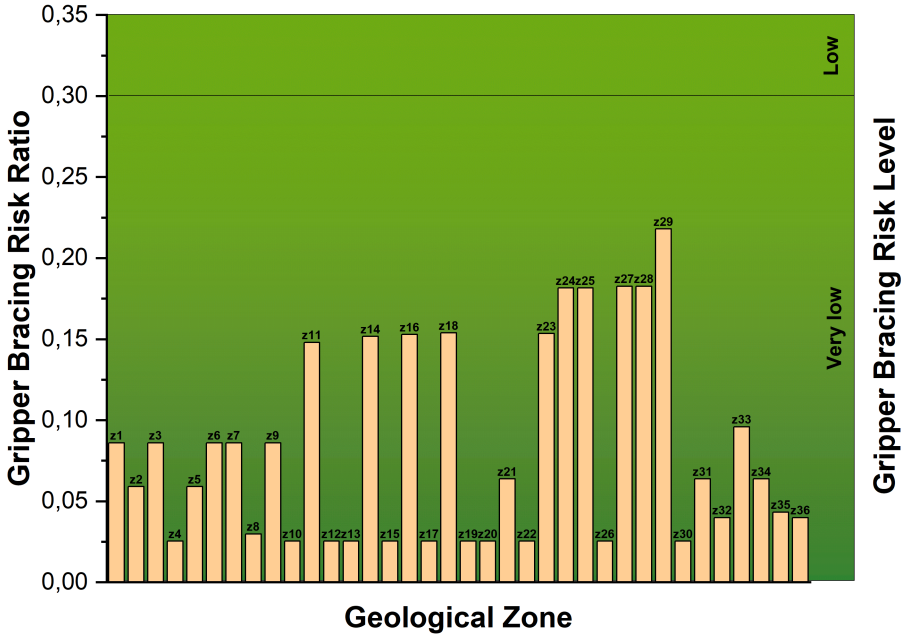

Figure 4.30: The extent of gripper bracing risk level in all the geological zones of Golab tunnel

Determination of the TBM Risk Index

Following the individual evaluation of different sources of risks, the total TBM Risk Index for squeezing is summed over entire tunnel length based on the significance factors introduced in Table 3.4 and the results are presented in Table 4.7. As expected, the use of the single shielded TBM with a lubricated shield can significantly reduce the extent of risks.

Table 4.7: The estimated value of TBM squeezing risk index for different machine types and mitigating measures

The machine type and the mitigating measures	TBM Squeezing Risk Index
DS TBM (existing condition-Max DR = 6cm)	3.59
DS TBM (Max DR = 8cm)	3.47
DS TBM assuming lubricated shield	3.18
SS TBM	2.8
SS TBM with lubricated shield	2.3

4.1.2 The probabilistic analysis of squeezing risks

The risk assessment procedure introduced in this research is on the basis of a probabilistic approach using Monte Carlo simulation. A specific number of iterations for considering the variability of parameters is chosen in the beginning. For this case study of Golab tunnel, the analysis is conducted using 100 iterations in the input parameters introduced in Tables 4.4, 4.5 and 4.6 for all the geological zones by assuming a normal distribution function. Figures 4.31 and 4.32 show the distribution of deformation modulus and compressive strength of rock mass for the critical geological zones of Golab tunnel, respectively.

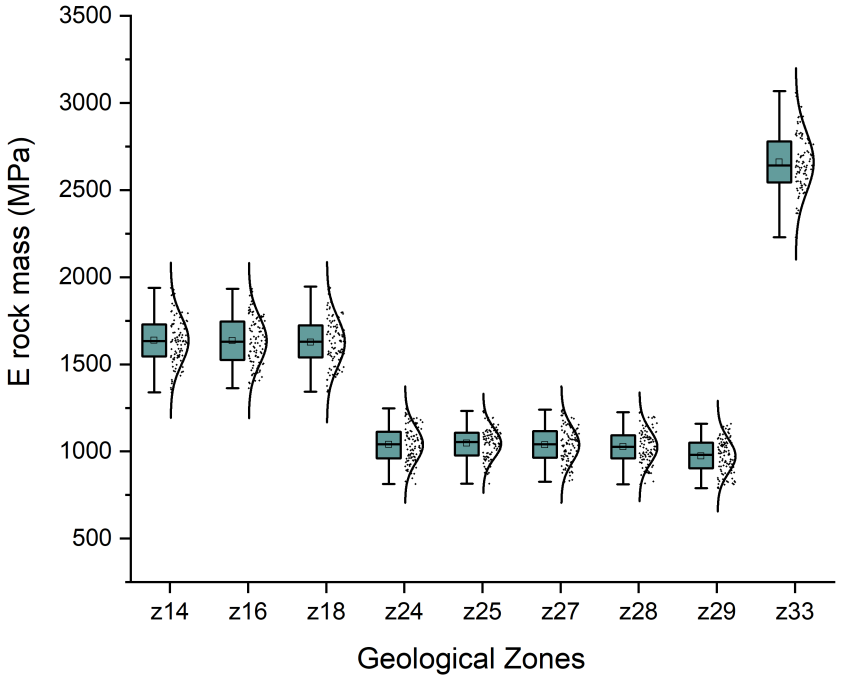

Figure 4.31: The probabilistic selection of the Deformation Modulus of rock mass for the critical zones in Golab tunnel

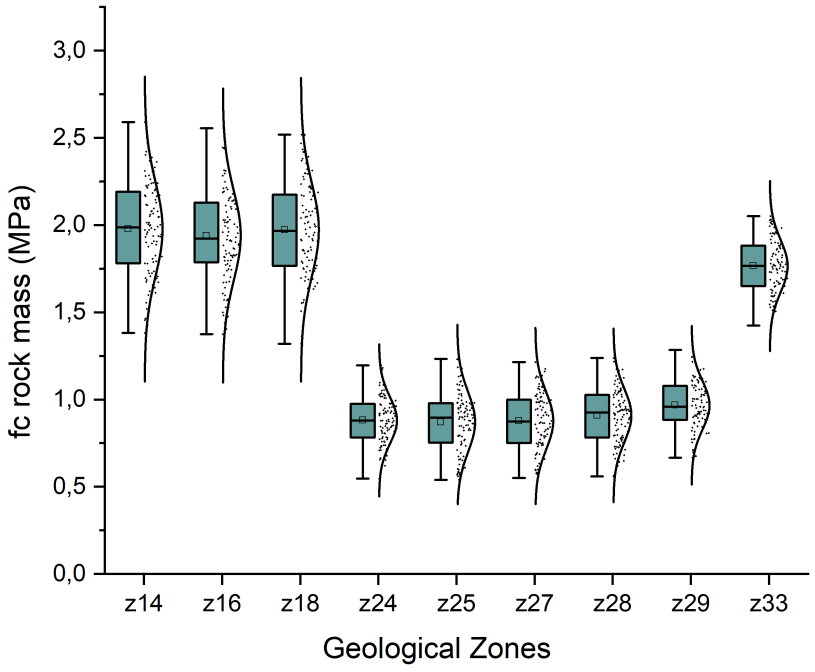

Figure 4.32: The probabilistic selection of the Compressive strength of rock mass for the critical zones in Golab tunnel

Amongst the two critical squeezing consequences in Golab tunnel i.e., shield jamming and support damage, the jamming risk exhibited higher sensitivity to the input parameters variation. The variation of regripping pressure in the slate formation (z25) shown in Figure 4.9 clearly verifies this fact. Thus, prior to the analysis of the total risk index (TBM_{RI}), this section mostly focuses on the jamming risk and its magnitude based on the variation of input parameters.

Probabilistic evaluation of the shield frictional force

The results obtained from the two main methods for evaluation of the shield friction force, namely the parametric 3D modeling and the analytical solution, are plotted through histograms and compared with the actual recorded data from the machine. The results for zones z14, z16, z18, and z23 are depicted in Figure 4.33. It is evident that the analytical method based on closed-form solutions (CC) underestimates the rear shield friction force, while the 3D modeling parametric method overestimates the values and in many instances warns against jamming of the shield, which in practice does not occur in these zones. For the more critical zones 24, 25, 27, and 28, as shown in Figure 4.34, the analytical method tends to overestimate, but the values are closer to the actual data compared to the 3D modeling method. In the most critical zone (z25), where jamming occurred five times, the 3D modeling method provides a safer margin for prediction. Similar findings can be deduced from the histograms pertaining to zones 29 and 33 in Figure 4.35. Although the analytical solution provides estimates that are closer to the actual data, the more conservative estimations by the 3D modeling are preferable in a risk management procedure. It should be noted that part of the overestimation could be attributed to the fact that the 3D modeling considers the whole length of the Double shield TBM, whereas the actual data represents the rear shield friction force alone.

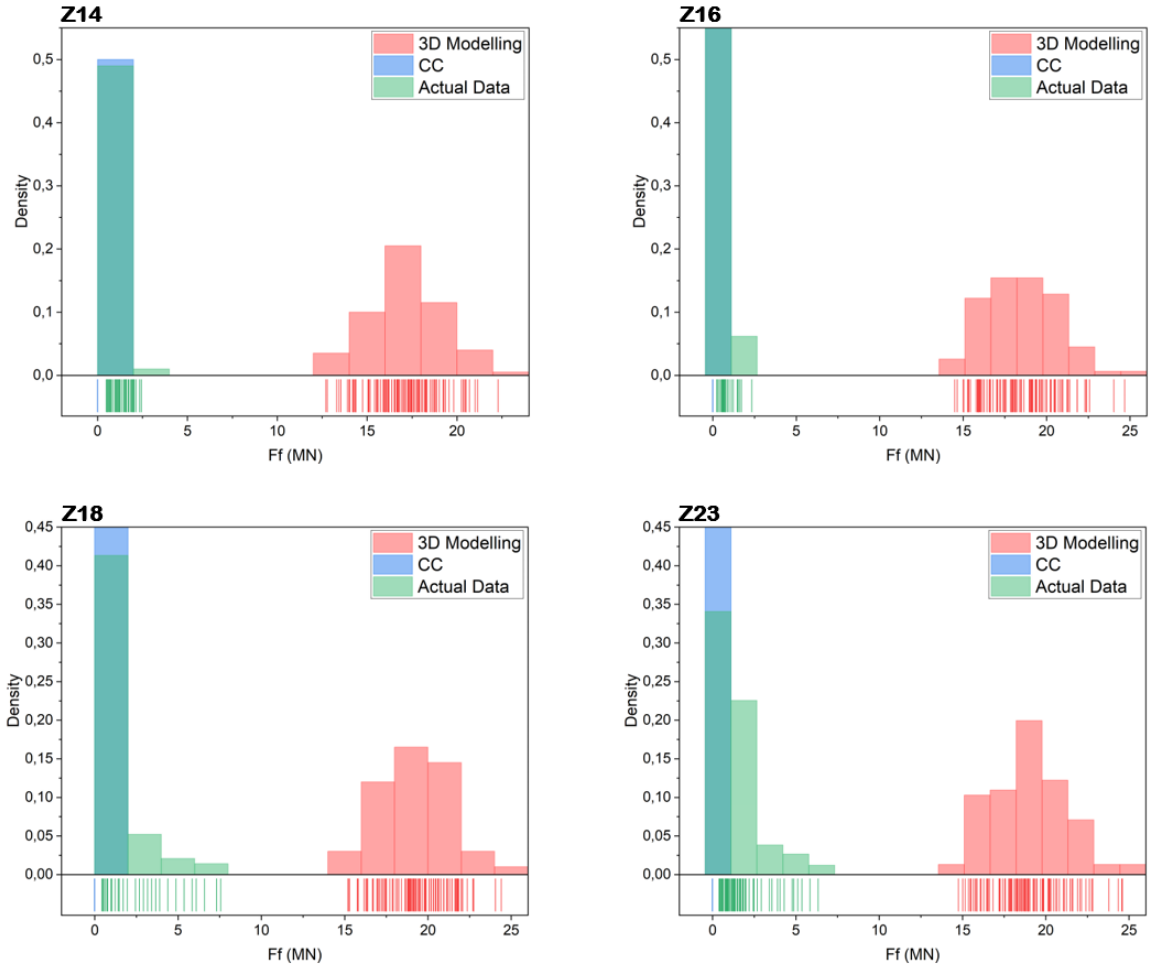

Figure 4.33: The distribution of shield friction forces and comparison with actual data from the regripping pressure for zones 14, 16, 18 and 23

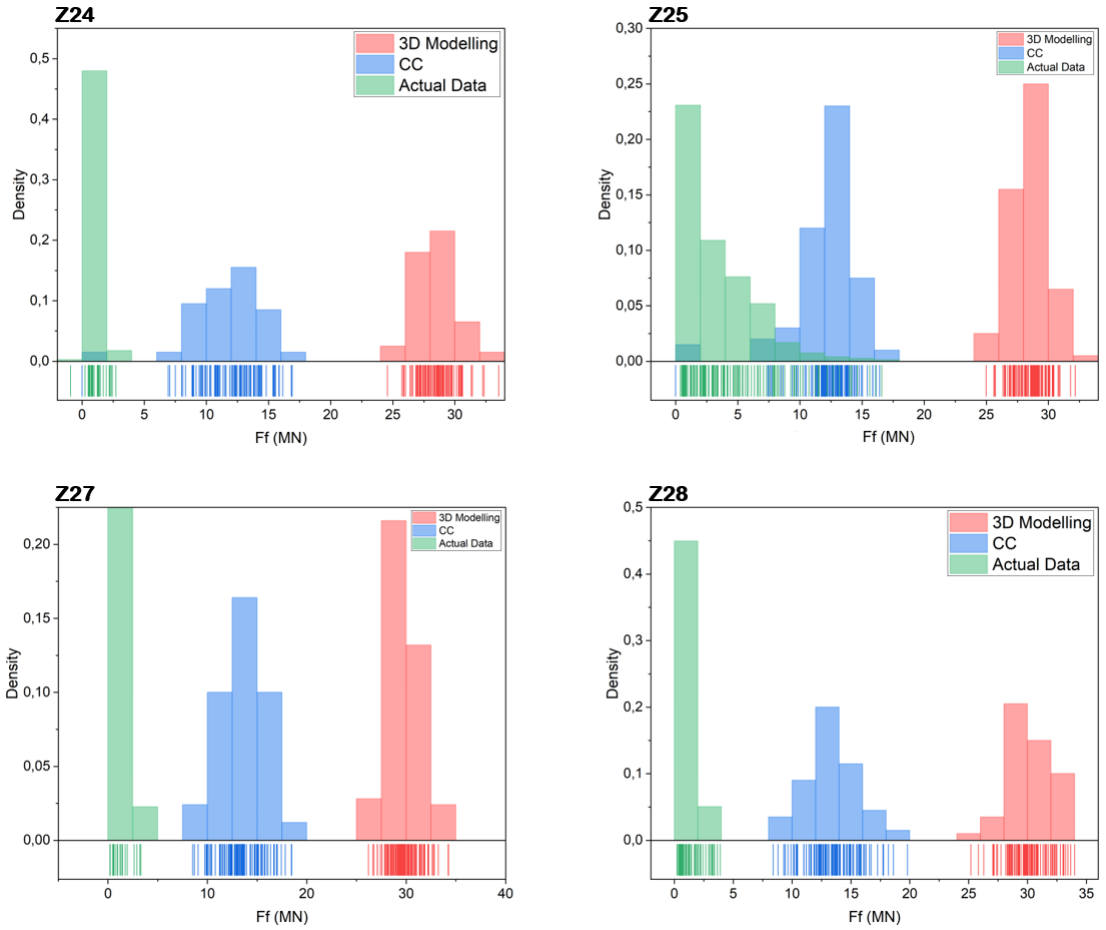

Figure 4.34: The distribution of shield friction forces and comparison with actual data from the regripping pressure for zones 24, 25, 27 and 28

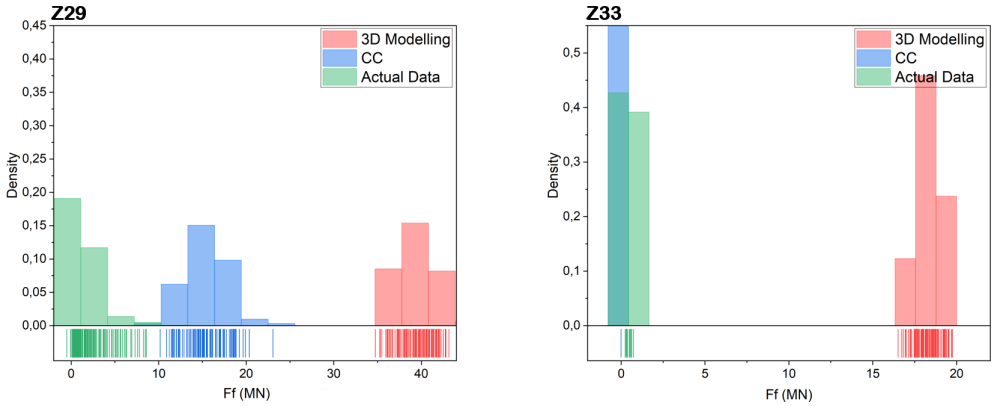

Figure 4.35: The distribution of shield friction forces and comparison with actual data from the regripping pressure for zones 29 and 33

By considering the 3D modeling method as the default prediction tool, the effect of mitigating measures already described in section 4.1.1 on the jamming risk in zones 25 and 29 are studied and the results are plotted in Figures 4.36 and 4.37.

In order to better see the effect of measures with regards to the jamming risk level categorization, additional histograms were drawn by using the values of the jamming risk ratio and plotted in Figures 4.38 and 4.39. The results show the highest effectiveness for the single shielded TBM with a shield length to radius ratio of 3.5 which is lubricated.

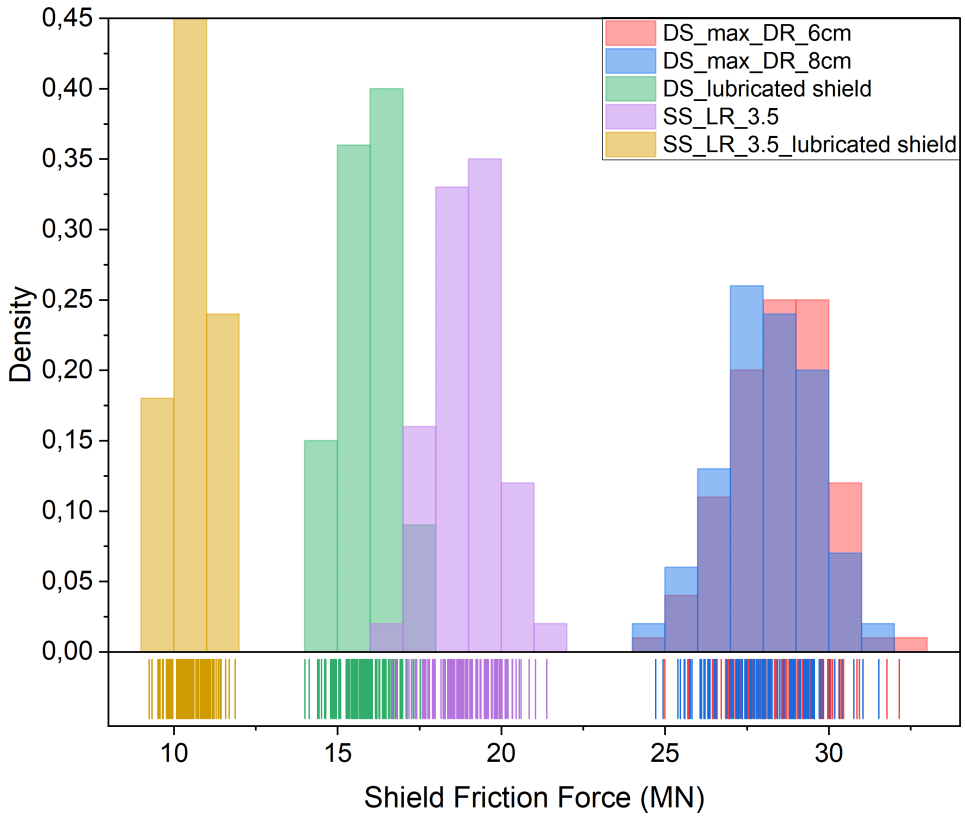

Figure 4.36: The distribution of shield friction forces using the 3D modeling method and the effect of mitigating measures and different machine types (z25)

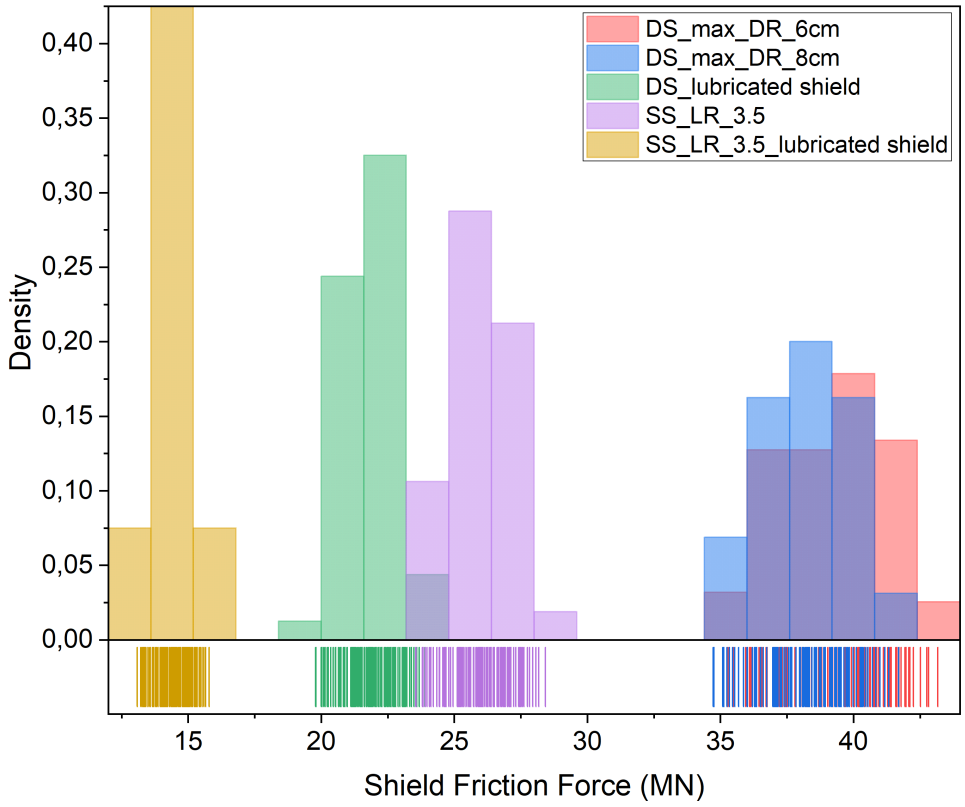

Figure 4.37: The distribution of shield friction forces using the 3D modeling method and the effect of mitigating measures and different machine types (z29)

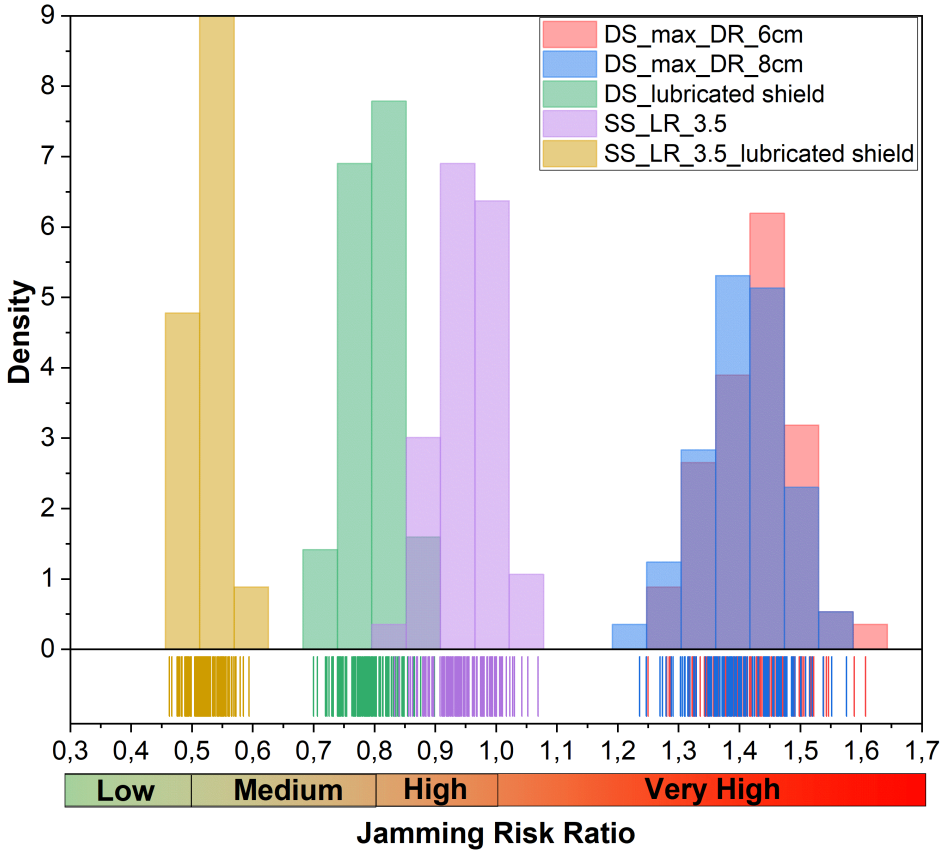

Figure 4.38: The distribution of jamming risk ratio using the 3D modeling method and the effect of mitigating measures and different machine types (z25)

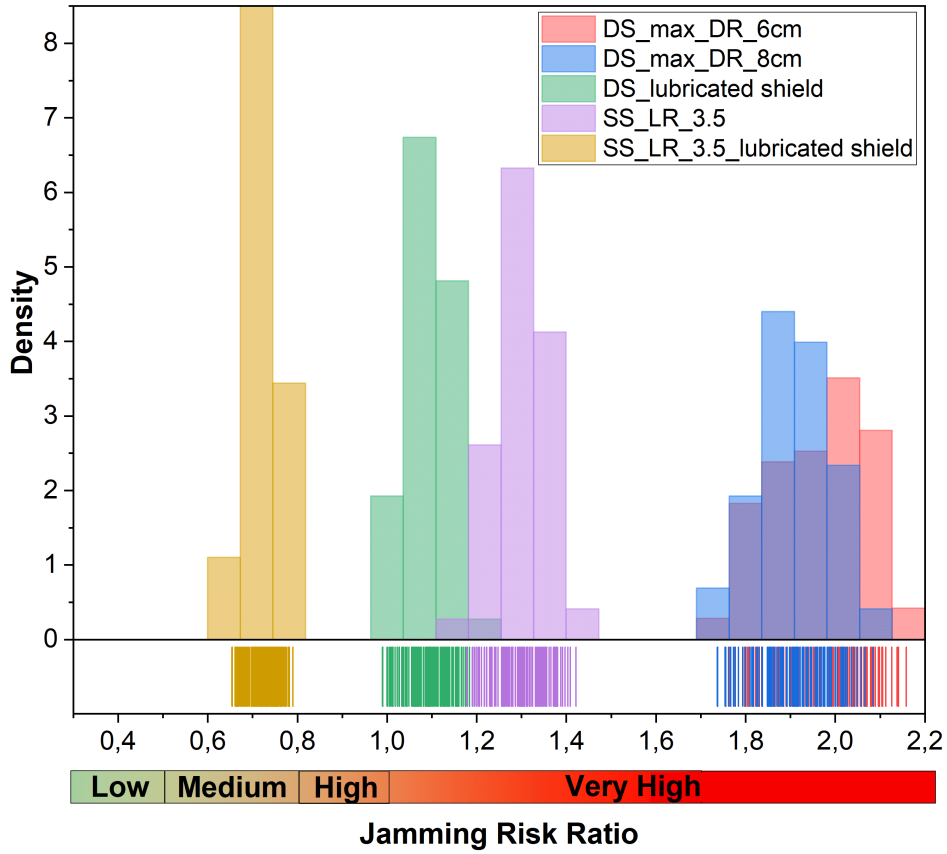

Figure 4.39: The distribution of jamming risk ratio using the 3D modeling method and the effect of mitigating measures and different machine types (z29)

To enhance the analysis of the probability of certain risks and the effectiveness of mitigating measures in controlling the consequences, the utilization of cumulative percent graphs can prove beneficial. In this particular analysis, three measures will be considered: the double-shielded TBM with lubrication, the single-shielded TBM without lubrication, and the single-shielded TBM with lubrication.

1. Double-shielded TBM with lubrication

   The cumulative percent graph is drawn for both zones 25 and 29 assuming that the double-shielded TBM is lubricated. According to Figure 4.40, 53% of the cases represent a medium level of jamming risk (JR_a of 0.5 to 0.8) and the rest of 47% would possess a high level of jamming risk (JR_a of 0.8 to 1). As for zone 29, 95% of the cases represent a very high level of jamming risk. By considering the medium level as the target, this measure is not sufficiently effective.

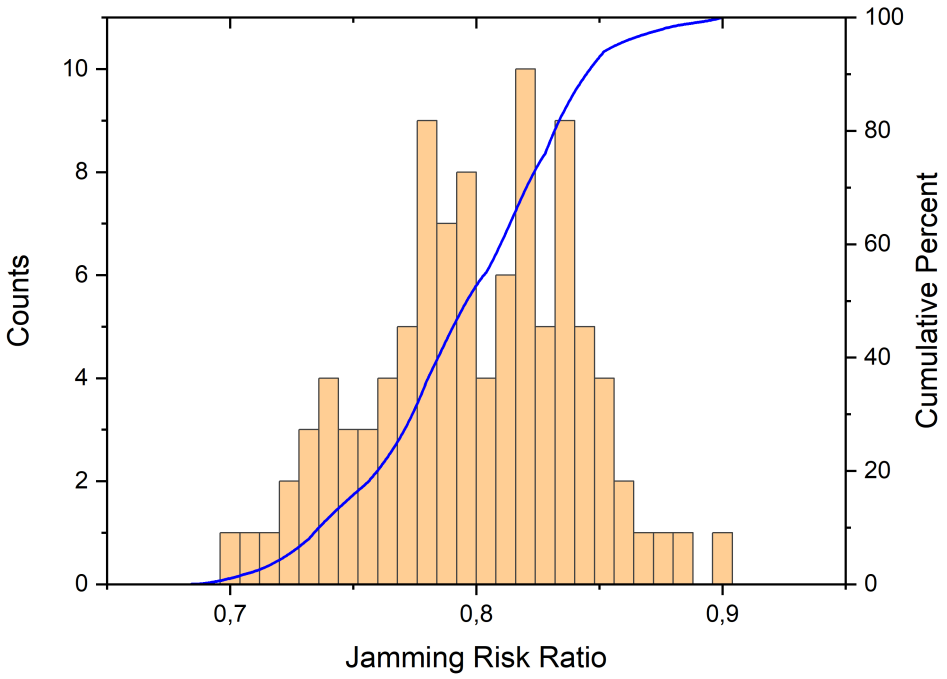

Figure 4.40: The cumulative percent graph for the jamming ratio in z25 when the Double-shielded TBM is actively lubricated

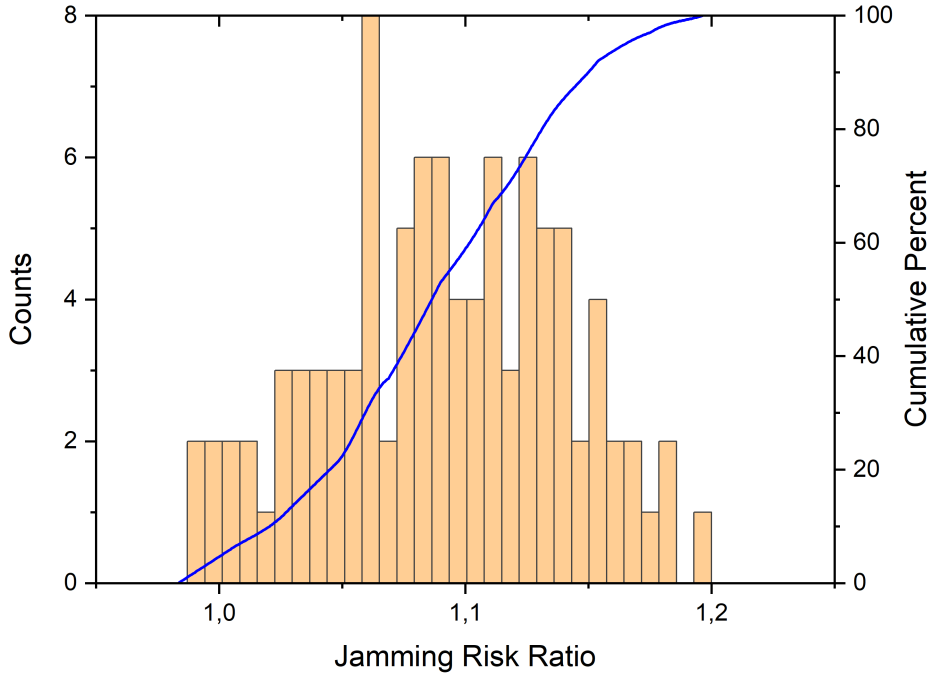

Figure 4.41: The cumulative percent graph for the jamming ratio in z29 when the Double-shielded TBM is actively lubricated

2. Single-shielded TBM without lubrication

   The application of a single-shielded TBM instead of a double-shielded TBM in zone 25 shows in 91% of the cases a high level of jamming risk and a very high level in 9% of the instances (See Figure 4.42). In zone 29, it is noteworthy that all instances exhibit a very high level of jamming risk.

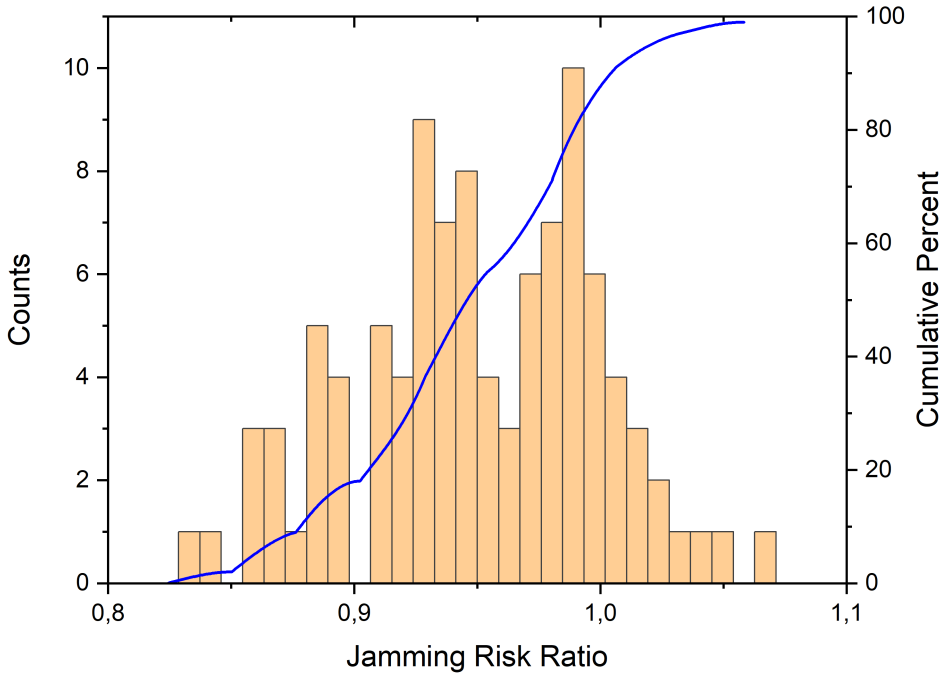

Figure 4.42: The cumulative percent graph for the jamming ratio in z25 when a single shielded TBM is applied

3. Single-shielded TBM with lubrication

   Assuming active lubrication behind the shields for a single shielded TBM in zone 25, on the other hand, leads to a low level of jamming risk in 18% of the iterations and a medium jamming risk for 82% of them (See Figure 4.43). The same mitigating measure applied in zone 29 would lower all the risks to the medium level (See Figure 4.44).

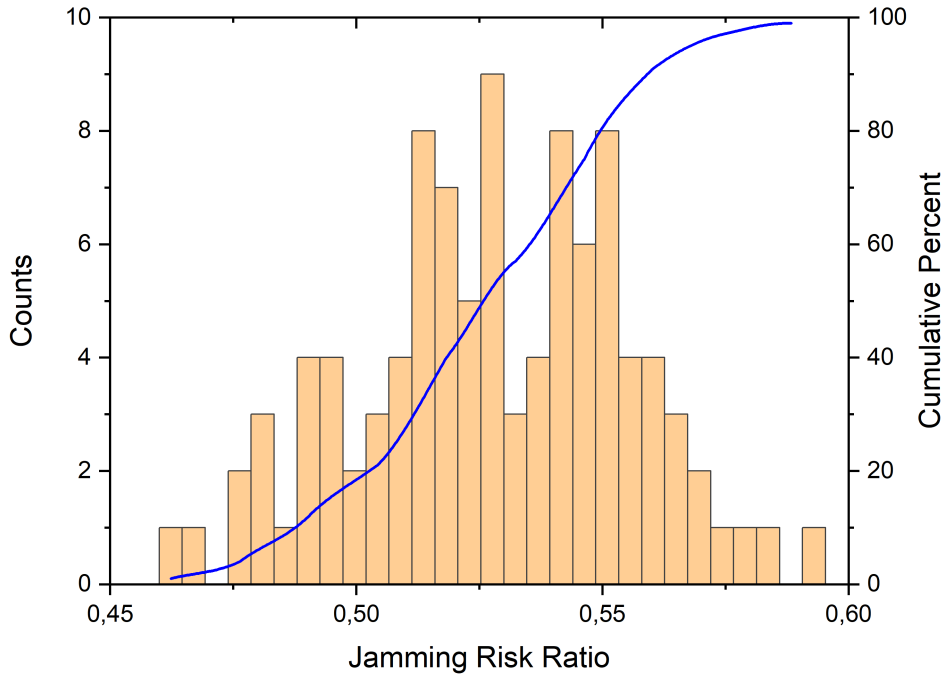

Figure 4.43: The cumulative percent graph for the jamming ratio in z25 when a single shielded TBM is applied with active lubrication

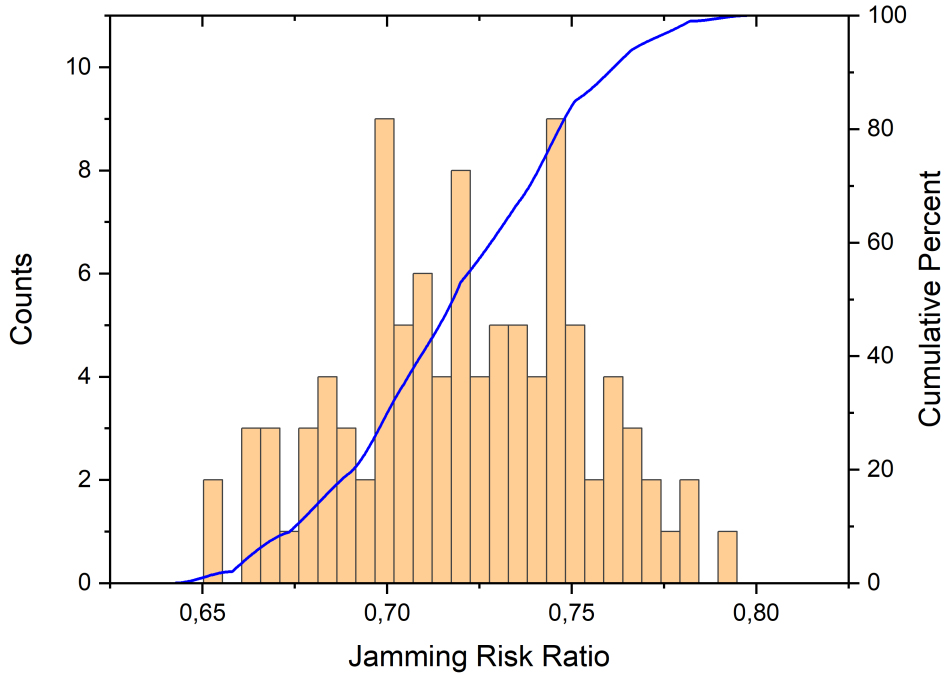

Figure 4.44: The cumulative percent graph for the jamming ratio in z29 when a single shielded TBM is applied with active lubrication

Table 4.8 presents a concise summary of the proportions of each geological zone 25 and 29 containing certain levels of jamming risks. This information serves as a valuable tool for decision-making, as it clearly indicates the likelihood of each level of risk. These results suggest that applying a single shielded TBM with active lubrication behind the shield would have enabled crossing the squeezing grounds with a low to medium level of jamming risk.

Table 4.8: The proportion of different levels of jamming risk in z25 and z29 using a probabilistic manner

Geological zone	The mitigating measure	The level of jamming risk			
		Low	Medium	High	Very High
z25	DS TBM with lubrication	-	53%	47%	-
	SS TBM	-	-	91%	9%
	SS TBM with lubrication	18%	82%	-	-
z29	DS TBM with lubrication	-	-	5%	95%
	SS TBM	-	-	-	100%
	SS TBM with lubrication	-	100%	-	-

Probabilistic evaluation of the TBM Risk Index

Eventually, through the probabilistic approach developed in this study, a distribution of the TBM Risk Index (TBM_{RI}) for all the instances is achieved, which is depicted in Figure 4.45. By examining this index, it becomes evident how different machine selections and mitigation strategies can directly impact the level of the squeezing risk. This analysis offers valuable insights into the efficacy of each approach in managing the squeezing risk in the Golab tunnel.

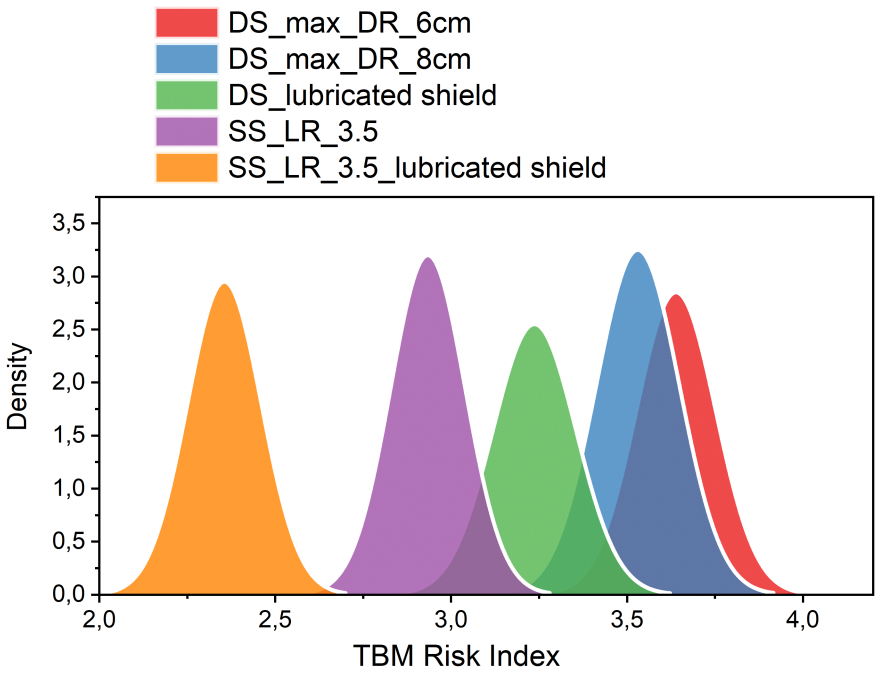

Figure 4.45: The distribution of TBM Risk Index for the 6400 length of Golab tunnel considering different machines and mitigating measures

4.2 Introduction of a case study for the rockburst risk assessment

The introduced methodology for assessment of the rockburst risk is now implemented in the TBM (Tunnel Boring Machine) excavated tunnel of the Jinping II project. Its objective is to facilitate a quantitative assessment of the consequences associated with rockburst events.

4.2.1 Project Overview

The Jinping II hydropower project, situated in the Sichuan province of China consists of seven parallel tunnels. These tunnels include a drainage tunnel, two transportation tunnels, and four diversion tunnels. The average length of the tunnels is 16.7 km with a maximum depth of 2525 m. Different excavation methods were

applied in this project. The No. 1 and No. 3 diversion tunnels were excavated using tunnel boring machines (TBMs), both of which have circular cross-sections with a diameter of 12.4 meters. The No. 2 and No. 4 diversion tunnels were excavated through blasting, and they have horseshoe-shaped cross-sections with a diameter of 13.0 meters (See Figure 4.46). Additionally, the drainage tunnel with a diameter of 7.2 m was also excavated by a TBM.

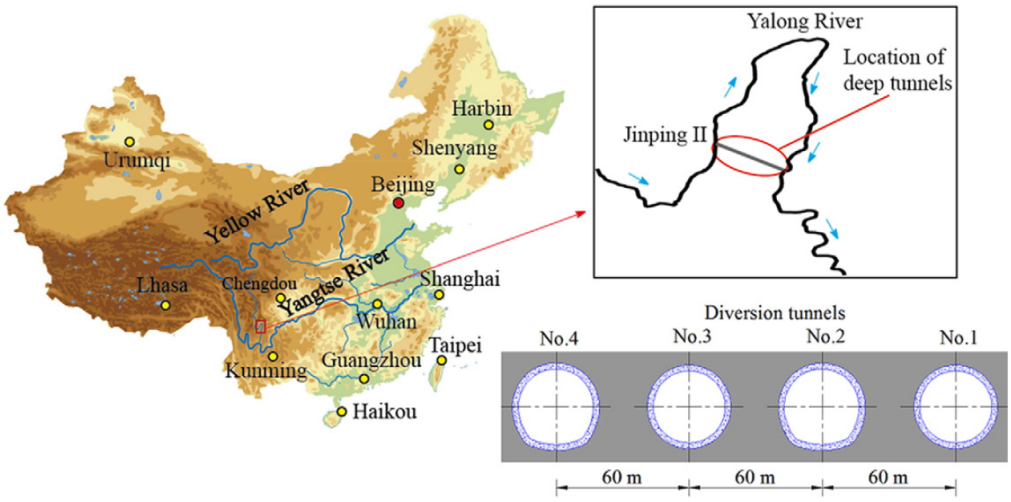

Figure 4.46: The Jinping II project location with the cross-section of the diversion tunnels [101]

The geological composition of these tunnels is predominantly made up of marble, sandy slate, and chlorite schist. Amongst them, marble from the Baishan Formation has a higher potential for strainbursts due to its increased energy storage and brittleness properties. Intense rockbursts have occurred multiple times during the excavation of the tunnels. This investigation focuses on the T2b-class II marbles, specifically from chainage 5+500 km to 10+450 km, as this section experienced the majority of rockburst incidents. The range of geotechnical parameters from this formation is inserted in Table 4.9.

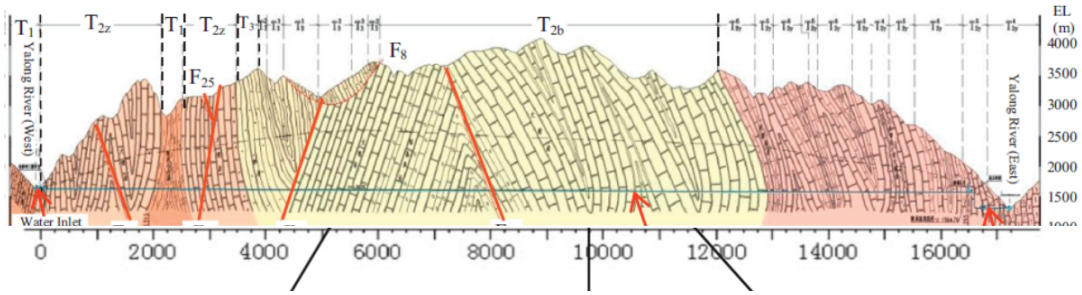

Figure 4.47: The geological profile of the Jinping II hydropower station project(adapted from [104])

Table 4.9: The geotechnical parameters of the main marble formation in Jinping II project [105] ,[104] and [106]

Main Lithology	Statistical Measures	density (kg/m3)	σ_{ci} (MPa)	GSI	Crack initiation stress (MPa)	T (MPa)	E_i (GPa)	ν
Marble-T2b-Class II	Mean (μ)	2750	113.7	60	60.2	4.5	42.8	0.23
	Standard Deviation (σ)	-	13.7	3	10.2	0.5	10.7	-

According to the existing geotechnical parameters, the most common equations based on the in-situ stress and rock strength are applied. The vertical stress is assumed as the gravitational stresses estimated by the overburden in every meter of the chainage 5+500 km to 10+450 km. By the Monte Carlo simulation, geotechnical values of rock are selected by assuming normal distributions from Table 4.9, and five main methods are employed for the analysis. The outcomes of the analysis are communicated through separate histograms, which can be found in Figures 4.48, 4.49, 4.50, and 4.51. Furthermore, a summary of the value ranges is included in Table 4.10. This table provides a convenient reference to the anticipated ranges of rockburst extent, indicating a range of moderate to heavy. Based on the findings discussed in Section 3.3.1, where it was highlighted that mechanical excavation is more prone to experiencing the consequences of rockbursts, the higher extent of heavy rockbursts is assumed as the prevailing type.

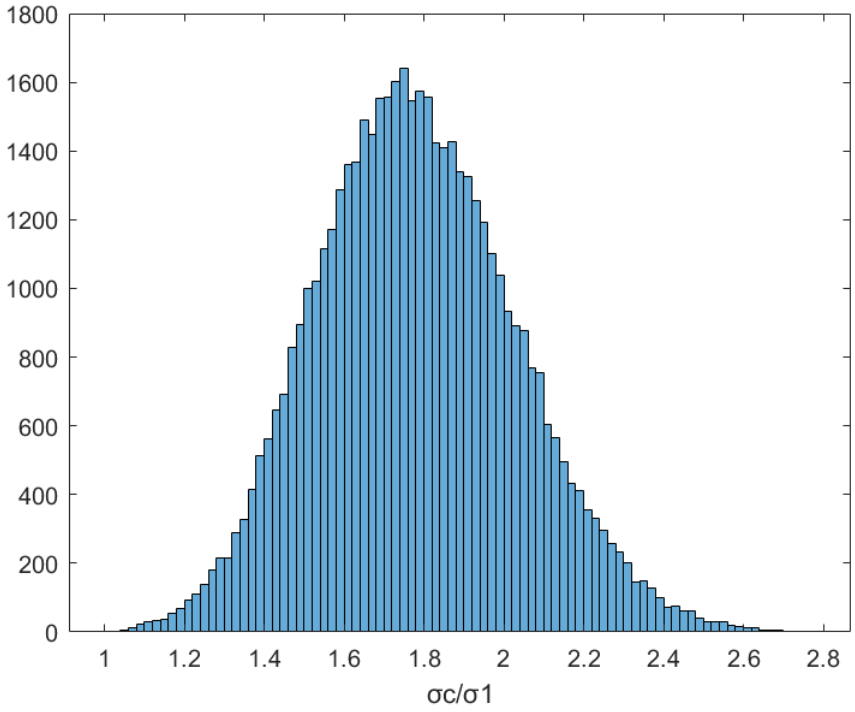

Figure 4.48: The distribution of UCS to max. principal stress for the Marble-T2b-Class II

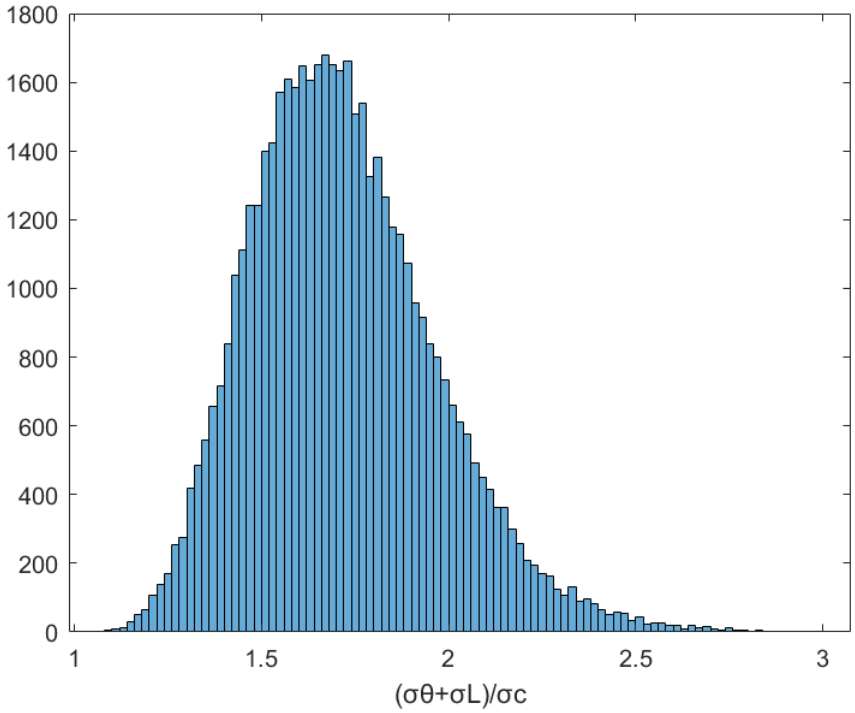

Figure 4.49: The distribution of the stress-strength criterion by Turchaninov and Markov (1981) for the Marble-T2b-Class II

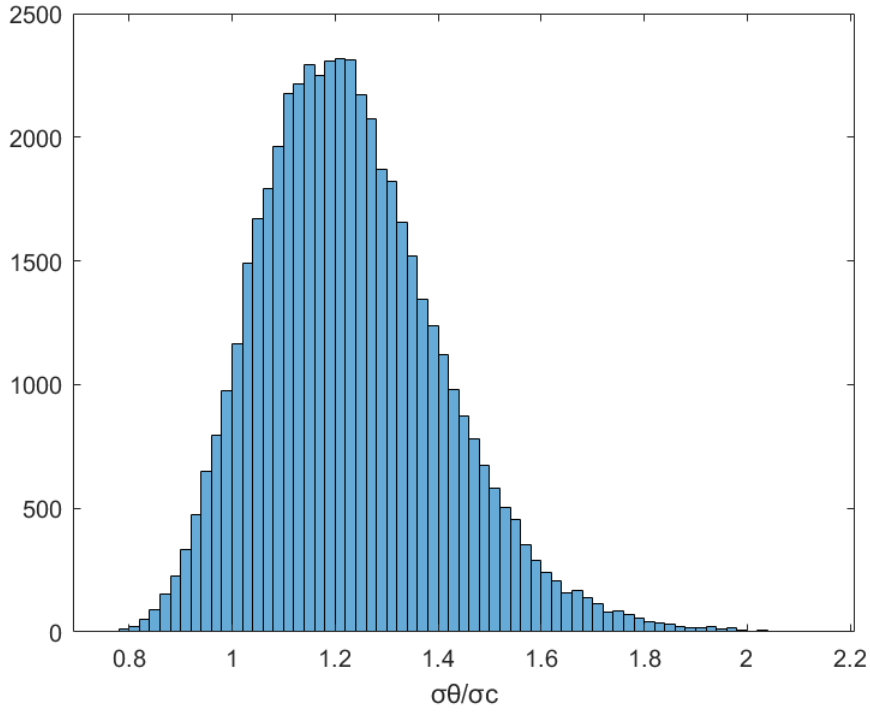

Figure 4.50: The distribution of max. tangential stress to UCS for the Marble-T2b-Class II

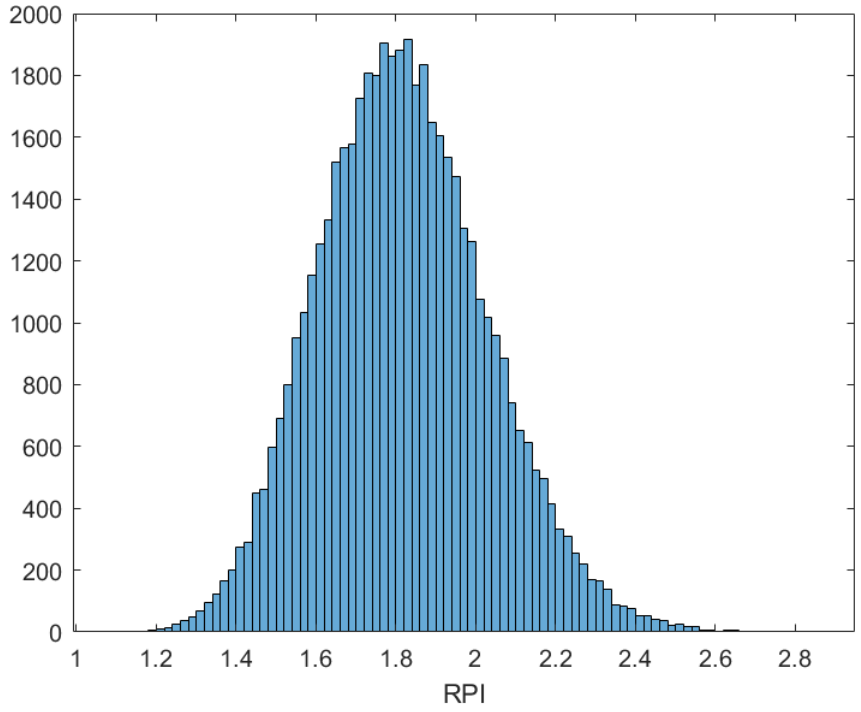

Figure 4.51: The distribution of the RPI factor by Ma et al. (2018) for the Marble-T2b-Class II

Table 4.10: The intensity of rockburst using rockburst prediction tools

Criterion	σ_c/σ_1	$(\sigma_\theta + \sigma_L)/\sigma_c$	σ_θ/σ_c	Spalling extent (m)	RPI	Rockburst intensity
Barton et al. (1974)	1-2.7					Moderate to heavy rockburst
Turchaninov and Markov (1981)		1-2.8				Heavy rockburst
Hoek and Brown (1980)			0.8-2			Heavy rockburst
Martin and Christiansson (2009)				3-18		-
Ma et al. (2018)					1-2.6	Moderate to heavy rockburst

In the next stage of the assessment, the criterion introduced in Table 3.19 is employed together with the rockburst location (RB_l) randomly selected based on the distribution function introduced in Figure 3.38 for assessment of the Rockburst Risk Index. The question here similar to the squeezing risk assessment procedure is to determine the suitable type of TBM that possesses the lowest extent of risk. Three typical types of TBMs with the same diameter of 7.2 m and the following characteristics are assumed in the analysis:

- Gripper TBM with 6m shield length- 4m of the initial support section
- Single Shield TBM with 9m shield length
- Double Shield TBM with 13m of total shield length

Taking these options into consideration and assuming the suitable coefficients for the machines, Table 3.19 will be modified to Table 4.11. Some notes regarding the logic for the selection of the factors are explained as follows:

- Since the support system in a gripper TBM develops itself as the tunnel advances, the parameter SM_{3G} or the functionality of the support system in a gripper TBM against high energy events is different in each chainage. It is here assumed that the support system is not active in the RB_l of 6 m to 9 m and therefore the support damage is not concerned in this range. From $RB_l > 9m$, it is assumed that the functionality of the support system will increase, and therefore, the $SM_{3G} = 0.5$. This signifies that the support system can mitigate the effects of support damage by a factor of two. On the other hand, the

functionality of segmental lining against high-energy events is assumed to be two times less than the support in the gripper TBM ($SM_{3S} = 1$).

- The mitigating effects of the support system in a gripper TBM against equipment damages (SM_{4G}) and injuries (SM_{5G}) are also expected to vary based on the location of the rockburst (RB_l). For the range of $6m < RB_l \leq 9m$, both parameters (SM_{4G} and SM_{5G}) are expected to be equal to 1, indicating a lack of mitigating effect due to the absence of a support system. As of $RB_l > 9m$ a mitigating effect of 30% is assumed or: $SM_{4G} = SM_{5G} = 0.7$

- The mitigating effect of segmental lining in shielded TBMs against equipment damages (SM_{4s}) and injuries (SM_{5s}) is assumed to be 20%. This value shows only a marginal decrease when compared to the gripper TBM because although the segmental lining is expected to have a higher risk of damage due to its low energy-absorbing characteristics, it provides a protected area for personnel and equipment. This protection functions well as long as the support system itself is not significantly damaged.

To conduct the analysis, we perform 100000 iterations to determine the location of the rockburst and apply this data to calculate the Rockburst Risk Index for each type of machine, following the established criteria. Figure 4.52 shows the distribution of rockburst risk index values for each type of machine. As can be seen, the values are very discrete, which is due to the fact that the main input parameter which is the intensity of the rockburst is not changing and was assumed as 4 (heavy rockburst) in the whole region of this analysis. The only variation lies in the location of the rockburst which is very much focused in the front area of the tunnel according to the distribution defined in Figure 3.38. In order to have a better comparison between the different TBM types, the average values of TBM_{RI} are evaluated and inserted in Table 4.12. As can be seen, the higher protection provided by the larger shields in single and double-shielded TBMs leads to lower risk indices compared to the gripper TBMs. The injury and fatality risks are especially lower for shielded TBMs. This is primarily attributed to the high exposure of personnel to the rock bursts in a

gripper TBM compared to shielded TBMs. Another factor is that according to the distribution function introduced in Figure 3.38, most of the rockbursts are expected to have occurred before the distance from the tunnel face (RB_l) reaches 13 m. As a result, the primary risk for the double-shield TBM in this region is damage to the shield and cutterhead. Based on the rockburst risk index criterion, the double-shield TBM, with a total risk index value of 4.9, is considered a superior choice for excavation in high-rockburst risk zones.

Table 4.11: The criterion for evaluation of the TBM rockburst consequences in Jinping II drainage tunnel with parameters modification according to TBM types

Distance of event (RB_l)	Gripper TBM		SS TBM		DS TBM	
	Damage/time-consuming operation	Injury/fatality	Damage/time-consuming operation	Injury/fatality	Damage/time-consuming operation	Injury/fatality
$0.2 < RB_l \leq 6$	$RB_2 + RB_{6G}$	-	RB_2	-	RB_2	-
$6 < RB_l \leq 9$	$RB_4 + RB_{6G}$	RB_5	RB_2	-	RB_2	-
$9 < RB_l \leq 13$	$0.5RB_{3G} + 0.7RB_4 + RB_{6G}$	$0.7RB_5$	$RB_{3S} + 0.8RB_4$	$0.8RB_5$	RB_2	-
$13 < RB_l \leq 70$	$0.5RB_{3G} + 0.7RB_4 + RB_{6G}$	$0.7RB_5$	$RB_{3S} + 0.8RB_4$	$0.8RB_5$	$RB_{3S} + 0.8RB_4$	$0.8RB_5$

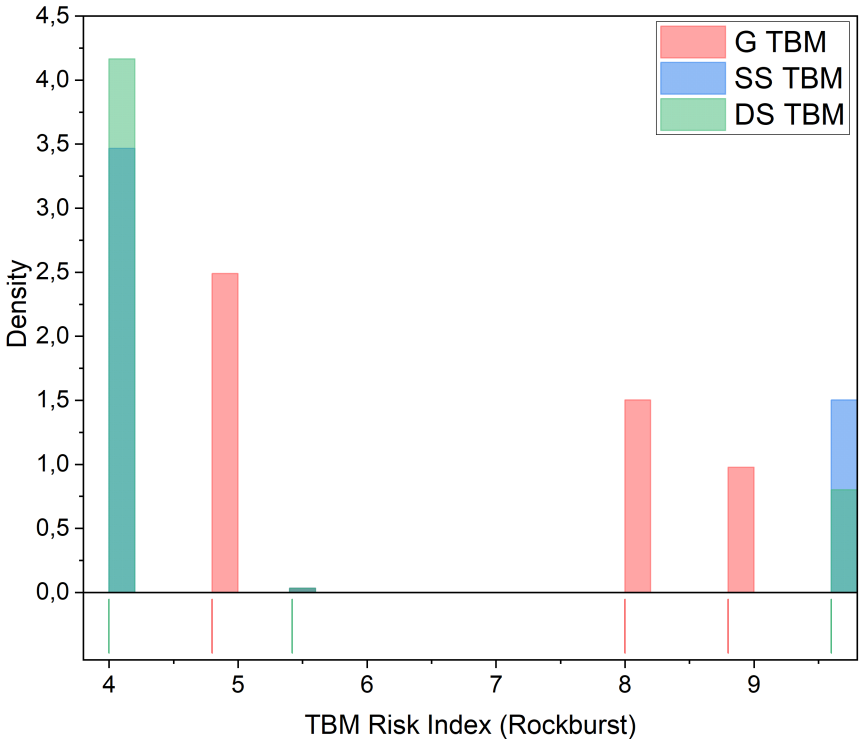

Figure 4.52: The distribution of the TBM Risk Index for different types of TBMs

Table 4.12: The average TBM rockburst risk index for different machine types

Consequence	Gripper-TBM Risk Index	Single-Shield TBM Risk Index	Double-Shield TBM Risk Index
Damage/time-consuming operation	4.92	4.72	4.38
Injury/fatality	1.63	0.97	0.52
Total	6.55	5.69	4.9

4.2.2 Discussion of the results

This section presents some observations regarding the outcomes obtained from the investigation into the rockburst risk index:

- Predicting the intensity of rockburst in a tunnel is an inherently challenging

task. When assessing the rockburst risk associated with TBM application, this procedure becomes even more complex. An example of a case study (Jinping II drainage tunnel 7.2 m diameter) was introduced in this chapter of the thesis. The extent of the database was very limited and therefore, in the first step which was the prediction of the rockburst intensity, the methods based on the strength and stress state of rock were applied for a whole 5 km length of the tunnel and instead of a distribution of rockburst intensities, only one single category of heavy rockburst was chosen. This is certainly not a sufficiently accurate estimation. Moreover, the subsequent stage of rockburst consequence estimation relied exclusively on the geometry of the TBM and its features as well as the assumption of rockburst location approximation based on statistical data obtained from a project with similar dimensions (Neelum-Jhelum tunnel with 6.8 m diameter). It must be noted that assuming the same rockburst intensity for all the rockbursts occurring is an overestimation. What can certainly reduce the complexity and uncertainties in this research is the broader extent of databases from similar projects.

- The coefficients introduced in Table 3.19 and later adapted in Table 4.11 are assumptions. Some parameters such as the mitigating effect of the support system in controlling the consequences highly depend on the intensity of rockbursts and the type of support system itself. Therefore, these factors are very project specific and need to be chosen based on actual data from similar projects which was very difficult to access in this research.

- The methodology developed for the assessment of the rockburst consequences in this research is exclusively related to strainbursts which are more common in mechanically excavated tunnels. Therefore, the rockbursts which are triggered by faults require an additional factor. For instance, an intensifier factor can be considered for the zones where the possibility of fault-triggered rockburst exists. As for the Jinping II drainage tunnel, a sudden slip of a rigid fault sub-parallel to the tunnel axis in the chainage of 9 + 283 km to 9 + 322 km is known to have caused an intensive rockburst leading to 7 deaths, one injury,

and total destruction of the TBM [107]. Figure 4.53 shows different images pertaining to the rockburst destructive consequences as well as the position of the fault adjacent to the tunnel section.

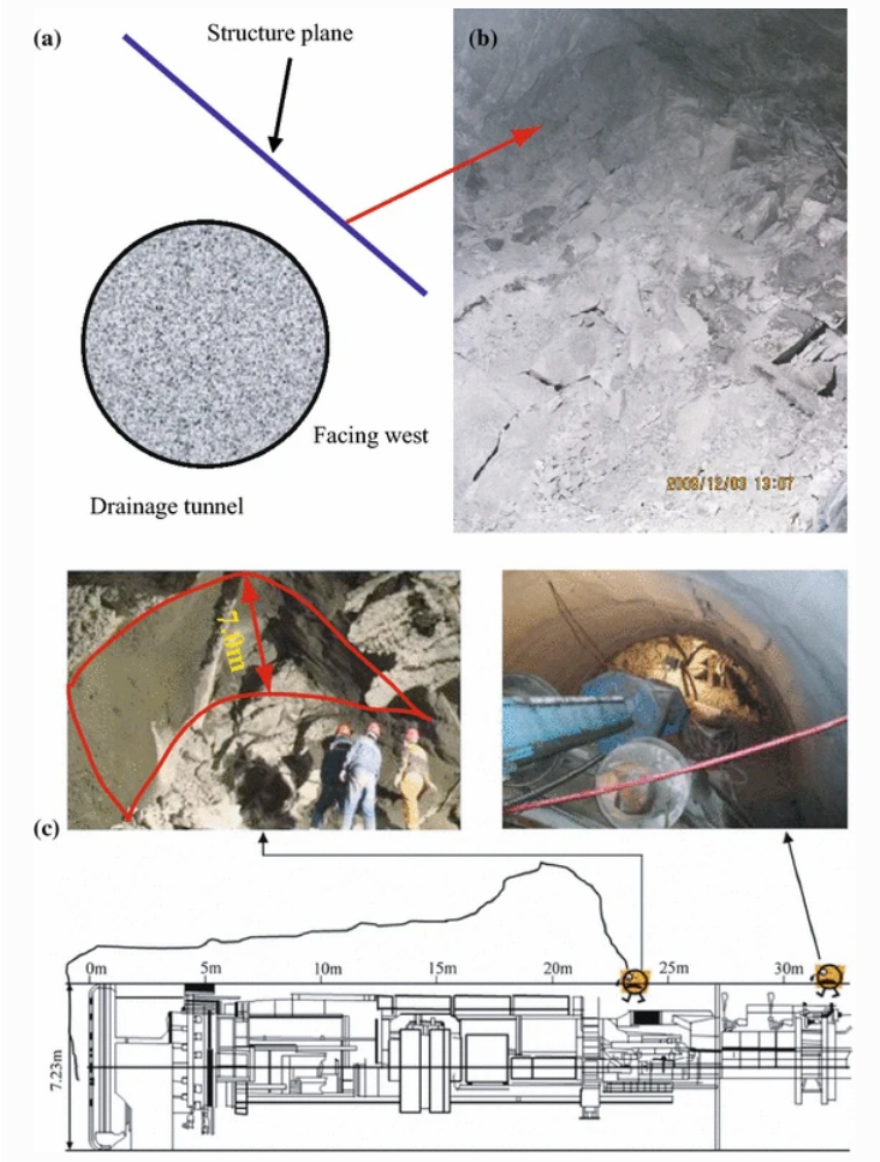

Figure 4.53: The very intensive rockburst occurred in the chainage 9+285 km of the drainage tunnel in Jinping II project [107]

- One notable limitation of the rockburst risk index, which is similar to the squeezing risk index, is its lack of a definitive classification for the severity of consequences based solely on the introduced numerical values. Instead, the rockburst risk index allows for a comparison between various TBMs, mitigation measures, and other factors, aiding in the selection of the approach with the lowest extent of risk.

4.3 Representation of squeezing and rockburst in one risk index

In the previous sections, two case studies each encountering harsh squeezing and rockburst risks were presented and the TBM risk indices for these risks were evaluated accordingly. As for the case study of Golab tunnel, squeezing risks including shield jamming and support system damage were predominant. The findings indicated that utilizing a single-shielded TBM with a shorter shield along with the implementation of shield lubrication as a mitigating measure, would significantly reduce the squeezing risk index. Conversely, the risk index evaluations in the case study of the drainage tunnel of Jinping II project suggest that a shorter shield would result in higher exposure of personnel and machine components to seismic events when rockburst risk is predominant. The question that arises here is: Which type of machine is suitable if both of these risks are present in a project? In order to answer this question, a case study having both risks was required. Attempts made to get access to data pertaining to such case studies were not successful. In this concluding phase of the investigation, we rely on assumptions, combining geotechnical data from the two case studies to guide the analysis. The assumption is that within a tunneling project, three primary types of ground conditions may be encountered: normal ground conditions, squeezing ground conditions, and ground with a risk of rockbursts. From these conditions, three distinct scenarios are distilled:

- Scenario 1: An equal proportion of all behavior types (Figure 4.54).
- Scenario 2: A scenario predominantly characterized by squeezing ground behavior (Figure 4.55).
- Scenario 3: A scenario where the predominant concern is the risk of rockbursts (Figure 4.56).

The geometrical and operational characteristics of the Golab tunnel are used in this respect. The geotechnical parameters pertaining to the Meta shales with the zoning number of z29 were picked for the squeezing risk from Table 4.4, and the ones

from the Marble formation in Jinping II from Table 4.9 were assumed for the zone having the rockburst risk. The effect of the proportion of each ground condition is considered through the length normalizing factor ($\frac{L_i}{L_t}$) in equation 3.1.

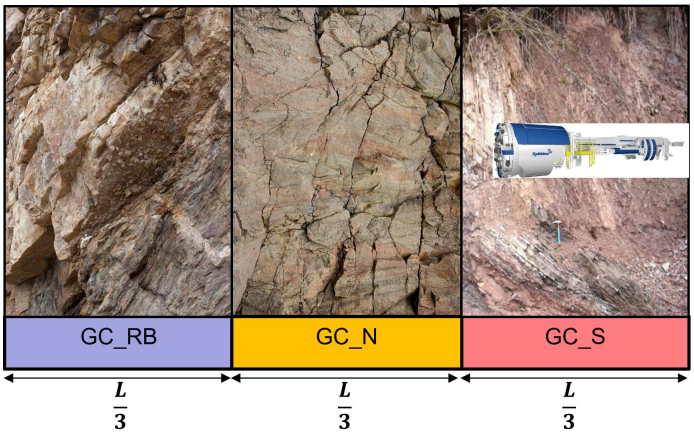

Figure 4.54: The presumed scenario for a tunnel with equal proportions of normal ground (GC_N), ground with squeezing risk (GC_S) and ground with rockburst risk (GC_RB)

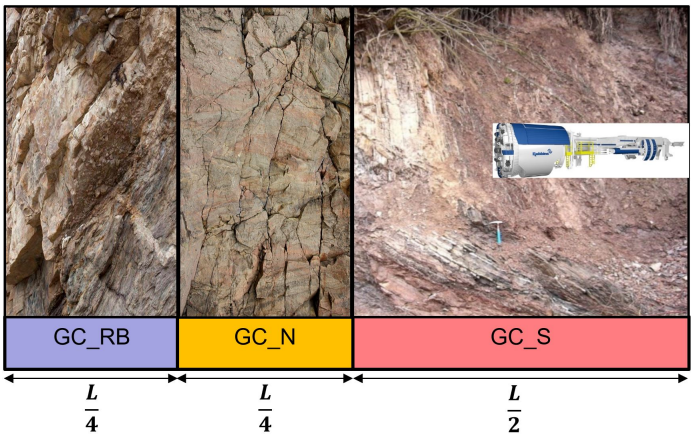

Figure 4.55: The presumed scenario for a tunnel with dominant squeezing behavior (GC_S) and equal proportions of normal ground (GC_N) and ground with rockburst risk (GC_RB)

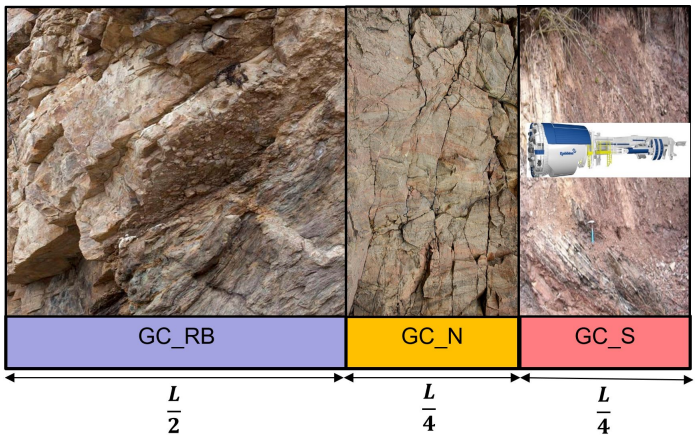

Figure 4.56: The presumed scenario for a tunnel with dominant rockburst hazards (GC_RB) and equal proportions of normal ground (GC_N) and ground with squeezing risk (GC_RB)

All types of machines introduced in section 4.1.1 together with a gripper TBM are included in this analysis. The main performance parameters for the assumed gripper TBM are inserted in Table 4.13. The support system also needs to be taken into consideration in the analysis of a gripper TBM. Since the support system is not a fixed structure in gripper TBMs compared to shielded TBMs, more detailed characteristics including the distance of the support installation point to the tunnel face need to be specified. Rock support measures are usually started shortly behind the Gripper-TBM's L1 section (See Figure 3.37). Examples of support element installation methods include steel support erecting machines, rockbolt drilling machines, or mesh laying devices. The installation of shotcrete takes place in the rear section. In this instance, we are assuming that in the very harsh squeezing grounds of Meta Shales, steel support together with systematic bolting installation are immediately installed after the TBM shield, and afterward in a distance of 8 m to the tunnel face, a shotcrete layer is also sprayed on the tunnel surface. The mechanical characteristics of the support system are inserted in Table 4.14. The maximum support pressure and the support stiffness of the entire system were estimated utilizing the Rocsupport Software V. 5.002 [108]. The results indicate a maximum support pressure of 2.72 MPa and a support stiffness of 164.15 MPa/m. It should be noted that based on equation 3.15, an SF_{sig1} of 1.5 was considered to take account of the anisotropies in the deformation due to the schistosity of the rock

mass in the Meta-Shales. This factor is assumed lower compared to the segmental lining, as the more flexible support system is supposed to be more efficient with regards to anisotropic deformations.

The same assumptions made for the strainburst location distribution made in section 4.2 according to Figure 3.38 are also made for this investigation. Using these data, five types of machines and associated mitigating measures are analyzed together and the total TBM Risk Indices are calculated. Figures 4.57 and 4.58 summarize the process applied for selection of the suitable squeezing and rockburst indices, respectively.

Estimation of the TBM risk index starts with separate calculation of squeezing and rockburst risk consequences as indicated in Table 4.15. The indices are subsequently summed together according to the different proportion of zones containing squeezing and rockburst risk in each scenario (See Table 4.16). The summary of TBM risk indices evaluated from the three scenarios are depicted in Figure 4.59.

Table 4.13: The assumed gripper TBM performance parameters

Radius(m)	L_{sh} (m)	R_{sh}(m)	μ	Max. Thrust Force (MN)
2.27	3	2.21	0.45	10

Table 4.14: The support system mechanical parameters assumed for the gripper TBM

Rockbolts					Wide flange ribs			Shotcrete			
D (mm)	Capacity (MN)	E (GPa)	L (m)	Circumferential and longitudinal spacing(m)	Section depth (mm)	Area (mm^2)	Out of plane spacing(m)	Thickness (mm)	UCS (MPa)	E (GPa)	ν
25	0.354	207	3	1.2	150	4080	1.2	200	25	3	0.2

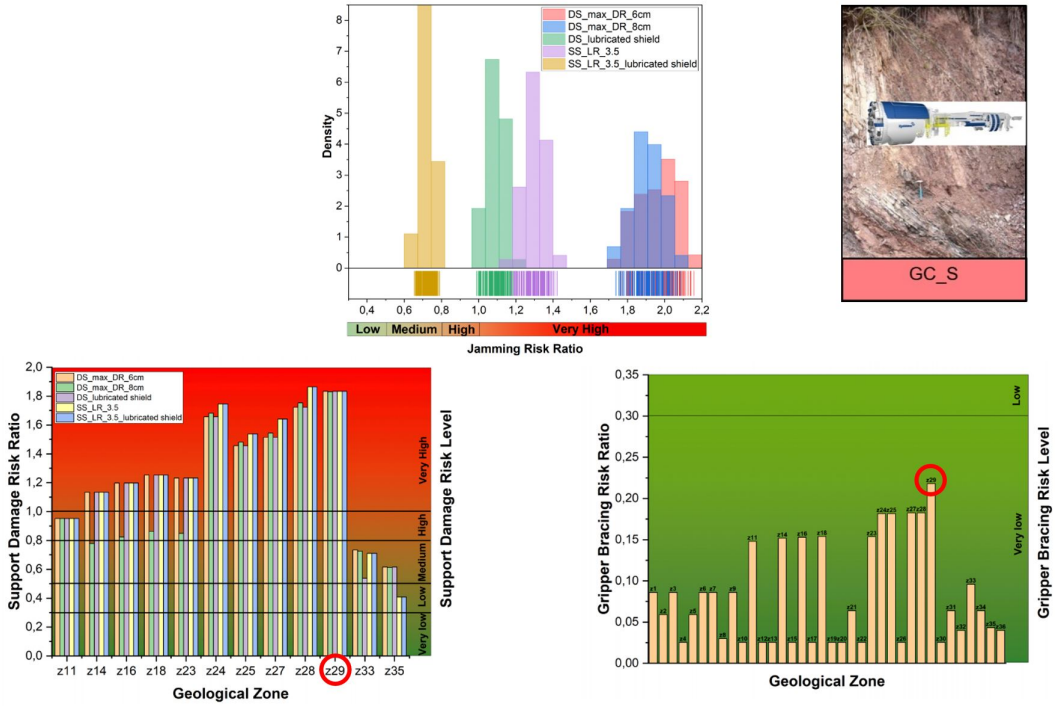

Figure 4.57: Deterministic selection of squeezing consequences for the Meta shale zone in Golab tunnel (zone z29) based on the assessments conducted in section 4.1

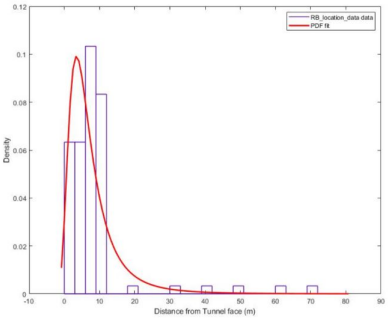

Rockburst degree	The Consequence extent	The consequence quantity RB_j
No Rockburst	Insignificant	1
Light Rockburst	Minor	2
Medium Rockburst	Moderate	3
Heavy Rockburst	Major	4
Serious Rockburst	catastrophic	5

Figure 4.58: Using the presumed rockburst location distribution, the rockburst category together with the machine geometrical properties for the ground class with rockburst possibility

Table 4.15: Estimation of the squeezing and rockburst risk indices for different types of machines and mitigating measures

The machine type and measures	Average Squeezing Risk Index (Sq_{RI}) = $\sum_{j=1}^{3} S_j \cdot W_{S_j}$						Average Rockburst Risk Index (RB_{RI}) based on the criterion in Table 4.11				
	Jamming Risk (JR)		Support damage Risk (DR)		Gripper bracing risk (GR)		Shield damage (RB2)	Support damage (RB3)	Equipment Damage (RB4)	Gripper bracing issues (RB6)	Injuries or fatalities (RB5)
	Consequence(S_1)	Weight(W_{S_1})	Consequence(S_2)	Weight(W_{S_2})	Consequence(S_3)	Weight(W_{S_3})	Damage and time consuming operation				
DS TBM (Max DR = 6cm)	4	1.00	4	0.80	-	-	4.52				0.7
	7.20						5.22				
DS TBM (Max DR = 8cm)	4	1.00	4	0.80	-	-	4.52				0.7
	7.20						5.22				
DS TBM assuming lubricated shield	4	1.00	4	0.80	-	-	4.52				0.7
	7.20						5.22				
SS TBM	4	1.00	4	0.80	-	-	4.84				1.14
	7.20						5.98				
SS TBM with lubricated shield	2	1.00	4	0.80	-	-	4.84				1.14
	5.20						5.98				
GTBM	0.00	1.00	4.00	0.80	2.00	0.20	4.93				2.72
	3.60						7.65				

Table 4.16: Estimation of the TBM_{RI} for different types of machines and mitigating measures based on the three presumed geological scenarios

The machine type and measures	TBM_{RI} scenario 1 ($\frac{Sq_{RI}}{3} + \frac{RB_{RI}}{3}$)	TBM_{RI} scenario 2 ($\frac{Sq_{RI}}{2} + \frac{RB_{RI}}{4}$)	TBM_{RI} scenario 3 ($\frac{Sq_{RI}}{4} + \frac{RB_{RI}}{2}$)
DS TBM (Max DR = 6cm)	4.14	4.91	4.41
DS TBM (Max DR = 8cm)	4.14	4.91	4.41
DS TBM assuming lubricated shield	4.14	4.91	4.41
SS TBM	4.39	5.1	4.79
SS TBM with lubricated shield	3.73	4.1	4.29
GTBM	3.75	3.71	4.73

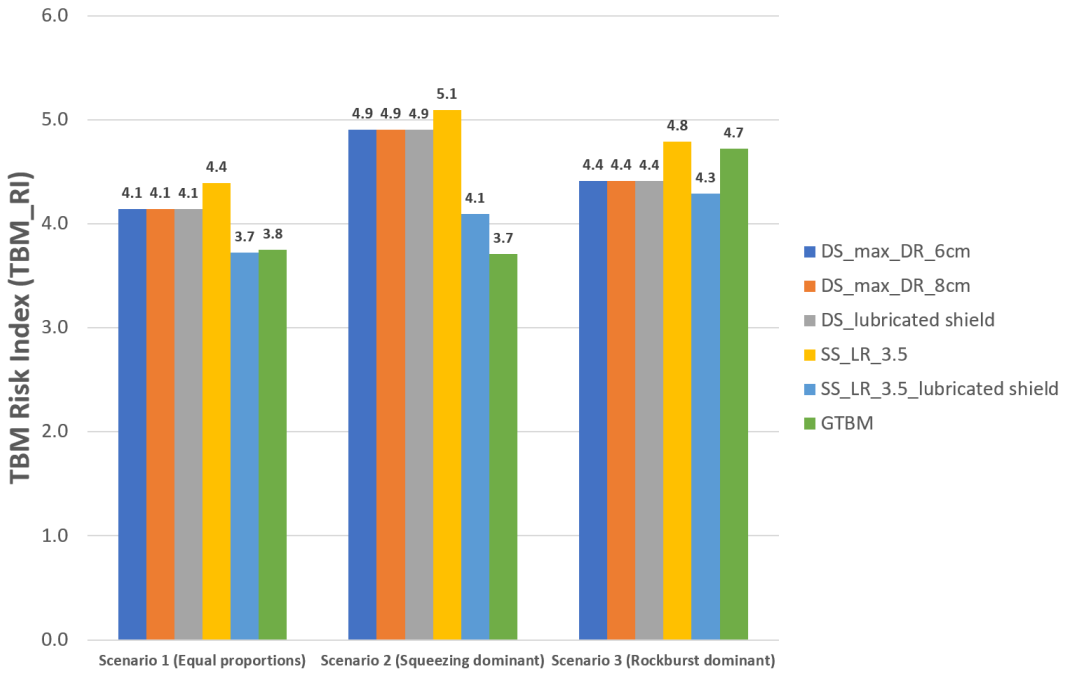

Figure 4.59: The results of TBM_{RI} for the three presumed geological scenarios

The analysis results yield the following findings:

- As can be seen in Table 4.15, the shield length has the highest effect on the extent of jamming risk. By shortening the shield of the machine from 11 m in a double-shielded TBM down to 3 m in a gripper TBM, the jamming risk can be fully reduced from a consequence extent of 4 to 0 i.e, fully treated. It is important to highlight that the support system highly affects the jamming risk, and without immediate installation of a suitable support system as close as possible to the tunnel face, the high deformations can impose high pressures

on the shield of a gripper TBM. This is especially important because the maximum thrust force the machine can provide in a gripper TBM depends on the ground conditions and the capability of gripper shoes in providing the required reaction forces for excavation and advance of the machine. In this example, we assumed that the grippers can provide a maximum thrust force of 10 MN which is half of the maximum values for the shielded TBM.

- Although the jamming risk is highly treated through lubrication of a single shielded TBM or application of a gripper TBM, the support system risk was not addressed and the risk extent is the same for all options. As for the shielded TBMs, this can be addressed by using more deformable segmental linings. Shielded TBMs are not very flexible in this regard, whereas gripper TBMs offer more flexibility in choosing a variety of support systems that can well fit to a squeezing ground. The main issue here compared to the shielded machines is the time-consuming operation needed for the support installation which would certainly reduce the advance rate to a certain extent. In spite of the facts mentioned, the selection of the support system in all types of machines requires a more comprehensive investigation e.g., using numerical modeling to properly design the components and consider the operational implications.

- An interesting fact from the results is the moderate level of gripper bracing risk for the gripper TBM in the squeezing grounds, which was anticipated, because of the very low strength of the rock in the Meta-shales. However, it is worth noting that this risk is not critical, as there are measures that can be taken to address it effectively. One such measure involves installing timbers behind the gripper shoes to increase the pressurizing area. This sort of implementation helps distribute the forces exerted by the gripper shoes more evenly, minimizing the risk of bracing-related issues.

- It can be deduced that gripper TBMs have the lowest extent of squeezing risk compared to other machines. Their main disadvantage which is not considered in the risk index is the lower advance rate especially when extensive support

systems need to be installed in weak grounds. On the other hand, gripper TBMs, as was also seen in the Jinping II case study, have the highest extent of rockburst risk, especially with regard to the higher exposure of personnel to rockburst events.

- In the first scenario with equal proportions of all ground types, the total TBM_{RI} for a single shielded TBM that uses lubrication is the lowest, but only slightly lower than a gripper TBM as the next best alternative. An interesting observation is that without lubrication, the single-shielded TBM would actually become the worst alternative. Therefore, the effectiveness of a shielded machine in such a scenario relies heavily on the implementation of mitigating measures to control the jamming risk.

- In the second scenario, where the predominant concern is the risk associated with squeezing, it is noteworthy that a gripper TBM exhibits a notably lower risk index in comparison to all other available options. Conversely, in the third scenario, where rockbursts are the primary risk factor, a single shielded machine with appropriate lubrication emerges as the most favorable choice. What makes shielded machines and especially double-shielded machines a better alternative compared to a gripper TBM in this scenario is mainly the high-risk extent of gripper TBMs with regards to injuries and fatalities (RB_5). This extent of risk can be alleviated by further mitigating measures. Brox (2019) suggests some measures to counteract the issues: extension of TBM finger shields, use of the McNally Tunnel roof support system, drilling of radial drill holes, and de-stress blasting [109]. Drilling of radial drill holes and de-stress blasting are considered very difficult due to the lack of space in front of the tunnel and can dramatically reduce the advance rate of the TBM. However, the use of the Mc Nally tunnel roof support system, as mentioned before, has proven to be very effective in controlling the safety risks of using gripper TBMs in deep tunneling conditions. Assuming that systems such as the Mc Nally system can alleviate the safety risks pertaining to heavy rockbursts, the TBM_{RI} for a gripper TBM in Table 4.16 can be further reduced. As the effectiveness

of this measure is not quantitatively evaluated in this study, no conclusion can be made upon the best method for the third scenario. Nevertheless, it can be generally stated that a gripper TBM with mitigated rockburst consequence using measures such as the Mc Nally system encompasses the lowest TBM risk index in the first and second scenarios.

- Referring to some other case studies and an overview of the projects where both squeezing and rockburst were concerns shows a preference among contractors for using gripper TBMs primarily to avoid machine entrapment in squeezing zones. For instance, in the planning stage of Neelum-Jhelum hydroelectric project, the high-stress environment was analyzed in terms of two distinct rock behaviors, namely the tendency of competent brittle rock to experience rock bursts and the potential of weak rock to undergo extreme deformations of up to 500 mm due to squeezing. In this case, using a gripper TBM would mitigate the jamming risk and even the support damage risk because of the adaptability of the machine to different support systems. The variability of the ground condition and lack of geotechnical data from the deep underground conditions can also be another reason for choosing the gripper TBMs with more potential in changing the support system [110]. However, despite these considerations for squeezing risk, a severe rockburst with a Richter magnitude of 2.0 at a depth of 1300 m in the chainage of 09+706 to 09+793 led to deep over breaks. As a result, three workers died and a few others were injured on the 31st of May 2015. The severe impact of the seismic events destroyed the whole support systems and the TBM itself (See Figure 4.60). The concentration of stresses resulting from geological structures was identified as the main reason for the severe damages, similar to the high energy seismic event that occurred in the drainage tunnel of the Jinping II project [111]. Due to the lack of details regarding the support system, it is difficult to establish a direct correlation between this accident, the chosen machine type, and the existing support system.

Figure 4.60: The damages caused by the rockburst on the May 31, 2015 in Neelum Jhelum project [111]

Despite this case, there have been also successful examples of using gripper TBMs in conditions where both squeezing and rockburst were regarded as critical risks. For instance, 85 km of the whole 157 km rail tunnel system in Gotthard tunnel was excavated successfully with similar gripper TBMs [110]. These case studies underscore the significance of conducting comprehensive geotechnical investigations while considering the most significant risks.

Chapter 5

Summary and outlook

In this final chapter, a summary of the key conclusions from this research are presented. Subsequently, in the recommendations section, pertinent issues related to the study's limitations will be addressed, highlighting areas that require further investigation.

5.1 Conclusions

In spite of their advantages, TBMs have encountered challenges when employed in hard rock mines, primarily due to difficult ground conditions, limited adaptability to mining infrastructures, and intensive launching operations. Improper rock engineering design in difficult ground conditions can result in hazards that jeopardize the safety of personnel, cause delays in tunnel completion, and lead to financial losses. This research focused on assessing the risks posed by difficult ground conditions and aimed to develop a quantitative risk assessment index to investigate the suitability of TBMs for different rock formations, with a specific emphasis on squeezing and rockburst. A summary of the main considerations and findings are presented as follows:

- This study employed Fault Tree Analysis (FTA) and Event Tree Analysis (ETA) as methodologies for primary risk analysis according to the type of machine and its characteristics. The main outcomes of squeezing and rockburst in

relation to the use of TBMs include worker injuries, equipment damage, shield jamming, support system damage, and challenges related to gripper bracing in weak grounds.

To quantitatively assess the extent of these consequences, a Monte Carlo simulation approach was suggested, provided that a probabilistic approach is feasible. An integrated risk assessment index known as the TBM Risk Index (TBM_{RI}) was developed. This index analyses the geological risks in two groups of rockburst and squeezing, and provides a measure of the overall risk level. It considers the cumulative effect of these risks, through consideration of the entire length of the excavation. The index is able to incorporate certain mitigating measures aimed at minimizing the risks. The key components of the TBM Risk Index are specific prediction tools chosen from various methods introduced in the literature. These tools enable the assessment of potential risks associated with squeezing and rockburst in TBM tunneling.

- The research findings suggest that for shield jamming, the parametric method based on previously conducted 3D numerical models and the adapted convergence confinement (CC) method introduced in this study yield more accurate results compared to the parametric method based on previously conducted 2D models. The 2D parametric method tends to overestimate the values of shield frictional force in most cases due to its underlying conservative assumptions. For shielded TBMs experiencing jamming, the 3D parametric method is considered the primary approach. In the case of gripper TBMs, the adapted convergence confinement (CC) method can be customized to consider certain support systems. It is crucial to note that for gripper TBMs, the specific details of the support system, including the mechanical properties and location of the support system must be considered in the risk assessment process.

- Damage to the support system represents a notable consequence of squeezing ground conditions. The methodology introduced in this research was mainly associated with segmental lining in shielded TBMs. However, it is easily adaptable to other kinds of support systems in gripper TBMs as well. The main

causes of support system damage in shielded TBMs are excessive radial deformation on the exterior side of the support system and longitudinal cracks on the segmental lining resulting from high jack forces on the segments. Analytical methods based on the adapted convergence confinement method and the parametric study based on previously conducted 2D asymmetric numerical simulations were applied for evaluation purposes.

- The quantification of the rockburst consequences in a TBM tunneling project was inevitably evaluated through a different approach compared to squeezing. This approach primarily relies on two crucial parameters: the intensity and location of rockburst events, both of which are inherently difficult to ascertain due to their dependence on various geological and operational variables. The location of a rockburst carries significant implications for the type of TBM and its associated features, such as shield length and support type. These factors, in turn, define the level of exposure to hazards for both equipment and personnel.

- Initially, rockburst prediction tools are employed to evaluate the potential intensity of rockbursts based on available input parameters. Subsequently, a Monte Carlo simulation is used to randomly determine the location of rockburst based on a presumed probability distribution function.

- Two case studies each having one of the main classes of introduced risks, namely squeezing and rockburst were applied for validation purposes. In the case study of the Golab tunnel, squeezing risks including shield jamming and support system damage were dominant. The study showed that using a single-shielded TBM with a shorter shield, along with the implementation of shield lubrication, would substantially reduce the squeezing risk index compared to the double-shielded TBM that was originally employed. On the other hand, the case study of the drainage tunnel in Jinping tunnel was selected as an example of a tunnel where rockburst is the main dominant risk. Unlike the Golab tunnel case study, the risk index evaluations conducted in the drainage

tunnel of the Jinping II project revealed that opting for a shorter shield would lead to higher risks by increasing the exposure of personnel and machine components to seismic events.

To determine the suitable machine type when both squeezing and rockburst risks are significant in a project, a case study with both risks was necessary. However, attempts to access relevant data from such case studies were not successful. Consequently, for this final investigation, assumptions were made by combining geotechnical data from the aforementioned case studies. Three scenarios of different proportions of squeezing, rockburst and normal ground conditions were taken for this purpose. A fundamental assumption underlying all these scenarios was that the three main types of Tunnel Boring Machines (TBMs) operated at approximately equal excavation speeds, avoiding complexities related to time-dependant deformations. In a first scenario, it was assumed that the tunnel consists of three equally long sections: one with high squeezing risk, one with high rockburst-associated risks and the rest without any of these risks. Based on the approximation method presented in this research, the single shielded TBM using lubrication has the lowest total TBM risk index (TBM_{RI}) and is only slightly lower than the gripper TBM. Assuming that the gripper TBM is capable of employing a mitigation measure such as the Mc Nally system, the high exposure of personnel and equipment can be partially addressed. Therefore, an optimum option can be chosen between a single-shielded TBM with active lubrication to avoid jamming or a gripper TBM using mitigating measures to avoid rockburst consequences.

- In case a significant proportion of a tunnel is composed of squeezing grounds, the TBM risk index in this research would yield the lowest value for a gripper TBM. However, this decision needs to be carefully considered in the pre-design stage of the TBM. In order to effectively manage high convergences occurring in close proximity to the tunnel face, it is crucial for the machine to be equipped with support installation components in the L1 zone. This ensures the implementation of essential control measures before the full installation of

the support system in the L2 zone. In extreme squeezing grounds, the issue of gripper bracing together with the difficult and time-consuming process of support system installation can reduce the advance rate of the TBM. One of the shortcomings of the introduced risk index in this research would prevail here, which is the negligence of the advance rate of different types of machines and its effect on the time-dependant deformations in ground, which in the case of long standstills can question the superiority of a gripper TBM in this scenario. It is generally questionable in this scenario if using a TBM would become actually advantageous over conventional tunneling. This once again indicates the importance of a wider risk management procedure that can consider other excavation methods, in addition to mechanized excavation using TBMs.

The last scenario with predominant rockburst risk has obviously indicated the superiority of shielded TBMs over gripper TBMs in reducing the exposure of machine components and the personnel to seismic events.

5.2 Outlook

- It is of high importance to mention that the initial decision between conventional tunneling and mechanized excavation was not in the scope of the study. This aspect is suggested for future work, where further investigation into this procedure is recommended.

- The CC method used in this research has certain limitations that should be taken into consideration. According to Cantieni and Anagnostou (2009), the CC method (using the Plane strain assumption) is deemed unsuitable for heavily squeezing rocks when the distance to the support installation is long and a stiff support system is employed [74]. Furthermore, another study by Vrakas and Anagnostou(2014) highlights the limitation of the CC method using the common Duncan Fama and Carranza-Torres closed-form solutions, as they are more suitable for small strain analysis. A further study can be the introduc-

tion of the closed-form solution proposed by Vrakas and Anagnostou (2014) for large strain cases [58].

- It has been proved that the advance rate of the TBM can highly affect the extent of jamming risk due to the time-dependent nature of many weak rocks. This phenomenon was not considered in this research due to a lack of data related to the time-dependent behavior of rock mass in many cases. In this research, we operated under the assumption that various types of Tunnel Boring Machines (TBMs) advance at a relatively consistent speed, with minimal interruptions.

- Using gripper TBMs in squeezing grounds can present the challenge related to gripper shoes. The evaluation of gripper bracing difficulties in such conditions involves assessing the rock's capacity to provide the necessary reaction force. To comprehensively address this issue, a numerical investigation is highly recommended, as it enables the computation of stress redistribution, considers gripper shoe force exertion, and if necessary can incorporate geological discontinuities. This approach is particularly suited for assessing potential instabilities due to the exertion of gripper forces to the ground. However, considering the aim of this study to provide a quick and straightforward procedure, the research primarily involved studying the gripper bracing issue through an analytical process. This approach also deserves additional research efforts.

- In this research, the rockburst location determination method was based on the rockburst event distribution observed in the Neelum-Jhelum project case study as just an example. This may defer from many other case studies. Thus, further work should involve extensive data analysis of different projects, enhancing the effectiveness of the proposed procedure.

  The same applies to the significance factors introduced in this research for both squeezing and rockburst consequences. Integration of these risks into one index required defining weighting coefficients representing the criticality of each type of risk and their consequences. These factors were defined based

on subjective judgments and would benefit from calibration using actual data from TBM tunneling projects and acquiring the knowledge of experts in the field. In case a sufficient amount of data can be provided that can correlate each risk with time and cost consequences, the significance factor of each type of consequence can be evaluated in a more certain way.

- The proposed methodologies and approaches in this research for support systems in shielded TBMs can provide a preliminary evaluation of the loads exerted on the segmental lining. However, these methods do not eliminate the need for more accurate assessments such as tailored numerical analyses. For instance, the simultaneous effect of ground pressure on the segmental lining and the pressure exerted by the jacks in the grounds with high jamming risk can only be analyzed with further relevant investigations. This aspect deserves careful consideration to ensure the optimal design and performance of the support system.

  Moreover, the introduced approaches have limitations that they do not account for the tensile strength of the support system and fail to capture damages caused by anisotropic ground deformations. For instance, buckling is an outcome of anisotropic schistosity in the rock mass. Further investigation in this direction can provide valuable insights into the extent of its effect on the support damage consequence as well as the jamming in a tunneling project. To surpass these limitations in this research, a safety factor was assumed to evaluate the structural integrity of the segmental lining.

- In spite of the above limitations, in the process of identifying the TBM with the lowest level of risk, the quantitative risk index introduced in this research can serve as a valuable primary step. It can be used as a framework to effectively differentiate between various types of risks within a deep tunneling project facing rock mechanical issues. Specifically, it can be applied for gaining an understanding of an integrated risk landscape. It is important to note that the significance factors assigned to different risk types and machine types are presumed values and are subject to further studies. Therefore, additional data

analysis is necessary to improve the accuracy of estimations and refine the risk assessment process.

Bibliography

[1] Y.L. Zheng, Q.B. Zhang, and J. Zhao. "Challenges and opportunities of using tunnel boring machines in mining". In: *Tunnelling and Underground Space Technology* 57 (2016), pp. 287–299. ISSN: 0886-7798. DOI: 10.1016/j.tust.2016.01.023. URL: https://www.sciencedirect.com/science/article/pii/S0886779815303680.

[2] Roohollah Narimani Dehnavi, Nikolaus Sifferlinger, and Jamal Rostami. "Assessment of the Rockburst Risk Associated with Use of TBMs in Deep Mines". In: *The 5th International Conference on Tunnel Boring Machines in Difficult Grounds*. 2022, pp. 132–137.

[3] Xing Huang et al. "Application and prospect of hard rock TBM for deep roadway construction in coal mines". In: *Tunnelling and Underground Space Technology* 73 (2018), pp. 105–126. ISSN: 0886-7798. DOI: 10.1016/j.tust.2017.12.010. URL: https://www.sciencedirect.com/science/article/pii/S0886779817300202.

[4] Robbins. "Robbins Co. Webinar". In: Robbins, 2019.

[5] Alexander Vyazmensky. "Numerical modeling of surface subsidence associated with block cave mining using a FEM/DEM approach". PhD thesis. Simon Fraser University, 2008.

[6] Roohollah Narimani Dehnavi et al., eds. *The Performance of a TBM in Difficult Ground Conditions of Golab Water Transfer Tunnel: A Case Study in Iran*. 2016.

[7] ITA. "TBM Excavation of Long and Deep Tunnels Under Difficult Rock Conditions". In: (2017).

[8] Jamal Rostami. "Performance prediction of hard rock Tunnel Boring Machines (TBMs) in difficult ground". In: *Tunnelling and Underground Space Technology* 57 (2016), pp. 173–182. ISSN: 0886-7798. DOI: 10.1016/j.tust.2016.01.009. URL: https://www.sciencedirect.com/science/article/pii/S0886779815301991.

[9] DAUB-Working Group. *Recommendations for the Selection of Tunnel Boring Machines*. 2022.

[10] Matthew Leitch. *ISO 31000:2009—The New International Standard on Risk Management*. 2010. DOI: 10.1111/j.1539-6924.2010.01397.x.

[11] Rita L. Sousa. "Risk Analysis for Tunneling Projects". PhD thesis. 2010.

[12] Stacey, T.R.* & De Jongh C.L.**. "Stress fracturing around a deep-level bored tunnel". In: *Journal of the Southern African Institute of Mining and Metallurgy* 78.5 (1977), pp. 124–133. DOI: 10.10520/AJA0038223X{\textunderscore}820.

[13] Simon Loew, Giovanni Barla, and Mark Diederichs. "Engineering geology of Alpine Tunnels: Past, present and future (keynote lecture)". In: 2010.

[14] Masoud Ghorbani et al. "A critical review on the developments of rock support systems in high stress ground conditions". In: *International Journal of Mining Science and Technology* 30.5 (2020), pp. 555–572. ISSN: 2095-2686. DOI: 10.1016/j.ijmst.2020.06.002. URL: https://www.sciencedirect.com/science/article/pii/S2095268618307213.

[15] Wulf Schubert and Juan Manuel Davila Mendez. "Influence of Foliation Orientation on Tunnel Behavior". In: *Procedia Engineering* 191 (2017), pp. 880–885. ISSN: 1877-7058. DOI: 10.1016/j.proeng.2017.05.257. URL: https://www.sciencedirect.com/science/article/pii/S1877705817323974.

[16] Q. M. Gong et al. "Rock burst and slabbing failure and its influence on TBM excavation at headrace tunnels in Jinping II hydropower station". In: *Engineering Geology* 124 (2012), pp. 98–108. ISSN: 0013-7952. DOI: 10.1016/j.enggeo.2011.10.007. URL: https://www.sciencedirect.com/science/article/pii/S0013795211002602.

[17] Horst Wagner. *Rock Engineering for Deep Mines_Module 8_Management of Rock Pressure Risk*. 2020.

[18] Chuanqing Zhang et al. "Case Histories of Four Extremely Intense Rockbursts in Deep Tunnels". In: *Rock mechanics* 45.3 (2012), pp. 275–288. ISSN: 1434-453X. DOI: 10.1007/s00603-011-0218-6.

[19] Emilio Rosenblueth. "Point estimates for probability moments". In: *Proceedings of the National Academy of Sciences* 72.10 (1975), pp. 3812–3814. DOI: 10.1073/pnas.72.10.3812.

[20] Eleyas Assefa et al. "Slope Stability Evaluation for the New Railway Embankment using Stochastic Finite Element and Finite Difference Methods". In: *Electronic Journal of Geotechnical Engineering* 22 (2017), pp. 33–49.

[21] Brent Henderson and Elisabeth Bui. "Determining Uncertainty in Sediment & Nutrient Transport Models for Ecological Risk Assessment". In: (2023).

[22] Manchao He et al. "Rockburst laboratory tests database — Application of data mining techniques". In: *Engineering Geology* 185 (2015), pp. 116–130. ISSN: 0013-7952. DOI: 10.1016/j.enggeo.2014.12.008. URL: https://www.sciencedirect.com/science/article/pii/S0013795214003421.

[23] L. M. Castro, Robert Bewick, and Trevor Carter. "An overview of numerical modelling applied to deep mining". In: *Innovative Numerical Modeling in Geomechanics* (2012), pp. 393–414. DOI: 10.1201/b12130-22.

[24] Jian Zhou, Xibing Li, and Hani S. Mitri. "Evaluation method of rockburst: State-of-the-art literature review". In: *Tunnelling and Underground Space Technology* 81 (2018), pp. 632–659. ISSN: 0886-7798. DOI: 10.1016/j.tust.

2018.08.029. URL: http://www.sciencedirect.com/science/article/pii/S0886779817309094.

[25] I. A. Turchaninov and G. A. Markov, eds. *Conditions of Changing of Extra-hard Rock Into Weak Rock Under the Influence of Tectonic Stresses of Massifs*. ISRM-IS-1981-090, 1981.

[26] N. Barton, R. Lien, and J. Lunde. "Engineering classification of rock masses for the design of tunnel support". In: *Rock mechanics* 6.4 (1974), pp. 189–236. ISSN: 1434-453X. DOI: 10.1007/BF01239496.

[27] B. F. Russenes. "Analysis of rock spalling for tunnels in steep valley sides". PhD thesis. Norwegian Institute of Technology, 1974.

[28] Evert Hoek and E. T. Brown. *Underground excavations in rock*. London: Institution of Mining and Metallurgy, 1980. ISBN: 0900488549 9780900488542 0900488557 9780900488559.

[29] Tao Zhen-Yu, ed. *Support Design of Tunnels Subjected to Rockbursting*. Vol. All Days. ISRM International Symposium. 1988.

[30] A. Palmström, ed. *Characterizing rock burst and squeezing by the rock mass index*. 1995.

[31] Z. Hosseini et al., eds. *Mining Strategies of Multi-Sill Pillars In Burst Prone Ground Conditions At Vale Inco's Coleman Mine*. Vol. All Days. U.S. Rock Mechanics/Geomechanics Symposium. 2010.

[32] N. Wiseman. *Factors effecting the the design andcvonditions of mine tunnels*. Johannesburg, South Africa, 1979.

[33] Horst Wagner. "Deep Mining: A Rock Engineering Challenge". In: *Rock mechanics* 52.5 (2019), pp. 1417–1446. ISSN: 1434-453X. DOI: 10.1007/s00603-019-01799-4.

[34] Tan Yian, Sun Guangzhong, and Guo Zhi. "A COMPOSITE INDEX Krb CRITERION FOR THE EJECTION CHARACTERISTICS OF THE BURST ROCK". In: *Chinese Journal of GeologyVL - 26* 2 (1991). URL: http://www.dzkx.org//article/id/geology_10255.

[35] Z. Peng, Y.-H. Wang, and T.-J. Li. "Griffith theory and the criteria of rock burst". In: *Chinese Journal of Rock Mechanics and Engineering* 15.SUPPL (1996), pp. 491–495. URL: https://www.scopus.com/inward/record.uri?eid=2-s2.0-33746690570&partnerID=40&md5=077db38908dfe9f40f605264b309c7c2.

[36] T. Feng et al. "Brittleness of rocks and brittleness indexes for describing rockburst proneness". In: *Mining and Metallurgical Engineering* 20.4 (2000), pp. 18–19. URL: https://www.scopus.com/inward/record.uri?eid=2-s2.0-48549104943&partnerID=40&md5=57b5107fdf89fb22e6e313abc530841d.

[37] G. Zhang, J. Chen, and B. Hu. "Prediction and control of rockburst during deep excavation of a gold mine in China". In: *Yanshilixue Yu Gongcheng Xuebao/Chinese Journal of Rock Mechanics and Engineering* 22.10 (2003), pp. 1607–1612. URL: https://www.scopus.com/inward/record.uri?eid=2-s2.0-0442311775&partnerID=40&md5=7d882ca7ee5fdcf0c77f7c378d1ac9ce.

[38] G. Zhang, J. Chen, and B. Hu. "Prediction and control of rockburst during deep excavation of a gold mine in China". In: *Yanshilixue Yu Gongcheng Xuebao/Chinese Journal of Rock Mechanics and Engineering* 22.10 (2003), pp. 1607–1612. URL: https://www.scopus.com/inward/record.uri?eid=2-s2.0-0442311775&partnerID=40&md5=7d882ca7ee5fdcf0c77f7c378d1ac9ce.

[39] J.-A. Wang and H. D. Park. "Comprehensive prediction of rockburst based on analysis of strain energy in rocks". In: *Tunnelling and Underground Space Technology* 16.1 (2001), pp. 49–57. ISSN: 0886-7798. DOI: 10.1016/S0886-7798(01)00030-X. URL: https://www.sciencedirect.com/science/article/pii/S088677980100030X.

[40] N.G.W. Cook et al. *Rock mechanics applied to the study of rockbursts*. Johannesburg: South African Institute of Mining and Metallurgy, 1966.

[41] J. A. Ryder. "Excess shear stress in the assessment of geologically hazardous situations". In: *Journal of the Southern African Institute of Mining and Metallurgy* 88.1 (1988), pp. 27–39. DOI: 10.10520/AJA0038223X$\backslash${\textunderscore}1867.

[42] B. Neyman, Z. Szecowka, and W. Zuberek, eds. *Effective methods for fighting rock burst in Polish collieries*. 1972.

[43] H. S. Mitri, B. Tang, and R. Simon. "FE modelling of mining-induced energy release and storage rates". In: *Journal of The South African Institute of Mining and Metallurgy* 99 (1999), pp. 103–110.

[44] J. Zhou, X. B. Li, and H. S. Mitri, eds. *A critical survey of empirical methods for evaluating rockburst potential*. 2017.

[45] Hani S. Mitri. "Assessment of horizontal pillar burst in deep hard rock mines". In: *International Journal of Risk Assessment and Management* 7.5 (2007), pp. 695–707. ISSN: 1466-8297. DOI: 10.1504/IJRAM.2007.014094.

[46] Gyan Lal Shrestha. "Stress Induced Problems in Himalayan Tunnels with Special Reference to Squeezing". PhD thesis. 2006.

[47] Bhawani Singh et al. "Correlation between observed support pressure and rock mass quality". In: *Tunnelling and Underground Space Technology* 7.1 (1992), pp. 59–74. ISSN: 0886-7798. DOI: 10.1016/0886-7798(92)90114-W. URL: https://www.sciencedirect.com/science/article/pii/088677989290114W.

[48] R. K. Goel, J. L. Jethwa, and A. G. Paithankar. "Tunnelling through the young Himalayas — A case history of the Maneri-Uttarkashi power tunnel". In: *Engineering Geology* 39.1 (1995), pp. 31–44. ISSN: 0013-7952. DOI: 10.1016/0013-7952(94)00002-J. URL: https://www.sciencedirect.com/science/article/pii/001379529400002J.

[49] Ö. Aydan, T. Akagi, and T. Kawamoto. "The squeezing potential of rocks around tunnels; Theory and prediction". In: *Rock Mechanics and Rock Engineering* 26.2 (1993), pp. 137–163. ISSN: 1434-453X. DOI: 10.1007/BF01023620.

[50] Evert Hoek and P. Marinos. "Predicting Tunnel Squeezing Problems in Weak Heterogeneous Rock Masses". In: *Tunnels and Tunnelling International* 32 (2000), pp. 45–51.

[51] R. K. Goel. "Correlations for predicting support pressures and closures in tunnels". PhD thesis. India: Nagpur University, 1994.

[52] Rohola Hasanpour. "Evaluation of applicability of double shielded Tunnel Boring Machines (DS-TBM) in potential squeezing grounds". PhD thesis. 2013.

[53] Rocscience. *Rocsupport introduction manual*. 2019. URL: https://static.rocscience.cloud/assets/verification-and-theory/RocSupport/Introduction_Manual.pdf.

[54] C. Carranza-Torres and C. Fairhurst. "Application of the Convergence-Confinement method of tunnel design to rock masses that satisfy the Hoek-Brown failure criterion". In: *Tunnelling and Underground Space Technology* 15.2 (2000), pp. 187–213. ISSN: 0886-7798. DOI: 10.1016/S0886-7798(00)00046-8. URL: https://www.sciencedirect.com/science/article/pii/S0886779800000468.

[55] B.H.G. Brady and E. Brown. *Rock Mechanics for underground mining*. 2006. ISBN: 978-1-4020-2064-3. DOI: 10.1007/978-1-4020-2116-9.

[56] Mary E. Duncan Fama. "3 - Numerical Modeling of Yield Zones in Weak Rock". In: *Analysis and Design Methods*. Ed. by CHARLES FAIRHURST. Oxford: Pergamon, 1993, pp. 49–75. ISBN: 978-0-08-040615-2. DOI: 10.1016/B978-0-08-040615-2.50009-5. URL: https://www.sciencedirect.com/science/article/pii/B9780080406152500095.

[57] C. Carranza-Torres. "Elasto-plastic solution of tunnel problems using the generalized form of the hoek-brown failure criterion". In: *International Journal of Rock Mechanics and Mining Sciences* 41 (2004), pp. 629–639. ISSN: 1365-1609. DOI: 10.1016/j.ijrmms.2004.03.111. URL: https://www.sciencedirect.com/science/article/pii/S1365160904001583.

[58] Apostolos Vrakas and Georgios Anagnostou. "A finite strain closed-form solution for the elastoplastic ground response curve in tunnelling". In: *International Journal for Numerical and Analytical Methods in Geomechanics* 38.11 (2014), pp. 1131–1148. ISSN: 0363-9061. DOI: 10.1002/nag.2250.

[59] C. Carranza-Torres. "Dimensionless Graphical Representation of the Exact Elasto-plastic Solution of a Circular Tunnel in a Mohr-Coulomb Material Subject to Uniform Far-field Stresses". In: *Rock Mechanics and Rock Engineering* 36.3 (2003), pp. 237–253. ISSN: 1434-453X. DOI: 10.1007/s00603-002-0048-7.

[60] P. Kaiser and M. Cai. "Design of rock support system under rockburst condition". In: *Journal of rock mechanics and geotechnical engineering* 4 (2012), pp. 215–227.

[61] M. P. McNally and C. McNally. "Method and apparatus for feeding a tunnel roof support system from the roof shield of a TBM". Pat. EP1033473A1. 2000.

[62] Lock Home and Desiree Willis. *Keep your TBM moving against the odds*. 2017. URL: https://www.tunneltalk.com/TunnelTECH-Jun2017-TBM-operations-in-difficult-ground.php.

[63] Detlef Jordan, ed. *The Brenner Challenge – TBMs Versus Drill & Blast in High Cover Conditions*. Vol. All Days. ISRM EUROCK. 2015.

[64] Georg H. Erharter, Robert Goliasch, and Thomas Marcher. "On the Effect of Shield Friction in Hard Rock TBM Excavation". In: *Rock Mechanics and Rock Engineering* 56.4 (2023), pp. 3077–3092. ISSN: 1434-453X. DOI: 10.1007/s00603-022-03211-0.

[65] Lok Home and Gary Brierley. "The Risks Associated with TBM Procurement and the Next Steps Towards Industry Change". In: (2018).

[66] E. Hoek and R. Guevara. "Overcoming Squeezing in the Yacambú-Quibor Tunnel, Venezuela". In: *Rock Mechanics and Rock Engineering* 42.2 (2009), pp. 389–418. ISSN: 1434-453X. DOI: 10.1007/s00603-009-0175-5.

[67] Ebrahim Farrokh, Ali Mortazavi, and Gholamreza Shamsi. "Evaluation of ground convergence and squeezing potential in the TBM driven Ghomroud tunnel project". In: *Tunnelling and Underground Space Technology* 21.5 (2006),

pp. 504–510. ISSN: 0886-7798. DOI: 10.1016/j.tust.2005.09.003. URL: http://www.sciencedirect.com/science/article/pii/S0886779805000799.

[68] Rohola Hasanpour. "Advance numerical simulation of tunneling by using a double shield TBM". In: *Computers and Geotechnics* 57 (2014), pp. 37–52. ISSN: 0266-352X. DOI: 10.1016/j.compgeo.2014.01.002. URL: https://www.sciencedirect.com/science/article/pii/S0266352X14000032.

[69] Rohola Hasanpour et al. "Prediction of TBM jamming risk in squeezing grounds using Bayesian and artificial neural networks". In: *Journal of Rock Mechanics and Geotechnical Engineering* 12.1 (2020), pp. 21–31. ISSN: 1674-7755. DOI: 10.1016/j.jrmge.2019.04.006. URL: https://www.sciencedirect.com/science/article/pii/S1674775519307346.

[70] A. Jafari, M. Mollaee, and H. Shamsi. "Investigation Into Ground Convergence Effect On TBM Performance In Squeezing Ground". In: 2007, ISRM–11CONGRESS–2007–205.

[71] Mahdi Rasouli Maleki and Roohollah Narimani Dehnavi. "Influence of Discontinuities on the Squeezing Intensity in High In Situ Stresses (a Tunnelling Case Study; Actual Evidences and TBM Release Techniques)". In: *Rock mechanics* 51.9 (2018), pp. 2911–2933. ISSN: 1434-453X. DOI: 10.1007/s00603-018-1476-3.

[72] N. Vlachopoulos and M. S. Diederichs. "Improved Longitudinal Displacement Profiles for Convergence Confinement Analysis of Deep Tunnels". In: *Rock mechanics* 42.2 (2009), pp. 131–146. ISSN: 1434-453X. DOI: 10.1007/s00603-009-0176-4.

[73] M. Ramoni and G. Anagnostou. "Thrust force requirements for TBMs in squeezing ground". In: *Tunnelling and Underground Space Technology* 25.4 (2010), pp. 433–455. ISSN: 0886-7798. DOI: 10.1016/j.tust.2010.02.008. URL: https://www.sciencedirect.com/science/article/pii/S0886779810000374.

[74] Linard Cantieni and Georgios Anagnostou. "The Effect of the Stress Path on Squeezing Behavior in Tunneling". In: *Rock mechanics* 42.2 (2009), pp. 289–318. ISSN: 1434-453X. DOI: 10.1007/s00603-008-0018-9.

[75] Rohola Hasanpour and Jürgen Schmitt. "Evaluation of Ground Reaction and Convergence Relative to Possibility of Entrapment for Shielded Tunnel Boring Machines". In: 2016, ISRM–ISRS–2016–060.

[76] Ömer Aydan and Rohola Hasanpour. "Estimation of ground pressures on a shielded TBM in tunneling through squeezing ground and its possibility of jamming". In: *Bulletin of Engineering Geology and the Environment* 78.7 (2019), pp. 5237–5251. ISSN: 1435-9537. DOI: 10.1007/s10064-019-01477-3.

[77] Ö. Aydan, T. Akagi, and T. Kawamoto. "The squeezing potential of rock around tunnels: Theory and prediction with examples taken from Japan". In: *Rock mechanics* 29.3 (1996), pp. 125–143. ISSN: 1434-453X. DOI: 10.1007/BF01032650.

[78] Pierpaolo Oreste. "Analysis of the Interaction between the Lining of a TBM Tunnel and the Ground Using the Convergence-Confinement Method". In: *American Journal of Applied Sciences* 12.4 (2015). DOI: 10.3844/ajassp.2015.276.283.

[79] Pierpaolo Oreste et al. "Analysis of the behavior of the two-component grout around a tunnel segmental lining on the basis of experimental results and analytical approaches". In: *Transportation Geotechnics* 29 (2021), p. 100570. ISSN: 2214-3912. DOI: 10.1016/j.trgeo.2021.100570. URL: https://www.sciencedirect.com/science/article/pii/S221439122100060X.

[80] M. Ramoni, N. Lavdas, and G. Anagnostou. "Squeezing loading of segmental linings and the effect of backfilling". In: *Tunnelling and Underground Space Technology* 26.6 (2011), pp. 692–717. ISSN: 0886-7798. DOI: 10.1016/j.tust.2011.05.007. URL: https://www.sciencedirect.com/science/article/pii/S088677981100071X.

[81] M. Ramoni and G. Anagnostou. "The Interaction Between Shield, Ground and Tunnel Support in TBM Tunnelling Through Squeezing Ground". In: *Rock mechanics* 44.1 (2011), pp. 37–61. ISSN: 1434-453X. DOI: 10.1007/s00603-010-0103-8.

[82] Alessandro Graziani, Capata Aldo, and R. Paolo. "Analysis of rock-TBM-lining interaction in squeezing rock". In: 2007.

[83] Marco Ramoni and Georg Anagnostou. *Numerical analysis of the development of squeezing pressure during TBM standstills*. 2007.

[84] Francesco Amberg, ed. *Numerical simulations of tunnelling in soft rock under water pressure*. Aedificatio Publishers, 2009.

[85] Jürgen Schmitt. *Spannungsverformungsverhalten des Gebirges beim Vortrieb mit Tunnelbohrmaschinen mit Schild*. 2009. ISBN: 3-927610-80-1.

[86] Kai Zhao, Michele Janutolo, and Giovanni Barla. "A Completely 3D Model for the Simulation of Mechanized Tunnel Excavation". In: *Rock mechanics* 45.4 (2012), pp. 475–497. ISSN: 1434-453X. DOI: 10.1007/s00603-012-0224-3.

[87] Rohola Hasanpour et al. "Parametric study of the impacts of various geological and machine parameters on thrust force requirements for operating a single shield TBM in squeezing ground". In: *Tunnelling and Underground Space Technology* 73 (2018), pp. 252–260. ISSN: 0886-7798. DOI: 10.1016/j.tust.2017.12.027. URL: https://www.sciencedirect.com/science/article/pii/S0886779817302158.

[88] Shaokang Hou et al. "Prediction of shield jamming risk for double-shield TBM tunnels based on numerical samples and random forest classifier". In: *Acta Geotechnica* 18.1 (2023), pp. 495–517. ISSN: 1861-1133. DOI: 10.1007/s11440-022-01567-9.

[89] Rohola Hasanpour et al. "Examining the effect of adverse geological conditions on jamming of a single shielded TBM in Uluabat tunnel using numerical modeling". In: *Journal of Rock Mechanics and Geotechnical Engineering* 9.6

(2017), pp. 1112–1122. ISSN: 1674-7755. DOI: 10.1016/j.jrmge.2017.05.010. URL: https://www.sciencedirect.com/science/article/pii/S1674775517300689.

[90] Georg Anagnostou. "TBM tunnelling in complex rock formations". In: 2014, pp. 307–331. ISBN: 9788867890514.

[91] Nuh Bilgin and Melih Algan. "The performance of a TBM in a squeezing ground at Uluabat, Turkey". In: *Tunnelling and Underground Space Technology* 32 (2012), pp. 58–65. ISSN: 0886-7798. DOI: 10.1016/j.tust.2012.05.004. URL: https://www.sciencedirect.com/science/article/pii/S0886779812000983.

[92] I. Vicenzi et al. "Deep tunnelling in hardrock with large diameter TBM: What's up? An experience from the Gotthard Base Tunnel". In: (2007). DOI: 10.1201/NOE0415408073.ch44.

[93] Herrenknecht AG. *Single Shield TBM - Herrenknecht AG*. 4.04.2023. URL: https://www.herrenknecht.com/en/products/productdetail/single-shield-tbm/?chash=f99d7ff4ebec3652bb3baca964181f03&cHash=efb97119796c6781690

[94] *Double Shield TBM - Herrenknecht AG*. Apr. 2023. URL: https://www.herrenknecht.com/en/products/productdetail/double-shield-tbm/.

[95] ITA. "Guidelines for the design of segmental tunnel linings". In: (2019).

[96] ACI Committee 318. "318-19(22): Building Code Requirements for Structural Concrete and Commentary (Reapproved 2022)". In: *Technical Documents* ().

[97] Walter Wittke. *Stability analysis and design for mechanized tunneling*. Geotechnical Engineering in Research and Practice, 2007.

[98] Nuh Bilgin, Hanifi Copur, and Cemal Balci. *Mechanical excavation in mining and civil industries*. Boca Raton: Taylor & Francis/CRC, 2014. ISBN: 9780429074110.

[99] Jamal Rostami. "Study of pressure distribution within the crushed zone in the contact area between rock and disc cutters". In: *International Journal of Rock Mechanics and Mining Sciences* 57 (2013), pp. 172–186. ISSN: 1365-1609. DOI: 10.1016/j.ijrmms.2012.07.031. URL: https://www.sciencedirect.com/science/article/pii/S1365160912001682.

[100] R. Narimani Dehnavi, Sifferlinger N. A., and Jamal Rostami, eds. *Assessment of the Rockburst Risk Associated with Use of TBMs in Deep Mines*. 2022.

[101] Yong Fan et al. "Influence of tunneling methods on the strainburst characteristics during the excavation of deep rock masses". In: *Engineering Geology* 201 (2016), pp. 85–95. ISSN: 0013-7952. DOI: 10.1016/j.enggeo.2015.12.015. URL: https://www.sciencedirect.com/science/article/pii/S0013795215301101.

[102] J. Mierzejewski, G. Peach, and B. Ashcroft, eds. *Short-Term Rockburst Prediction in TBM Tunnels*. 2017.

[103] Hafeezur Rehman et al. "Impact of Construction Method and Ground Composition on Headrace Tunnel Stability in the Neelum–Jhelum Hydroelectric Project: A Case Study Review from Pakistan". In: *Applied Sciences* (2021).

[104] Peng Lin, Hongyuan Liu, and Weiyuan Zhou. "Experimental study on failure behaviour of deep tunnels under high in-situ stresses". In: *Tunnelling and Underground Space Technology* 46 (2015), pp. 28–45. ISSN: 0886-7798. DOI: 10.1016/j.tust.2014.10.009. URL: https://www.sciencedirect.com/science/article/pii/S0886779814001771.

[105] J. A. Hudson and X.-T. Feng. *Rock Engineering Risk (1st ed.)* CRC Press, 2015.

[106] Weizhang Liang et al. "Assessing the Probability of Strainburst Potential Via an Integration of Monte Carlo Simulation and Machine Learning Algorithms". In: *Rock mechanics* 56.1 (2023), pp. 129–142. ISSN: 1434-453X. DOI: 10.1007/s00603-022-03067-4.

[107] N. W. Xu et al. "Microseismic Monitoring of Strainburst Activities in Deep Tunnels at the Jinping II Hydropower Station, China". In: *Rock Mechanics and Rock Engineering* 49.3 (2016), pp. 981–1000. ISSN: 1434-453X. DOI: 10.1007/s00603-015-0784-0.

[108] Rocscience. *Rocsupport*.

[109] Dean Brox. "Technical considerations for TBM tunneling for mining projects". In: (2013).

[110] Irfan Ullah, Gary Peach, and Muhammad Nadeem. "Tunnel Boring Machine Advance Ground Investigation in Rockburst-Prone Ground Conditions on Neelum Jhelum Project". In: *Engineering Challenges for Sustainable Underground Use*. Ed. by Sherif Agaiby and Piergiorgio Grasso. Cham: Springer International Publishing, 2018, pp. 53–75. ISBN: 978-3-319-61636-0.

[111] Abdul Muntaqim Naji et al. "Impact of Shear Zone on Rockburst in the Deep Neelum-Jehlum Hydropower Tunnel: A Numerical Modeling Approach". In: *Energies* 11.8 (2018). ISSN: 1996-1073. DOI: 10.3390/en11081935. URL: https://www.mdpi.com/1996-1073/11/8/1935.

List of Figures